

Investigation of Head and Brain Response in Football Helmet Impacts using a Finite Element Model of the Head and Neck with Active Muscle

by

David Bruneau

A thesis

presented to the University of Waterloo

in fulfillment of the

thesis requirement for the degree of

Master of Applied Science

in

Mechanical and Mechatronics Engineering

Waterloo, Ontario, Canada, 2019

© David Bruneau 2019

Author's Declaration

This thesis consists of material all of which I authored or co-authored: see Statement of Contributions included in the thesis. This is a true copy of the thesis, including any required final revisions, as accepted by my examiners.

I understand that my thesis may be made electronically available to the public.

Statement of Contributions

Some of the material in this thesis has been published in a journal article:

“Head and Neck Response of an Active Human Body Model and Finite Element Anthropometric Test Device During a Linear Impactor Helmet Test”. **Bruneau, D.**, Cronin, D.S. *J Biomech Eng*, 2019 (Accepted). doi: 10.1115/1.4043667. Copyright © 2019 by ASME

Duane Cronin was the principal investigator and a reviewer of the pre-print of the manuscript (15%). David Bruneau contributed to 85% of the published work.

Abstract

Among high school and college athletes, ~50% of American football players report a concussion each year, and at least 30% of players sustain more than one concussion per year, which may be reduced in part through improvements in head protection. Football helmets are commonly assessed experimentally using a linear impactor test, where a helmet is donned on a Hybrid III Anthropometric Testing Device (ATD) head and neck affixed to a sliding carriage, and is struck by a deformable impactor. The biofidelity of the Hybrid III ATD is known to have some limitations: the ATD was developed to predict anterior-posterior response while the current test includes multi-directional loading, and the passive neck structure does not simulate active muscle. Additionally, the linear impactor test does not include the body of the player, which may influence the head response. The current study used an advanced Human Body Model (HBM) combined with a validated finite element model of a modern football helmet to assess the importance of the aforementioned limitations, and was then extended to investigate the response of the brain to impact scenarios. A virtual evaluation tool provides the advantage of assessing changes to current helmet designs, and new helmet designs prior to the construction of a physical prototype.

An existing ATD head and neck model validated in the linear impact configuration, and a validated football helmet model previously assessed with 60 impact cases, were used as a baseline for the assessment of head response in football impact scenarios. The Global Human Body Models Consortium (GHBMC) head and neck model (HNM) and Full Human Body Model (FBM) were integrated with the helmet and linear impactor, and assessed using the same boundary conditions as the ATD. The HNM allowed for the investigation of muscle activation, using a muscle activation scheme representing a player braced for impact, and a baseline case with no activation. The models were used in three studies to assess: (1) the kinematic response of the ATD and HNM, (2) the effect of ATD and HNM boundary conditions on brain response, and (3) the role of the whole body mass and inertia on head and brain response.

The first study compared the head kinematics of the HNM to those of the ATD simulation using the boundary conditions of the linear impactor test. It was found that the HNM and ATD had similar head acceleration and angular velocity in the primary direction of impact, and exhibited similar responses regardless of muscle activation. Differences between the ATD and HNM were identified in the axial head acceleration, attributed to axial neck stiffness, and longer term metrics measured at the base of the neck differed but did not have a large effect on the short-term head response assessed using existing head response metrics (HIC, BrIC, HIP).

In the second study, two boundary conditions were investigated for a head FE model: (1) a commonly-used simplified boundary condition where head model kinematics are prescribed from experimentally measured

ATD kinematics and (2) a full simulation of the HNM, helmet and linear impactor. The second approach enables the opportunity to assess the effect of modifications to the helmet. While the lateral and rear impacts exhibited similar levels of Maximum Principal Strain (MPS) in the brain tissue using both the prescribed kinematics and simulated HNM boundary condition, differences were noted in the frontal orientation (MPS varied by <43%), attributed to geometric differences between the physical ATD and simulated HNM which influenced the angular kinematics in this orientation. It was also found that Cumulative Strain Damage Measure was more sensitive to the boundary condition than MPS.

The objective of the third study was to investigate the role of whole body mass and inertia on head and brain response in a football impact. The helmet was integrated with an unconstrained FBM and the response was compared to the HNM integrated with the helmet. While the motion at the base of the neck differed after 20 ms (no rotation occurred here in the HNM), the kinematic response of the head in the FBM and HNM remained mostly similar until late in the impact (50 ms), regardless of muscle activation, which had little effect on both the FBM and HNM. Comparing the FBM and HNM, the brain response exhibited some small (<15%) differences between 30 and 50 ms, attributed to small differences in angular velocity during this time.

Overall, the three studies demonstrated that biofidelic HBM predict similar head kinematics to those measured using the linear impactor testing of an ATD and the comparable ATD FE model. The primary exception was differences in axial head acceleration, which was attributed to the high axial stiffness of the ATD neck compared to a more human-like neck model. For the short timeframes considered using conventional head response metrics, the two muscle activation schemes considered did not have a considerable effect on the head kinematics or brain deformation. In the future, the coupled HNM and helmet could be used as a tool for improving helmet performance by directly simulating the effect of design changes on head and brain response, prior to building physical prototypes.

Acknowledgements

First, thanks to Dr. Duane Cronin for providing me with a great project opportunity, for bringing me to an international conference, and for encouraging me to publish my work, even when the paper reaches the fifty-second revision. Perhaps most importantly, for teaching me some of the subtleties of academic communication. I'd also like to thank Jack Callaghan and Naveen Chandrashekar for reviewing this thesis and for asking excellent questions during my seminar.

Thanks to the sponsors of the work including Biocore, the Natural Sciences and Engineering Research Council of Canada and the Ontario Government (Ontario Graduate Scholarship). I'd also like to acknowledge and thank the teams at Biocore and the University of Virginia for providing some of the experimental data and models used in this thesis.

I'd also like to thank Chi-Hsaing Liao for being an excellent social coordinator for the research group over the last couple of years, and Prusodman Sathananthan, for all the help with coursework. Thanks to David Shen and Bartek Pilarczyk for the help with neck related questions, and I appreciate Kaab Omer for teaching me the importance of $ELF = 16$.

Finally, I'd like to thank my parents for the encouragement and for helping me put things in perspective. And finally, thanks to Anna Polak, for all the support, especially during thesis time!

Table of Contents

Author's Declaration	ii
Statement of Contributions	iii
Abstract.....	iv
Acknowledgements.....	vi
List of Figures.....	xii
List of Tables	xvii
1. Introduction.....	1
1.1. Motivation for Research.....	1
1.2. Objectives, Approach and Outline	3
2. Background.....	6
2.1. Head and Neck Anatomy	6
2.1.1. Coordinate System.....	6
2.1.2. Anatomy of the Head.....	7
2.1.3. Anatomy of the Neck.....	9
2.2. Concussive Head Injury.....	11
2.2.1. Concussion in American Football.....	12
2.2.2. The Biomechanics of Concussion.....	13
2.3. Football Helmet Impact Testing	14
2.3.1. Anthropometric Testing Devices for Football Helmet Impacts	14
2.3.2. NOCSAE Drop Test.....	16
2.3.3. Pendulum Test	17
2.3.4. Linear Impactor Test.....	18

2.3.5.	Hybrid III Head and Neck and Linear Impactor FE Models.....	23
2.3.6.	Kinematic Head Response Metrics	25
2.4.	Human Body Modelling.....	28
2.4.1.	Modelling of the Head	28
2.4.2.	Brain Response Metrics	30
2.4.3.	Modelling of the Neck	34
2.4.4.	Global Human Body Models Consortium Human Body Model.....	38
2.5.	Objective Rating Methods	45
2.6.	Football Helmet Modelling.....	46
2.6.1.	Existing Football Helmet Finite Element Models.....	47
2.6.2.	Xenith X2e Football Helmet Model.....	48
2.6.3.	Material Level Testing.....	50
2.6.4.	Component Level Validation	51
2.6.5.	Full Helmet Validation.....	52
2.6.6.	Integrating Football Helmet Models with HBMs	54
2.7.	Summary	55
3.	Methods.....	56
3.1.	Head and Neck FE Model Repositioning.....	56
3.2.	Linear Impactor Boundary Conditions.....	58
3.3.	Helmet Fitting on the GHBMC Head Model.....	60
3.4.	Study 1: Head and Neck Response of an Active Human Body Model and Finite Element Anthropometric Test Device During a Linear Impactor Helmet Test	61
3.5.	Study 2: Simulated and Experimental Boundary Conditions for a Human Head Model Comparing Brain Response in Football Helmet Impacts.....	64
3.6.	Study 3: The Role of the Whole Body Mass and Inertia in Football Helmet Impacts.....	65

3.7.	Measurement of Head, Neck and Brain Response	66
4.	FE Model Verification	68
4.1.	Verification of Hybrid III ATD and Helmet Models	68
4.1.1.	Verification Test Cases for Helmeted and Bare Head ATD Models	68
4.1.2.	Helmet and ATD Model Verification Results	69
4.2.	Verification of HNM Response	72
4.2.1.	Head and Neck FE Model Boundary Conditions.....	72
4.2.2.	Head and Neck Model Verification Results.....	73
5.	Study 1: Head and Neck Response of an Active Human Body Model and Finite Element Anthropometric Test Device During a Linear Impactor Helmet Test	75
5.1.	Qualitative Description of Head Response to Impact	76
5.2.	Results – Kinematic and Kinetic Response of Head and Neck.....	78
5.2.1.	Comparison of the ATD FE Model to the HNM with No Activation.....	78
5.2.2.	Comparison of the HNM with and Without Muscle Activation	82
5.3.	Discussion – Kinematic and Kinetic Response of Head and Neck.....	84
5.3.1.	Comparison of the ATD and HNM Head and Neck Kinematics	84
5.3.2.	The Effect of Muscle Activation on Head Kinematics	85
6.	Study 2: Simulated and Experimental Boundary Conditions for a Human Head Model Comparing Brain Response in Football Helmet Impacts.....	88
6.1.	General Description of Brain Response	89
6.1.1.	Frontal Impact.....	89
6.1.2.	Lateral Impact	90
6.1.3.	Rear Impact	91
6.2.	Results - Comparison of Simulated Impact and Prescribed Kinematics.....	92
6.2.1.	Whole Brain Maximum Principal Strain.....	92

6.2.2.	Whole Brain Cumulative Strain Damage Measure	94
6.2.3.	Regional Brain Response	95
6.2.4.	Effect of Balanced Muscle Activation	96
6.3.	Discussion - Simulated Impact and Prescribed Kinematics Approach	96
6.3.1.	Comparison of Prescribed Kinematics Approach and Simulated HNM Impacts	96
6.3.2.	Regional Brain Response	98
6.3.3.	The Influence of Balanced Muscle Activation.....	99
7.	Study 3: The Influence of the Whole Body Mass and Inertia on Head Response in Football Helmet Impacts.....	100
7.1.	Qualitative Description of Impact Response.....	101
7.2.	Head Kinematics Comparison	102
7.3.	Spine Kinematics Comparison.....	104
7.3.1.	T1 Motion	104
7.3.2.	Full Cervical Spine Motion.....	105
7.4.	Brain Deformation Comparison.....	106
7.4.1.	Maximum Principal Strain	106
7.4.2.	Cumulative Strain Damage Measure	108
7.5.	Discussion – The Role of the Whole Body.....	110
8.	Summary, Conclusions and Recommendations.....	113
8.1.	Summary and Conclusions.....	113
8.1.1.	Comparison of Head Kinematics of the ATD and HNM.....	113
8.1.2.	Prescribed Kinematics vs. Simulated HNM Impact	114
8.1.3.	The Role of the Whole Body Mass and Inertia.....	114
8.2.	Limitations	115
8.3.	Recommendations.....	116

9. References.....	118
Appendix A: Verification of HNM Response.....	132
Appendix B: Progression of Bare Head Impact.....	135
Appendix C: Head Kinematics and Other Metrics in All Impacts.....	136
Head Kinematics and Kinetics for All Cases.....	136
Out of Plane Kinematics	139
Muscle Force-Time Profiles	141
Appendix D: Brain Deformation of Simulated HNM Impacts and Prescribed Kinematics approach.....	143
Maximum Principal Strain (95 th Percentile)	143
Bare-Head Impact	143
Helmeted Impact.....	146
Cumulative Strain Damage Measure (CSDM15) in all impacts	149
Bare-Head Impact	149
Helmeted Impact.....	151
Appendix E – 3 DOF Angular Head Kinematics of HNM and ATD – experiment	154

List of Figures

Figure 1.1	A typical linear impactor test, rear impact at 9.3 m/s.....	2
Figure 1.2	Graphical outline of thesis: (a) chapter 2, (b) chapter 3, (c) chapter 4, (d) chapter 5, (e) chapter 6, (f) chapter 7.....	5
Figure 2.1	(a) Anatomical planes for the full body (adapted from [49]), (b) Frankfurt Plane and Sagittal Plane of the head (adapted from [50]), (c) head local coordinate system used in this thesis. Note that the head local coordinate system has z positive downwards.	7
Figure 2.2	Head segmentation (adapted from Yoganandan, 2009).....	7
Figure 2.3	Tissue layers of the head from the surface of the brain to the outermost tissues, including the meninges [54].....	8
Figure 2.4	(a) Sagittal and (b) coronal cross sections of the brain, adapted from Armstrong (2018) and Budday (2017)	9
Figure 2.5	(a) Cervical spine and T1 (b) C1 vertebra structure (c) C2 vertebra structure and (d) C3 – C7 and T1 vertebra structure	10
Figure 2.6	Flexor and extensor muscles in the neck (adapted from Gray, 1918)	11
Figure 2.7	(a) NOCSAE headform, (b) Hybrid III head mounted on Hybrid III neck	15
Figure 2.8	Hybrid III ATD Head and Neck Angle	16
Figure 2.9	(a) Twin wire drop test used by NOCSAE [16], (b) NFL drop tower, (c) Modified drop tower with Hybrid III neck incorporated [84].....	17
Figure 2.10	(a) Virginia Tech pendulum impactor and sliding carriage [15]	18
Figure 2.11	Linear impactor test apparatus (adapted from [17])	18
Figure 2.12	Linear impactor construction.....	19
Figure 2.13	(a) NFL reconstruction methodology (from [77]), (b) linear impactor test, (c) Full-scale reconstruction, used to verify NFL reconstruction methodology (from [91])	22
Figure 2.14	Time history of Biocore linear impactor test, shown here in the lateral orientation at 9.3 m/s	23
Figure 2.15	(a) Hybrid III ATD head and neck model, (b) Linear Impactor Model.....	24
Figure 2.16	GHBMC M50-O, version 4.4.....	38

Figure 2.17	GHBMC M50-O head and neck model extraction.....	39
Figure 2.18	GHBMC brain model, showing only brain tissues.....	40
Figure 2.19	(A) Full neck model, (b) neck model with skin and subcutaneous tissues removed, (c) isolated cervical spine.....	41
Figure 2.20	1D muscle element inputs.....	42
Figure 2.21	Neck musculature, showing flexor and extensor muscles.....	43
Figure 2.22	(a) Progression rating, (b) phase rating, (c) size rating (From Thunert 2012).....	45
Figure 2.23	(A) Foam force-displacement response, (b) material considerations for absorption of linear impacts (taken from [6]).....	46
Figure 2.24	(a) Helmet with foam liner, (b) Xenith X2e helmet with decoupled shell and air-venting liner, (c) Vicis Zero1 helmet with columnar liner.....	47
Figure 2.25	Helmet FE models: (a) 2016 Riddell Speed Classic (b) 2016 Schutt AirXP Pro (c) 2017 Vicis Zero1 (d) 2016 Xenith X2e.....	48
Figure 2.26	(a) Physical Xenith X2e helmet, (b) physical helmet liner (c) Xenith X2e helmet model, (d) Xenith X2e model liner.....	49
Figure 2.27	The development process of the Xenith X2e helmet model.....	49
Figure 2.28	(a) Compression shock material response, (b) 27 mm compression shock experimental and simulated response (from [46]).....	52
Figure 3.1	(a) The Frankfurt plane of the GHBMC model in the default seated position, (b) original vertebrae COG locations of the HNM in the default seated position.....	57
Figure 3.2	ATD Experiment (a), ATD Simulation (b), HNM (c), frontal impact configuration. The location of the occipital condyle is marked “OC”.....	58
Figure 3.3	(a) Lateral, (b) Frontal and (c) Rear impact orientations, corresponding to the NFL “C”, “F” and “R” orientations respectively.....	58
Figure 3.4	(a) Linear impactor test dimensions for lateral, frontal and rear orientations, (b) table of dimensional offsets for each orientation.....	59
Figure 3.5	(a) Scaled head geometry, (b) tightening straps and adjusting helmet position, (c) final helmet fit.....	61

Figure 3.6	Flexor and extensor AL curves for flexor and extensor active elements for the “balanced activation” condition.....	62
Figure 3.7	Exemplar impact simulation timeline, for “balanced activation” condition in a frontal impact at 5.5 m/s (a) bare head, (b) helmeted.....	63
Figure 3.8	Resultant linear and angular velocity prior to linear impact for three conditions	64
Figure 3.9	Lateral impact at 9.3 m/s, showing (a) the ATD experiment (prescribed kinematics approach) and (b) the HNM with balanced activation (simulated HNM impact).....	65
Figure 3.10	Unconstrained FBM integrated with football helmet and linear impactor (frontal configuration).....	66
Figure 4.1	Verification cases (3x Bare Head, 9x Helmeted). Note that there were three repeat experiments completed for the bare head cases, and single experiments for the helmeted cases.	68
Figure 4.2	Simulated (verification and original) and experimental response of the bare head ATD in a lateral impact at 5.5 m/s (a) head Y acceleration, and (b) head X angular velocity	69
Figure 4.3	Simulated (verification and original) and experimental response of the helmeted ATD in a lateral impact at 5.5 m/s (a) head Y acceleration, and (b) head X velocity	71
Figure 4.4	HNM verification cases (4 Total).....	72
Figure 4.5	T1 boundary conditions for 15g frontal impact scenario.....	73
Figure 4.6	T1 boundary conditions for 7g Lateral impact scenario	73
Figure 4.7	Simulated response of the HNM in a 15g frontal impact, overlaid with the corridors from the NBDL experiments	74
Figure 4.8	Simulated response of the HNM in a 7g lateral impact, overlaid with the corridors from the NBDL experiments	74
Figure 5.1	Study 1 simulation matrix.....	76
Figure 5.2	Progression of helmeted impacts: (a) ATD simulation, lateral 5.5 m/s, (b) HNM w. no activation, lateral 5.5 m/s, (c) ATD simulation, frontal 5.5 m/s, (d) HNM w. no activation, frontal 5.5 m/s, (e) ATD simulation, rear 5.5 m/s, (f) HNM w. no activation, rear 5.5 m/s	77
Figure 5.3	Helmeted impact kinematics, 5.5 m/s, (a) lateral, (b) frontal, (c) rear.....	80
Figure 5.4	Neck compression in helmeted impact (a) lateral, (b) frontal, and (c) rear helmeted impact at 5.5 m/s.....	81

Figure 6.1	Simulation matrix, Study 2	89
Figure 6.2	Progression of maximum principal strain in a frontal helmeted impact of the HNM (no activation) at 9.3 m/s. The visible shearing of the cerebrum grey and white matter elements in the center of the cranial fissure is highlighted.	90
Figure 6.3	Nodal traces showing the movement of the middle of the brain in a frontal impact, relative to the cerebrum grey matter	90
Figure 6.4	Maximum Principal Strain of the brain, at the time of peak deformation in a simulated 9.3 m/s impact of the HNM with No Activation. (a) Frontal orientation, transverse plane, (b) lateral orientation, transverse plane, (c) frontal orientation, coronal plane, (d) lateral orientation, coronal plane.	91
Figure 6.5	Progression of maximum principal strain in a rear helmeted impact of the HNM (no activation) at 9.3 m/s.....	92
Figure 6.6	9.3 m/s impact, 95 th percentile MPS in the (a) lateral orientation, (b) frontal orientation, (c) rear orientation.....	93
Figure 6.7	9.3 m/s impact, CSDM15 in the frontal orientation	94
Figure 6.8	9.3 m/s impact, maximum value of 95 th percentile MPS in each brain region across impact orientations.....	96
Figure 7.1	Head and Neck Model (HNM), compared to the Full human Body Model (FBM), shown in the frontal configuration	100
Figure 7.2	Simulation Matrix, Full Body Model Compared to Head and Neck Model.....	101
Figure 7.3	Motion of the 5.5 m/s frontal impact (no muscle activation), showing (a) the HNM and (b) the FBM.....	102
Figure 7.4	Head kinematics and impactor Force (a) lateral 5.5 m/s, (b) lateral 9.3 m/s, (c) frontal 5.5 m/s, (d) frontal 9.3 m/s, (e) rear 5.5 m/s, (f) rear 9.3 m/s	103
Figure 7.5	T1 displacement and rotation for the FBM and HNM in the global coordinate system, at 5.5 m/s with no muscle activation in the (a) lateral, (b) frontal, and (c) rear orientation. Note that the HNM can only translate in the global X direction.....	105
Figure 7.6	Motion of the cervical spine in a 5.5 m/s frontal impact (no muscle activation), comparing the HNM and the FBM	106

Figure 7.7 95th Percentile Maximum Principal Strain (MPS) in helmeted impacts (a) Lateral 5.5 m/s, (b) Lateral 9.3 m/s, (c) Frontal 5.5 m/s, (d) Frontal 9.3 m/s, (e) Rear 5.5 m/s, (f) Rear 9.3 m/s 108

Figure 7.8 Cumulative Strain Damage Measure (CSDM) with a cutoff threshold of 0.15 (CSDM15) in helmeted impacts (a) Lateral 5.5 m/s, (b) Lateral 9.3 m/s, (c) Frontal 5.5 m/s, (d) Frontal 9.3 m/s, (e) Rear 5.5 m/s, (f) Rear 9.3 m/s 110

List of Tables

Table 2.1	Incidence of concussion in NFL football.....	12
Table 2.2	NFL impact locations [17].....	20
Table 2.3	Hybrid III ATD model element formulation and material constitutive models.....	24
Table 2.4	Linear impactor material models	25
Table 2.5	Relation of kinematic injury predictors to observed concussions.....	27
Table 2.6	List of published three-dimensional head models used for concussion.....	29
Table 2.7	Relation of tissue-level injury predictors to observed concussions	33
Table 2.8	List of published head and neck models	36
Table 2.9	Summary of all brain tissue regions.....	40
Table 2.10	Solid element material properties, brain tissue and CSF	41
Table 2.11	Summary of neck muscles included in model and extensor/flexor classification.....	43
Table 2.12	Summary of material models used in the HNM	44
Table 2.13	Targeted nominal strain rates for material tension and compression experiments for the predominant subcomponents of the Xenith X2E helmet	50
Table 2.14	Xenith X2E subcomponent experimental modes of loading, target nominal rates and strains, and validation models	51
Table 2.15	Helmet validation cases	53
Table 2.16	Overall average CORA ratings for the full helmet model	54
Table 3.1	Comparison of geometric and mass properties of the Hybrid III experiment, Hybrid III simulation, and the GHBMC HBM	60
Table 4.1	CORA ratings between bare head ATD simulations and experiments	70
Table 4.2	CORA ratings between helmeted ATD simulations and experiments.....	71
Table 5.1	CORA ratings between HNM simulations and ATD simulations with no activation	79
Table 5.2	Response Metrics of HNM: HIC, BrIC and HIP, and ratio of HNM with no activation to ATD simulation response (bold indicates average response)	81

Table 5.3	CORA ratings between HNM simulations and ATD simulations with balanced activation .	82
Table 5.4	Response Metrics of HNM: HIC, BrIC and HIP, and ratio of HNM with balanced activation compared to ATD simulation response (bold indicates average response)	83
Table 6.1	MPS peak values and timing for the whole brain (darker red boxes indicate higher peak values, while darker green values indicate earlier peak values).....	93
Table 6.2	CSDM15 peak values and timing for the whole brain (darker red boxes indicate higher peak values, while darker green values indicate earlier peak values)	94
Table 6.3	Angular velocity peak values and timing for the whole brain (darker red boxes indicate higher peak values, while darker green values indicate earlier peak values).....	95

1. Introduction

1.1. Motivation for Research

Concussion is a persistent injury in contact sports, especially American football. In high school and college athletes, approximately 50% of football players report a concussion each year, and over 30% sustain more than one concussion [1]. In recent years, there has been a growing concern about the long-term effects of concussion, with a high prevalence of Chronic Traumatic Encephalopathy (CTE) found post-mortem in American Football players [2]. This disease has resulted in cognitive and behavioral disturbances later in life, which have led to depression, violence and suicide [1]. In the National Football League, concussion prevalence has risen in recent years [3,4], which may be attributed, in part, to improved diagnosis of concussion. Of all sports played in the US, American football has the greatest number of concussions, but also has the highest number of participants [5]. Helmets have reduced the risk for focal head injuries in American football, such as skull fracture [6]; however, improving helmet design to reduce the risk of concussion is an ongoing challenge [5,7]. While many metrics have been proposed to quantify concussion risk using linear and rotational kinematics of the head [8,9], concussion has been increasingly linked to rotational kinematics [7,10–12]. While helmets effectively limit the linear head accelerations linked to focal head injuries, helmet designs and testing standards have only recently attempted to mitigate head rotation, and not all newer helmets have exhibited significant reductions in rotational response metrics compared to traditional designs [13].

In addition to commonly used drop tests [14] and pendulum impact testing [15], a newer method to assess helmet performance experimentally is the linear impactor test (Figure 1.1) [16,17]. The linear impactor test imitates a player's kinematic properties during a concussive impact to the head, determined from reconstructions of National Football League (NFL) concussions [18] using simplified representations of the struck and striking player. The struck player is represented by a helmeted head and neck from a Hybrid III Anthropometric Testing Device (ATD), which is a crash test dummy developed for automotive testing. The striking player is represented by an impactor with the effective mass and stiffness properties to an incoming player wearing a helmet. Several tests are undertaken with impacts delivered to the helmet in multiple orientations at the same range of velocities experienced during gameplay (5.5 – 9.3 m/s) from the NFL reconstructions [13,19]. Importantly, the flexible neck of the Hybrid III ATD, made from aluminum and rubber, allows rotation of the head after impact; the previous NOCSAE drop test ((ND)002-17m19) for football helmets used a headform fixed to a carriage and allowed little to no rotation of the head relative to the carriage [8]. Another commonly used helmet test is the pendulum impact test that uses the same ATD and sliding carriage as the linear impactor test and provides very repeatable impact responses [15]. The

pendulum impactor is stiffer and heavier than a striking player compared to the linear impactor [18] and therefore may not simulate the head kinematics during concussion events. The linear impactor test has been used to evaluate helmets in academic studies for some time [13,19,20], is currently used by the National Football League (NFL) to rank helmet performance, and will be used by National Operating Committee on Standards for Athletic Equipment (NOCSAE) to certify helmets as of May 2019 [16].

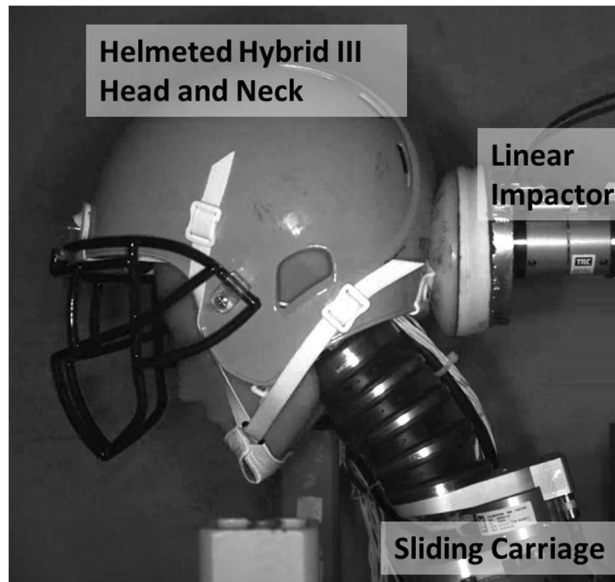


Figure 1.1 A typical linear impactor test, rear impact at 9.3 m/s

While the Hybrid III ATD provides repeatable loading conditions that allow for rapid testing of helmets, this human surrogate has been reported to have some limitations in biofidelity [8,19–23]. One of the more commonly cited limitations of using the Hybrid III in football impact testing is the neck stiffness in different loading directions, as the ATD was designed for Anterior-Posterior loading [19,23,24]. The Hybrid III ATD has no representation of neck muscle activity, which affects neck stiffness and has been suggested to be important in head impacts, but the exact effects are not well understood [20,21,25]. In addition, the sliding carriage used to represent the body of the ATD could further limit the biofidelity of the linear impactor test, because the body of the player (below the neck) can exhibit motion as early as 7 ms after a helmeted impact, which could influence the head response [26].

Human Body Models (HBM), simulated using the Finite Element (FE) method, provide additional anatomical detail compared to anthropometric testing devices [27]. These models represent the material properties and geometry of a human by modelling ligaments, bones, muscles and other tissues relevant to impact loading [27–29], which allows for more detailed investigations than ATD experiments. For example, HBMs can be used to investigate the effect of muscle activation, by tensing certain muscle groups at different levels [30]. HBMs can also be used to investigate the effect of the whole body inertia and mass

during a football impact, which would be time consuming and expensive to perform experimentally using ATDs. Combined with computational helmet models, HBMs can be used to predict tissue level injury [25,26,28,29], which is not possible with current ATDs. Some HBMs model the individual structures of the brain [31–33], which are not represented in the Hybrid III ATD. The predicted deformation of brain tissue within human brain models has been demonstrated to be a better predictor of concussion than metrics that include only the kinematics of the head [34–38], and certain regions of the brain, such as the corpus callosum and thalamus, have been better linked with concussion than others [35,36,39,40]. While it is common to prescribe the kinematics from an ATD experiment to an isolated head model from a HBM (“prescribed kinematics” approach), the behavior of the ATD neck has potential to affect the brain response. While current HBM are capable of simulating football helmet impacts, previous efforts have had limited helmet model validation [25,26], and have used boundary conditions which do not simulate the mass, stiffness or speed of an incoming player [26,41]. Currently, one of the most advanced HBMs is the Global Human Body Models Consortium (GHBMC) 50th percentile male model [42]. Recently, four detailed FE models of modern football helmets, along with models of helmet assessment tools have been made publically available [43,44], which have been more extensively validated than any yet published in the literature. The author of this thesis was involved with the development of the Xenith X2e helmet model [45–47], which achieved good to excellent validation outcomes [43].

1.2. Objectives, Approach and Outline

The current thesis was completed to investigate the biofidelity of the linear impactor helmet test using a contemporary Human Body Model. Specifically, three studies were carried out:

1. The first study compared the head kinematics of the ATD and HBM head and neck model (HNM), and examining the effect of neck muscle activation. Helmeted impacts were compared to bare-head impacts, to establish a baseline response without the added complexity of the helmet. The time history of head kinematics, impactor kinematics and lower neck kinematics were compared using cross correlation and head response metrics (Head Injury Criterion, Brain Injury Criterion, Head Impact Power) were also investigated. Direct comparison of ATD and HBM response serves to highlight the relative importance of the neck, and the impact boundary condition, when considering head response.
2. The purpose of the second study was to assess two boundary conditions for a HBM head model using brain deformation metrics. Simulated boundary conditions, using the HNM integrated with a helmet were compared to the approach of prescribing kinematics from an ATD experiment to an isolated head model. The time history of two commonly used brain deformation metrics were

compared. Full brain responses were reported, as well as localized brain deformation in brain regions that have been closely linked to concussion.

3. A third study investigated the effect of whole body mass and inertia in a football helmet impact, comparing the HNM constrained at the First Thoracic (T1) vertebra and an unconstrained Full Human Body Model (FBM). Head kinematics, brain deformation metrics and the motion of the neck vertebrae were compared, and the effect of muscle activation was assessed with the FBM.

These studies rely on the integration of three previously developed and validated FE models: a contemporary detailed HBM (GHBMC 50th percentile male model, v4.4), a model of the head and neck from a 50th percentile male Hybrid III ATD, a linear impactor model, and a detailed contemporary football helmet model (Xenith X2e). The current studies are the first, to the knowledge of the author, to combine an extensively validated finite element model of a football helmet with a HBM. Additionally, this is the first study to examine helmeted head and brain response in both sagittal and coronal plane impacts with a HBM.

This thesis consists of eight chapters (Figure 1.2). Chapter 2 provides the relevant background on concussion in American football and helmet testing. The role of human surrogate choice and neck musculature in head impacts relevant to American football (Figure 1.2a) are outlined, and the existing models used in the current thesis are detailed. Chapter 3 describes the novel methods used for the three studies (Figure 1.2b). Chapter 4 presents a verification of the HNM, ATD, and helmet models against the available experimental data (Figure 1.2c). Chapter 5 (Study 1) presents the comparison of head kinematics of the ATD and HNM (Figure 1.2d), while chapter 6 (Study 2) presents the prediction of brain deformation from the HNM, compared to the prescribed kinematics approach (Figure 1.2e). Chapter 7 (Study 3) investigates the effect of whole body mass and inertia, comparing head-neck and full human body models (Figure 1.2f). Finally, chapter 8 presents the overall conclusions of the studies and recommendations for future work.

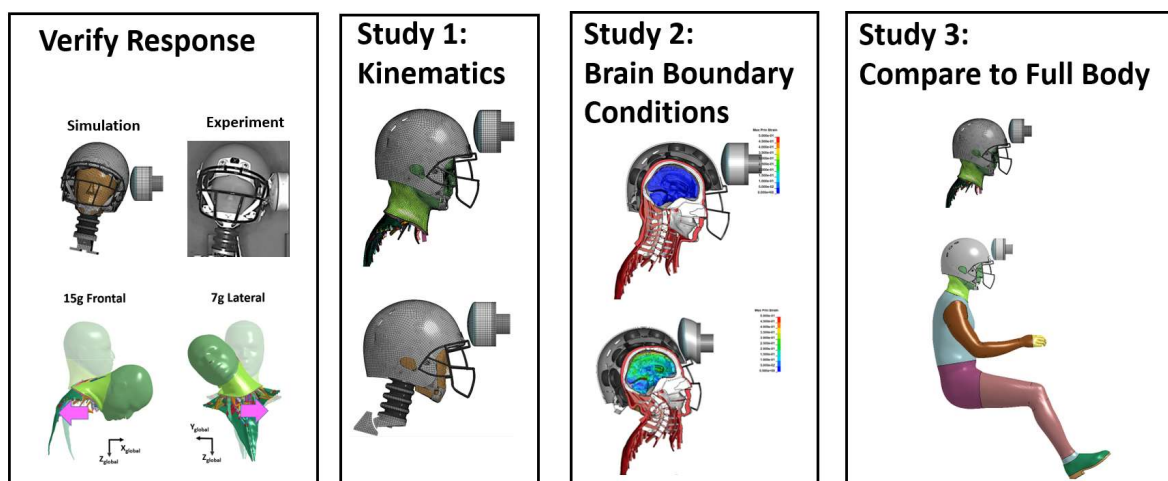
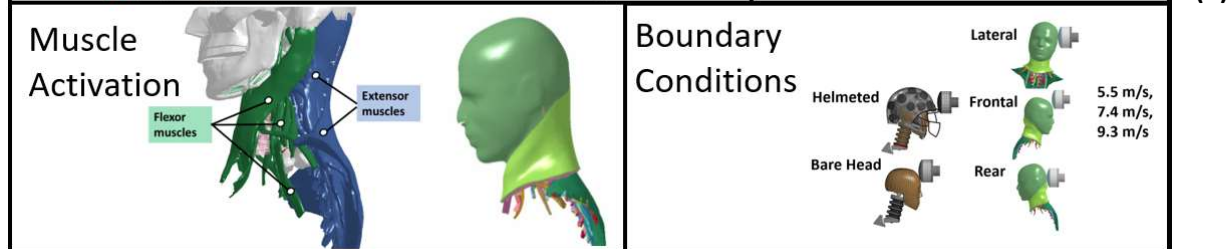
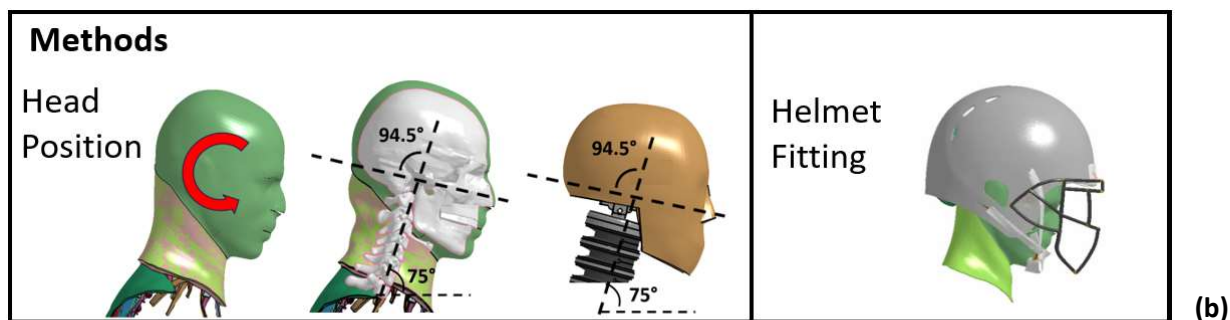
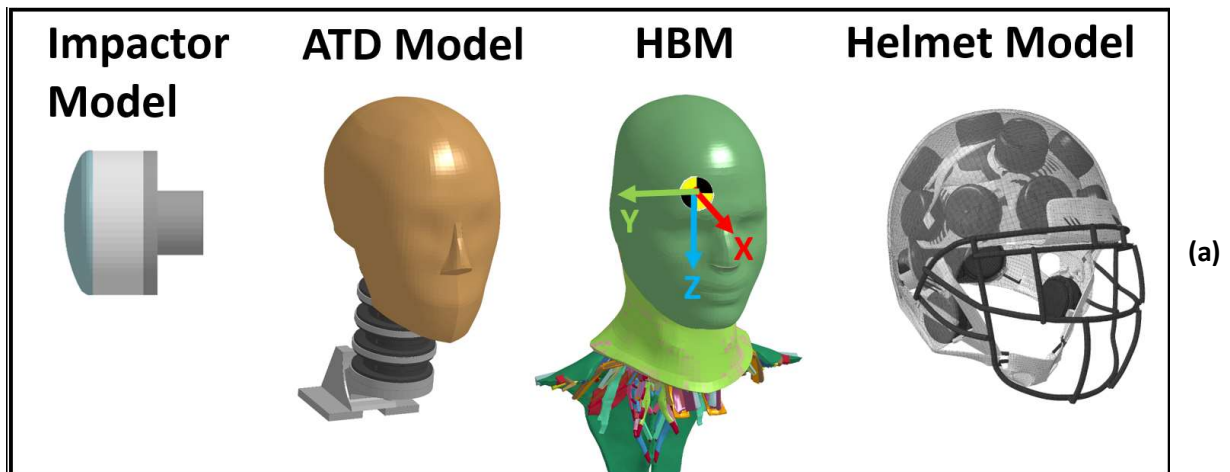


Figure 1.2 Graphical outline of thesis: (a) chapter 2, (b) chapter 3, (c) chapter 4, (d) chapter 5, (e) chapter 6, (f) chapter 7

2. Background

This chapter provides the background information relevant to the three studies in this thesis. Anatomy of the head and neck are first outlined, followed by a review of concussive head injury in American Football. Anthropometric Testing Devices (ATDs) used to evaluate the performance of football helmets are described, as well as modern testing of football helmets and the biofidelity limitations of the testing methods. Computational Human Body Models (HBMs) are introduced, and previous studies that relate brain deformation from HBM head models to observed concussion are summarized. Objective rating methods used to evaluate surrogate fidelity are described and finally, contemporary football helmet designs and FE modelling of helmets are outlined.

2.1. Head and Neck Anatomy

2.1.1. Coordinate System

Three planes are commonly used to define the coordinates of the human body; sagittal, coronal and transverse (Figure 2.1a). The sagittal plane divides the body into the left and right side. The coronal plane divides the body into the anterior (front) and posterior (back) section. The transverse plane divides the body into the top section and a bottom section. In addition to the planes used to define the body, the Frankfurt plane is used to precisely define the X and Y axes of the human head [48] using anatomical landmarks (Figure 2.1b). It is defined as the plane that passes through the bottom of the eye socket (the infraorbital) and the top of ear canal (the tragion). A local coordinate system (the Society of Automobile Engineers (SAE) coordinate system) for the head is used throughout this thesis, with the X-axis pointing in the anterior direction (forwards), parallel to the Frankfurt plane and the Z-axis pointing in the inferior direction (downwards) (Figure 2.1c).

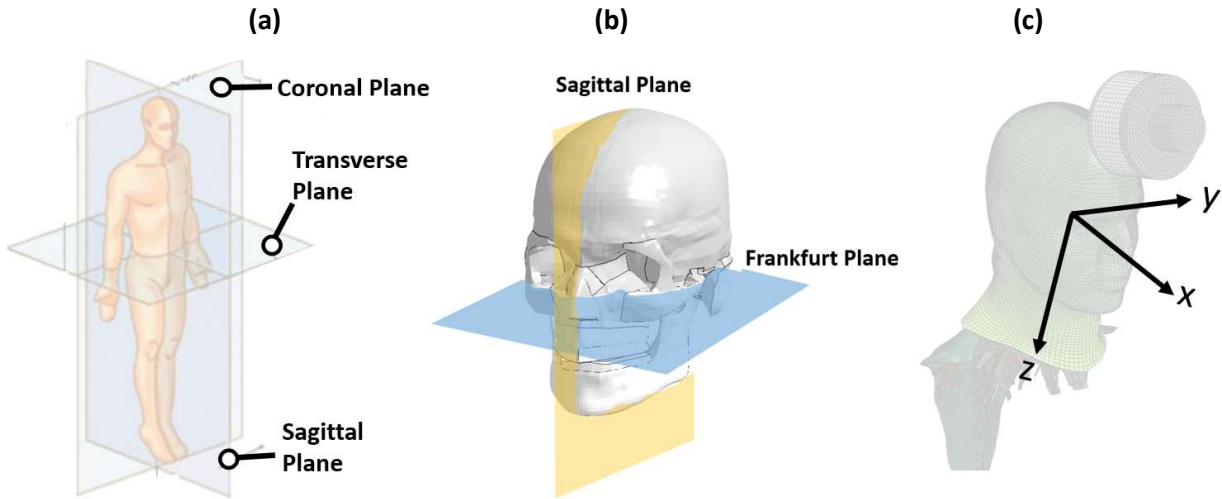


Figure 2.1 (a) Anatomical planes for the full body (adapted from Creative Commons), (b) Frankfurt Plane and Sagittal Plane of the head, (c) head local coordinate system used in this thesis. Note that the head local coordinate system has z positive downwards.

2.1.2. Anatomy of the Head

The head comprises of all tissues above the bottom of the skull and those contained within the jawbone (Figure 2.2). The major structures of the head are the skin, subcutaneous tissue, skull, cerebrospinal fluid (CSF) and most importantly, the brain. The 50th percentile male head has been found to have an average head mass of 4.5 kg [48], and a sagittal-plane moment of inertia ranging between 164 and 244 kg-cm² [48].

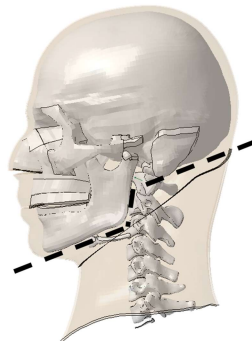


Figure 2.2 Head segmentation

Starting at the skin, many layers of tissue, fluid and bone surround and protect the human brain [27,50] (Figure 2.3). Below the skin are layers of subcutaneous tissue such as muscle and fat, then deeper is the thin membrane of aponeurosis, then periosteum enveloping the skull (Figure 2.3). The skull is comprised of 28 separate bones that are attached together with cartilage, a tough but flexible connective tissue [50]. The cranium refers to the portion of the skull surrounding the brain, and inside the cranium is the intracranial

region containing the brain, nerves, blood vessels, meninges and cerebrospinal fluid (CSF) [50]. The meninges are three concentric layers of tissue, which surround the brain and spinal cord [27,32,50] (Figure 2.3), and are each separated by Cerebrospinal Fluid (CSF), a fluid comprising primarily of water [27,51], of which there is approximately 125-150 ml distributed throughout the inside of the skull [51]. The outermost layer of the meninges is the thick, dense and fibrous dura mater. Part of the dura mater occupies the longitudinal fissure between the two hemispheres of the brain, called the falx [52]. Below the dura mater is the arachnoid, which is much thinner than the dura mater. The microscopically thin pia mater is the innermost meninge and adheres to the contours of the brain.

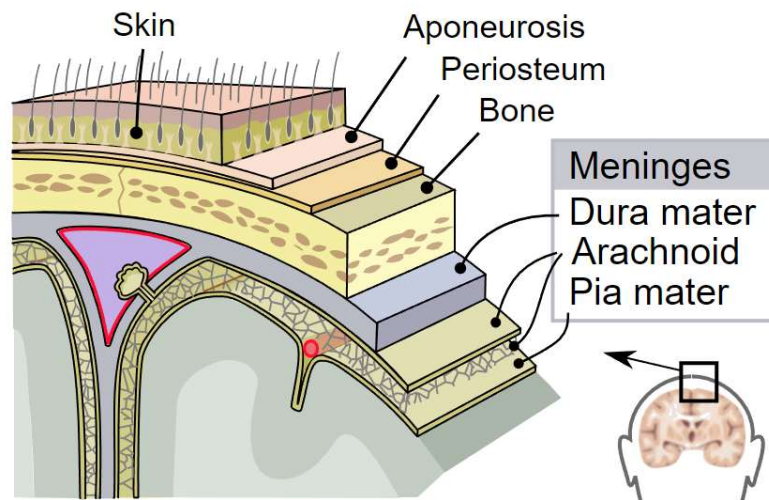


Figure 2.3 Tissue layers of the head from the surface of the brain to the outermost tissues, including the meninges (from Creative Commons)

The brain comprises the brainstem and regions of white matter and grey matter [27,32,50,54]. Grey matter is composed mostly of neurons (cells that are the fundamental units of the brain) while white matter consists of axons, which are fiber pathways that connect neurons together. A common approach to subdivide the brain considers eight regions (Figure 2.4) [32,35,40]. Regions of the brain that have been associated most commonly with concussion, indicated by reduced brain tissue volume include the corpus callosum, the thalamus and the midbrain [35]. The corpus callosum is the largest white matter pathway of the brain, and forms an arch approximately 10 cm long [50] that links the two hemispheres of the cerebrum together. The corpus callosum itself is divided into three regions, the splenium at the anterior end, the body in the middle, and the genu at the posterior end [50]. Many studies have linked increased deformation of the corpus callosum to concussion [34,35,39,40,55–57] (see Section 2.4.2), possibly attributed to its proximity to the stiff falx [52,58]. Another region commonly linked to concussion is the thalamus, which is about 4cm long, consists mostly of grey matter and is responsible for processing sensory information [50,59]. It has been suggested that deformation of the corpus callosum and thalamus are linked [58]. Another brain region

linked to concussion, the midbrain is above the brainstem and connects the brainstem and cerebellum to the rest of the brain [50]. Similarly to the corpus callosum, the increased deformation of the midbrain during concussive impact has been attributed to its proximity to a stiff structure, the tentorium [37]. Some studies have linked the brainstem to concussion [35,40]; however, most FE models of the head do not include the spinal cord past the base of the brainstem [31], which could influence brain deformation. Other regions that have been less frequently linked with concussion include the white and grey matter of the cerebrum, the cerebellum and the basal ganglia (see Section 2.4.2).

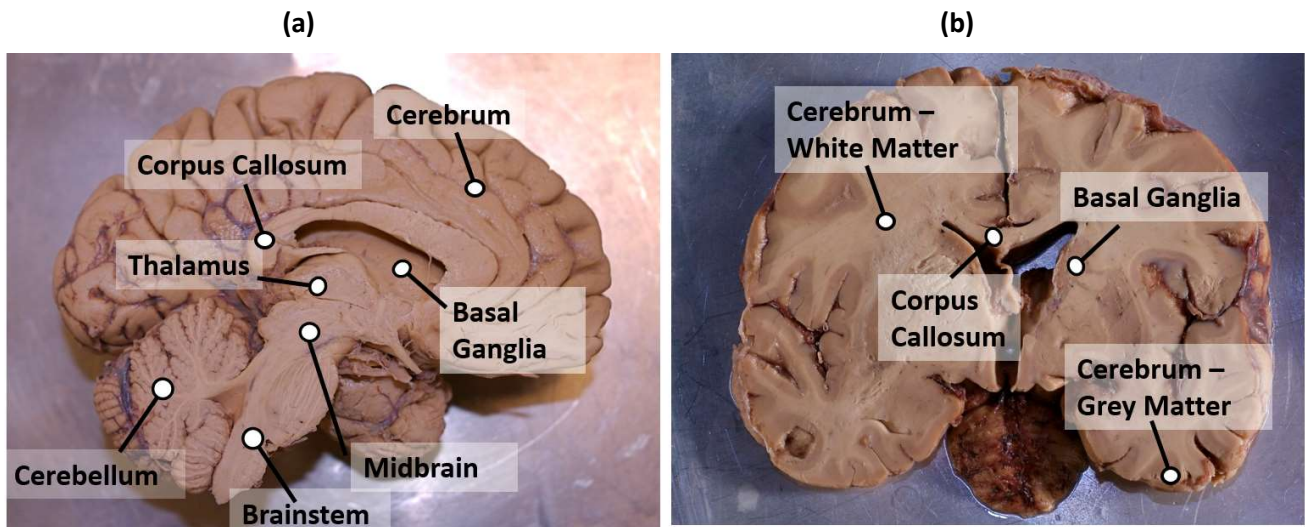


Figure 2.4 (a) Sagittal and (b) coronal cross sections of the brain, adapted from Creative Commons

2.1.3. Anatomy of the Neck

The neck consists of all tissues below the bottom of the skull, up to the first thoracic vertebra (T1) and all relevant muscles extending into the torso [27,50]. From a mechanical perspective, the major structural tissues in the neck are the vertebrae, the discs, ligaments and muscle [27]. Surrounding the cervical spine and muscles, there are layers of non-structural soft tissues including skin and fat. Other structures that are non-structural include veins, nerves and the spinal cord [27]. Of particular interest in this study are the muscles, as it has been commonly hypothesized that neck muscle strength is an important factor in concussive head injury, although this hypothesis lacks experimental evidence [41].

The human spine contains seven cervical vertebrae which comprise the neck, and twelve thoracic vertebrae and five lumbar vertebrae [27]. The seven cervical vertebrae are labelled C1 to C7, while the thoracic vertebrae are labelled T1 to T12. The C3 to C7 vertebrae, and the first thoracic vertebra (T1) have a similar structure, while the C1 and C2 are distinctly different in geometry and function (Figure 2.5). The joint

between the C1 and skull is called the Occipital Condyle (OC), which is responsible for most of the “nodding” motion of the skull in the sagittal plane. The joint between the C1 and C2 vertebrae allows most of the axial rotation of the head. The vertebrae are composed of a layer of cortical bone surrounding a volume of trabecular bone [50]. Cervical ligaments are soft, fibrous tissues that connect bones to other bones [27] and their purpose is to hold the cervical spine together and bear tensile loads. Synovial fluid acts as a lubricant between the cervical vertebrae [27] and intervertebral discs bear compressive loads in the spine [60]. The only other bone in the neck is the hyoid, which is connected via hyoid muscles and ligaments to the clavicle and the skull and is not considered part of the cervical spine.

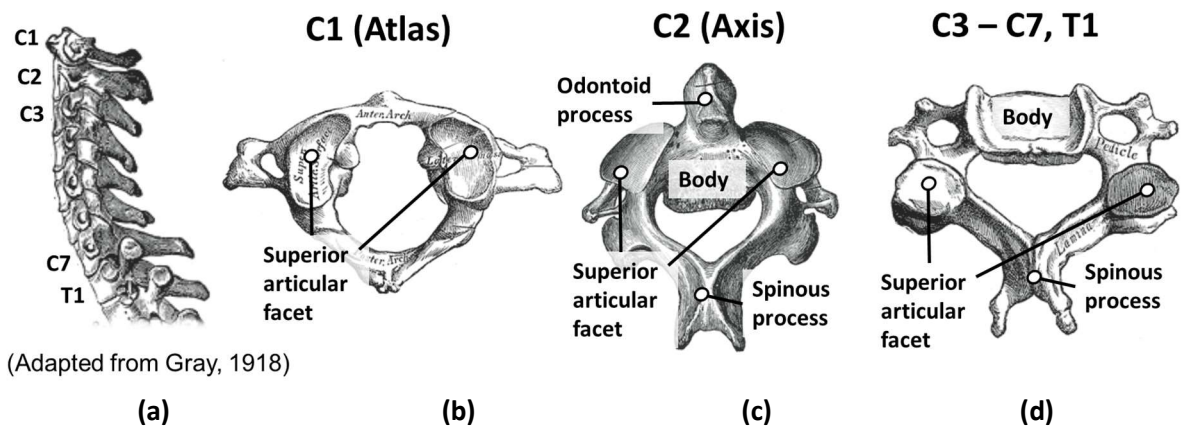


Figure 2.5 (a) Cervical spine and T1 (b) C1 vertebra structure (c) C2 vertebra structure and (d) C3 – C7 and T1 vertebra structure

Neck muscles enable movement of the head and cervical spine. There are 26 pairs of muscles in the neck, that are typically considered for modelling purposes, with the hyoid muscles are grouped together [27]. These muscle pairs are symmetrical about the sagittal plane. The neck muscles can be divided into flexor muscles, which rotate the head forwards in the sagittal plane, and extensor muscles, which rotate the head backwards in the sagittal plane (Figure 2.6) [61]. The largest of the neck flexor muscles is the sternocleidomastoid, while the largest neck extensor muscle is the trapezius [61]. Muscles consist of fibers that lie along a line of action, and attach to bones via tendons, which are high strength tissues comprised of collagen fibers [27,50]. In a live human, muscles generate a contractile force which is transmitted through tendons to two or more bones, and this force is dependent on the level of activation and stretch of the muscle.

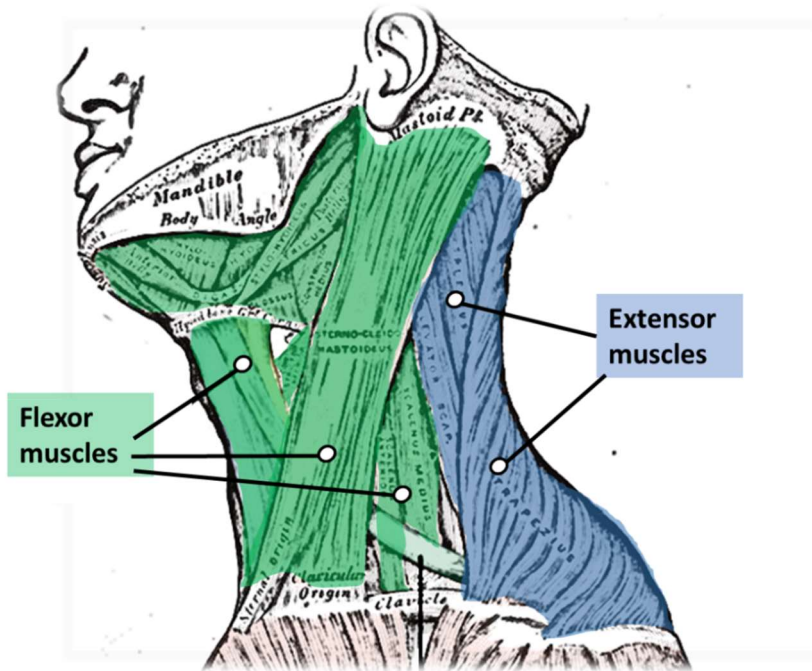


Figure 2.6 Flexor and extensor muscles in the neck (adapted from Gray, 1918)

2.2. Concussive Head Injury

The definition of concussion, having evolved from the pre-1970s meaning (impacts that cause a loss-of-consciousness), has remained consistent since the early 2000s, after which the majority of the cited studies in this thesis were written. Beckwith et al. [62] defined concussion as an “Alteration in mental status as reported or observed by the player or the team’s medical staff, resulting from a blow to the head which may or may not have involved loss of consciousness”. Other definitions have noted that head rotations which cause concussions can result from impacts to other parts of the body, not necessarily the head [5,7]. Most studies attempting to relate head motions to concussion have used a yes or no diagnosis of concussion, sometimes excluding concussions that were self-reported after leaving the game. Daneshvar et al. [5] described the symptoms of concussion as: physical signs (loss of consciousness, amnesia), behavioral changes (irritability), cognitive impairment (reaction time), sleep disturbances, somatic symptoms (headache), cognitive symptoms and/or emotional symptoms [5]. Daneshvar et al. [5], and others [6,63] have differentiated concussion from catastrophic head injury, which was defined as “a head injury caused by direct contact during competition resulting in a fatal, nonfatal permanent, or serious nonpermanent injury”, which can include skull fracture, contusion or diffuse axonal injury. Concussion is a prevalent injury in contact sports, including American Football.

2.2.1. Concussion in American Football

A 1995 – 1997 study reported levels as low as 3.66 concussions per 100 player-seasons at the high school level, as reported to medical professionals, while a retroactive survey of athletes after the 1996 – 1997 season found that 110 out of 233 players had experienced at least one concussion [5]. While rates of concussion in American Football are known to be high [4,5], the prevalence is difficult to quantify, especially at the high school level where there is a lower presence of medical professionals and rates are thought to be underreported [5]. It has been suggested that college football has a higher incidence of concussion than high school football, although there is also better access to medical professionals in college football [5]. Professional football has an even higher reported prevalence than college or high school football [2,5]. In the NFL, concussion prevalence has risen in recent years (Table 2.1), which may be partly attributed to the awareness and diagnosis of concussion improving, leading to more reported concussions [5].

Period	Concussion Incidence Per Season [4]		Concussion Incidence Per Season [3]					
	1996 – 2001 (Avg.)	2002 – 2007 (Avg.)	2012	2013	2014	2015	2016	2017
# Concussions Reported	147.8	142.3	265	244	212	279	250	291

Table 2.1 Incidence of concussion in NFL football

Concussion is understood to be a serious injury, with potential for long term consequences if the player has a history of repeated head impacts [1,2]. In 2005, Omalu et al. dissected the brain of a professional football player who had experienced cognitive impairment, mood disorders and Parkinsonian symptoms. Chronic Traumatic Encephalopathy (CTE) was discovered in the player’s brain [64], which had previously found to be only present in the brains of boxers. The problem was later discovered to be widespread, with a 2017 study finding that CTE was present in 110 of the 111 donated brains of NFL football players [2], with a lower prevalence in College (48 out of 53) and High School (3 out of 14) players. In one study, five players diagnosed with CTE experienced sudden deaths between the age of 36 and 50 years, two of which were due to suicide [65]. While concussion is still prevalent in American Football, some studies have shown that current helmets vary considerably in performance when assessed with head injury metrics [13], indicating that head motion associated with concussion could be reduced with improved helmet design [66].

2.2.2. The Biomechanics of Concussion

In 1974, Ommaya and Gennarelli proposed a prevailing theory about the mechanism of concussion [67], called the “centripetal theory of concussion”, stating that “...increasing severity of disturbance in the level and content of consciousness is caused by mechanically induced strains affecting the brain in a centripetal sequence of disruptive effects on function and structure”. In other words, rotation of the skull is transmitted to the outer surface of the brain and inertial effects cause the inner regions to lag behind, inducing shear strain, which causes axonal damage leading to concussion symptoms. The theory also stated that the centripetal progression of diffuse disruption of axons is enhanced in areas of structural inhomogeneity within the brain [12] such as the boundaries between white and grey matter. The theory of axonal damage or disruption has been supported by other studies [68,69]. In addition to being a proposed cause of concussion, brain tissue deformation predicted from numerical simulations has also been correlated with concussion in numerous studies [35,39,56,70]. While intracranial pressure (linked to catastrophic head injury) is influenced by linear acceleration of the head, studies have shown that brain tissue deformation is caused primarily by rotational motion of the head [10,71], and influenced regionally by the intracranial partitioning membranes and material properties of the tissue [7,52]. It is difficult to cause unconsciousness with constrained linear acceleration, but introducing a rotational component increases the likelihood of unconsciousness considerably [12]. This is attributed to the mechanical behavior of brain tissue. Brain tissue has a high bulk modulus and therefore low compressibility, due in part to its high water content, but is one of the least stiff biological materials and deforms readily in shear. For a given magnitude of rotational acceleration, patterns of strain are directionally dependent.

It has been shown that coronal plane rotations are most likely to produce concussion symptoms for a given magnitude of rotational acceleration [11,72] and affect the deep structures of the brain [11], although similar injuries can occur in the other planes of motion, if a higher magnitude of rotational acceleration is applied. Interestingly, in a recent review of NFL concussions, Lessley et al. [73] found that over 50% of concussions for 2015-2016 NFL season were caused by impacts to the side of the helmet, which induce motion in the coronal plane. Despite occurring predominantly in the sagittal plane, rear impacts are important for quarterbacks [73], and ground impacts to the rear of the helmet are a common cause of concussion in football [74]. Frontal impacts have been shown to be among the most common in gameplay [75], but have not caused concussion as commonly as the other impact orientations [20], and typically represent the striking player in most concussion-causing impacts to the struck player [76].

2.3. Football Helmet Impact Testing

There are multiple experimental methods that have been used to assess the head kinematics in a football helmet impact. These tests vary in complexity, from drop tests with a linearly translating headform, to full body reconstructions using the Hybrid III ATD. The purpose of helmet testing is to simulate impacts with similar kinematics to the range of possible impacts in football [18]. The NOCSAE drop test is used to certify helmets, and the linear impactor test is being introduced for this purpose in 2019 [77]. The NFL uses three tests to rate helmets: the NOCSAE drop test, the linear impactor test and the pendulum test.

2.3.1. Anthropometric Testing Devices for Football Helmet Impacts

ATDs, more commonly known as crash test dummies, are meant to simulate a human during impact loading. The purpose of the Hybrid III ATD was to predict occupant response for frontal automotive crash tests [78], however this ATD has been widely used in other areas including sports applications [79]. ATDs are designed to mimic human response, provide repeatable data without incurring damage, and provide an estimate of injury risk for specific body regions and impact scenarios [23,79]. For Football helmet testing, the most commonly used ATDs are the NOCSAE headform [19] and the 50th percentile Hybrid III ATD head and neck [79].

The National Operating Committee on Standards for Athletic Equipment (NOCSAE) headform is used to certify football helmets [16] (Figure 2.7a). The headform was developed to match the mechanical response and geometry of human cadaver heads [19]. The inertial properties represent that of a 50th percentile male head, with a polyethylene inner skull filled with gelatin to simulate the brain, and polyurethane to simulate the flesh and skin [19]. The mounting hardware is located at the base of the neck [19]. The NOCSAE headform is currently used for assessing helmet performance in a drop test configuration.

The 50th percentile male Hybrid III ATD was developed in the 1970's as a surrogate for automotive crash testing [78]. The Hybrid III head is made of aluminum with a mass of 4.54 kg and covered in a vinyl skin. The head has internally mounted accelerometers to record kinematics at the head center of gravity (COG). The neck from the Hybrid III is the most commonly used for football helmet testing, which is typically used with the Hybrid III head [80]. The Hybrid III neck is a passive structure consisting of rubber and metal discs, which allows for deformation of the neck (e.g. flexion) and therefore rotation of the head (Figure 2.7b). This neck is made of aluminum discs, rubber, with a cable running down the middle, with a total mass of 1.54 kg. The neck contains an upper load cell at the Occipital Condyle (OC) and a lower load cell at the base of the neck.

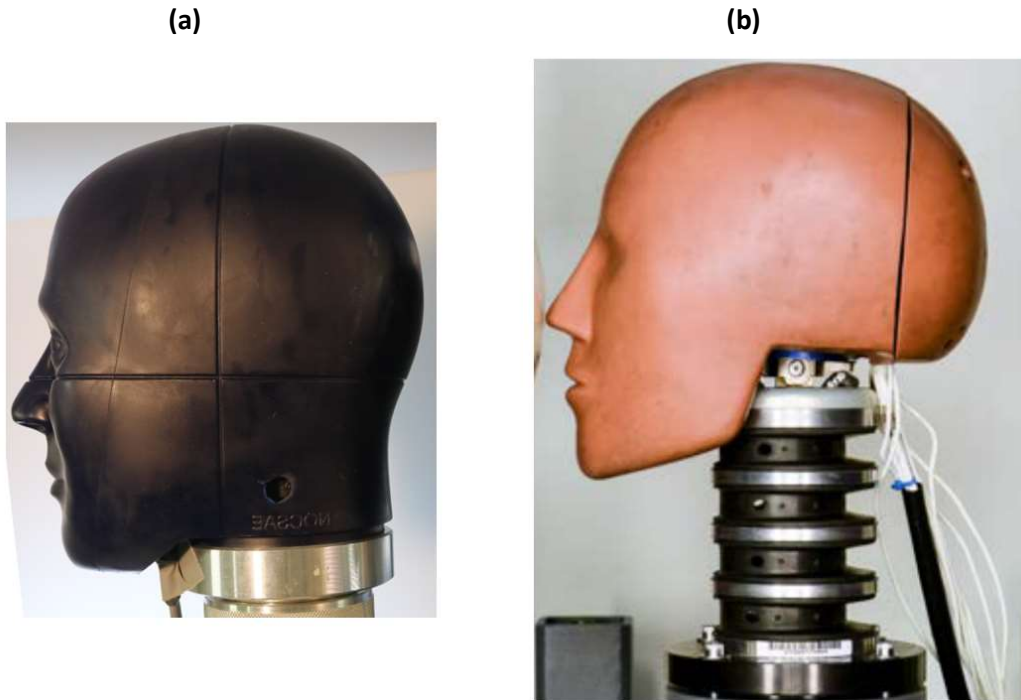


Figure 2.7 (a) NOCSAE headform, (b) Hybrid III head mounted on Hybrid III neck

The Hybrid III head uses a SAE J211 [48] coordinate system, with the origin at the head COG. The X-axis points from the COG through the bridge of the nose (Figure 2.8). The Y-axis is directed from the ATD's left to right side, and the Z-axis pointed down through the neck (Figure 2.8). Anatomical landmarks that are typically used to determine the Frankfurt plane, and thus the anatomical coordinate system, are not present in the Hybrid III ATD. The Frankfurt Plane of the Hybrid III head has been suggested to be parallel to its local axes [81,82]. It is accepted in the literature [82,83] that the X-axis and Z-axis of the Hybrid III head run parallel to the two flat surfaces of the head, and that the Y-axis is perpendicular to sagittal plane. If the neck of the Hybrid III is aligned vertically, the local X-axis of the head is tilted 4.5° up from horizontal (Figure 2.8). The neck of the Hybrid III is a cylindrical structure that had a cable running from top to bottom, and thus it is easy to define the neck axis angle.

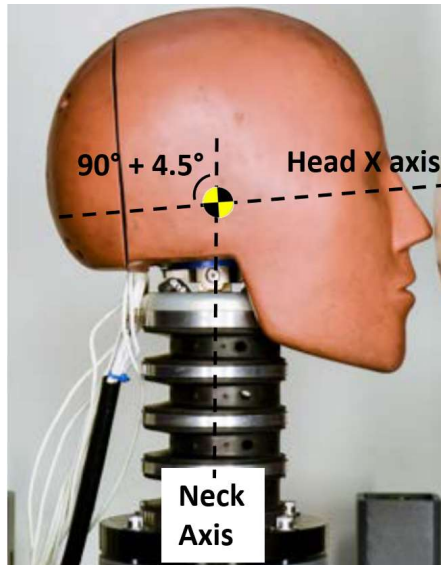


Figure 2.8 Hybrid III ATD Head and Neck Angle

2.3.2. NOCSAE Drop Test

The NOCSAE drop test (Figure 2.9a) has been used from the 1970s to the present and is the most commonly used test to certify football helmets [8]. In this test, the headform is rigidly mounted to the drop tower without a deformable neck, thereby restricting head rotation during the test. A twin wire setup is used by NOCSAE (Figure 2.9a), where a rigid structure (carriage) supporting the headform is guided by two wires, and propelled by gravity into a firm rubber pad outfitted with a load cell [19]. The NFL uses a twin rail structure (Figure 2.9b) which better constrains the carriage movement, and can accommodate either a Hybrid III or NOCSAE headform [14]. The headform measures head linear and rotational accelerations, the carriage translational acceleration is recorded and the load cell measures the impact force. Drop testing is effective for measuring head linear acceleration, which is useful for evaluating helmets for their ability to mitigate catastrophic head injury, but the test does not effectively represent the rotational kinematics that are the primary causes of brain deformation leading to concussion [8]. More recently, some studies have incorporated the Hybrid III neck with the NOCSAE headform and drop tower to provide additional compliance and allow for more head rotation [84] during the impact. However, the incorporation of a neck is more commonly used to investigate bicycle helmet impacts than football helmet impacts (Figure 2.9c).

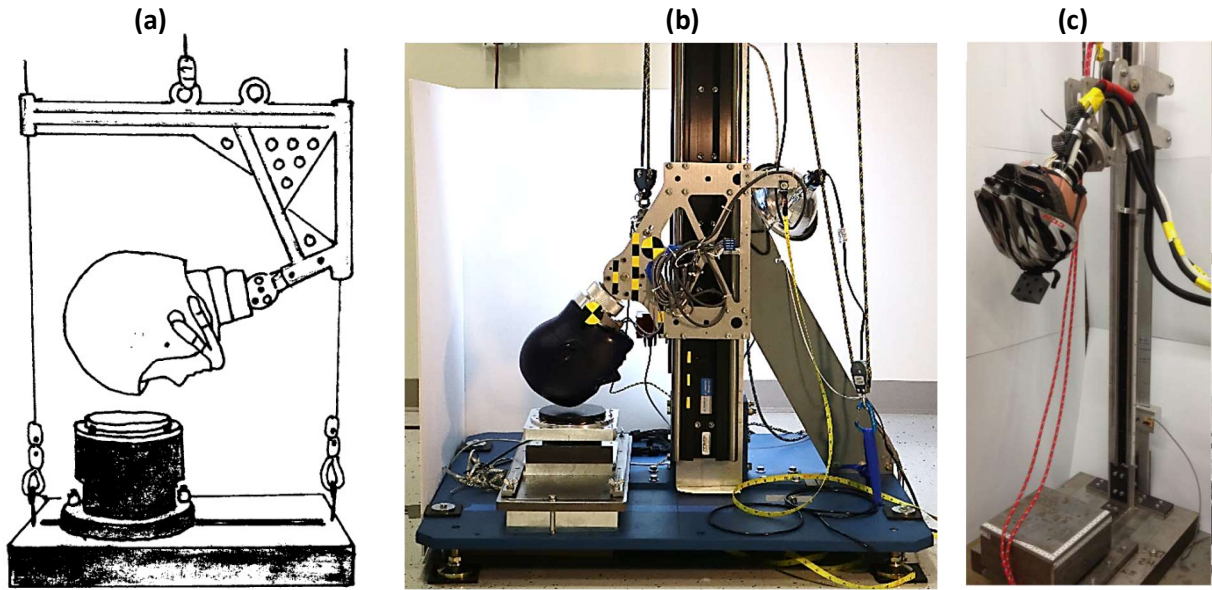


Figure 2.9 (a) Twin wire drop test used by NOCSAE [16], (b) NFL drop tower, (c) Modified drop tower with Hybrid III neck incorporated [84]

2.3.3. Pendulum Test

The Virginia Tech pendulum test (Figure 2.10) uses a highly stiff pendulum to strike a helmeted Hybrid III head and neck mounted on a sliding carriage with a combined mass of 23.1 kg [15]. Incorporation of the neck is intended to produce a more biofidelic response compared to the NOCSAE drop test, where little rotation is possible [76]. The carriage height and neck orientation is adjustable so that different impact orientations can be tested. The pendulum consists of a 37kg arm and hammer assembly with a moment of inertia of 72 kg m², that delivers a repeatable impact to the headform. The nylon end cap of the pendulum hammer has a high stiffness, to highlight the differences between helmets [15]. In addition to 1 DOF pendulum rotational acceleration, the 6 DOF acceleration of the head is measured, and 6 DOF forces and moments are also measured with the upper and lower neck load cells. By nature of the heavy, stiff impactor used, it was found that the impact speed required to produce the kinematics observed in reconstructions of NFL concussions was between 4.5 – 6 m/s, while 9.3 m/s was the average impact speed for a concussed player [76]. It was found that the pendulum required different impact speeds in each impact orientation to achieve similar kinematics to those observed during concussion events, and therefore pendulum testing at the standardized speeds does not necessarily generate the head kinematics observed during concussion events [76].



Figure 2.10 (a) Virginia Tech pendulum impactor and sliding carriage [15]

2.3.4. Linear Impactor Test

The linear impactor test incorporates the head and neck from a Hybrid III 50th percentile male ATD mounted on the same sliding carriage used in the pendulum test, which is free to translate in same direction as the impact direction (Figure 2.11). The boundary conditions of the linear impactor test are based on reconstructions of NFL concussions which used two ATDs [76].

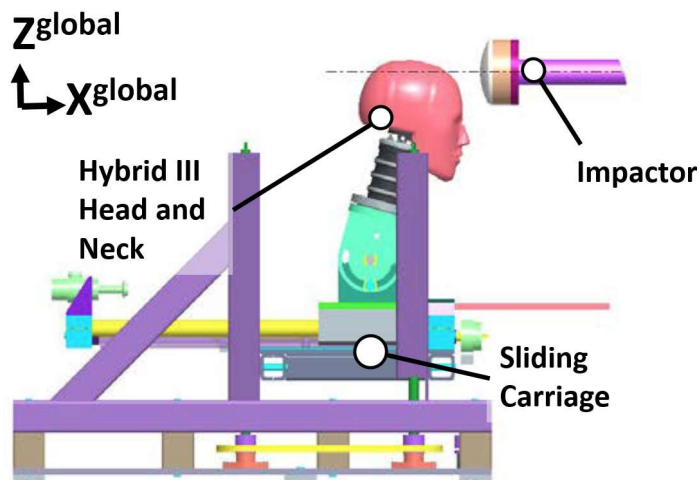


Figure 2.11 Linear impactor test apparatus (adapted from [17])

The impact velocities in the linear impactor test, determined from the NFL reconstructions, range from regular gameplay (5.5 m/s) to speeds that potentially cause concussion (7.4 and 9.3 m/s) [13,18]. The stiffness and 15.4 kg mass of the linear impactor simulate the mass and stiffness of a striking player at impact velocities that cause concussion, in contrast with the pendulum impactor [18]. The impactor properties resulted in peak resultant head acceleration within 16% of the earlier NFL concussion reconstructions, which was deemed acceptable [76]. The impactor is composed of a thrust rod, a vinyl-nitrile foam layer and an end cap (Figure 2.12). The rounded end cap is made from Nylon and had a radius-of-curvature of 127 mm. The foam layer was made of DerTex VN600 foam, with a diameter of 127mm and a thickness of 41.3 mm. The thrust rod was constrained to motion in the X direction and has a circular backing plate.

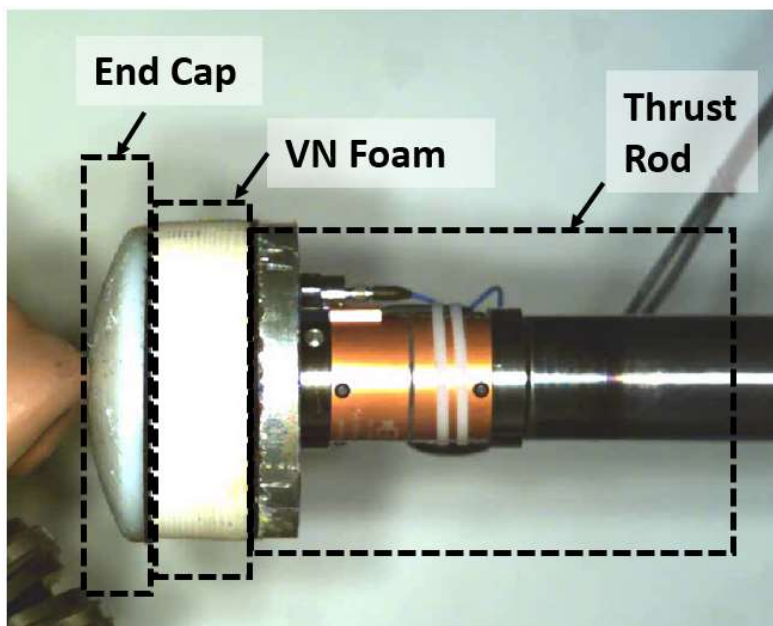


Figure 2.12 Linear impactor construction

The NFL Linear Impactor Helmet Test Protocol [17] consists of eight impact locations, four of these locations are impacts to the helmet shell, and four are impacts to the facemask of the helmet (Table 2.1). The impact locations represent a range of impacts associated with concussion in NFL players [13]. From the linear impactor test, the 6 DOF acceleration of the head is measured [85]. The 6 DOF forces and moments are also measured with the upper and lower neck load cells. The acceleration in the direction of translation, and the 6 DOF forces are measured by the ram load cell. The carriage acceleration is reported in the direction of translation.

	Impact Site	Neck Angle		Head COG location	
		α (deg)	β (deg)	Y_{Global} (mm)	Z_{Global} (mm)
Shell	F	0	15	15	-90.1
	C	-95	11	9.3	-7.4
	D	-157	11	20.1	-4.6
	R	180	-15	15	-9.1
Facemask	A	-25	7	19.5	15.7
	A'	0	-10	15	33.4
	B	-55	7	12.4	-7.5
	UT	-90	0	72.7	39.5

Table 2.2 NFL impact locations [17]

Limitations of the Hybrid III ATD Neck

The Hybrid III neck is commonly used in football helmet testing and impact reconstruction, as it provides repeatable loading conditions and allows the experimentalist to measure head rotations. How the head kinematics of the Hybrid III compare to those of a more biofidelic human model is still not well understood [20,76], and the passive structure of the Hybrid III neck does not simulate muscle activity [19]. A previous study [23] has shown that the Hybrid III neck exhibits less flexion and extension in a car crash scenario compared to cadaver specimens, while others have suggested that the Hybrid III neck is not stiff enough for football impact testing [19]. The Hybrid III neck has been shown to lack biofidelity in axial loading; Yoganandan et al. [86] found that the compressive stiffness of the Hybrid III neck was between 2.4 and 4x stiffer than cadaveric cervical spines, at a 2.54 mm/s loading rate. The Hybrid III was designed for anterior-posterior loading, while the linear impactor test comprises of loading in multiple directions [24], leading to lateral neck loading, axial rotation, and often combined modes of loading. The biofidelity of the Hybrid III is often cited as a limitation of studies which use it to predict head kinematics [20,24,70,87].

Despite the cited limitations, some experimental studies using ATDs have shown that large variations in neck stiffness have had relatively little effect on head kinematics and brain deformation in direct impacts to the head [88]. Rosseau et al. [88] found that neck stiffness had an insignificant effect on brain response metrics when doubling and halving the neck stiffness, and another study [89] found that head angular accelerations with a stiffer neck were up to 8% higher than the standard Hybrid III neck. These studies performed frontal impacts on a Hybrid III head and neck using a linear impactor [89], and prescribed the head kinematics to the UCDBTM head model [88].

The Influence of Full Body Mass and Inertia on Head Kinematics

In the linear impactor test, the base of the Hybrid III ATD neck is constrained to translate only horizontally, with a carriage mass of 17.7 kg [13]. When one examines the available literature concerning the development of this boundary condition for the neck, the origin of the boundary condition is not explained in detail. Originally, the linear impactor test was proposed because the head kinematics represented those of the NFL reconstructions [76] (Figure 2.13a) accurately, however, the NFL reconstructions on which the test have recently been shown to have some limitations [90], indicating a need to reinvestigate this boundary condition.

The NFL reconstructions [76] were completed between 1998 and 2002 [91] and consist of 31 impact reconstructions of head impacts in professional football. These reconstructions used the head and neck of one helmeted Hybrid III ATD to represent the struck player, and the head, neck and torso of another helmeted Hybrid III ATD to represent the striking player, based on video review of concussions during gameplay. Two different methods were used to justify the simplification of the struck player in Newman et al. [91]. The first were multi-body simulations, which indicated that changing the torso mass of the struck player had no effect on head acceleration, which in turn was used to justify the reconstruction techniques, but little detail on these simulations was provided. The second method was a series of full-scale reconstructions using two full Hybrid III ATDs (Figure 2.13c), which found differences in peak resultant linear acceleration ranging from 6% to 17%, and differences in peak angular acceleration between 4% and 14% when compared to the NFL reconstructions (Figure 2.13a). The NFL reconstructions were used as a basis for further simplifications in the linear impactor test.

The sliding carriage representing the body of the struck player in the linear impactor test (Figure 2.13b) was first published in the 11th installment of the “Concussion in Professional Football” series of studies [18]. In the development of the standard linear impactor test method [18], the carriage was first proposed as an alternative to simply fixing the neck in place [18]. This study reported that fixing the neck in place resulted in high stress on the neck, and interestingly, that head kinematics that “did not simulate those seen in the NFL video or reconstructions, while adding the carriage resulted in “more natural” motion. In the Pellman et al. study [74], three testing methodologies were examined for the testing of football helmets, including the current linear impactor test, a pendulum impact test with the same sliding carriage as the linear impactor test, and a linear impactor test with a Hybrid III torso mounted on a sliding carriage. The head response measured with these three methodologies was evaluated for accuracy against the previously completed NFL reconstructions [76]. The criteria used to compare the proposed test methods were ΔV , Severity Index, and peak acceleration, over an interval of 20 ms. The linear impactor test was chosen as the

NOCSAE methodology because it most accurately represented the early head response of the struck player measured in the Pellman et al. [76] reconstructions.

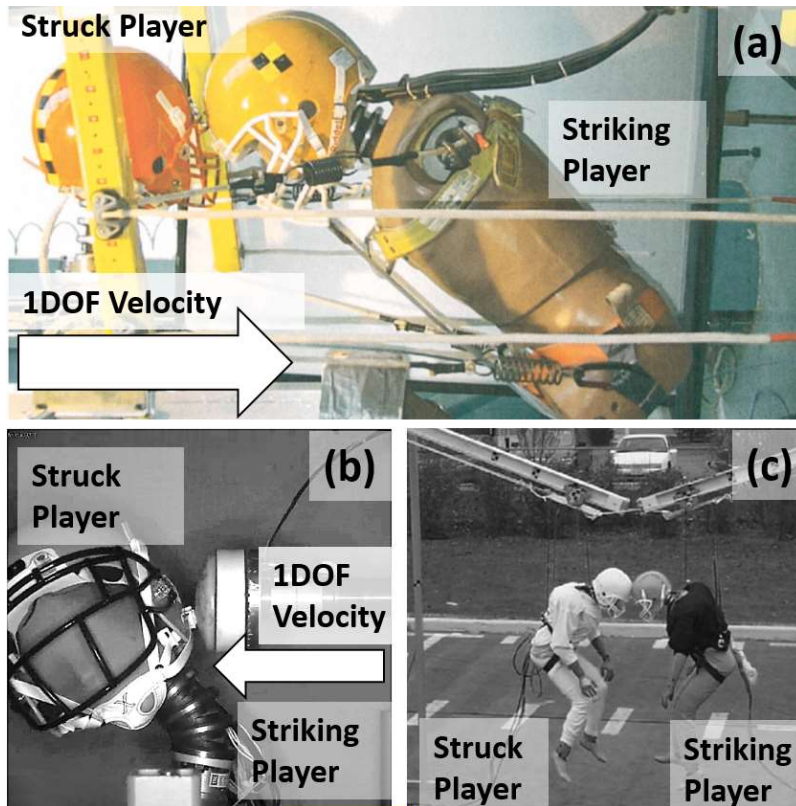


Figure 2.13 (a) NFL reconstruction methodology (from [76]), (b) linear impactor test, (c) Full-scale reconstruction, used to verify NFL reconstruction methodology (from [91])

Some uncertainties remain concerning the head and neck constraint in the linear impactor test, which was justified by comparing the kinematic data from this test to the NFL reconstructions [76]. The first is that only linear kinematics were compared to justify the neck constraint in the linear impactor test, over a short timeframe of 20 ms; which is not long enough for the maximum deformations of the brain tissue to occur [90] and therefore may not be representative. The second is that the original constraint in the NFL reconstructions was justified using more Hybrid III ATD testing, which has some biofidelity limitations. A third limitation is that the head angular velocity from the NFL reconstructions has been recently shown to have significant errors; the median peak angular velocity of all the reconstructions was found to be 17% higher than initially reported [90]. In summary, it is clear that there is a need to investigate the role of the body in the linear impactor test, due to the compounding uncertainties in the dataset used to justify this boundary condition, especially considering the angular kinematics of the head. The head and neck kinematics of a constrained head and neck may be different than those of a full human body without this constraint.

Biocore Linear Impactor Experiments

A comprehensive set of linear impactor experiments were completed on the Xenith X2e football helmet (Biocore, LLC [17]), including the eight standard impact orientations and three impact velocities (5.5 m/s, 7.4 m/s and 9.3 m/s). Bare head impacts were also completed in all eight orientations at 5.5 m/s only, to avoid damage to the ATD. All acceleration data was filtered using a CFC 180 filter, and all forces and moments were filtered using a CFC 600 filter.

The geometry and boundary conditions of the test setup were well documented [17]. The Hybrid III head was covered by two stockings to simulate hair and make the helmet easier to don and remove from the head. The helmet was fitted using a consistent procedure, and checked for a consistent fit after each test. To accomplish this, the helmet was positioned 75mm from the tip of the Hybrid III nose to the brow of the helmet. The helmet straps were tightened so that they could be fastened without undue effort and the straps were marked so they could be tightened consistently.

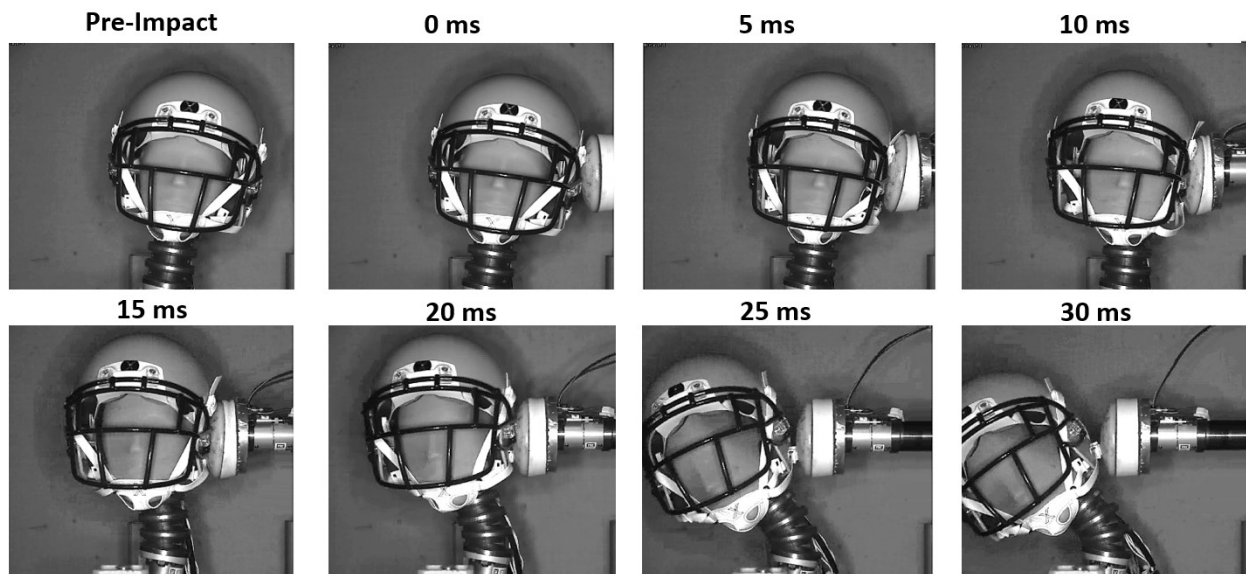


Figure 2.14 Time history of Biocore linear impactor test, shown here in the lateral orientation at 9.3 m/s

2.3.5. Hybrid III Head and Neck and Linear Impactor FE Models

The Anthropometric Testing Device (ATD) used in the current study was a previously developed model of a 50th percentile male Hybrid III head and neck (Figure 2.15a) [44]. The linear impactor model was created to match the impactor used in the NFL Linear Impactor Helmet Test Protocol (Figure 2.15b) [17]. These models were developed by J.S Giudice et al. [44], and are publically available at the Biocore LLC website [85].

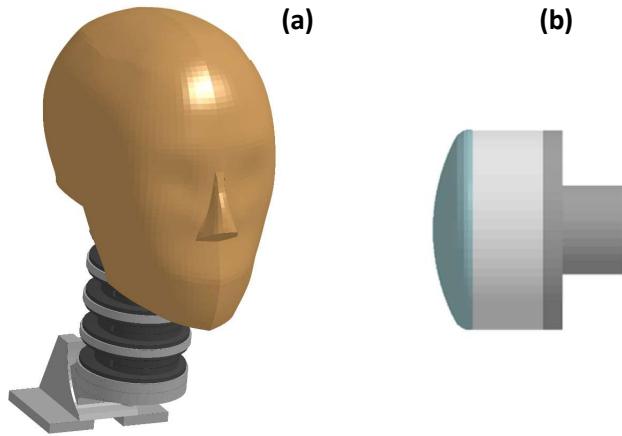


Figure 2.15 (a) Hybrid III ATD head and neck model, (b) Linear Impactor Model

The Hybrid III FE model was developed by measuring the material properties, and applying them to a mesh constructed from Computer Aided Design (CAD) geometry. All metal components of the Hybrid III head and neck were assumed to be rigid solid elements, with the exception of the neck cable. The neck cable consisted of 50 axial elements with elastic material properties (Table 2.3) and a cross-sectional area of 50 mm², with no pre-tension in the cable. The head skin was modelled as a rubber material with no rate effects, defined by a uniaxial stress-strain response from experimental testing. The neck rubber was defined as a viscous foam material, which consists of a nonlinear spring in parallel with a viscous damper, and the neck cable was assumed to be an elastic material. To attach the head to the neck, a torsional spring was used at the OC pin, with different stiffness in negative and positive sagittal head rotation to represent the nodding block. The base of the neck mount was constrained so that free translation could only occur in the direction of impact, with all other directions fixed. A mass of 17.7 kg was prescribed to the base of the neck, to simulate the mass of the carriage. The Hybrid III ATD model consists of 57762 elements total.

Component	Material	Element Type	Material Model	Visco-elastic?
Skull	Aluminum	Solid	Elastic (*MAT_001)	No
Skin	Vinyl	Solid	Hyperelastic rubber (*MAT_181)	No
Neck Discs/Mount	Steel/Aluminum	Solid	Rigid	No
Neck Cable	Steel	Axial	Elastic (*MAT_001)	No
Neck Rubber	Butyl Rubber	Solid	Viscous Foam (*MAT_062)	Yes

Table 2.3 Hybrid III ATD model element formulation and material constitutive models

The ram, foam and end cap which comprise the impactor were meshed from technical drawings, and these three parts that were attached together using shared nodes [44]. The ram was constrained so that free translation could occur only in the direction of impact, with all other directions fixed. The ram was treated as rigid, due to its high stiffness compared to the compliant impactor. The Nylon end cap was modelled using an elastic material model. The Vinyl-Nitrile foam was modeled as a hyperelastic, viscoelastic foam (Table 2.4), with interpolation between stress-strain curves based on experimental data [80]. The foam was tested quasi-statically at strain rates of 10^{-3} , 10^{-2} , 10^{-1} s⁻¹, and dynamically at impact velocities of 4.6, 8.0, and 9.3 m/s. The maximum strain observed in each test was 0.18, 0.26, and 0.6, while the maximum strain rates were 84, 97.5, and 131 s⁻¹. A total mass of 15.4 kg was used for the linear impactor model, matching the experimental test device, and the model consisted of 9409 elements total.

Component	Material	Element Type	Material Model	Visco-elastic?
Foam Disc	Vinyl-Nitrile Foam	Solid	Fu-Chang Foam (*MAT_181)	Yes
End Cap	Nylon	Solid	Elastic (*MAT_001)	No
Ram	Metals (assembly)	Solid	Rigid	No

Table 2.4 Linear impactor material models

The Hybrid III ATD and linear impactor models were developed for use in LS-Dyna (LSTC, single precision, R7.1.2). The model was validated against linear impactor experiments with a bare head, achieving an average Correlation and Analysis (CORA) rating of 0.87 against experiments in eight orientations at 5.5 m/s [80]. The model also achieved good validation outcomes with four experimental pendulum tests [44] and in helmeted configurations [43].

2.3.6. Kinematic Head Response Metrics

Linear and angular velocity and acceleration of the head have been correlated with concussion (Table 2.5), however, there is no consensus on the best head response metric for predicting concussive injury out of the many that exist [34]. Head response metrics range in complexity from peak values of a certain velocity or acceleration, to more complex empirical formulae that incorporate multiple kinematic responses that are assigned different weights. These metrics are typically curve-fits to an injury database; some metrics were developed solely for concussion [92] while others were developed for a range of injuries of differing severity [9,93,94].

It is well established that angular kinematics of the head are a greater contributor to brain deformation than linear kinematics [10,71]. Ommaya and Gennarelli [12] suggested that rotational components of

accelerative trauma result in a centripetal progression of axonal disruption which is largest at the periphery of the brain and increased at sites of structural inhomogeneity [12]. They suggested that the linear components of acceleration produced only focal injuries. Multiple studies have shown that pressure in the brain is not significantly influenced by rotational kinematics, while the strain response of the brain is not significantly influenced by the linear kinematics [40,62] when linear or rotational kinematics are applied in isolation. Despite the small influence on brain deformation, linear kinematics of the head have been correlated with concussion [37,76], but this could be because rotational kinematics of the human head are typically accompanied by linear motion [10,71].

Kinematic response metrics provide an estimation of injury based solely on the head kinematics after impact. The Head Injury Criterion (HIC), Brain Injury Criterion (BrIC) and Head Impact Power (HIP) are some of the most commonly used [36–38,40,95,96]. BrIC has been shown to be one of the best correlated kinematic response metrics to brain deformation by Gabler et al. [95]. The study correlated 15 different kinematic response metrics measured from 660 experimental head impacts to MPS and CSDM in the GHBMC and SiMON head models, with the purpose of highlighting which kinematic response metrics are most appropriate for predicting brain response.

Study	Methodology	Significant Metrics	Threshold	Statistical Significance (-2 log likelihood ratio)
Hernandez (2015)	Instrumented mouth guard 2 Concussive impacts, 511 Non-concussive impacts (American Collegiate Football, Boxing and MMA)	α_{peak} HIP GAMBIT	N/A N/A N/A	P<0.03 P<0.05 P<0.05
Patton (2015)	Rigid body reconstructions of observed concussions, from videos. 27 concussion and 13 non-concussion cases (Aussie-rules football)	α_{peak} (Coronal)	50% Chance of Concussion 1747 $\text{rad}\cdot\text{s}^{-2}$	P<0.001
Viano (2006)	Hybrid III ATD reconstructions of observed concussions, from video. 22 concussive, 6 non-concussive Professional American Football	HIC SI	Mean Concussed HIC=339 SI=422	P<0.000 P<0.000
Beckwith (2018)	Helmet measurement (HIT?) Football (High School and Collegiate) 45 immediately diagnosed concussions (105 total), 161732 control impacts	Peak Linear Acceleration		

Pellman (2003)	Hybrid III ATD reconstructions of observed concussions, from video. 25 Concussion, 157 No-Injury	Peak Linear Acceleration	98g (mean concussed)	P<0.001
Zhang (2004)	Hybrid III ATD reconstructions of observed concussions 24 concussive impacts	HIC GSI Ar Rr	N/A N/A N/A N/A	P=0.001 P=0.001 P=0.001 P=0.001

Table 2.5 Relation of kinematic injury predictors to observed concussions

Three widely used and proposed head response metrics include: the Head Injury Criteria (HIC), Brain Injury Criteria (BrIC), and Head Impact Power (HIP). The kinematic criteria for head response assume the head to be a rigid structure, and are calculated using the rigid body kinematics of the head COG.

The head injury criterion (HIC) (Eqn. 1) is a commonly used metric for head response [94,97].

$$\text{HIC} = \max_{t_1, t_2} \left\{ \frac{1}{(t_2 - t_1)^{3/2}} \left[\int_{t_1}^{t_2} a(t) dt \right]^{5/2} \right\} \quad (1)$$

Where acceleration (a) is the resultant acceleration with the units of g , and time is in s . For HIC₁₅, the maximum value of $t_2 - t_1$ is 15 ms.

The Brain Injury Criterion (BrIC) (Eqn. 2) is a rotational response criterion calculated from the angular velocity of the head. It was developed from a combination of animal response data, ATD testing data and strain estimates from human FE Models [93].

$$\text{BrIC} = \sqrt{\left(\frac{\omega_x}{\omega_{xC}}\right)^2 + \left(\frac{\omega_y}{\omega_{yC}}\right)^2 + \left(\frac{\omega_z}{\omega_{zC}}\right)^2} \quad (2)$$

Where ω_x , ω_y , and ω_z are the individual peak values of the angular velocity over the entire impact, and ω_{xC} , ω_{yC} , and ω_{zC} are constants equal to 66.2 rad/s, 59.1 rad/s and 44.2 rad/s respectively.

Head Impact Power (HIP) (Eqn. 3) has been correlated with observed concussions in football [36] and considers all 6 degrees-of-freedom. $\text{HIP} = \max \left[m a_x(t) \int a_x(t) dt + m a_y(t) \int a_y(t) dt + m a_z(t) \int a_z(t) dt + I_{xx} \alpha_x(t) \int \alpha_x(t) dt + I_{yy} \alpha_y(t) \int \alpha_y(t) dt + I_{zz} \alpha_z(t) \int \alpha_z(t) dt \right]$

(3)

Where the mass (m) is 4.5 kg, and the moments of inertia, I_{xx} , I_{yy} and I_{zz} are 0.016, 0.024 and 0.022 kg m², respectively. These constants represent the mass properties of a 50th percentile male head [38].

2.4. Human Body Modelling

Computational Human Body Models (HBMs) provide more anatomical detail than an ATD, and have the ability to model muscle activation and predict tissue-level strain. Some recent studies have used FE modelling to investigate brain deformation, where football helmet models have been integrated with HBMs [25,26,66]. When investigating some of the limitations of the Hybrid III head and neck, an appropriate Head and Neck Model (HNM) could highlight important differences.

2.4.1. Modelling of the Head

FE models of the human head are the most commonly used tool to predict deformation of the brain, which has been associated with concussion [20,25,36,39,40,55–57]. There are many brain models which exist, but comparatively little experimental data on the cadaveric brain with which to validate these models (Table 2.6), due to the difficulty of measuring displacement of the cadaveric human brain [98], which changes quickly post-mortem and cannot be frozen without compromising the mechanical properties [54]. The existing data with which to validate head models comprises of brain pressure and displacements of selected points [32,98], and many models have shown good agreement with this data [99] (Table 2.6).

Model	First Published	Brain Model Experimental Validation	Total Elements	Brain Regions (#)	Brain Material Model	Integrated with neck model
KTH FE Human Head Model	2007 (Isotropic) [40]	intracranial pressure, intracerebral acceleration, relative brain-skull motion, skull fracture	21,000 (Full Head) 7,128 (Brain)	7	2 nd Order Ogden w. Viscoelasticity	Yes
	2014 (Anisotropic) [35]	intracranial pressure, intracerebral acceleration, relative brain-skull motion	21,000 (Full Head) 7,128 (Brain)	7	2 nd Order Ogden w. Viscoelasticity and anisotropy	No
Simulated Injury MONitor (SiMON)	2008 [100]	intracranial pressure, brain motion	40,708 (Full Head)	3	Kelvin-Maxwell Linear Viscoelastic	No
Total Human Model for Safety (THUMS)	2006 [101]	intracranial pressure, brain motion	49,579 (Full Head)	6	Linear Viscoelastic	Yes
University College Dublin Brain Trauma Model (UCDBTM)	2003 [102]	intracranial pressure, brain motion	28,000 (Full Head)	1	Linear Viscoelastic	No

Worcester (previously Dartmouth) Head Injury Model (WHIM or DHIM)	2015 [103]	Brain motion	115,228 (Full Head)	4	2 nd Order Ogden w. Viscoelasticity	No
Global Human Body Models Consortium (GHBMC) head model	2013 [32] (GHBMC)	intracranial pressure, brain motion	270,552 (Full Head)	8	Kelvin-Maxwell Linear Viscoelastic	Yes

Table 2.6 List of published three-dimensional head models used for concussion

All models have been partially validated against the brain motion experiments from Hardy et al. [98] and the intracranial pressure from the experiments of Nahum (1977). In the Hardy et al. [98] study, an impact was delivered to 8 cadaver head and neck specimens using a pneumatic impactor. The brain motion in the experiments was measured by tracking neutral density targets with a high speed X-Ray. In the Nahum (1977) study, pressure was measured after the impact of 6 cadaver heads.

In terms of mechanical behavior, human brain tissue is highly viscoelastic [54], which means that the rate of loading governs the stiffness of the material. It is also highly dependent on the post-mortem treatment and time prior to testing [54,104]. The measured shear modulus of brain tissue can vary by an order of magnitude or more, depending on the study [54]. Most commonly brain tissue models include viscoelasticity [31], and others include effects such as hyperelasticity, meaning that the response is non-linear [40] and direction-dependent properties [35].

Available head models typically have the geometry of a 50th percentile male, matching the predominance of 50th percentile ATDs in automotive regulatory environment [27]. While the 50th percentile male may not represent the typical football player, current football helmet testing uses 50th percentile male ATDs [13,17,18], and as such, 50th percentile head models are listed (Table 2.6). These head models range in element count from 21,000 to 270,000 (Table 2.6). Recently, it has become common to use two or more models of the head in the same study [21,31,62,103,105], to compare the responses of independently developed models. It has been shown recently that one of the most important parameters in FE modelling of the brain is the mesh size [31,106,107]. Mao et al. [106] demonstrated that a brain model with 65,000 elements had not achieved mesh convergence, and differences in brain displacement up to 30% were observed compared to a model with a finer mesh. Additionally, Zhao and Ji [107] found that at 202,000 elements were required for mesh convergence of a human brain model. With 270,552 elements, the GHBMC head model has the finest mesh of all models surveyed, and importantly, the mesh of this model achieved convergence [32]. The GHBMC head model and SIMON models were shown to have similar responses in terms of maximum principal strain when the same kinematics were applied [21]. The WHIM and SIMON models were shown to give similar responses when comparing regions but with different

magnitudes [62], which was a result of the different material properties used in each model. For the current study, only models integrated with a neck could be used, because investigating neck muscle behavior is an objective of this thesis.

2.4.2. Brain Response Metrics

Brain responses from FE models (Table 2.7) have been shown to be more effective in predicting concussions than metrics calculated from the gross kinematics of the head [34–38]. Multiple studies have found increased maximum principal strain in any region the brain to be a statistically significant ($p < 0.001$) predictor of concussion [39,56,62]. However, some studies have postulated that certain brain regions, in particular the corpus callosum, are better predictors of concussions than others [36,39,56,70], however there is no agreement among studies that one region of the brain is most predictive of concussion. Which metric is the best predictor of concussion is also not settled, and proposed thresholds for concussion (if a metric exceeds the threshold, a 50% likelihood of concussion is predicted) vary considerably (Table 2.7) [62].

FE Model Metrics

Maximum Principal Strain (MPS) is one of the most commonly used predictors of concussion in FE models (Table 2.7), as it has been commonly correlated with observed concussions [20,25,36,39,40,55–57]. It is linked mechanistically to concussion; as stretching of axons has been theorized to be the mechanism of concussion [12]. While arguably the most commonly used brain deformation metric [25,31,35,36,40,56,93,100,107,108], Cumulative Strain Damage Measure (CSDM) has not been as strongly related to concussion as MPS [35,36,40,56]. In addition, this metric is highly sensitive to the threshold chosen, and there is no agreement on a CSDM threshold strain for concussion [35,40]. When a linear viscoelastic constitutive model is used, MPS and CSDM are calculated using logarithmic, or true strain [109].

Other metrics have been used to predict concussion, albeit less commonly. Strain rate has correlated well with concussion in some studies [57], as well as the product of strain and strain rate, but these metrics have been shown to be less effective predictors than MPS [56]. Von-Mises Stress has been shown to be a good indicator of concussion [56], but has been examined less frequently than other measures. Pressure has been examined in the past as a potential indicator of concussion, and grey matter pressure was found to be the best predictor of concussion by Kleiven [40]. However, pressure typically arises from linear accelerations, and pressure is not mechanistically linked to concussion. Another metric, Maximum Axonal Strain (MAS) has been shown to be a strong predictor of concussion [35], but the calculation of axonal strain is not possible in most head FE models.

The 95th percentile MPS refers to the value of MPS which is exceeded by 5% of the elements in a given brain region. This metric has been presented as an alternative to the maximum (100th percentile) value of maximum principal strain because the use of the 95th percentile value prevents the simulation result from being driven by the response of a single element [9,95]. Gabler et al. [95] found that using the 95th percentile MPS correlated better with kinematic injury criteria and CSDM than the 100th percentile MPS, when considering a database of 660 physical head impacts, using both the SiMON and GHBM head models.

Regional Dependence

The corpus callosum is very frequently found to be associated with concussion in the literature [34,35,39,40,55–57]. The strain threshold for concussion in the corpus callosum is frequently found to be lower than the cerebrum white matter [35,40,56,62] when predicted with a number of different head models. Changes in neuroimaging parameters related to brain injury were also found to correlate with higher strain and strain rate in the corpus callosum after concussive impacts [57]. The thalamus has also frequently been found to be associated with concussion, and was the best predictor of concussion with the lowest strain threshold for concussion in some studies [56,70]. The brainstem, including the midbrain is frequently found to be associated with concussion in the literature [35,37]. However, using a FE head model alone to predict the strains in the lower brainstem, as most past studies have done, could result in errors, because the brainstem is not connected to a spinal cord which would influence the strains. The choice of boundary condition at the base of the brainstem could influence the resulting strains. The white matter in the cerebrum is often found to be associated with concussion; however, the white matter strain threshold for concussion has often been found to be higher than that in the corpus callosum and thalamus [35,56,62]. The cerebrum grey matter [40] and cerebellum [35,57] have been associated with concussion as well, although strains in these regions are not as frequently found to predict concussion as the strains in other regions.

Study	Methodology	Brain Model	Significant Brain Region	Most Significant Metrics (Ordered more to less significant)	Threshold	Statistical Significance (-2 log likelihood ratio)
Hernandez (2015)	Instrumented mouthguard 2 Concussive impacts, 511 Non-concussive impacts (American Collegiate Football, Boxing and MMA)	KTH (Iso)	Corpus Callosum	Peak MPS	N/A	P<0.03
Patton (2014)	Rigid body reconstructions of observed concussions, from videos. 27 concussion and 13 non-concussion cases (Aussie-rules football)	KTH (Iso)	Thalamus Corpus Callosum White Matter	Stress (V-M) MPS Stress (V-M) MPS MPS	2.24 kPa 0.13 3.51 kPa 0.15 0.26 (50% chance concussion)	P<0.001 P<0.001 P<0.001 P<0.001 P<0.001
Viano (2006)	Hybrid III ATD reconstructions of observed concussions, from video. 22 concussive, 6 non-concussive (Professional American Football)	WSUHIM	Cerebrum Hippocampus Midbrain Parahippocampus, Uncal Regions Midbrain	MPS Max S. Rate	0.416 0.448 0.108 79.3 (Mean concussed)	P<0.002 P<0.007 P<0.017 P<0.012
Beckwith (2018)	Helmet kinematics Football (High School and Collegiate) 45 immediately diagnosed concussions (105 total), 161732 control impacts	WHIM	Whole Brain Cerebrum Cerebellum Brain stem Corpus Callosum	MPS	0.16 0.18 0.09 0.14 0.13 (Mean concussed)	P<0.001 P<0.001 P<0.001 P<0.001 P<0.001
		SIMon (2 nd gen)	Whole Brain Cerebrum Cerebellum Brain stem	MPS	0.12 0.14 0.06 0.10 (Mean concussed)	P<0.001 P<0.001 P<0.001 P<0.001

Kleiven (2007)	Hybrid III ATD reconstructions of observed concussions, from video. 25 Concussion, 33 No-Injury (Professional American Football)	KTH (Iso)	Grey Matter Corpus Callosum	MPS	0.26 0.21 (50% chance concussion)	P<0.001 P<0.001
Giordano (2014)	Hybrid III ATD reconstructions of observed concussions, from video. 25 Concussion, 33 No-Injury (Professional American Football)	KTH (Aniso)	Brainstem Midbrain Corpus Callosum	MAS	0.1461 0.1078 0.0736 (50% chance concussion)	P= 1.09e-3 P= 2.69e-4 P= 1.89e-3
Zhang (2004)	Hybrid III ATD reconstructions of observed concussions 24 concussive impacts (Professional American Football)	WSUHIM	Midbrain Thalamus	Max Shear Stress	7.8 kPa N/A (50% chance concussion)	P<0.001 P=0.001
King (2003)	Hybrid III ATD reconstructions of observed concussions 22 concussive impacts (Professional American Football)	WSUHIM	Midbrain	Product of Strain and Strain Rate	18 s ⁻¹ (50% chance concussion)	p<0.0000

Table 2.7 Relation of tissue-level injury predictors to observed concussions

Impact Orientation Dependence

The orientation of impact plays a role in the pattern of brain deformation and the likelihood of concussion [36,39,56,110]. FE models of head response also have shown a dependence on impact orientation, comparable to studies with observations of living subjects. Using an early model of the brain (WSUHIM), Zhang et al. found higher positive pressures in a lateral impact compared to a sagittal plane impact [110]. Perhaps more interestingly, this study found higher shear stresses in the core regions of the brain (specifically the corpus callosum). Patton et al. [39,56] and Hernandez et al. [36,58] obtained kinematics from concussions in football, and found that high strains in the corpus callosum and thalamus, and coronal angular acceleration correlated best with concussion.

While the linear impactor test has been used to investigate brain deformation by prescribing head kinematics from the test to an isolated head model, the inner regions of the brain were not investigated. Post et al. [20]

conducted linear impactor tests of a helmeted Hybrid III head and neck at 7.5 m/s, with three different helmet models, considering nine impact configurations. The experimental kinematics of the Hybrid III were prescribed to the UCDBTM head model, and the brain was divided into segments rather than specific organ structures [20]. It was found that a centric (directed through the COG) coronal impact produced regional strains almost twice as high as those in the centric frontal impact. A later study by Post et al. [111], using the same impact orientations, used the WSUHIM to examine the variation in MPS related to impact location, considering 4 different helmet models. The brain model was subdivided into white matter, grey matter, the cerebellum and the brain stem. This study also found that higher values of MPS resulted from impacts to the side of the helmet. However, large variations in head kinematics between different helmet models in the frontal impact orientation, with variations as large as a factor of three observed in the angular acceleration [111]. Elkin et al. [21] used a similar test methodology with even more impact orientations, at two speeds (5.5 m/s and 9.3 m/s) and also found that impact direction had a strong influence on MPS within the brain. The percentage of energy transfer to the head was calculated, and found to be highest for coronal impacts, and lower for frontal and crown impacts. Similar regional strains were calculated using both the SiMON and GHBMC models, which both predicted that frontal impacts resulted in a lower value of MPS than lateral impacts; however, the inner regions of the brain were not considered separately in this study. These studies did not suggest a mechanistic cause for higher strains resulting from lateral impact, however, Smith et al. [7] suggested that proximity of the falx could be the cause of high strains in the corpus callosum in lateral impacts. This is supported by Ho et al. [52], who used a detailed FE model to show that the presence of the falx had a large effect strains on the corpus callosum, in an oblique lateral impact.

In summary, the corpus callosum, thalamus, and the midbrain appear to be most strongly linked to concussion, therefore, these brain regions were investigated in detail in the current study. MPS and CSDM are the most commonly used metrics, so these metrics were considered. Comparing the response of MPS and CSDM with human body models and head models driven by ATD kinematics may highlight reasons for the lower correlation of CSDM with concussion.

2.4.3. Modelling of the Neck

FE models of the neck have been created with the objective of predicting head response and the behavior of the cervical spine in automotive crashes [112–114] (Table 2.8). There has been only limited use of computational neck models in the field of sports injury [25,26], compared to head models which have often been used to predict brain deformation. While many neck models have been shown to achieve good validation outcomes in terms of head response, different muscle implementations have been used.

Muscle activation is a process where muscles undergo contraction [27], and has often been suggested to play a role in head impacts in football [25,115–117]. Muscle contraction refers to a complex process in the constituents that make up the muscle fibers, and can involve shortening of the muscle, maintaining a constant length or lengthening of the muscle. In contrast to a living human, cadavers have no muscle activity, and thus muscles in a cadaver exhibit only passive behavior. When activated, muscles also stiffen in the transverse direction. The extensor muscles in the neck, which include the trapezius have been found to be stronger than the neck flexor muscles, the strongest of which is the sternocleidomastoid [61]. For a tackle position with the head up, activation level of the upper, middle and lower trapezius have been shown to be 14%, 37%, and 83% of sternocleidomastoid (flexor) activation, respectively [118]. Passive muscle properties of humans have been measured in vitro, exhibiting a non-linear response and viscoelasticity [119], while active properties in muscles have been estimated from in vivo testing, via electromyography [118] or external force measurements [115].

The simplest approach used in FE models of muscles is to use 1D Hill-type muscle elements to account for both the active and passive properties [113]. Using a single 1D element to represent an entire muscle can provide an accurate response in uniaxial tension, but do not account for the wrapping behavior of muscles, and the curved line of action that a real muscle would exhibit [120]. To account for wrapping behavior, recent models have segmented the 1D elements and connected them rigidly to the cervical spine to provide a realistic line of action [120]. Another approach is to use 3D elements to represent the passive properties, connected in parallel with 1D elements to represent the active properties. The combined 3D and 1D approach accounts for the wrapping behavior and the line of action of the muscles, as well as the transverse and shear stiffness of the muscle [27].

Many different muscle activation strategies have been used in human body models. Panzer et al. [121] applied a pulse with a delay of 74 ms to all muscles when simulating a frontal 8G and 15G volunteer sled impact. Brodin et al. used a similar strategy of prescribing muscle activation curves with a delay in response to a frontal and lateral crash [113]. Others have used control systems to maintain specific postures during driving maneuvers [122]. In the few studies which have used HBM necks to study football helmet impacts, muscles have not been activated [26] or the muscles have all been activated at the same level [25] or recently, at levels which maintain head stability [41]. In a player braced for impact, the head should remain stationary, and the muscle activation level should remain within measured physical levels [41].

A variety of data exists with which to validate neck models; however, data at injurious loads in living subjects does not exist due to ethical constraints. The most useful data available for validation of a neck model with active musculature are volunteer sled tests, which range in intensity from 2g to 15g and cover frontal [28] and lateral impacts. In these experiments, six living subjects were subjected to the 8g frontal

and 7g lateral impacts, and five subjects were subjected to a 15g frontal impact for the Naval Biodynamics Laboratory (NBDL). In the NBDL experiments, the head motion of the volunteer subjects was measured with a mouth-mounted accelerometer, while the neck accelerometer was mounted outside the body at the spinous process of the T1 vertebra [123]. In a later study, the T1 measurement was corrected based on video data [124]. The participants were belted to the sled using a number of restraints for the torso, pelvis and arms. The data from the experiments have been arranged into corridors, which are 1 standard deviation above and below the mean. While the NBDL volunteer data does not cover rear impacts, detailed cadaveric data exists [125]. Deng [125] performed 7g rear impacts using 6 whole-body cadaver specimens in a sled without a head restraint [125]. The cadaver was belted to a rigid, flat seatback which was angled back at 20 degrees. The head and the T1 vertebra were instrumented with accelerometers fixed directly to the bone as well as the vertebrae (C1-C7). Tensile tests of the full cervical spine [28] also exist, and many experiments have been completed at the motion segment level [126].

Model	First Published	Model Experimental Validation	Total Elements	Muscle Material Model
KTH Head and Neck Model	2014 [120]	Motion segment, volunteer sled tests	-	1D Hill, combined active and passive properties, w. realistic line of action
Total Human Model for Safety (THUMS) neck model	2006 [101]	Neck flexion, cervical axial compression	12,586	1D Hill, combined active and passive properties
UW neck model	2011 [28,29]	Volunteer sled tests, cadaver sled tests, tension of cervical spine, motion segment	108,354 [60]	1D Hill, combined active and passive properties
Global Human Body Models Consortium (GHBMC) neck model	2018 [27]	Volunteer sled tests, cadaver sled tests, tension of cervical spine, many motion segment level tests	212,000	3D hyperelastic-viscoelastic Ogden for passive properties, 1D Hill contractile only for active properties, w. realistic line of action

Table 2.8 List of published head and neck models

The role of muscle strength and activity in concussion is not well understood, with some studies showing decreased severity of head acceleration with stronger neck musculature [25,115] and others showing an increase in severity or no effect of stronger neck musculature [116,117]. The majority of these studies have

focused on living subjects and have not measured muscle activity at the time of impact. In football helmet impacts, the impact is transmitted directly to the head, in contrast with the more prevalent studies concerning car crashes where the impact is translated from the body to the head and neck muscle activity has had a significant effect on the head kinematics [29]. Studies that examined the influence of neck stiffness on brain deformation have also showed contrasting results [25,88], indicating a need for further research.

Results from experimental studies have been somewhat contradictory [25,116]. Eckner et al. [115] observed a correlation between anticipatory muscle activity and decreased head angular velocity in a test on human participants, using non-injurious impulses directly to the head (resultant angular velocity of 2 – 3.5 rad/). A braced and relaxed condition were tested, with the braced condition exhibiting 15% lower angular velocity. Schmidt et al. [116] found that higher measured cervical stiffness and lower angular displacement (responses to a cervical perturbation) reduced the chances of sustaining head impacts with high linear acceleration, when examining 49 collegiate football players with wearable sensors. In the same study, higher cervical muscle strength and size actually increased the odds of sustaining a moderate head impact (compared to a mild head impact) by 1.75 times.

The GHBMC neck model has been used to model head and neck response in car crash scenarios, where active musculature has been shown to have a significant effect on the head kinematics [29]. However, only one study of a football helmet impact to a HBM has considered the effect of active musculature. Jin et al. [25] studied the effect of muscle activation during football helmet impacts using the GHBMC head and neck model, with part of the torso included. Jin et al. [25] found that early activation of musculature reduced the angular velocity of the head. A single lateral impact at a speed of 9.5 m/s was simulated, based on an impact reconstruction from Pellman et al. [74] which used two Hybrid III ATDs [76]. The exact positioning of the ATDs and helmet in the reconstruction was unknown, so the HBM was positioned by guessing the head position, then adjusting the position so that the translational acceleration traces of the HBM head and the ATD matched as closely as possible. Four muscle activation schemes were selected, and with muscle activation prior to impact, a 20% decrease in peak rotational velocity was observed. In this study, the flexor and extensor muscles were given the same muscle activation curve, which causes the GHBMC head to rotate quickly backwards. Because the impact timing in this study varied, the changes in head response observed in this study that were attributed to active musculature could have been caused by the head moving into a different position prior to impact. While this study was a promising investigation into the effect of active musculature, it would be beneficial to investigate the effect of impact orientation and speed, while using a football helmet model with more experimental validation and known positioning of the ATD and helmet at the time of impact. In contrast, Eckersley et al. [41] considered a hybrid III headform integrated

with the Duke University Neck Model. This study found no significant influence of muscle activation considering multiple impact orientations, when using a muscle activation scheme which held the head in equilibrium; however, this study did not model helmeted impacts.

2.4.4. Global Human Body Models Consortium Human Body Model

The Head and Neck Model (HNM) and the Full Human Body Model (FBM) from the Global Human Body Models Consortium (GHBMC) 50th percentile male (v4.4) were used in the current study. The GHBMC model was well-validated with experimental data at the cervical spine level [126–129], and the overall head and neck had good validation performance [28,29]. Importantly, the brain model had a high mesh density, and the combined 3D passive and 1D active muscle implementation captured wrapping behavior and transverse muscle stiffness (Figure 2.16). The mid-sized male seated vehicle occupant (Figure 2.16) (M50-O) was developed from CT and MRI scans of a 26-year-old living male, who had similar anthropometric measurements to the Hybrid III ATD [27].



Figure 2.16 GHBMC M50-O, version 4.4

The HNM has been previously extracted from the GHBMC model (Figure 2.17) to examine head and neck behavior without the added computational time of the remainder of the body [29]. The head model was developed at Wayne State University [32] and the neck model was developed at the University of Waterloo [60]. The HNM was validated in 16 cases, including spine-level cases and sled tests considering the whole head and neck [130]. These validation cases included cadaveric testing and volunteer sled tests which account for muscle activation. The HNM consisted of the entire head and neck and all supporting muscles,

which are constrained to the T1 vertebra (Figure 2.17) [29]. The HNM consisted of 420 components total, and contained a total of 482257 elements.

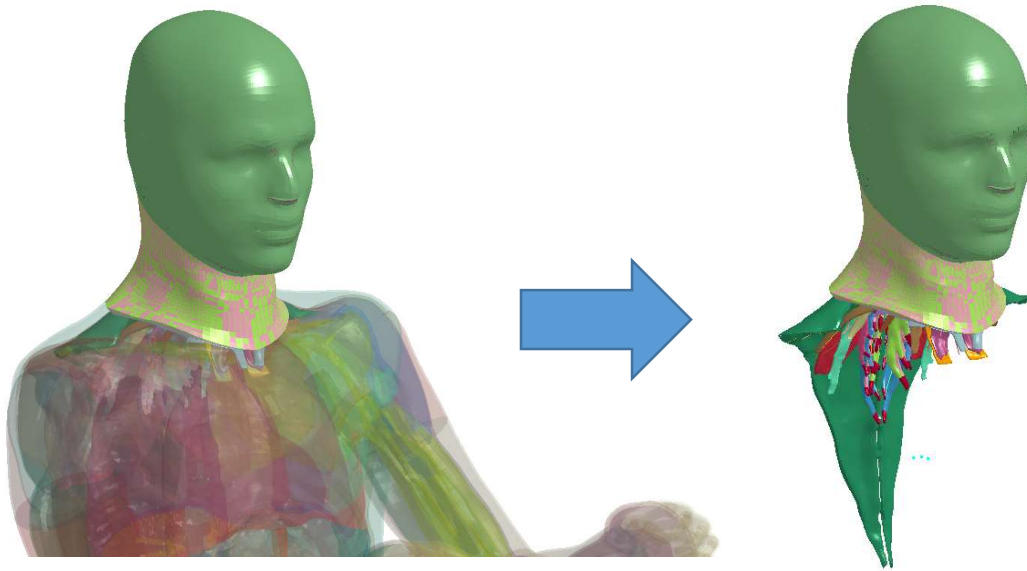


Figure 2.17 GHBMC M50-O head and neck model extraction

Head and Brain Model

The GHBMC full head model was validated against cadaveric experiments from the literature, including brain motion and pressure, and bone deformation. Intracranial pressure was validated against 6 experiments from Nahum (1977), additional experiments from Trosseille (1992) and Hardy et al. [98]. Brain motion was validated against 8 experiments from Hardy et al. [98], with the model showing mostly good agreement with the experiments. In Hardy et al. [98], an impact was delivered to 8 cadaver head and neck specimens using a pneumatic impactor. The brain motion in the experiments was measured by tracking neutral density targets with a high speed X-Ray. In the Nahum (1977) study, pressure was measured after the impact of 6 cadaver heads. Skull deformation was evaluated against four independent studies from the literature [112].

The brain region model (Figure 2.18) consisted of 22 components total, including the brain tissues, cerebrospinal fluid (CSF), the pia mater, the arachnoid, and the falx and tentorium. Quadrilateral elements were used for the shell elements and hexahedral elements were used for the solid elements. All brain elements and CSF elements consisted of hexahedral solid elements with a single integration point [32]. The brain tissue was divided into eight brain regions with constant material properties in each region. The corpus callosum was assumed to consist entirely of white matter, while the cerebellum, thalamus and basal ganglia were assumed to consist entirely of grey matter. Brainstem regions (Midbrain, Brainstem) used a stiffer

material, and the cerebrum was split into a grey matter region on the outside and a white matter region on the inside (Table 2.9).

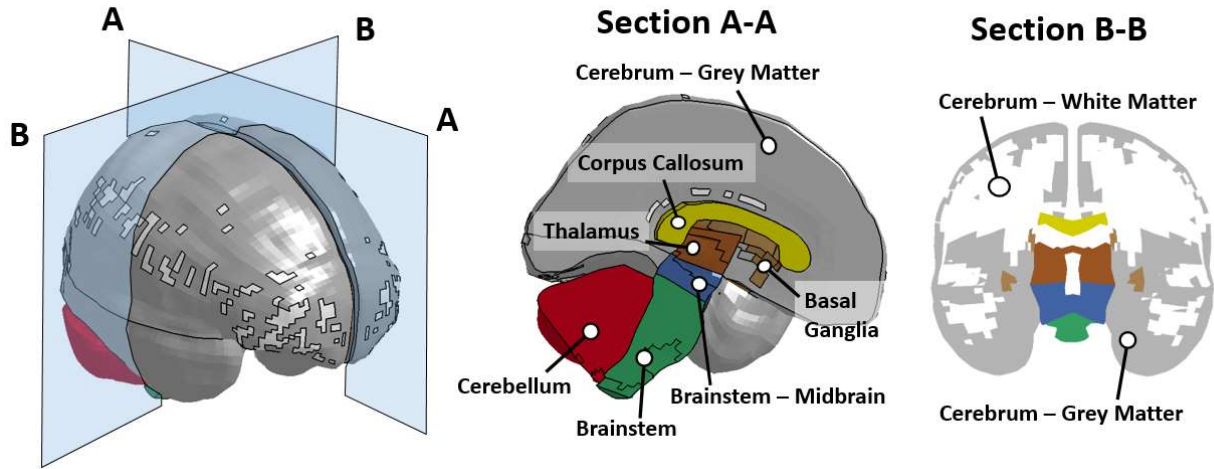


Figure 2.18 GHBM brain model, showing only brain tissues

The brain tissue in the model had a total mass of 1.16 kg. The model had 65628 elements, with most of these making up the cerebrum.

Brain Region	Material	# of Elements	Mass (kg)
Cerebellum	Grey Matter	14280	0.123
Cerebrum Grey Matter	Grey Matter	22700	0.491
Corpus Callosum	White Matter	980	0.021
Thalamus	Grey Matter	260	0.012
Brainstem - Midbrain	Brainstem	504	0.010
Brainstem (Pons and Medulla)	Brainstem	2280	0.022
Basal Ganglia	Grey Matter	1284	0.026
Cerebrum White Matter	White Matter	23340	0.455
	Total	65628	1.16

Table 2.9 Summary of all brain tissue regions

The brain tissues, as well as the CSF were modelled using a Maxwell Viscoelastic Model [131]. The shear modulus given by the Maxwell model is a function of the short-time shear modulus (G_0), the long-time shear modulus (G_∞), and the decay constant (β) (Eqn. 1).

$$G(t) = G_\infty + (G_0 - G_\infty)e^{-\beta t} \quad (4)$$

The material properties of the brain tissue were determined using values from the literature, as well as in-house testing data from Wayne State University [32] (Table 2.10).

Brain Material	Density (kg/m ³)	Bulk Modulus (GPa)	Short-time shear modulus (kPa)	Long-time shear modulus (kPa)	Decay Constant (β)
Grey Matter	1060	2.19	6.00	1.20	80
White Matter	1060	2.19	7.50	1.50	80
Brainstem	1060	2.19	12.0	2.40	80
CSF	1040	2.19	5.00	1.00	80

Table 2.10 Solid element material properties, brain tissue and CSF

The meninges, including the falx and tentorium, were modeled using shell elements and an elastic material model [32]. The pia mater and the arachnoid were also modeled using shell elements with an elastic material model.

Neck Model

The GHBMC neck region model included the muscles, vertebrae, ligaments and other relevant tissues to impact loading (Figure 2.19). Validation of the cervical spine model includes approximately 60 cases total, while at least 12 cases exist for the full neck model. The cervical spine experiments used for validation included testing at both quasi-static and high rates in tension, flexion and extension at the motion segment level from C2-C3 to C7-T1 [112]. Axial rotation experiments were also used, at levels from C0-C1 to C7-T1, and the full cervical spine was compared to a full cervical spine tensile experiment [112]. At the full neck level, the validation cases include sled testing of live volunteers, at a range of loads from 2-15 g in frontal impact, at 7g in a lateral impact and 4g in a rear impact [112]. Cadaver testing in a rear impact at 7g is also used for validation [112].



Figure 2.19 (A) Full neck model, (b) neck model with skin and subcutaneous tissues removed, (c) isolated cervical spine

Muscles in the GHBMC neck model consisted of 3d passive muscle elements, attached in parallel with 1D axial elements modelling the active properties, which were interspersed at small increments. This implementation is thought to replicate the wrapping behavior of the muscles better than a purely 1D approach. Passive muscle elements were modeled using a hyperelastic Ogden material model with viscoelastic effects, fit to experimental data (Figure 2.20). The 1D active muscle elements were modeled using contractile elements with a simplified Hill-type muscle model [25]. The force in the 1D active muscle elements was a function of three curves: (1) elongation of the element, (2) the rate of loading, and (3) the Activation Level (AL), which is a dimensionless parameter representing the level of muscle activation as a function of time (Figure 2.20). The default values of these three curves are shown in Figure 2.20, which are described in detail in Panzer, 2006 [121]. The default AL curve represented a startle response, with a 74 ms delay prior to impact. The muscle elements were held in place by 1D elements that were fixed to the vertebrae.

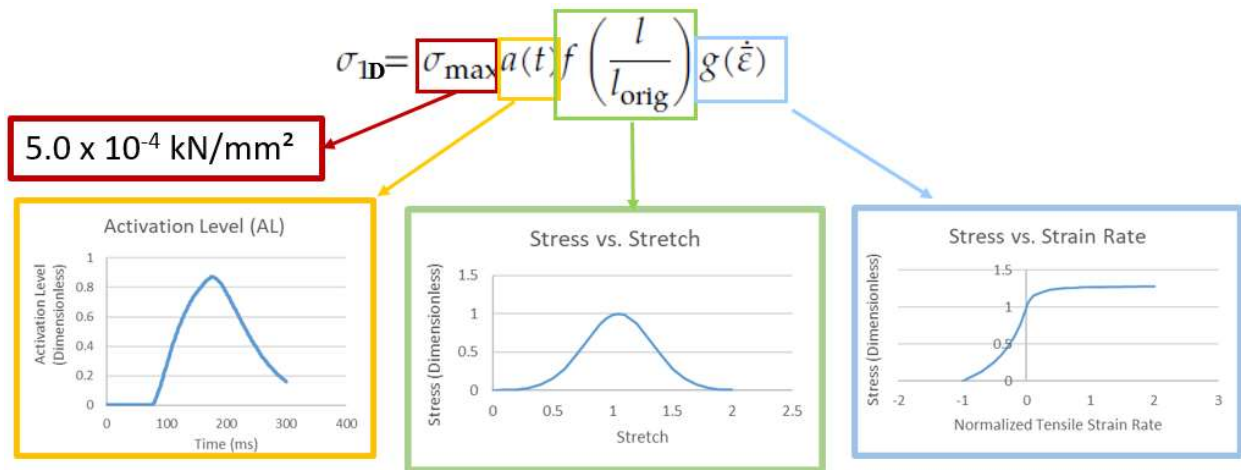


Figure 2.20 1D muscle element inputs

The muscles in the GHBMC neck were classified as flexor muscles and extensor muscles (Figure 2.21). The AL curve was scaled by a certain factor for the flexor muscles and by a different value for the extensor muscles. All flexor muscles were assigned the same AL, and all the extensor muscles were assigned the same AL.

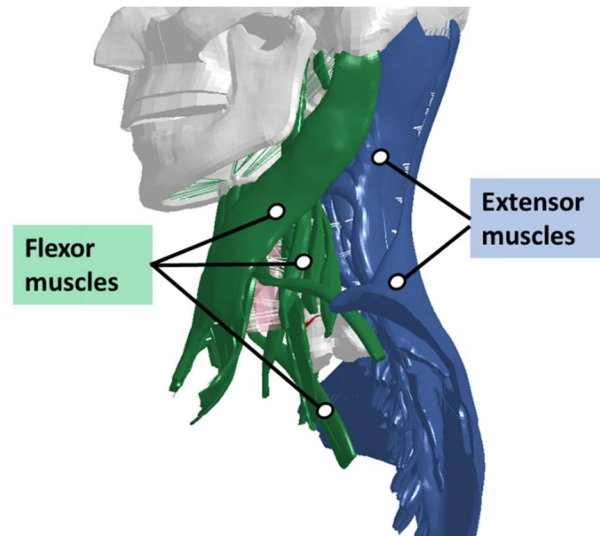


Figure 2.21 Neck musculature, showing flexor and extensor muscles

The classification of each muscle in the neck is shown in Table 2.11. Extensor muscles tend to pull the head backwards, and the flexor muscles tend to pull the head forwards.

Muscle	Function	Model	Muscle	Function	Model
Anterior Scalene	Flexor	1D Active + 3D Passive	Multifidus	Extensor	1D Active + 3D Passive
Middle Scalene			Semispinalis Capitis		
Posterior Scalene			Semispinalis Cervicis		
Rectus Capitis Anterior			Longissimus Capitis		
Rectus Capitis Lateral			Longissimus Cervicis		
Omohyoid			Iliocostalis		
Sternocleidomastoid			Splenius Capsitis		
Longus Capitus			Splenius Cervicis		
Longus Colli			Levator Scapula		
Sternohyoid			Oblique Capitis Inferior		
Sternothyroid			Oblique Capitis Superior		
Thyrohyoid			Rectus Capitis Posterior Major		
Mylohyoid			Rectus Capitis Posterior Minor		
Stylohyoid			Minor Rhomboid		
Digastric			Trapezius		
Geniohyoid					
		1D Spring			

Table 2.11 Summary of neck muscles included in model and extensor/flexor classification

The skin of the GHBMC neck was modeled with a fully integrated shell elements using a linear viscoelastic material. Below the skin, attached via shared nodes was the subcutaneous tissue, modeled using solid

elements with a simplified rubber material. The cervical ligaments in the model were modeled using 1D axial elements. The material properties of these ligaments were measured from experimental tensile tests. The intervertebral disc was modeled using a combination of anisotropic fibrous (fabric) elements and a hill foam matrix for the articular cartilage, and an elastic fluid material for the synovial fluid. The vertebrae were modeled using a piecewise plasticity model. The anterior soft tissues, including the trachea were simplified to a cylindrical structure that used a simplified rubber material based on tensile experiments of the whole throat. The material models used in the HNM are summarized in Table 2.12.

Region	Part	Element Type	Material Model	Visco-elastic?
Outer Tissue	Skin	Shell	Linear viscoelastic (*MAT_006)	Yes
	Subcutaneous Tissue	Solid	Hyperelastic rubber (*MAT_181)	No
Soft Tissue - Head	Brain Tissue	Solid	Linear Viscoelastic (*MAT_061)	Yes
	Lateral Ventricle, CSF	Solid	Linear Viscoelastic (*MAT_061)	Yes
	Meninges	Shell	Elastic (*MAT_001)	No
	Bridging Veins	Beam	Elasto-Plastic (*MAT_024)	No
Soft Tissue - Neck	Passive Muscle	Solid	Viscoelastic Ogden (*MAT_77_O)	Yes
	Active Muscle Attachments	Beam	Discrete Spring (*MAT_074)	No
	Anterior Tissue	Shell	Hyperelastic rubber (*MAT_181)	No
	Hyoid Inferior/Superior Springs	Axial	Elastic spring (*MAT_S01)	No
Skull	Skull	Solid	Elasto-Plastic (*MAT_024) and Elastic (*MAT_001)	No
	Teeth	Solid	Rigid	-
Cervical Spine	Ligaments	Axial	Discrete Spring (*MAT_074)	Yes
	Annulus Matrix	Solid	Hill Compressible Foam (*MAT_177)	No
	Nucleus 3D	Solid	Elastic Fluid (MAT_001_Fluid)	Yes
	Fibrosis	Shell	Fabric (*MAT_034)	No
	Cortical Bone	Shell	Bi-Linear Plastic (*MAT_003)	No
	Trabecular Bone	Solid	Bi-Linear Plastic (*MAT_003)	No

Table 2.12 Summary of material models used in the HNM

2.5. Objective Rating Methods

Objective rating methods are commonly used to compare the responses of human surrogates, including ATDs [80] and HBMs [126,132]. One of the most commonly used is Correlation and Analysis (CORA), developed by Partnership for Dummy Technology and Biomechanics [133]. This rating methodology can be used to compare the response of a simulation to an experiment, or the response of an ATD to a cadaveric response. Due to the detailed, objective rating of simulation response [134], CORA has been used in many recent biomechanics publications to assess HBM response [126,132,134], which is typically compared to an experiment, but CORA can also be used to compare HBM response to another simulation.

The rating method can consist of a cross correlation rating and/or a corridor rating. The cross-correlation component of the rating compares two curves, and examines of three aspects of the response: (1) a progression (shape) rating (K_V), (2) a phase shift rating (K_P), and (3) a size rating which compares area under the curves (K_G) (Figure 2.22). The cross-correlation rating method requires only a single experimental response, or the average response of multiple experiments. The cross-correlation ratings range from 0 to 1, with an average rating of 0 representing no correlation between the curves, and an average of 1 representing perfectly overlapping curves. The three components of the cross-correlation rating are weighted using user defined factors; the default weight for K_V , K_P and K_G are 0.5, 0.25 and 0.25 respectively [133], and the sum of the weighted components represents the overall cross-correlation rating. These default weights, and all other user-adjustable parameters for that matter, have been used commonly [28,44,46,99,128,134]. The corridor rating is often used to compare simulation responses to large sample sizes of volunteer [28] or cadaveric [135] human experiments, where there is a high variability in the data. The corridor upper and lower bound are made from the average plus and minus a multiple of the standard deviation between the experimental curves [133]. The rating refers to the percentage of the curve that falls within the corridor.

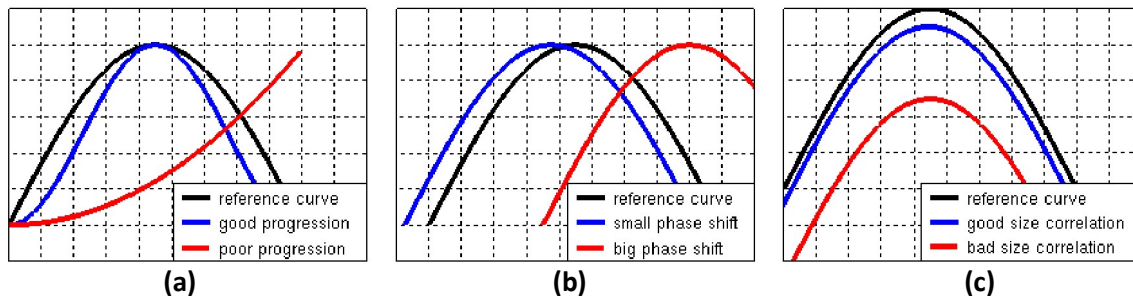


Figure 2.22 (a) Progression rating, (b) phase rating, (c) size rating (From Thunert 2012)

2.6. Football Helmet Modelling

The purpose of the modern football helmet has expanded to include protecting the head from concussion, in addition to the original purpose of protecting the head from catastrophic injuries, which include contusions and skull fracture [6,63]. Improvements in helmet design have vastly reduced the incidence of catastrophic head injuries [6,63], especially when compared to the leather helmets that remained in use until 1940's [6]. Unfortunately, concussion remains prevalent in all levels of American Football [3–5]. Because the seriousness of concussion is now better understood, helmet manufacturers have introduced new helmet designs that attempt to mitigate rotational motions that cause concussion.

The primary purpose of a football helmet, like most protective equipment, is to reduce force transmitted to the head by spreading an impact out over a longer period of time and over a larger area, and to dissipate the energy of an impact [6]. Traditionally, high density foam has been used as an energy absorbing liner, which has a relatively constant force-displacement response until it consolidates. This is desirable because, prior to the final consolidation region, there are no spikes in force transmitted to the head. A traditional liner material maintains force below a certain threshold for the duration of an impact; too stiff a material exceeds the peak force right away, and too soft a material exceeds the peak force after consolidating (Figure 2.23). Foam liners are effective in reducing linear acceleration of the head; however, traditional foam liners (Figure 2.24a) are not intended to reduce the rotational acceleration of the head, which is now understood to be closely linked to concussion [12].

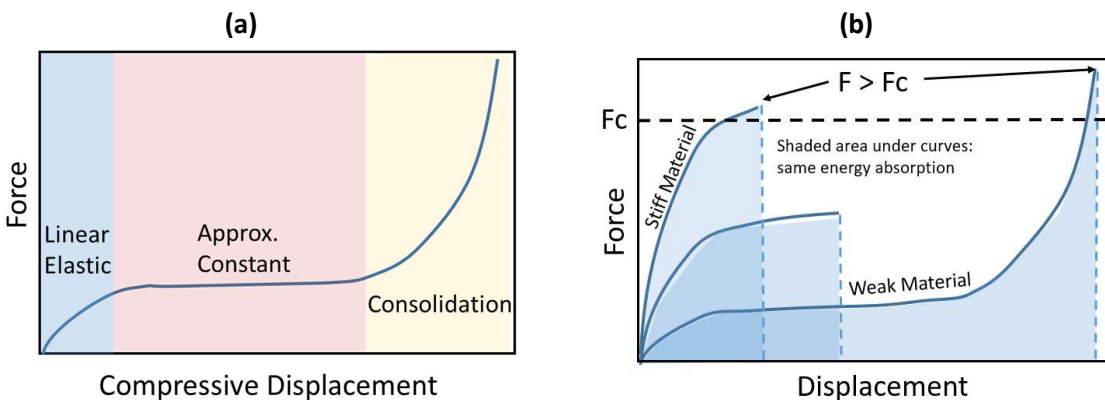


Figure 2.23 (A) Foam force-displacement response, (b) material considerations for absorption of linear impacts

In addition to introducing new energy absorbing structures made from polymers, at least three manufacturers have designed helmets where the helmet shell can rotate relative to the innermost surface of the liner. Two manufacturers, Xenith (Figure 2.24b) and Schutt have introduced designs which decouple the energy absorbing liner from a traditional shell. Another manufacturer, Vicis (Figure 2.24c), has

introduced a helmet with a softer outer shell that is coupled to an inner shell by a columnar structure which acts as a both a rotational and linear energy absorber.

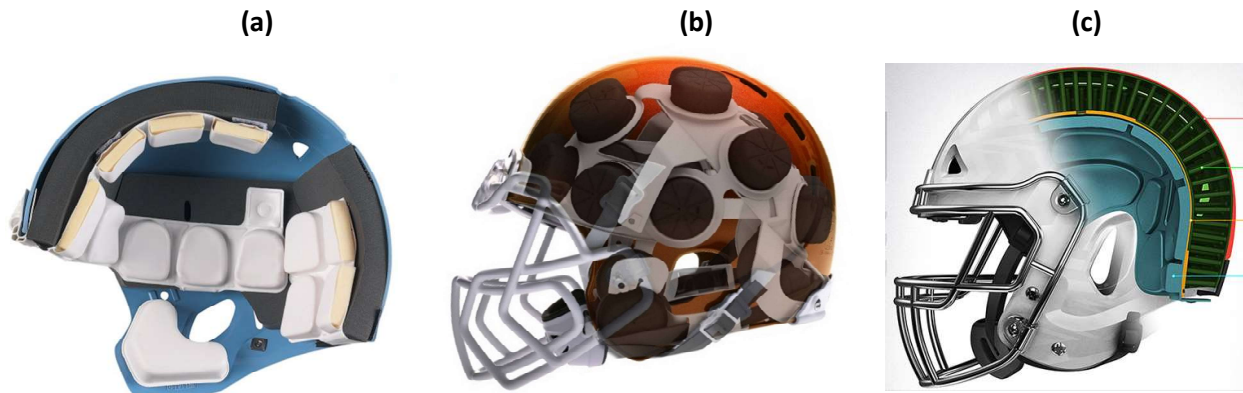


Figure 2.24 (a) Helmet with foam liner, (b) Xenith X2e helmet with decoupled shell and air-venting liner (from Xenith, 2018), (c) Vicis Zero1 helmet with columnar liner (from Vicis, 2018)

2.6.1. Existing Football Helmet Finite Element Models

Improvements to the design of football helmets may be enabled with advanced FE modelling backed by experimental testing. FE modelling can inform design decisions by enabling parametric studies and optimization for certain modes of loading. The majority of helmet modelling has been focused on American football. Zhang et al. [136] introduced a FE model of a foam helmet design that was validated against 4 linear impacts of a helmeted Hybrid III head and neck, using a foam block as an impactor. The study suggested that the helmet was less effective at attenuating lateral and rear impacts than frontal impacts, having observed 90% foam compression in a 7 m/s linear impact. The model material properties were based on a combination of physical testing, manufacturer data and reverse engineering methods, where the material properties were adjusted until the best agreement between models and experiments was achieved. A rigid material was used for the facemask. Another model of a traditional foam helmet was created by Darling et al. [26]. A mesh refinement study was performed, which evaluated the helmet response in two linear impacts to the top and front of the helmet at 3.0 m/s, with three mesh sizes. Other studies have modified component geometry or material properties to minimize certain head injury metrics. Johnston et al. [137] made improvements to the helmet liner, to reduce rotational acceleration, using a combined experimental and simulation approach. Two football helmet designs were tested experimentally with linear impacts at 3.2 m/s to the facemask, and drop tests in five orientations at five different velocities. The helmeted experiments were modeled, then re-tested with an optimized liner, and a 28% reduction in head

rotational acceleration was observed. Johnson et al. [66] optimized the design of a football helmet facemask, using a full helmet model and linear impacts in two orientations.

Although previous FE models have shown promise in optimizing head protection, FE models of football helmets have been limited by a lack of validation data at the material and component level, resulting in models which have been calibrated to match a limited number of experiments. This has potential to achieve an accurate head response with the sub-components of the helmet exhibiting unrealistic behavior [46]. Another limitation of past models has been the simplification or removal of key features, such as a chin strap and face mask, which can change the response of the helmet considerably [138,139].

Recently, four open-source FE models of football helmets have been introduced by Biocore, LLC, in conjunction with four centers of expertise. These helmet models have been validated against 70 different full-helmet experiments, with the models achieving good to excellent correlation with the experiments. Prior to full-helmet validation, the models were validated with material-level and component-level testing for all key components. Importantly, the models range from a standard foam design (Riddell Speed Classic) (Figure 2.25a) to the most recent and best performing helmet designs, including the Schutt AirXP Pro (Figure 2.25b), Vicis Zero1 (Figure 2.25c) and the Xenith X2e (Figure 2.25d) which all include advanced liner systems designed to mitigate head rotation.

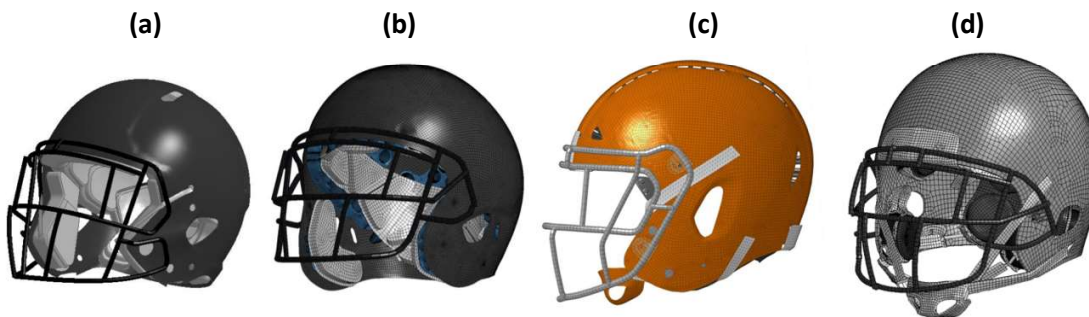


Figure 2.25 Helmet FE models: (a) 2016 Riddell Speed Classic (b) 2016 Schutt AirXP Pro (c) 2017 Vicis Zero1 (d) 2016 Xenith X2e

2.6.2. Xenith X2e Football Helmet Model

The football helmet model used in this study was a FE model of the Xenith X2E (Figure 2.26), an advanced helmet design which attempts to mitigate rotational acceleration of the head [140]. This helmet consists of a traditional helmet shell and facemask, with a more advanced energy absorbing liner and chin strap system. Instead of a traditional foam liner design, this helmet contains air-filled shock absorbers, called “compression shocks”, that are made of thermoplastic polyurethane. The liner consists of these compression

shocks and a soft foam layer that contacts the head. Unlike a traditional helmet, the liner is predominantly detached from the helmet shell, to permit rotation of the liner relative to the shell. The liner is secured to the head by a strap that attaches to the chin cup and wraps around the back of the head.

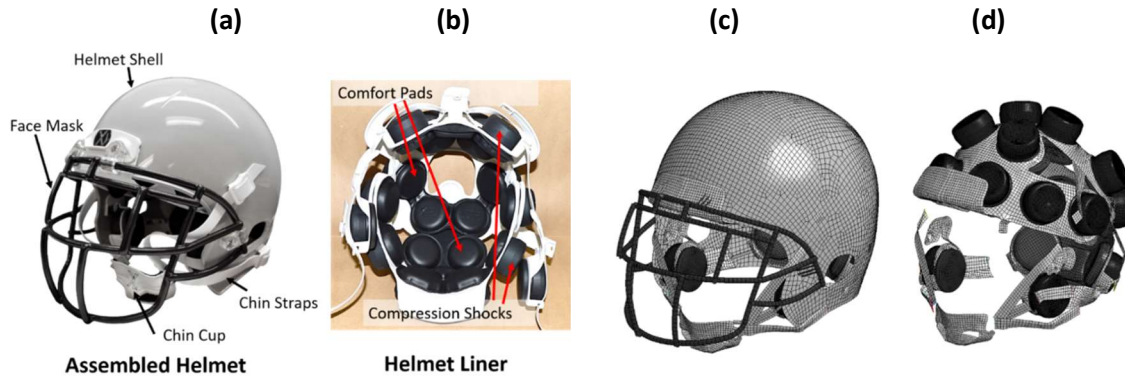


Figure 2.26 (a) Physical Xenith X2e helmet, (b) physical helmet liner (c) Xenith X2e helmet model, (d) Xenith X2e model liner

The FE model of the Xenith X2E used in this study was developed by the University of Waterloo, and is open source, and publically available to download [43]. The model was developed by measuring material properties of the components at multiple rates, then implementing these properties in component level models and validating them against experiments (Figure 2.27). These component level models were then assembled into the full helmet, which was validated against 70 experimental configurations. The helmet model consists of 182284 elements total. The helmet development is summarized in the following sections, which are adapted from Bustamante et al. [46] and Cronin et al. [43], and additional detail can be found in those documents.

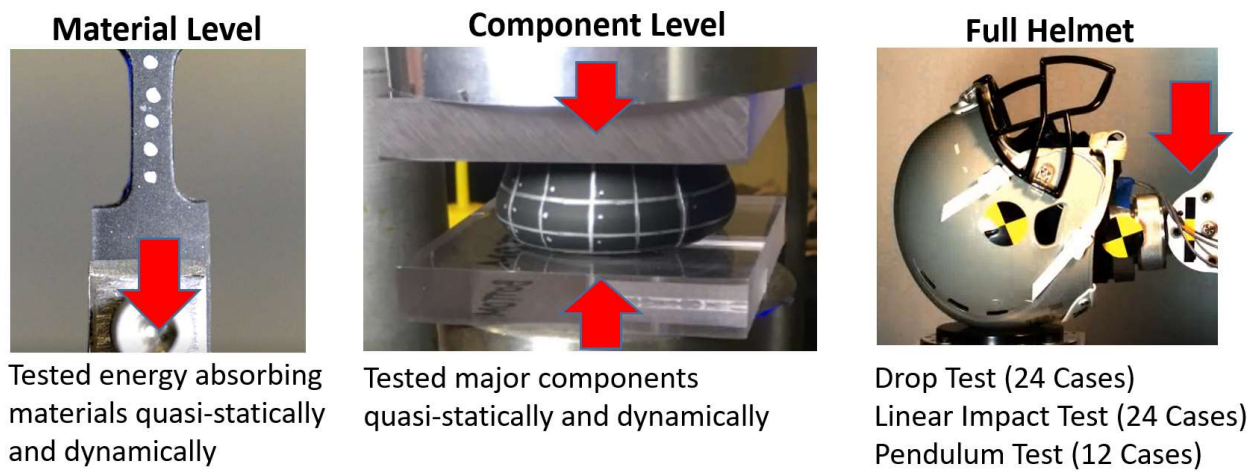


Figure 2.27 The development process of the Xenith X2e helmet model

2.6.3. Material Level Testing

The helmet materials were tested over a range of rates, in tension, compression or both. The relevant modes of loading and strain rates were identified based on the component function in the helmet. Cylindrical samples for the compressive tests were created using a coring tool, using multiple thin cylinders to achieve a good aspect ratio where necessary. For the tensile tests, custom stamping tools were used to create standard dog-bone samples when component sizes would allow; otherwise, samples were stamped using smaller dimensions. Displacements in all material tests were measured optically using high-speed imaging. A summary of material testing is shown (Table 2.13), which outlines the chosen material models to represent the properties, including the identifier for the model in LS-Dyna.

Material	Component	Strain Rates (s ⁻¹)		Material Model	Visco-elastic?
		Compression	Tension		
Polycarbonate	Helmet Shell	-	0.1, 10	Elastic (*MAT_001) (E = 2.45 GPa and v = 0.38)	No
Steel coated with Polyethylene	Face Mask	-	-	Elastic (*MAT_001) (E = 200 GPa and v = 0.32)	No
Thermoplastic Polyurethane (TPU)	Bonnet	-	0.01, 0.1, 1.0	Hyperelastic rubber (*MAT_181)	Yes
Polyurethane and Nylon	Strap System	-	0.01, 0.1, 1.0	Elastic (*MAT_001) (E = 2.45 GPa and v = 0.38)	No
TPU	Compression Shocks	0.01, 0.1, 10, 150	0.01, 0.1, 1.0, 10, 100	Hyperelastic rubber (*MAT_181)	Yes
High Density Polyurethane Foam	Comfort Pad	0.01, 0.1, 1.0, 30, 250, 1200	-	Fu-Chang Foam (*MAT_181)	Yes
Low Density Polyurethane Foam	Comfort Pad	0.01, 0.1, 1.0, 25, 185, 1000	-	Fu-Chang Foam (*MAT_181)	Yes
Medium Density Polyurethane Foam	Crown Pad	0.01, 0.1, 1.0, 30, 130, 1400	-	Fu-Chang Foam (*MAT_181)	Yes

Table 2.13 Targeted nominal strain rates for material tension and compression experiments for the predominant subcomponents of the Xenith X2E helmet

A larger number of tests were performed on the compression shock material relative to the other materials because the shocks were the primary energy-absorbing elements in the helmet. The material response exhibited a high degree of nonlinearity, viscoelasticity, and rate dependence (Figure 2.28). A simplified rubber [131] constitutive model was used to model the compression shock material, which interpolated between the experimental stress-strain curves at the measured rates.

2.6.4. Component Level Validation

Each subcomponent of the helmet was tested experimentally in at least one component-level experiment (Table 2.14). These tests were carried out in a hydraulic frame at low rates, and in a pendulum apparatus for the high rate experiments. Due to the highly viscoelastic nature of the materials, the foam comfort pads and the compression shocks were tested at two rates, while the facemask and helmet shell were tested only quasi-statically. It was verified via image analysis that the tested strains for the helmet shell, facemask and compression shocks were in excess of the strains seen during full helmet testing. The compression tests performed on the components represented the mode of loading that the component experienced in the full helmet testing.


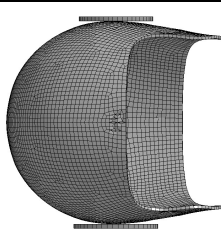


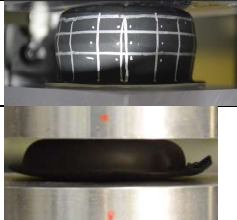
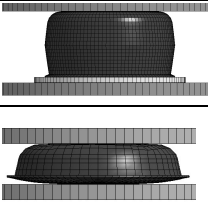

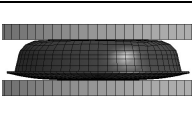
Test	Mode	Strain rates (s ⁻¹)	Strains (%)	Experiment	Simulation
Helmet Shell	Lateral Compression, Anterior-Posterior Compression	0.001 0.01	Load-unload in 5% increments up to 15%		
Facemask	Lateral Compression	0.0002	10		
Compression Shocks	Through-Thickness Compression	0.01 110- 120	Near consolidation		
Comfort Pads	Through-Thickness Compression	0.004 229	Near consolidation		

Table 2.14 Xenith X2E subcomponent experimental modes of loading, target nominal rates and strains, and validation models

The component level models of the helmet were created from computed tomography (CT) scans, and meshed in a pre-processing software (HyperMesh 14.0, Altair). The helmet shell model consisted of fully integrated shell elements with an average side length of 5 mm. The facemask model consisted of beam elements with a circular cross-section of 6.0 mm. The compression shock model consisted of fully-integrated shell elements with an average side length of 1.2 mm, which was required to capture the localized

folding and stick-slip behavior in the component level experiment. In addition, a simple airbag model with an orifice area of 2.25 mm² was implemented in the cavity of the compression shock. The simulation and experimental results for the large (27mm) compression shock were in good agreement considering both quasi-static and dynamic loading (Figure 2.28). The foam pads consisted of a 2mm single-integration point solid elements enclosed in shell elements representing the enclosing vinyl materials.

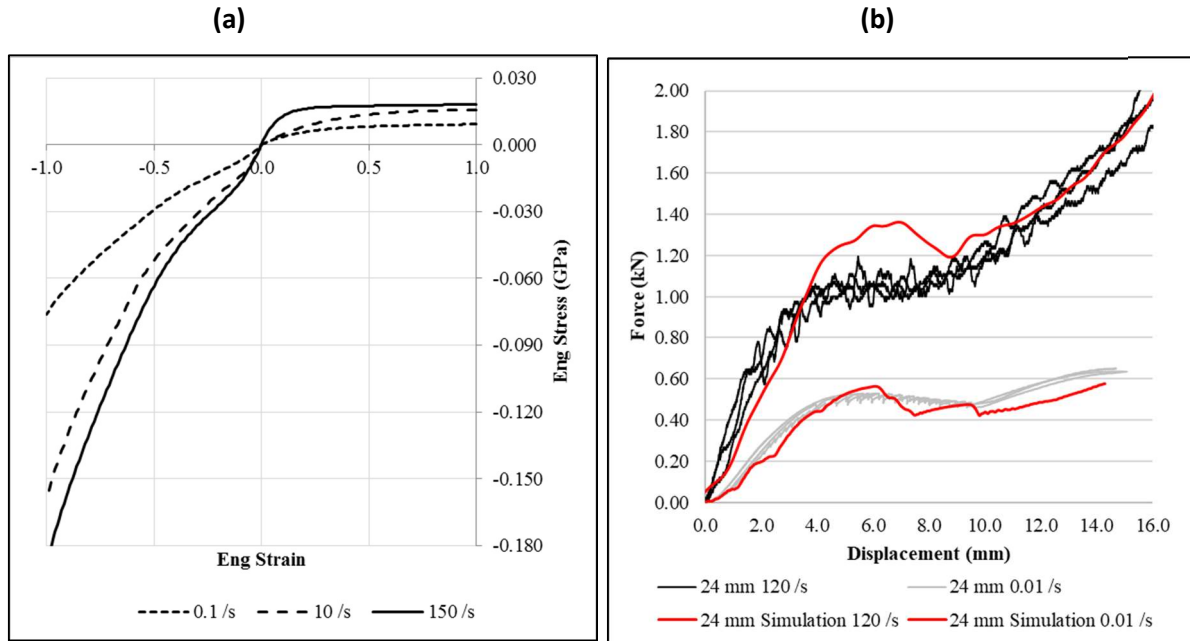


Figure 2.28 (a) Compression shock material response, (b) 27 mm compression shock experimental and simulated response (from [46])

The component models were assembled into the full helmet structure using shared nodes predominantly, and sliding contacts where required. Two meshes of the Xenith X2e helmet model were generated, one of which was fitted to a NOCSAE headform and the other to a Hybrid III headform. The fitting was completed by placing a scaled representation of the headform geometry inside the helmet, then expanding the geometry to its original size in a pre-simulation. The two meshes are identical with the exception of nodal coordinates of the foam and chin strap components. The headforms have a different shape and size, so the inner structures of the helmet conformed differently to each headform.

2.6.5. Full Helmet Validation

The full helmet was validated against 70 experimental configurations (Table 2.15). These range include drop tower tests using both a NOCSAE headform and a Hybrid III headform, a pendulum impact using a rigid pendulum and a sliding carriage, and the linear impactor test, using a sliding carriage and deformable

impactor (See Section 2.3 for details). The model responses considered for evaluation were contact force, headform angular and linear kinematics, and impactor acceleration. The helmet model response was compared to the experiment using CORA software (see section 2.5).

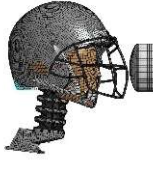

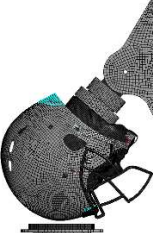

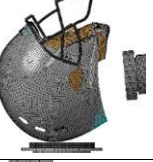

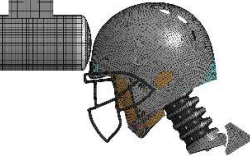
Test Setup	Impact Configuration		Evaluation Criteria (time history)				Simulation	Experiment
	Orientations	Impact Velocity [m/s]	Force	Linear Acceleration	Angular Velocity			
Linear Impactor	A, A', B, C, D, F, R, UT	5.5 7.4 9.3	Contact Force	Head COG (XYZ)	Impactor (Global X)	Head COG (XYZ)		
NOCSAE Drop Tower	Front, Side, Top	2.9 3.7 4.9 6.0	Contact Force	Head COG (XZ)	Carriage (Global Z)	N/A		
Hybrid III Drop Tower	Front, Back, Side, Top	2.9 4.9 6.0	Contact Force	Head COG (XYZ)	Carriage (Global Z)	N/A		
Pendulum	Front, Front Boss, Side, Top	3.0 4.6 6.1	N/A	Head COG (XYZ)	Impactor (Global X)	Head COG (XYZ)		

Table 2.15 Helmet validation cases

The CORA ratings for the head and impactor kinematics ranged from good to excellent (Table 2.16), where the NOCSAE and Hybrid III drop tests had the highest average ratings (0.93 and 0.88 respectively). The linear impactor tests had an overall average rating of 0.78 and the pendulum impact had a rating of 0.83. Similarly, the model response for helmet rotation in the linear impactor test was in good agreement with the experimental data measured from video analysis, with an overall CORA rating of 0.79.

Overall Weighted CORA Score	Drop Tower		Linear Impactor		Pendulum
	HIII	NOCSAE	HIII		HIII
	Head CG and impactor kinematics	Head CG and impactor kinematics	Head CG and impactor kinematics	Helmet rotation	Head CG and impactor kinematics
	0.88	0.93	0.78	0.79	0.83

Table 2.16 Overall average CORA ratings for the full helmet model

2.6.6. Integrating Football Helmet Models with HBMs

Recently, there have been a few studies which have integrated FE models of football helmets with detailed HBMs [25,26,66]. In existing studies of football helmet impacts using HBMs, the GHBMC model has been used predominantly [25,26]. However, in addition to the limitations of the helmet models used, the boundary conditions of the simulations were at times unclear, and may not have simulated the kinematics experienced during concussive impacts. Johnson et al. [66] considered facemask impacts in a linear impactor test scenario, however there was no mention of how the head model was constrained in the simulations as there was no neck included in the study. The head model was not extensively validated, only one case was used. One impact speed of 6 m/s was considered, which is not typically associated with concussive impacts [18]. Jin et al. [25] integrated the helmet from Zhang et al. [136] with the GHBMC HNM, with some torso mass included. In addition to the limitations of the helmet model, it was unclear how the striking and struck GHBMC models were constrained. Darling [141] used the GHBMC full body model fitted with a simplified football helmet model to investigate regional brain strains in frontal and crown impacts with a rigid impactor. Muscle activation was not considered in the study. Most importantly, the impactor weighed only 5 kg and was travelling at 3 m/s, which does not simulate the effective mass and speed that players experience during a concussive impact [13,18].

In previous studies, the simulations required to fit the helmet to the head were not described in detail. In Darling et al. [141], the helmet was loosely placed on the head, with a sliding contact with a friction coefficient of 0.01 defined between the head and the comfort foam of the helmet. No chin strap was included in the model. Zhang et al. [136] meshed the helmet model so that it fit the contours of the headform, and defined a sliding, penalty-based contact between the inside of the helmet and the headform with a friction coefficient of 0.3. Jin et al. [25] gave no detail about helmet model integration with the HBM head. Johnson et al. [66] did not mention how the helmet model was fitted to the HBM head model or how contact was modelled, but did mention that the chin strap was represented by coupling the HBM chin to selected points on the helmet with elastic connecting elements. Luo et al. [142] used a representation of HBM head geometry, which was expanded to fit the helmet model and allowed the helmet to fit the contours of the

head. However, this helmet model did not include a chin strap, which affects helmet performance [66,139]. Clearly, it is desirable for a helmet model to realistically fit the contours of the head and include a chin strap to accurately simulate the transmission of loading to the head [138].

2.7. Summary

From the review of the literature, it is clear that there are uncertainties with the current linear impactor helmet testing, and some of its applications which warrant further investigation.

1. The accuracy of the Hybrid III ATD head kinematics in a football helmet impact are not known, and the role of neck muscle activity on head kinematics is also not well understood.
2. The application of prescribed kinematics from the linear impactor test to a head and brain model has not been compared to a more biofidelic HNM, when considering the deformation of the whole brain or the comprising brain regions. The role of neck musculature on brain deformation has not been previously investigated using multiple impact orientations.
3. There is a need to investigate the influence of the human body mass of the struck player on the resulting head kinematics.

3. Methods

This chapter outlines the required enhancements to the existing models used to evaluate head response in a football helmet impact. This involved replicating the boundary conditions of the existing linear impactor experiments as closely as possible, with the existing Xenith X2e helmet model, the Hybrid III ATD model, the GHBMC HNM, and the GHBMC FBM.

For the first study, the HNM head was repositioned relative to the neck (T1) to match the head and neck angle of the ATD. The Xenith X2e helmet was fitted to the HNM head in a series of pre-simulations. The experimental boundary conditions corresponding to the mass and translation of the linear impactor carriage were applied to the HNM. A muscle activation scheme was developed to represent a fully braced player, which maintained the head position prior to impact with a high level of muscle force. For the second study, experimental kinematics from linear impactor tests were applied to the isolated HBM head to predict brain deformation, and compared to the fully integrated HNM and helmet FE model. In the third study, the FBM was positioned identically to the HNM in the previous studies. All FE models were solved using a commercial FE software (LS-DYNA R7.1.2, single precision) and analyzed using LS Pre-Post.

3.1. Head and Neck FE Model Repositioning

For the purpose of comparison, both the ATD and the HNM were positioned as similarly as possible, using anatomical landmarks. The default head coordinate system of the HBM had the same SAE J211 coordinate system as the ATD head. In seated position, the X-axis was horizontal pointing forwards and the Z-axis was vertical pointing downwards. The Frankfurt Plane was calculated by using the lowest point on the orbital and the highest point on the tragion when the head was horizontal, it was found to be within 0.5° of horizontal in seated position (Figure 3.1). For this reason, it was assumed that the built-in coordinate systems of the Hybrid III ATD and GHBMC HNM heads were equivalent. To calculate the angle of the neck axis, a least-squares regression line was plotted through the center of mass of each of the seven cervical vertebrae (C1 to C7). Using this definition, the neck axis was within 0.2° of vertical in seated position.

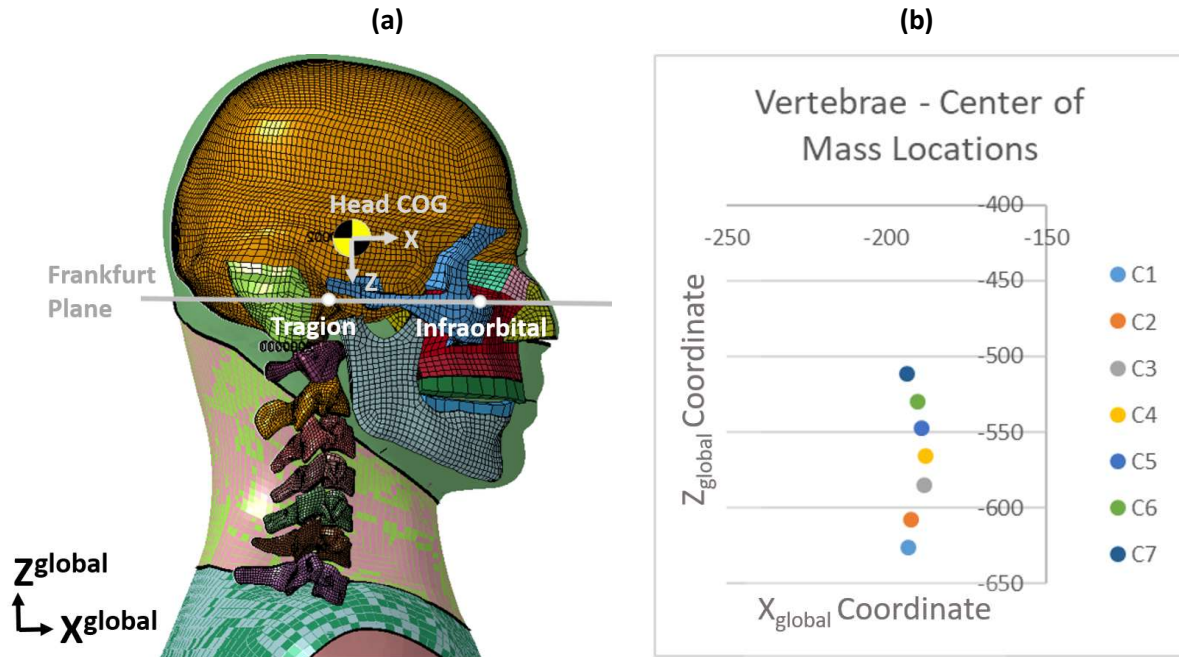


Figure 3.1 (a) The Frankfurt plane of the GHBMC model in the default seated position, (b) original vertebrae COG locations of the HNM in the default seated position

To match the ATD, the head of the HNM was repositioned so that the X-axis of the head made a 94.5° angle with the neck axis at the time of impact. In a pre-simulation, the vertebrae of the neck were fixed in place and the head was pushed at 0.16 m/s , then left to settle for 50 ms to allow the strains in the brain to settle. The nodal positions of the HNM head were exported from this pre-simulation to the main simulation so that the HNM head position matched the ATD head position in the linear impactor test. The final position of the head coordinate system of the ATD simulation, ATD experiment and HNM are shown in Figure 3.2, at a neck angle of 15° , where the head X-axis makes a 10.5° angle below horizontal. The location of the OC joint is also shown. For the GHBMC HBM, this joint was defined in the model. For the Hybrid III ATD, this point was marked by a cylindrical pin.

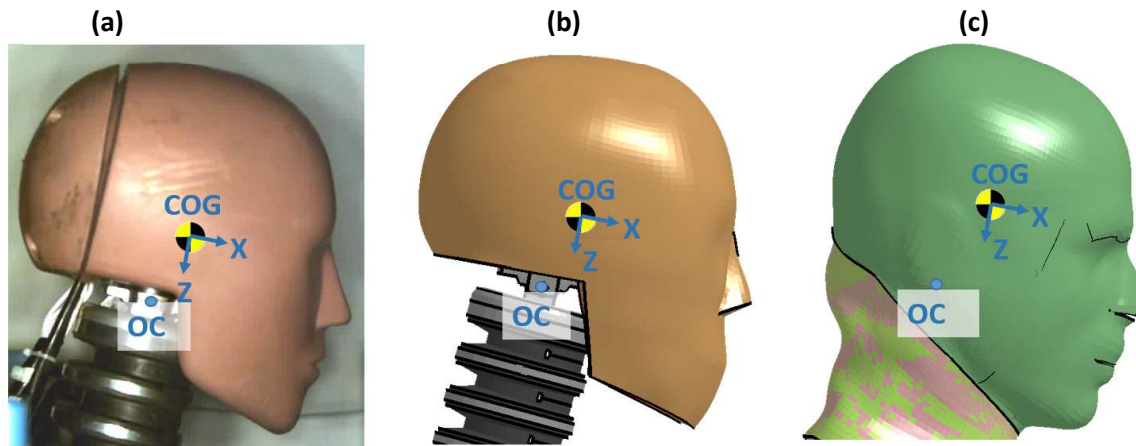


Figure 3.2 ATD Experiment (a), ATD Simulation (b), HNM (c), frontal impact configuration. The location of the occipital condyle is marked “OC”

3.2. Linear Impactor Boundary Conditions

In the current study, the “F” (frontal), “C” (lateral), and “R” (rear) impact were analyzed (Figure 3.3). These designations were applied as descriptors in the Biocore physical impact data, and were used in this study for consistency. The rear and frontal orientations resulted in almost pure sagittal rotation of the head. Importantly, the three impact orientations were approximately 90° apart, which flexed the neck in the lateral, anterior and posterior directions. These orientations induced motion primarily in a single plane, to clearly understand the effect of active musculature on the resulting head kinematics in the sagittal and coronal planes (an example of the out-of-plane motion is included in Appendix C, Figure C2 and Figure C3).

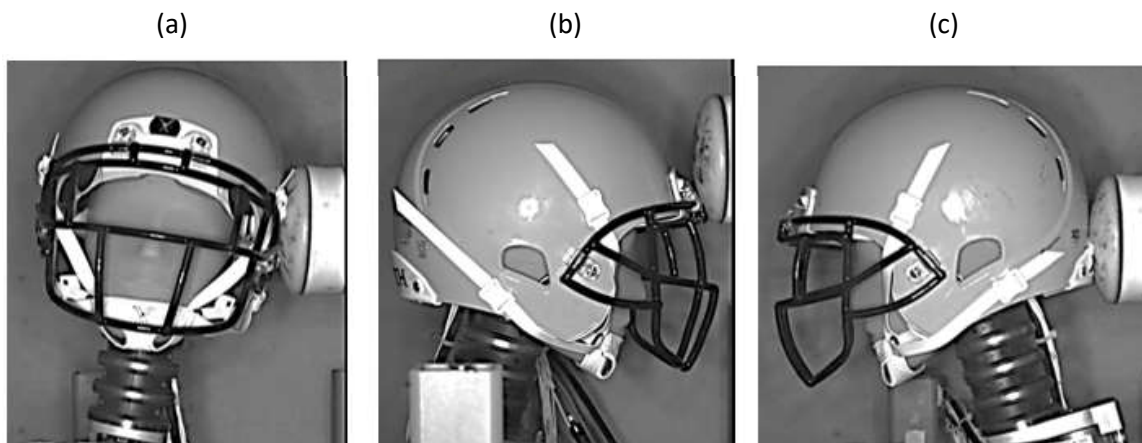


Figure 3.3 (a) Lateral, (b) Frontal and (c) Rear impact orientations, corresponding to the NFL “C”, “F” and “R” orientations respectively

In the HNM simulations, the linear impactor was positioned to match the ATD experiment and simulation, maintaining the same distance offsets relative to the head COG (Figure 3.4).

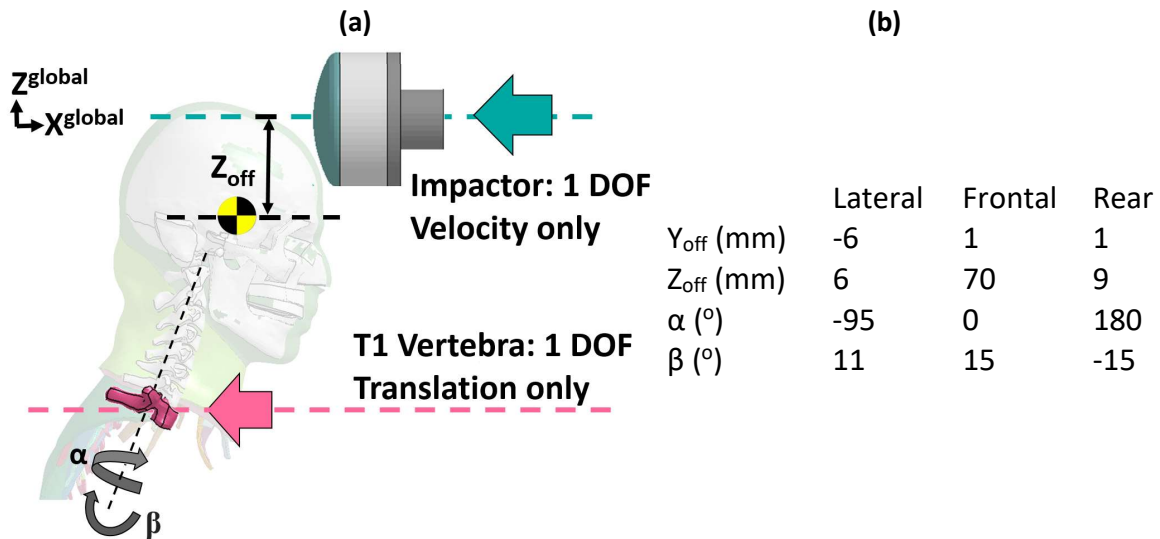


Figure 3.4 (a) Linear impactor test dimensions for lateral, frontal and rear orientations, (b) table of dimensional offsets for each orientation

The HNM was assigned the same boundary conditions used in the ATD linear impactor experiment and simulation (Figure 3.4). The inertial properties of the three headforms are shown in Table 3.1, calculated for the local coordinate systems for each model. The head moment of inertia and mass of the HNM were determined including the same regions as Walker et al. [55]. The head of the of the Hybrid III ATD is well defined, and was considered to include all parts above the OC. The same linear ram mass of 15.4 kg was used in the impact, with the thrust rod constrained to only move in the x direction. The head mass of the HNM was 4.41 kg, which was very similar to that of the ATD (4.54 kg). The moments of inertia of the HNM head were slightly higher than those of the ATD head about the X and Y axis, while the Z-axis value was slightly lower (Table 3.1). The mass of the HNM neck was higher than that of the ATD, because the HNM neck requires supporting muscles that extend into the torso. Mass was added to the T1 vertebra so that the HNM had the same combined carriage and neck mass of 19.2 kg used in the ATD experiment and simulation. The T1 was constrained to only move in the global X direction. A contact friction coefficient of 1.1 was defined between the impactor and the head for the bare-head HNM simulation, and friction coefficients of 0.1 and 0.3 were defined between the impactor and the helmet shell and facemask, respectively. These values were the same as those defined in the bare-head and helmeted validation cases used for the helmet development [43,80].

	Head Mass (kg)	Moment of Inertia (kg*mm ²)			COG Location (mm)			OC Location (mm)		
		Ixx	Iyy	Izz	X _{Global}	Y _{Global}	Z _{Global}	X _{Global}	Y _{Global}	Z _{Global}
Hybrid III ATD Experiment	4.53	15300	21000	18100	0.0	0.0	0.0	17.9	0.0	49.5
Hybrid III ATD Simulation	4.54	15338	21038	18100	0.0	0.0	0.0	17.8	0.0	48.3
GHBMC HBM	4.40	18854	22345	17386	0.0	0.0	0.0	25.0	0.0	58.3

Table 3.1 Comparison of geometric and mass properties of the Hybrid III experiment, Hybrid III simulation, and the GHBMC HBM

The impactor was constrained to move only in the direction of impact. The impactor was prescribed three initial velocities of 5.5 m/s, 7.4 m/s, 9.3 m/s. The impactor was allowed to coast in the direction of impact after the initial velocity was applied, consistent with the ATD simulations. After 30 ms, the impactor was decelerated by prescribing the experimental acceleration to the impactor. This simulated the braking force, which was applied to the ram in the experiments.

3.3. Helmet Fitting on the GHBMC Head Model

The model was fitted to the HNM head using the same method for fitting the helmet to the Hybrid III ATD head [43]. The initial helmet nodal coordinates were taken from the helmet fitted to the NOCSAE headform, because the HNM head had similar geometry to the NOCSAE headform, and less similar head geometry to the Hybrid III headform. The fitting process required two pre-simulations (Figure 3.5). In the first pre-simulation, a rigid representation of the skin geometry of the HNM, scaled to 0.9 of the original size, was centered inside the helmet. The seatbelt elements used for the chin strap were swapped with rigid axial elements for the first pre-simulation. The head was constrained so that the center of gravity was stationary and no rotation was possible, while the helmet was allowed to move freely. Over the course of the pre-simulation, the HBM head geometry was expanded to the final geometry, so that the soft foam elements of the helmet model deformed to fit the contours of the head. The helmet position was adjusted over a number of iterations to minimize helmet motion and foam deformation. The second pre-simulation involved tightening the upper strap and repositioning the crown of the helmet slightly downwards to the final position (a distance of 75mm from the tip of the nose to the crown of the helmet) to match the ATD experiment and simulation. The maximum principal strain in all foam components was below 0.1 in all pre-simulations, so no pre-stress or pre-strain was carried over to the main simulation. In the helmet model, each chin strap was attached to the helmet shell using a 1D axial element. At the start of the simulation, specific elements were assigned to retract with a specified force, enabling pre-tensioning of the strap system as in the physical tests which pre-compressed the foam components. This methodology was included in the original helmet model

development. Each chin strap was tightened with a force of 50N, which could produce some transient head motion prior to impact. An 80 ms delay was introduced prior to impact to ensure that the straps were tightened, and the head was stationary based on kinematic criteria ($V_{res} < 0.05$ m/s, $\omega_{res} < 0.15$ rad/s) and in the correct final position at the time of impact. A penalty-based contact was defined between the HBM head and the helmet with the same friction coefficient of 0.1 used in the ATD simulation [43].

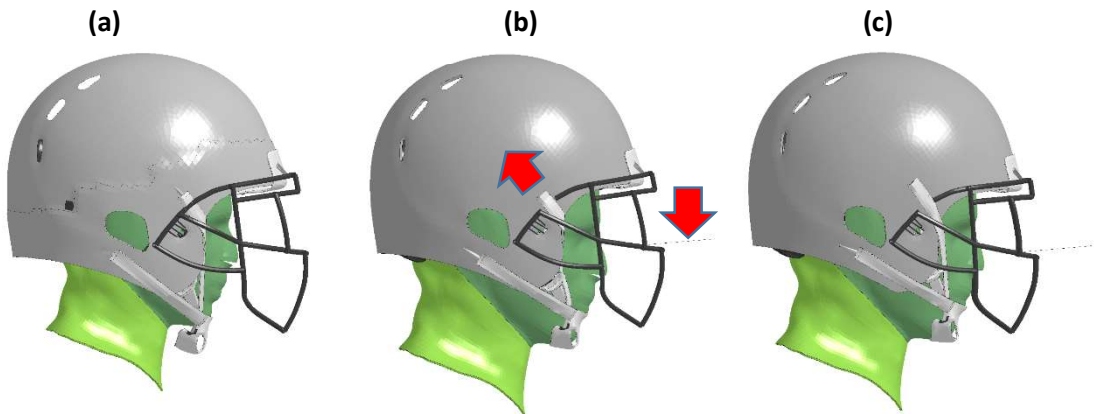


Figure 3.5 (a) Scaled head geometry, (b) tightening straps and adjusting helmet position, (c) final helmet fit

3.4. Study 1: Head and Neck Response of an Active Human Body Model and Finite Element Anthropometric Test Device During a Linear Impactor Helmet Test

For the current study, only the AL curve for the 1D flexor and extensor muscle elements were modified in the HNM. The AL was assumed to linearly increase from zero at $t = -80$ ms up to a constant maximum value at $t = -60$ ms of $AL = 0.871$, which was the maximum value of the default AL curve, representing the maximum possible level of muscle activation. The 20 ms rise time was included for numerical stability. Two conditions were investigated: (1) a balanced muscle activation scheme (balanced activation), to represent a player braced for impact, and a (2) baseline condition with no muscle activation (no activation). The two conditions represented extremes for the possible level of muscle activation, in reality there would be a small level of muscle activation at all times [143].

For the balanced activation condition, the flexor and extensor muscles in the neck were activated at different levels so that the head remained stationary with the same neck axis angle and head X-axis angle as that of the ATD and HNM with no activation. If the extensor muscles of the model were activated at the same level as the flexor muscles, the head would rotate backwards due to the higher strength of the extensor

muscles. With the balanced activation scheme, it was confirmed that the head was stationary and in the correct position just prior to impact ($V_{res} < 0.05 \text{ m/s}$, $\omega_{res} < 0.15 \text{ rad/s}$). To achieve equilibrium prior to impact with the correct head-neck angle, the initial head angle and level of extensor muscle activation were determined by trial and error. A range of initial head-neck angles from 84° and 90° and extensor muscle activation levels ranging from 0.13 to 0.18 were investigated with the flexor muscle activation level held constant. The iteration process was repeated until the head was in equilibrium and the HNM head-neck angle was within 0.5 degrees of the required ATD head-neck angle. The final head-neck angle is shown in Figure 3.7. The required ratio of flexor to extensor AL to balance the head and neck in the correct position was 20:3, so the AL curve in the GHMBC model was scaled by a factor of 1.0 for the flexor muscles, and 0.15 for the extensor muscles (Figure 3.6), which maintained a ratio similar to that suggested by electromyography data for a head up tackle position [118]. The magnitude of flexor AL used ($AL = 0.871$) was approximately 6x the overall level of activation measured in the sternocleidomastoid for a head-up tackle position [118], to represent a high level of muscle activation in the HNM, within physical limits.

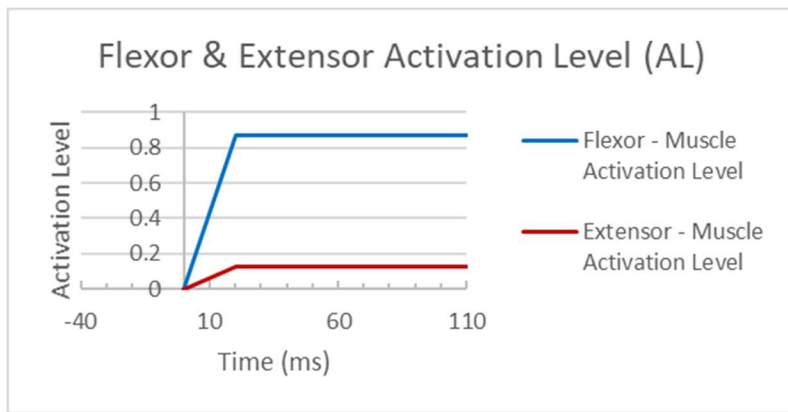


Figure 3.6 Flexor and extensor AL curves for flexor and extensor active elements for the “balanced activation” condition

The impact simulation consisted of an 80 ms delay prior to impact, where the head moved into the desired position and the helmet was tightened in the helmeted cases (Figure 3.7). Prior to impact, the sum of all 1D muscle forces at the time of impact was 1.1 kN, at a cross section of the neck 10 mm below the hyoid bone, which was within 10% of the 1.2 kN mean total muscle force in a frontal maximum voluntary contraction measured by Cheng [144].

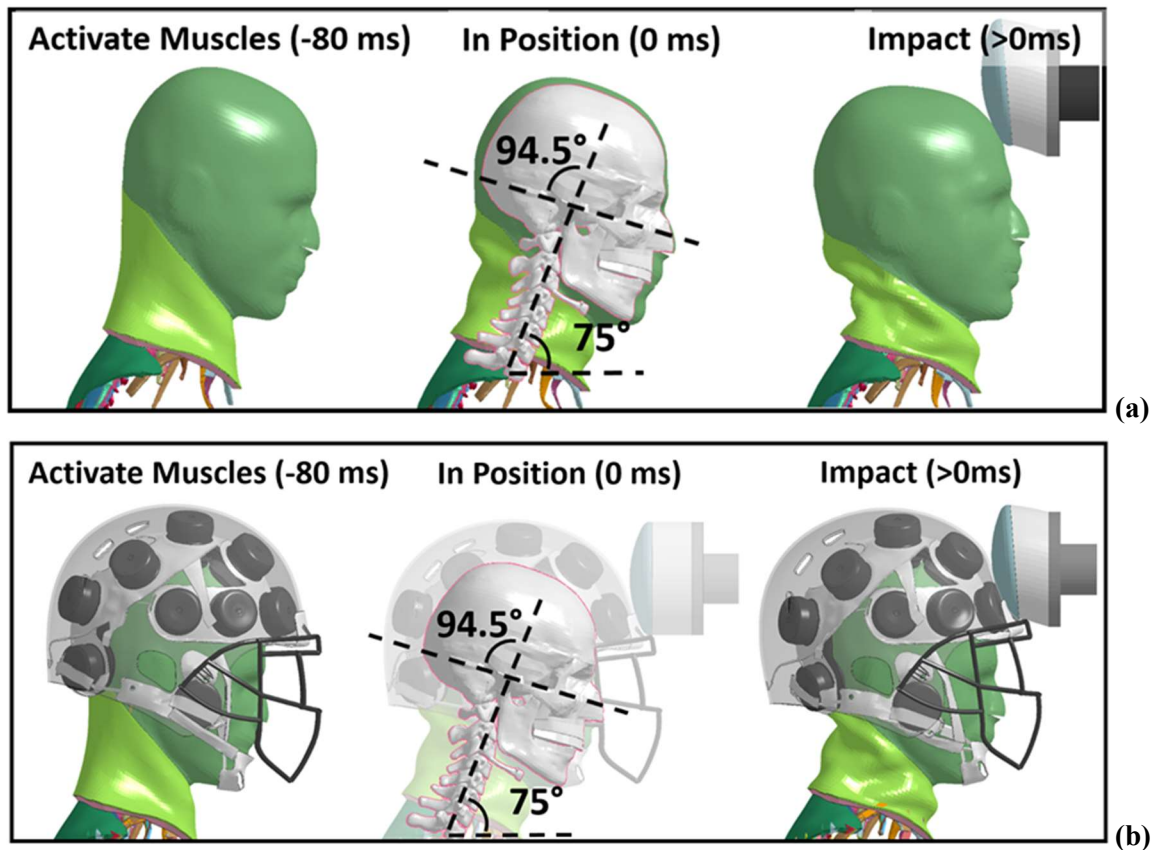


Figure 3.7 Exemplar impact simulation timeline, for “balanced activation” condition in a frontal impact at 5.5 m/s (a) bare head, (b) helmeted

There was some head motion prior to impact in all simulations with muscle activation or with the helmet included. With balanced activation, the head reached values of 0.3 m/s linear velocity and 2.7 rad/s angular velocity initially (Figure 3.8). The angular velocity of the head then decreased to 0.15 rad/s and the translational velocity fell to 0.05 m/s just prior to impact, for the helmeted and bare-head cases. The helmet tightening force influenced the response prior to impact (Figure 3.8), however it was confirmed that the head was stationary and in the correct position just prior to impact in all simulations ($V_{res} < 0.05$ m/s, $\omega_{res} < 0.15$ rad/s).

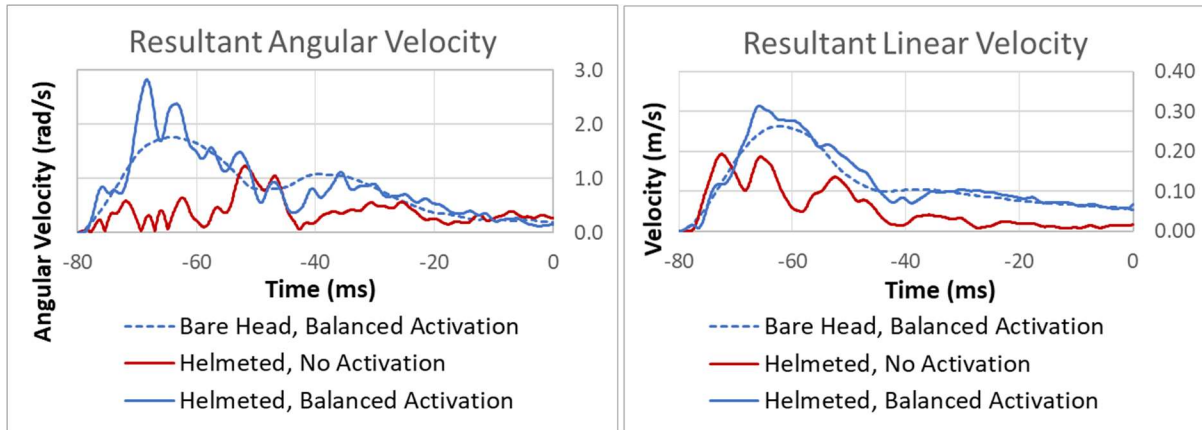


Figure 3.8 Resultant linear and angular velocity prior to linear impact for three conditions

Vertebral fracture was disabled in the HNM, because the Hybrid III ATD neck does not exhibit any fracture experimentally [17] and the current study was focused on head kinematics and response. Future studies should consider the effect of active musculature the potential for neck injury in football impacts. One additional change was made to the HNM. The element formulation of the trachea was changed from 2 to 16 for greater model stability, since instability was noted in some aggressive impact scenarios. The changes did not affect the model response considerably in the verification simulations (see Section 4.2.2).

3.5. Study 2: Simulated and Experimental Boundary Conditions for a Human Head Model Comparing Brain Response in Football Helmet Impacts

The Hybrid III ATD enables the measurement of head kinematics during an impact, but the ATD contains no representation of the brain and therefore cannot predict deformation of the brain directly. A common approach to predict brain strain has been to prescribe the kinematics measured from an ATD experiment to a human head model, as outlined in Section 2.4.2. In the current study, the 6 DOF kinematics of the ATD experiment were prescribed to the HBM head (Figure 3.9a), to calculate the brain response, for comparison with the fully simulated boundary condition using the HNM (Figure 3.9b). For the prescribed kinematics approach, the HBM head was separated from the neck at the base of the skull. The skull was changed from a deformable material to a rigid implementation. The 3 DOF linear velocity and the 3 DOF angular velocity were prescribed to the center of gravity of the rigid skull, and no other constraints were prescribed to the simulation. The head simulations with prescribed kinematics and the simulated HNM impacts ran for 70 ms, to allow sufficient time for brain deformation to occur, since the brain deformation lags behind the skull kinematics [25,90].

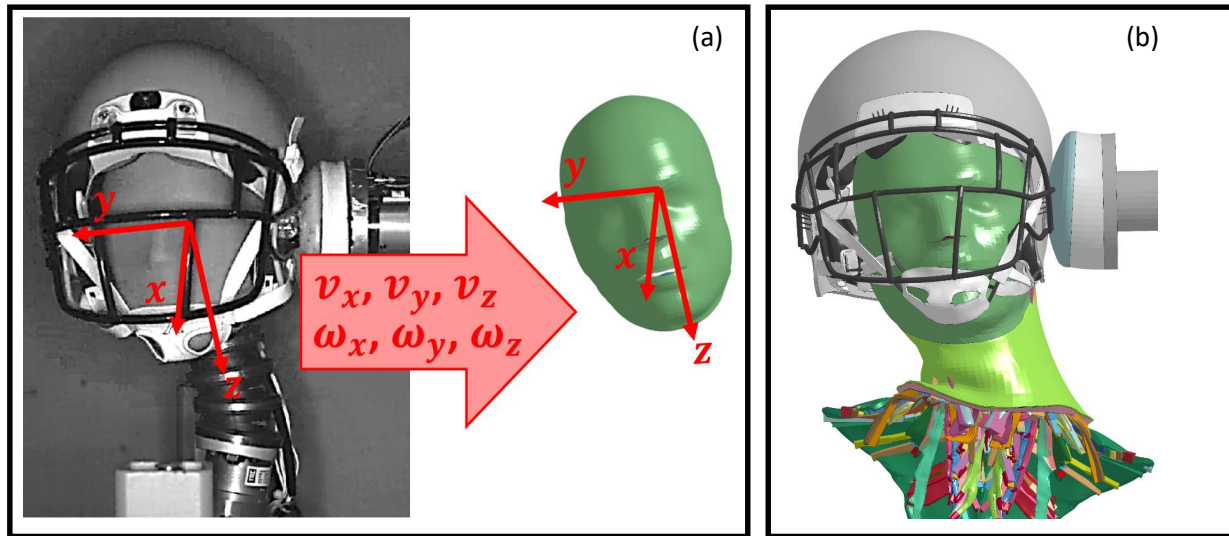


Figure 3.9 Lateral impact at 9.3 m/s, showing (a) the ATD experiment (prescribed kinematics approach) and (b) the HNM with balanced activation (simulated HNM impact)

3.6. Study 3: The Role of the Whole Body Mass and Inertia in Football Helmet Impacts

For all previous simulations, only the head and neck were considered, and the base of the neck was constrained so that only 1 DOF translation could occur. It is possible that this constraint has an effect on head kinematics, and that the inertia and mass of the whole body could play a role in impacts to the head [26]. To assess the role of the whole body mass and inertia on head kinematics and MPS in the brain, the FBM was compared to the constrained HNM used in the previous studies. The head, neck and helmet geometry, impactor boundary conditions and both muscle activation schemes from the HNM simulations were implemented identically for the full body model. The initial position of the head and neck of the FBM was identical to the constrained HNM. The only difference for the full body simulations was the presence of the torso and the remainder of the body, which were unmodified from the default seated position (Figure 3.10). In contrast to the HNM, the FBM was unconstrained for the duration of the impact simulation. In the constrained HNM, all neck muscles were attached rigidly to the T1 vertebra, which was constrained to only translate in the global X direction (Figure 3.10), in contrast with the full body simulations, where the neck muscles were attached to their anatomical insertion sites and the T1 vertebra was free to move.

Full Human Body Model (FBM)



Figure 3.10 Unconstrained FBM integrated with football helmet and linear impactor (frontal configuration)

3.7. Measurement of Head, Neck and Brain Response

The metrics of interest in the current thesis were the head kinematics, neck kinematics, kinematic response metrics for the head, and brain deformation response. The methods used to calculate these metrics are outlined in this section.

To objectively compare the response kinematics and kinetics of the ATD simulation to the HNM simulation, cross-correlation (CORA) values were calculated comparing the response curves. The same parameters were used to compare the ATD simulation and experiment (Section 4.1). The kinematic outputs assessed from the models and experiments were the linear acceleration and angular velocity of the head COG. In addition, the lower neck force, moment and translational acceleration were measured at the T1 and the ram acceleration and force were reported. The head COG kinematics were reported in the head local coordinate system (Figure 3.2). The acceleration and velocity data from the experiments and simulations were processed with a CFC 180 filter, while the force data was processed using a CFC 600 filter, consistent the development of the impactor model and helmet [17,43,80]. The signals from the ATD (simulated and experimental) were assessed using the recommended cross-correlation parameters in the CORA manual [133], while the corridor scoring method was not used. The shape parameter was given a weight of 0.5, and the size parameter and phase shift parameter were each given a weight of 0.25. These ratings were combined to give the overall CORA rating. An overall CORA rating of 1 indicated excellent

correspondence between the models, while a CORA rating of 0 indicated the ATD simulation and HNM results were not similar.

It has been shown [86] that the Hybrid III ATD neck is considerably stiffer than cadaveric necks in compression, which could contribute to the head response. In the current study, neck compression was measured for the HNM and the ATD simulation, which was defined as the overall change in length of the neck, measured along the arc of the cervical spine. Additionally, head response metrics including HIC, BrIC and HIP were measured for the ATD and HNM.

Maximum Principal Strain (MPS) and Cumulative Strain Damage Measure (CSDM) were calculated from the brain model, using logarithmic strain [109]. When considering the full brain MPS, only regions of brain tissue were considered, excluding the meninges, the bridging veins and CSF. All of the tissues considered as the full brain were split into 8 brain regions (Figure 2.18). In addition to calculating whole brain values for strain metrics, 3 brain regions were considered in the current study (corpus callosum, thalamus, midbrain), that have been most often correlated with the occurrence of concussion.

When calculating MPS, the 95th percentile value from each brain region was reported, and the 95th percentile value of the whole brain was considered to be the highest 95th percentile strain of any brain tissue region, to avoid the possibility of the whole-brain MPS being lower than the regional MPS. In addition to MPS, Cumulative Strain Damage Measure (CSDM) was calculated for all the simulations, which is a measure of the proportion of elements that have exceed a certain level of strain over the course of the entire impact, varying from 0 (no elements) to 1 (all elements). The value of CSDM increases monotonically over time when the brain is undergoing tensile stretch, and remains constant under other loading conditions [145]. A strain threshold of 0.15 was used to calculate CSDM, and in addition to the whole brain, CSDM was calculated for the corpus callosum, the thalamus and the midbrain regions. The time history of both MPS and CSDM was reported, similar to previous FE studies of the brain [26,40]. Reporting the time history of MPS and CSDM will serve to highlight differences in the brain responses, which may depend on the length of the time interval considered [90].

4. FE Model Verification

All models used in this thesis, including the ATD linear impactor test, the Xenith X2e helmet, and the HNM have been previously validated against experimental data. To ensure that all previously existing models behaved as expected, the model responses were verified against the available experimental data, and the previously measured simulation response.

4.1. Verification of Hybrid III ATD and Helmet Models

4.1.1. Verification Test Cases for Helmeted and Bare Head ATD Models

To verify the ATD model, impactor model and helmet model, the simulations were assessed against the available experiments in the configurations used in this thesis. The bare head response was verified against experiments at 5.5 m/s for frontal, lateral and rear impact, while the helmeted response was verified against experiments at 5.5 m/s, 7.4 m/s, and 9.3 m/s (Figure 4.1) for all three impact orientations.



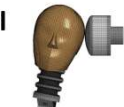





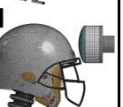
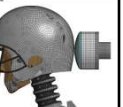
Bare Head Verification	3x Orientations	1x Impact Velocity	Helmeted Verification	3x Orientations	3x Impact Velocities
<p>ATD Simulation</p>  <p>ATD Experiment</p> 	<p>Lateral</p>  <p>Frontal</p>  <p>Rear</p> 	5.5 m/s	<p>ATD Simulation</p>  <p>ATD Experiment</p> 	<p>Lateral</p>  <p>Frontal</p>  <p>Rear</p> 	5.5 m/s 7.4 m/s 9.3 m/s

Figure 4.1 Verification cases (3x Bare Head, 9x Helmeted). Note that there were three repeat experiments completed for the bare head cases, and single experiments for the helmeted cases.

In the current study, an 80 ms delay was introduced prior to simulating the impact scenario for the HNM simulations (see Section 3.3) to allow the head to achieve equilibrium. During this time, the initial motion from the tightening of the helmet straps settled. Previously, the helmet model was validated on the ATD model with an impact occurring immediately at the start time of the simulation. In the current study, the 80 ms delay was included in the helmeted ATD simulation so that the head was in equilibrium prior to impact, as the tightening of the helmet caused some head motion initially (see Section 3.3). Additionally, lower

neck moment, lower neck force, and carriage acceleration were compared with the ATD experiment, which were not previously used for helmet validation [43].

4.1.2. Helmet and ATD Model Verification Results

The three bare-head ATD simulations (lateral, frontal and rear at 5.5 m/s) and nine helmeted ATD simulations used in this thesis were compared to the corresponding experiments using CORA. Additionally, two exemplar lateral impacts at 5.5 m/s are shown, overlaid with the original [43,146] bare-head and ATD helmeted response. The simulations of other impact orientations and speeds had similar verification outcomes when comparing the original and verification simulations. The original and verification simulations exhibited an identical response in the bare head impact, (Figure 4.2) and minor differences in the helmeted (Figure 4.3) configuration due to the 80 ms delay introduced in the verification simulation.

The bare head lateral response of the verification simulation at 5.5 m/s was in good agreement with the experiment, in terms of head Y acceleration and X angular velocity (Figure 4.2). The Y acceleration was over-predicted by the model, while the angular velocity achieved a similar peak response to the experiment. Overall, the verification simulations were in good agreement according to the objective ratings (Table 4.1) from CORA (0.83 for Y acceleration, 0.93 for angular velocity). The responses of the original and verification simulations were identical (Figure 4.2), indicating that the bare head ATD model ran as intended.

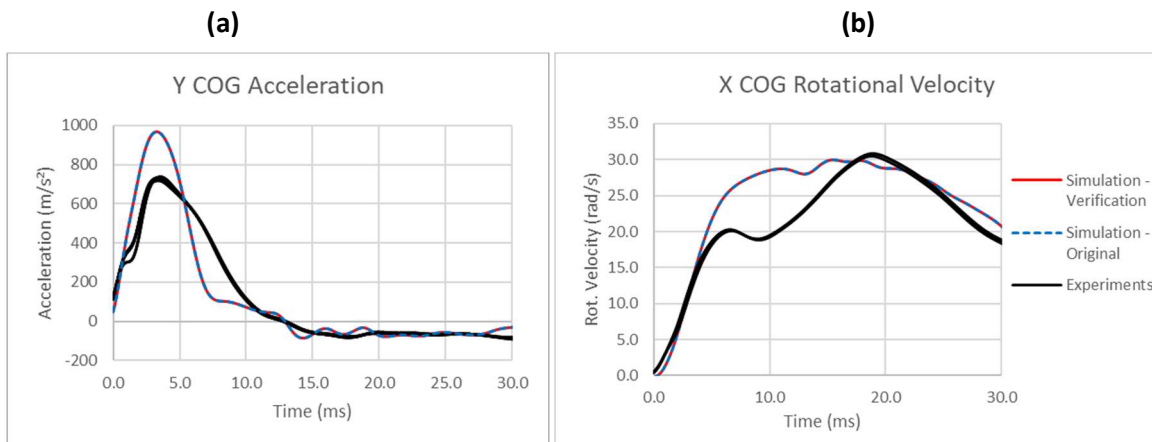


Figure 4.2 Simulated (verification and original) and experimental response of the bare head ATD in a lateral impact at 5.5 m/s (a) head Y acceleration, and (b) head X angular velocity

The overall average CORA rating (Table 4.1) for the bare-head simulation and experiment was 0.77. The rear orientation had a better correlation in the bare head test (average rating of 0.83) with the experiment than the frontal and lateral orientation (rating of 0.74 and 0.75 respectively). Overall, the primary axis head

kinematics (linear acceleration and angular velocity) were the most accurately predicted metrics by the model. The CORA ratings follow a similar trend to the original CORA ratings found during model development, with better correlation in rear impacts (Table 4.1); however, the values of the ratings differ due to the considerably different method used to calculate CORA (outlined in [146]).

	Acc. X	Acc. Y	Acc. Z	Ang. Vel. X	Ang. Vel. Y	Acc. Base	Fres Base	Mres Base	Acc. Ram	Fres Ram	Avg. Verif	Avg. Orig.
Lateral 5.5 m/s	-	0.83	0.72	0.93	-	0.73	0.53	0.71	0.74	0.79	0.75	0.85
Repeat 1	-	0.82	0.71	0.93	-	0.75	0.60	0.71	0.74	0.79	0.76	
Repeat 2	-	0.84	0.73	0.93	-	0.73	0.42	0.72	0.75	0.80	0.74	
Repeat 3	-	0.82	0.71	0.93	-	0.70	0.57	0.71	0.74	0.79	0.75	
Frontal 5.5 m/s	0.85	-	0.49	-	0.75	0.78	-	-	0.86	0.72	0.74	0.76
Repeat 1	0.85	-	0.47	-	0.75	0.81	-	-	0.88	0.72	0.74	
Repeat 2	0.87	-	0.55	-	0.78	0.77	-	-	0.87	0.73	0.76	
Repeat 3	0.83	-	0.47	-	0.73	0.78	-	-	0.82	0.70	0.72	
Rear 5.5 m/s	0.88	-	0.78	-	0.97	0.86	0.68	0.81	0.82	0.81	0.83	0.91
Repeat 1	0.90	-	0.79	-	0.96	0.83	0.72	0.82	0.82	0.83	0.83	
Repeat 2	0.85	-	0.75	-	0.98	0.84	0.64	0.78	0.80	0.78	0.80	
Repeat 3	0.88	-	0.80	-	0.98	0.92	0.68	0.82	0.84	0.81	0.84	
Avg.	0.87	0.83	0.66	0.93	0.86	0.79	0.60	0.76	0.81	0.77	0.77	0.84

Table 4.1 CORA ratings between bare head ATD simulations and experiments

The head Y acceleration in the helmeted simulation shown (Figure 4.3) was in excellent agreement with the experiment, while the head X angular velocity was in good agreement considering the complexity of the boundary condition. The verification simulation response was nearly identical to the original simulation response (Figure 4.3) as reported during the development of the helmet [43], indicating that the 80 ms delay prior to impact had little effect on the head response.

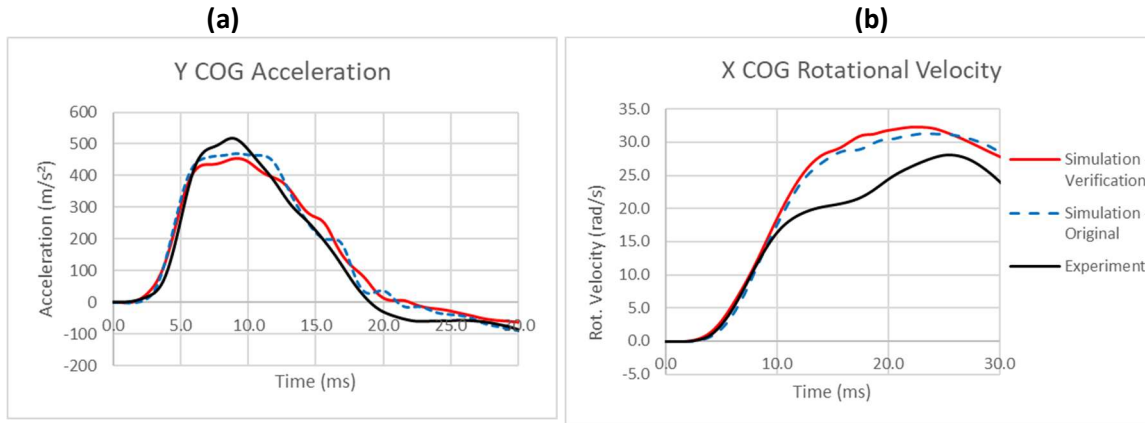


Figure 4.3 Simulated (verification and original) and experimental response of the helmeted ATD in a lateral impact at 5.5 m/s (a) head Y acceleration, and (b) head X velocity

The average CORA rating (Table 4.2) for the helmeted verification simulation and experiment was 0.81, indicating good correspondence of models and experiments. The rear and lateral impact orientation also show a better correlation with the experiment (ratings of 0.83, 0.85 respectively) than the frontal orientation (rating of 0.73). The CORA ratings from the verification simulations follow the same trends as those reported during the development of the helmet (Table 4.2), however the exact values differ due to the changes to the helmet and the different method used to calculate the CORA rating (outlined in [43]). In general, the higher speed impacts have a better correlation with the experiment, which is preferable because the impact speed of 9.3 m/s is associated with concussive impacts, while the low speed impact represents a normal hit during gameplay.

	Acc. X	Acc. Y	Acc. Z	Ang. Vel. X	Ang. Vel. Y	Acc. Base	Fres Base	Mres Base	Acc. Ram	Fres Ram	Avg. Verif	Avg. Orig.
Lateral		0.96	0.74	0.91		0.92	0.69	0.83	0.90	0.88	0.85	0.80
5.5 m/s		0.95	0.56	0.91		0.90	0.60	0.78	0.85	0.89	0.80	0.80
7.4 m/s		0.97	0.79	0.91		0.94	0.72	0.85	0.95	0.87	0.87	0.83
9.3 m/s		0.95	0.86	0.91		0.92	0.76	0.85	0.91	0.89	0.88	0.77
Frontal	0.77		0.51		0.74	0.75	-	-	0.77	0.85	0.73	0.66
5.5 m/s	0.74		0.39		0.60	0.69	-	-	0.58	0.81	0.64	0.60
7.4 m/s	0.75		0.54		0.77	0.80	-	-	0.88	0.87	0.77	0.67
9.3 m/s	0.81		0.59		0.86	0.74	-	-	0.86	0.85	0.79	0.71
Rear	0.86		0.70		0.87	0.93	-	-	0.88	0.84	0.83	0.81
5.5 m/s	0.79		0.64		0.85	0.90	0.77	0.70	0.80	0.79	0.78	0.72
7.4 m/s	0.88		0.69		0.84	0.96	0.78	0.73	0.88	0.82	0.82	0.80
9.3 m/s	0.92		0.76		0.91	0.93	0.84	0.82	0.97	0.91	0.88	0.91
Avg.	0.82	0.96	0.65	0.91	0.80	0.86	0.74	0.79	0.85	0.86	0.81	0.76

Table 4.2 CORA ratings between helmeted ATD simulations and experiments

4.2. Verification of HNM Response

The verification cases for the HNM included three sled impacts with live volunteers, and one sled test using cadavers, which were completed in previous studies [123–125]. The volunteer cases included 8g and 15g frontal crashes and a 7g lateral crash, while the cadaver test was a rear impact at 7g (Figure 4.4).

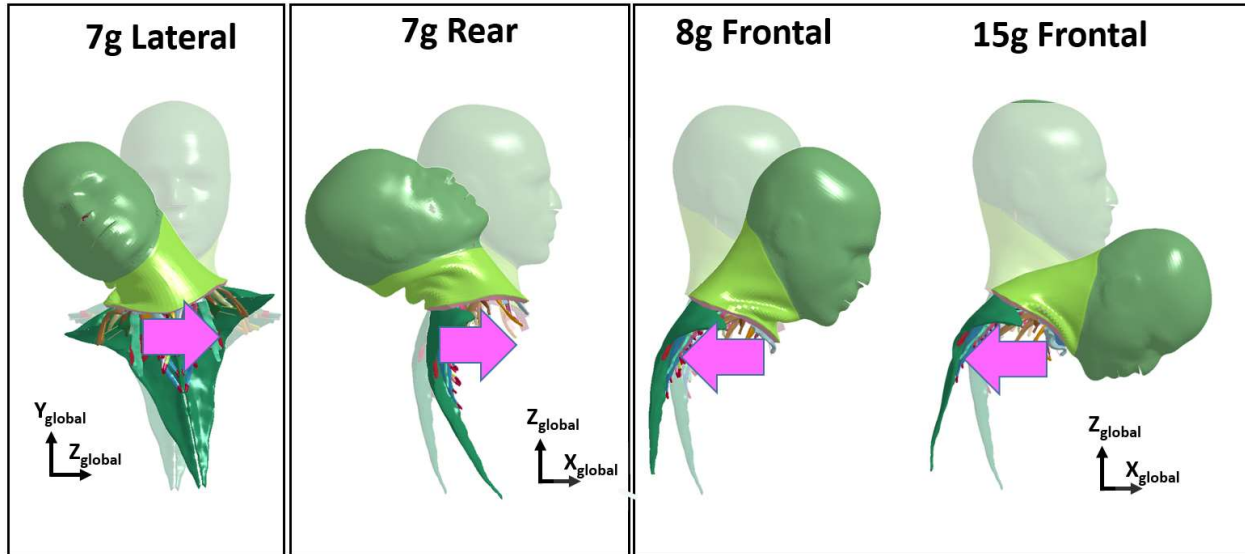


Figure 4.4 HNM verification cases (4 Total)

4.2.1. Head and Neck FE Model Boundary Conditions

For all verification cases, the boundary condition for the HNM was the average acceleration-time response at the T1 vertebra from the experiments as reported in Thunnissen et al. [124] and Ewing et al. [123]. The T1 angular and linear velocity were prescribed to the T1 in the model (Figure 4.5, Figure 4.6, Appendix A). In the frontal cases, T1 Y angular velocity and linear X velocity were prescribed, while the remaining DOF were constrained so that no motion could occur. In the rear case, the X and Z linear motion and Y angular motion were prescribed, with a fixed constraint in the other DOF. In the 7g lateral case, the Y linear acceleration and X angular velocity were prescribed, while the other DOF were fixed.

Muscle activation used the default muscle activation curve (Figure 2.20), as described by Panzer [121], which represented a 100 ms neural input, with a 74 ms delay prior to onset. In all frontal and lateral impacts, the extensor and flexor Activation Level (AL) was scaled by 1.0, which is a simplification [28]. In the rear impact, both flexor and extensor AL were set to 0.0 [29], because the 7g rear impact represented cadaveric data. In the verification simulations, the modifications outlined in Section 3.4 were retained, while the original simulation response was obtained internally from the model developers.

The output from the model was the linear and angular rotation of the head. The head COG kinematics were reported in the head global coordinate system as shown in Figure 4.4. The acceleration data from the simulations was processed with a CFC 180 filter [147].

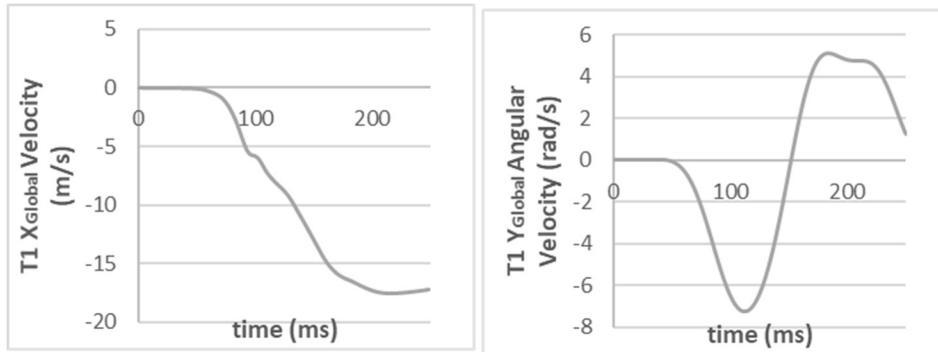


Figure 4.5 T1 boundary conditions for 15g frontal impact scenario

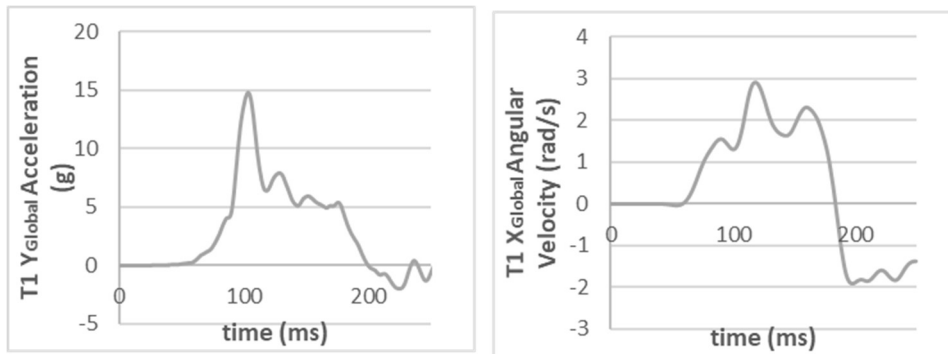


Figure 4.6 T1 boundary conditions for 7g Lateral impact scenario

4.2.2. Head and Neck Model Verification Results

In the 15g frontal case, the simulated Y COG angular acceleration of the HNM was in good agreement with the volunteer experiments, with the response falling mostly inside the tight corridor (Figure 4.7). The head X acceleration and head Z acceleration of the model were in reasonable agreement with the experiment, as they fell within one corridor of the experimental response. The first Z acceleration peak was slightly higher than the experiments, while the first X acceleration peak was slightly lower than the experiments. The peak timing was within 10 ms of the experimental peak for the three response components (Figure 4.7). The response of the verification simulation was nearly identical to the original simulation response, indicating that the changes to the model did not affect the response.

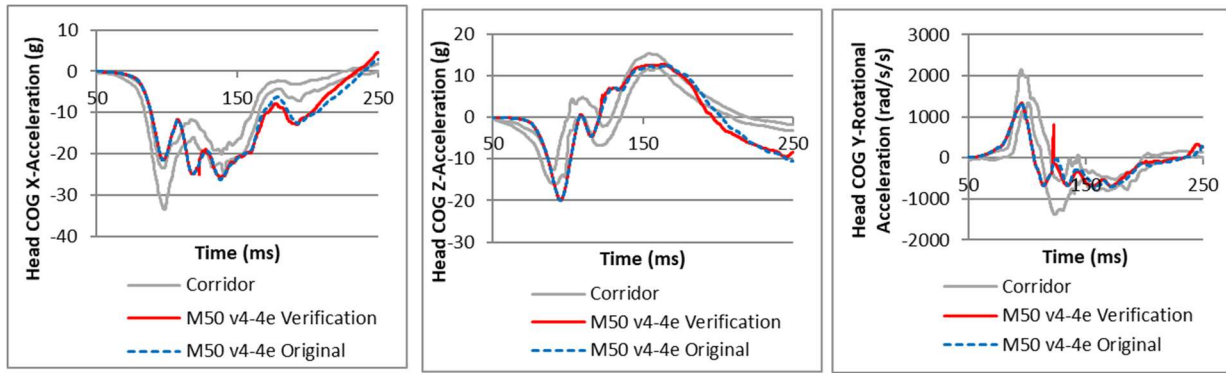


Figure 4.7 Simulated response of the HNM in a 15g frontal impact, overlaid with the corridors from the NBDL experiments

The 7g lateral response of the HNM was in good agreement with the experiment for the major acceleration components (Y, Z, X rotational) components, in terms of peak response and timing, and fell mostly within the tight corridors from the experiments (Figure 4.8). Similar to the 15g frontal case, the response of the verification simulation was in excellent correspondence with the original simulation response.

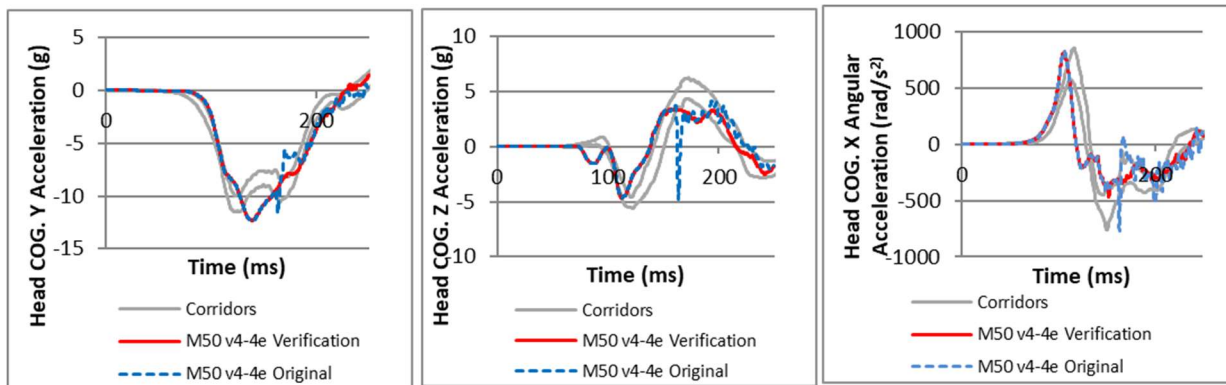






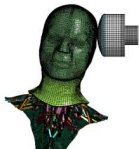
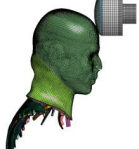
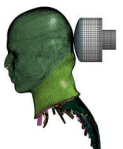
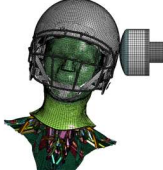
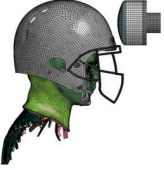
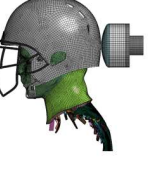


Figure 4.8 Simulated response of the HNM in a 7g lateral impact, overlaid with the corridors from the NBDL experiments

The remaining 8g Frontal and 7g Rear verification results are available in Appendix A (Figures A7 and A8), which also demonstrated good agreement with the experiments, and closely corresponded with the original recorded response of the model.

5. Study 1: Head and Neck Response of an Active Human Body Model and Finite Element Anthropometric Test Device During a Linear Impactor Helmet Test

The first objective of the current study was to compare the head kinematics of a detailed HNM to those of the Hybrid III ATD head and neck FE model using the boundary conditions of the linear impactor test (Figure 5.1). The effect of impact orientation and speed were examined for bare-head and helmeted impact scenarios. A secondary objective was to investigate the effect of active neck musculature in the HNM, by comparing a high level of muscle activation and no muscle activation in the HNM. It was hypothesized that the higher neck stiffness of the ATD compared to the HNM would affect head kinematics at long durations following the impact, but would not affect short-term head kinematics associated with current assessment criteria. The graphical results for head accelerations, angular velocity, reaction moment and impactor force are presented for lateral, frontal and rear helmeted impacts at 5.5 m/s. The remaining graphical results are presented in Appendix C. All head kinematics are stated in the head local coordinate system.

		Lateral	Frontal	Rear	
ATD Simulation	Bare Head				5.5 m/s 7.4 m/s 9.3 m/s
	Helmeted				5.5 m/s 7.4 m/s 9.3 m/s
HNM with No Muscle Activation	Bare Head				5.5 m/s 7.4 m/s 9.3 m/s
	Helmeted				5.5 m/s 7.4 m/s 9.3 m/s


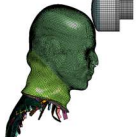
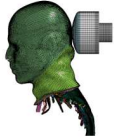

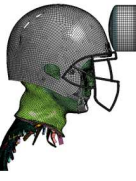
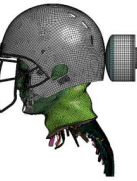
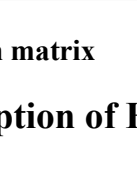


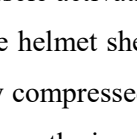
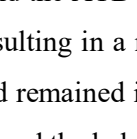
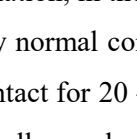
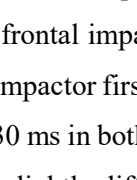
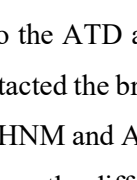
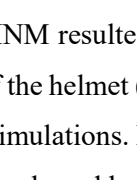
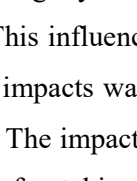
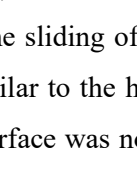
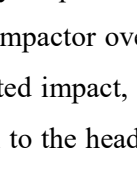
HNM with Balanced Muscle Activation	Bare Head				5.5 m/s 7.4 m/s 9.3 m/s
					
					
	Helmeted				5.5 m/s 7.4 m/s 9.3 m/s
					
					

Figure 5.1 Study 1 simulation matrix

5.1. Qualitative Description of Head Response to Impact

Considering the HNM with no muscle activation and the ATD simulation, in the lateral and rear helmeted impact, the impactor contacted the helmet shell resulting in a nearly normal contact surface (Figure 5.2). The impactor foam was uniformly compressed, and remained in contact for 20 – 30 ms depending on the impact speed. Similar sliding between the impactor and the helmet shell was observed in both the ATD and HNM simulation. In contrast, the frontal impacts to the ATD and HNM resulted in a non-normal contact surface because the bottom of the impactor first contacted the brim of the helmet (Figure 5.2). The impactor remained in contact for the entire 30 ms in both the HNM and ATD simulations. In the HNM and ATD, the initial contact of the impactor was slightly different, as the differently shaped heads of the HNM and ATD influenced the fit of the helmet. This influenced the sliding of the impactor over the front of the helmet. The progression of the bare head impacts was similar to the helmeted impact, with a similar duration of contact (Appendix B, Figure B1). The impactor surface was normal to the head surface in the lateral and rear impact, and non-normal in the frontal impact.

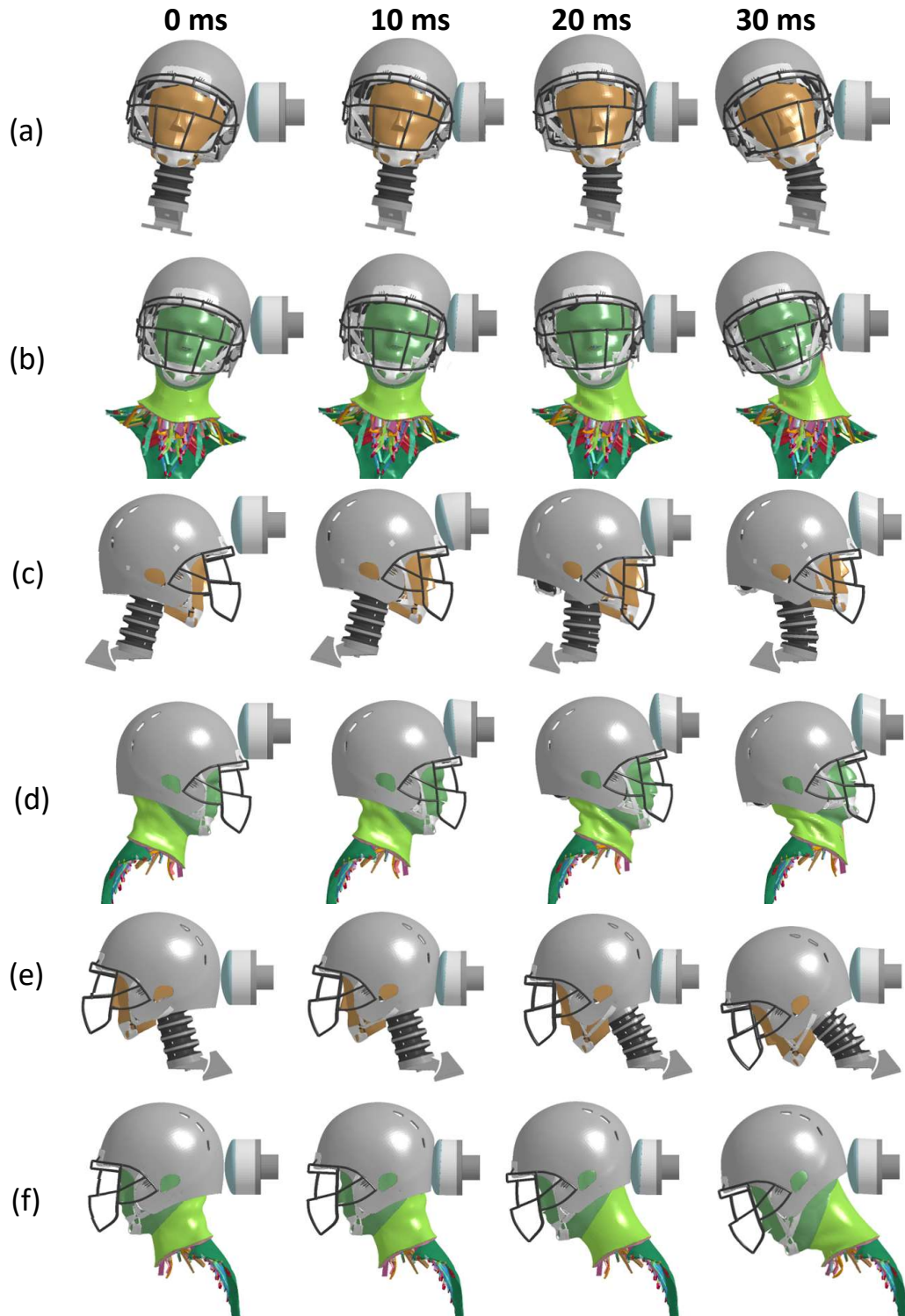


Figure 5.2 Progression of helmeted impacts: (a) ATD simulation, lateral 5.5 m/s, (b) HNM w. no activation, lateral 5.5 m/s, (c) ATD simulation, frontal 5.5 m/s, (d) HNM w. no activation, frontal 5.5 m/s, (e) ATD simulation, rear 5.5 m/s, (f) HNM w. no activation, rear 5.5 m/s

5.2. Results – Kinematic and Kinetic Response of Head and Neck

The graphical results for head accelerations, angular velocity, reaction moment and impactor force are presented for lateral, frontal and rear helmeted impacts at an impact speed of 5.5 m/s (Figure 5.3). The complete graphical results are presented in the Appendix C (Figure C1). All head kinematics are stated in the head local coordinate system. In this section, all cross-correlation (CORA) values were calculated comparing the response of the ATD simulation to the HNM, therefore a CORA value of 1 indicated excellent correspondence between the models, while a CORA value of 0 indicated the ATD simulation and HNM results were not similar.

5.2.1. Comparison of the ATD FE Model to the HNM with No Activation

Overall, the ATD simulation response was similar to the response of the HNM with no activation. The acceleration in the primary direction of impact (y direction for lateral orientation, X direction for frontal and rear orientation) was similar between the ATD and HNM impacts, with an overall average CORA rating of 0.89 for the bare head cases, and 0.90 for the helmeted cases (Table 5.1). The angular velocity in the primary direction was also similar for the HNM and the ATD (average of 0.88 in the bare head cases, 0.85 for the helmeted cases). In contrast, acceleration in the Z direction was not similar between the ATD and HNM, with an overall average rating of 0.43 for the bare-head cases, and 0.42 for the helmeted cases. In general, the CORA ratings were higher for the bare head cases than the helmeted cases. The ATD and the HNM ratings indicated a higher degree of correspondence in the lateral orientation compared to the frontal and rear orientations, with all CORA ratings exceeding 0.82 (except Z acceleration) in both the bare-head and helmeted cases in the lateral orientation.

Configuration	Orientation	Speed	Head COG					T1		Impactor		
			Acc. X	Acc. Y	Acc. Z	Ang. Vel. X	Ang. Vel. Y	Acc.	M _{res}	Acc.	F _{res}	
Bare Head	Lateral	5.5 m/s	-	0.93	0.46	0.97	-	0.79	0.84	0.87	0.97	
		7.4 m/s	-	0.93	0.52	0.95	-	0.84	0.83	0.88	0.96	
		9.3 m/s	-	0.93	0.56	0.94	-	0.87	0.79	0.92	0.96	
		Average	-	0.93	0.51	0.95	-	0.83	0.82	0.89	0.96	
	Frontal	5.5 m/s	0.92	-	0.33	-	0.81	0.69	0.28	0.83	0.81	
		7.4 m/s	0.84	-	0.38	-	0.82	0.64	0.57	0.73	0.81	
		9.3 m/s	0.69	-	0.47	-	0.83	0.47	0.54	0.58	0.65	
		Average	0.82	-	0.39	-	0.82	0.6	0.46	0.71	0.76	
	Rear	5.5 m/s	0.93	-	0.33	-	0.88	0.58	0.50	0.85	0.96	
		7.4 m/s	0.93	-	0.39	-	0.87	0.64	0.47	0.86	0.96	
		9.3 m/s	0.95	-	0.46	-	0.85	0.72	0.45	0.90	0.95	
		Average	0.94	-	0.39	-	0.87	0.65	0.47	0.87	0.96	
	Average			0.89		0.43	0.88		0.69	0.59	0.82	0.89
	Helmet	Lateral	5.5 m/s	-	0.96	0.49	0.93	-	0.94	0.82	0.95	0.98
			7.4 m/s	-	0.96	0.52	0.93	-	0.98	0.82	0.95	0.99
9.3 m/s			-	0.95	0.50	0.94	-	0.96	0.82	0.97	0.98	
Average			-	0.96	0.50	0.93	-	0.96	0.82	0.95	0.98	
Frontal		5.5 m/s	0.89	-	0.36	-	0.82	0.74	0.47	0.84	0.96	
		7.4 m/s	0.8	-	0.38	-	0.72	0.70	0.53	0.65	0.63	
		9.3 m/s	0.78	-	0.44	-	0.75	0.61	0.58	0.67	0.67	
		Average	0.82	-	0.40	-	0.76	0.68	0.53	0.72	0.75	
Rear		5.5 m/s	0.88	-	0.36	-	0.88	0.88	0.51	0.96	0.97	
		7.4 m/s	0.93	-	0.34	-	0.84	0.88	0.47	0.94	0.97	
		9.3 m/s	0.96	-	0.35	-	0.84	0.80	0.48	0.91	0.96	
		Average	0.93	-	0.35	-	0.85	0.85	0.49	0.93	0.97	
Average			0.90		0.42	0.85		0.83	0.61	0.87	0.90	

Table 5.1 CORA ratings between HNM simulations and ATD simulations with no activation

As expected, the head accelerations and angular velocities increased with increasing impact speed in all impact scenarios. Peak acceleration in the primary impact direction occurred at approximately 4 ms after initial contact for the bare-head cases (see Appendix C, Figure C1) and at approximately 10 ms for the helmeted cases (Figure 5.3). The HNM had 10% higher peak linear acceleration of the ATD, on average.

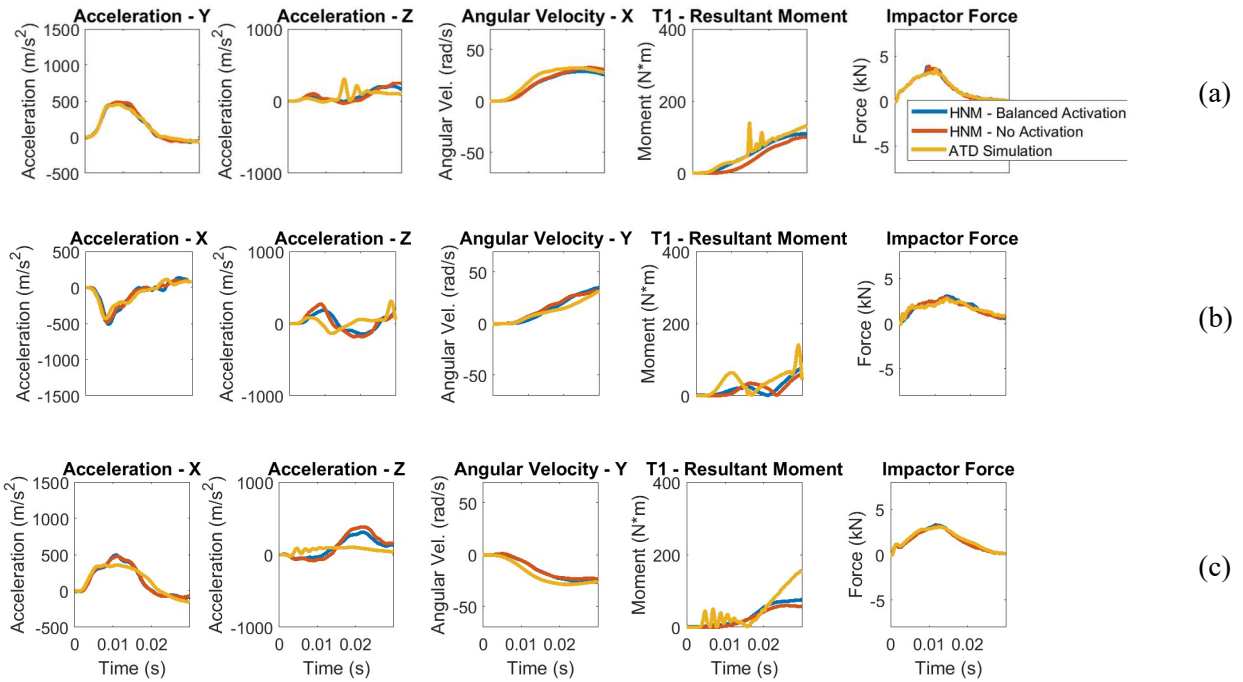


Figure 5.3 Helmeted impact kinematics, 5.5 m/s, (a) lateral, (b) frontal, (c) rear

The HNM reported higher values of HIC compared the ATD (37% , on average), while HIP was only slightly higher (11% on average) and BrIC was slightly lower (4% on average) (Table 5.2). Considering the HNM, HIC was reduced by 46% on average in the helmeted impacts compared to the bare head impacts (Table 5.2). Early kinematics governed HIC (10-15 ms) and HIP, while the peak values of angular velocity used to calculate BrIC occurred later in the simulation (25 – 30 ms).

Configuration	Orientation	Speed	HIC ₁₅ (HNM)	HNM/ATD (HIC ₁₅)	BrIC (HNM)	HNM/ATD (BrIC)	HIP (W) (HNM)	HNM/ATD (HIP)
Bare Head	Lateral	5.5 m/s	348	1.29	0.53	0.90	15651	1.16
		7.4 m/s	658	1.23	0.68	0.96	24871	1.10
		9.3 m/s	1095	1.18	0.82	0.95	38225	1.07
		Average		1.23		0.93		1.11
	Frontal	5.5 m/s	183	1.15	0.45	0.92	9716	0.79
		7.4 m/s	367	1.06	0.62	0.89	16217	0.76
		9.3 m/s	647	0.92	0.88	0.82	26442	0.56
		Average		1.04		0.88		0.93
	Rear	5.5 m/s	364	1.11	0.52	0.95	14977	0.64
		7.4 m/s	671	1.11	0.71	0.95	24489	0.67
		9.3 m/s	1133	1.05	0.75	0.79	39356	0.69
		Average		1.09		0.90		1.02
Average				1.12		0.90		1.02
Helmet	Lateral	5.5 m/s	133	1.14	0.51	1.00	8357	1.19
		7.4 m/s	264	1.09	0.64	1.01	14928	1.12
		9.3 m/s	586	1.18	0.74	1.01	26462	1.07
		Average		1.13		1.01		1.13
	Frontal	5.5 m/s	117	1.74	0.53	1.01	5250	1.27
		7.4 m/s	244	1.56	0.73	0.95	11574	1.02
		9.3 m/s	427	1.40	0.91	0.94	19465	1.05
		Average		1.57		0.96		1.11
	Rear	5.5 m/s	152	1.63	0.40	0.82	8055	1.23
		7.4 m/s	394	1.52	0.59	0.98	17588	1.04
		9.3 m/s	650	1.08	0.65	0.90	26869	0.96
		Average		1.41		0.90		1.08
Average				1.37		0.96		1.11

Table 5.2 Response Metrics of HNM: HIC, BrIC and HIP, and ratio of HNM with no activation to ATD simulation response (bold indicates average response)

The neck of HNM deformed considerably more in the axial direction (compression and tension) compared to the ATD neck (Figure 5.4); the neck of the HNM was stretched or compressed by 8 to 16 mm depending on the orientation, while the neck of the ATD stretched less than 3 mm in all impact orientations.

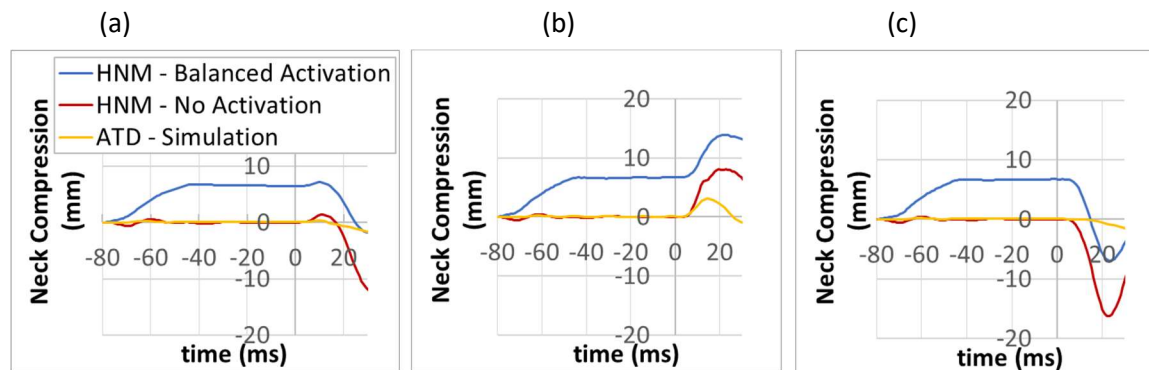


Figure 5.4 Neck compression in helmeted impact (a) lateral, (b) frontal, and (c) rear helmeted impact at 5.5 m/s

5.2.2. Comparison of the HNM with and Without Muscle Activation

Muscle activation had little influence on the HNM response, indicated by the similar CORA ratings achieved with the “no activation” condition and the “balanced activation” condition. The balanced activation condition caused the average CORA rating to increase (by 1% to 6% for all variables compared to the “no activation” condition, except the primary direction acceleration, which remained the same (Table 5.1 and Table 5.3). In the bare head cases, CORA ratings for the impactor, and head acceleration and angular velocity in the primary direction decreased by 2% to 4%, while ratings for T1 kinematics and Z acceleration increased by 3% to 5% with the balanced muscle activation scheme.

Configuration	Orientation	Speed	Head COG					T1		Impactor	
			Acc. X	Acc. Y	Acc. Z	Ang. Vel. X	Ang. Vel. Y	Acc.	M _{res}	Acc.	F _{res}
Bare Head	Lateral	5.5 m/s	-	0.91	0.60	0.94	-	0.83	0.97	0.84	0.93
		7.4 m/s	-	0.92	0.58	0.93	-	0.87	0.89	0.86	0.93
		9.3 m/s	-	0.84	0.59	0.91	-	0.92	0.81	0.80	0.85
		Average	-	0.89	0.59	0.93	-	0.87	0.89	0.83	0.90
	Frontal	5.5 m/s	0.95	-	0.35	-	0.76	0.79	0.35	0.86	0.84
		7.4 m/s	0.85	-	0.39	-	0.80	0.76	0.64	0.76	0.83
		9.3 m/s	0.67	-	0.50	-	0.83	0.56	0.59	0.55	0.65
		Average	0.82	-	0.41	-	0.80	0.70	0.53	0.72	0.77
	Rear	5.5 m/s	0.92	-	0.34	-	0.87	0.64	0.54	0.83	0.90
		7.4 m/s	0.90	-	0.39	-	0.86	0.67	0.49	0.83	0.87
		9.3 m/s	0.87	-	0.43	-	0.84	0.69	0.45	0.79	0.84
		Average	0.90	-	0.39	-	0.86	0.67	0.49	0.82	0.87
Average			0.87		0.46	0.86		0.75	0.64	0.79	0.85
Helmet	Lateral	5.5 m/s	-	0.99	0.57	0.91	-	0.87	0.92	0.96	0.98
		7.4 m/s	-	0.99	0.61	0.91	-	0.98	0.87	0.96	0.98
		9.3 m/s	-	0.97	0.59	0.93	-	0.97	0.78	0.89	0.99
		Average	-	0.98	0.59	0.92	-	0.94	0.86	0.94	0.98
	Frontal	5.5 m/s	0.84	-	0.43	-	0.89	0.77	0.61	0.91	0.94
		7.4 m/s	0.77	-	0.41	-	0.85	0.75	0.69	0.81	0.64
		9.3 m/s	0.78	-	0.48	-	0.85	0.70	0.68	0.70	0.79
		Average	0.79	-	0.44	-	0.86	0.74	0.66	0.81	0.79
	Rear	5.5 m/s	0.88	-	0.42	-	0.88	0.94	0.53	0.93	0.97
		7.4 m/s	0.93	-	0.37	-	0.85	0.88	0.48	0.95	0.98
		9.3 m/s	0.96	-	0.37	-	0.85	0.83	0.47	0.93	0.97
		Average	0.93	-	0.39	-	0.86	0.88	0.49	0.93	0.97
Average			0.90		0.47	0.88		0.85	0.67	0.89	0.91

Table 5.3 CORA ratings between HNM simulations and ATD simulations with balanced activation

When comparing the HNM with balanced activation and the HNM with no activation, the former reported 5% lower values of HIC, 3% higher values of BrIC and 2% lower values of HIP on average (Table 5.2 and Table 5.4). Interestingly, the HNM with balanced activation reported a higher value of BrIC in the rear and frontal orientations for both the bare head cases (average of 4% and 2% higher respectively), and the helmeted cases (average of 13% and 6% higher, respectively). In the lateral orientation, BrIC was reduced with balanced activation in the bare head (average of 5% lower) and helmeted cases (average of 3% lower),

when compared to the HNM with no activation. The largest changes in BrIC due to muscle activation were observed in the lowest severity impacts; in the helmeted impacts at 5.5 m/s, BrIC was reduced by 6% compared to the “no activation” condition, while BrIC increased by 11% in the frontal orientation and 15% in the rear orientation.

Configuration	Orientation	Speed	HIC ₁₅ (HNM)	HNM/ATD (HIC ₁₅)	BrIC (HNM)	HNM/ATD (BrIC)	HIP (W) (HNM)	HNM/ATD (HIP)	
Bare Head	Lateral	5.5 m/s	342	1.26	0.50	0.85	15350	1.13	
		7.4 m/s	644	1.21	0.65	0.91	24353	1.08	
		9.3 m/s	1085	1.17	0.78	0.91	37936	1.06	
			Average		1.21		0.89		1.09
	Frontal	5.5 m/s	180	1.13	0.49	1.00	9719	0.79	
		7.4 m/s	362	1.04	0.62	0.89	16208	0.76	
		9.3 m/s	627	0.89	0.86	0.81	25777	0.56	
			Average		1.02		0.90		0.93
	Rear	5.5 m/s	352	1.07	0.52	0.96	14692	0.64	
		7.4 m/s	649	1.07	0.69	0.92	23840	0.67	
		9.3 m/s	1098	1.02	0.85	0.89	38164	0.69	
			Average		1.05		0.92		0.99
Average				1.10		0.90		1.00	
Helmet	Lateral	5.5 m/s	112	0.96	0.48	0.95	6944	0.99	
		7.4 m/s	225	0.93	0.62	0.98	12957	0.97	
		9.3 m/s	550	1.11	0.73	0.99	25493	1.03	
			Average		1.00		0.97		1.00
	Frontal	5.5 m/s	106	1.57	0.59	1.11	5677	0.79	
		7.4 m/s	237	1.51	0.76	0.99	11963	0.76	
		9.3 m/s	434	1.42	0.93	0.96	20776	0.56	
			Average		1.50		1.02		1.18
	Rear	5.5 m/s	124	1.33	0.46	0.94	7748	0.64	
		7.4 m/s	347	1.34	0.63	1.04	17126	0.67	
		9.3 m/s	672	1.12	0.76	1.06	25685	0.69	
			Average		1.26		1.01		1.04
Average				1.25		1.00		1.07	

Table 5.4 Response Metrics of HNM: HIC, BrIC and HIP, and ratio of HNM with balanced activation compared to ATD simulation response (bold indicates average response)

Considering neck compression, the neck of the HNM with balanced activation was compressed 7 mm by the activation of the muscles, prior to the onset of impact (Figure 5.4). There was 10 – 20% smaller change in neck compression after the onset of impact in the helmeted impacts with balanced activation compared to the HNM with no activation. The 1D muscle force in the Trapezius and Sternocleidomastoid after impact are presented in Appendix C.

5.3. Discussion – Kinematic and Kinetic Response of Head and Neck

5.3.1. Comparison of the ATD and HNM Head and Neck Kinematics

Overall, the head acceleration in the primary direction from the ATD simulation was similar to that of the HNM with no activation and in all cases, the acceleration peak in the primary direction for the head COG occurred early in time. In all cases, the applied moment about T1, which is found by multiplying impactor force by the perpendicular distance to T1, ranged from 500 – 1500 Nm for the first 8 ms of contact. For the HNM, the measured reaction moment at T1 (Figure 5.3, Appendix C, Figure C1) was always at least 20x lower than the applied moment about T1 during the first 8 ms, and in the ATD simulation the reaction moment at T1 was always at least 6x lower. The considerably lower reaction moment demonstrates that, while the impactor was in contact with the head, the bending stiffness of the neck had little influence on the early kinematics. Since the impact force applied a larger moment than could be resisted by the neck, the mass and local stiffness at the contact site were the main contributors to the early kinematic response. Most of the acceleration peaks occurred during this time, and the angular velocity reached a value near its peak while the impactor was in contact. Comparing the helmeted and bare head cases, the helmeted impacts of the HNM were typically better correlated with the ATD simulation than the bare-head HNM, as indicated by higher CORA ratings. The HNM and ATD helmeted simulations had the same local stiffness properties at the impact site. Conversely, the bare-head HNM and ATD had different soft tissue properties at the location of the impact, resulting in different behavior; the HNM included a biofidelic skin and flesh model while the ATD had a rubber skin covering a metal skull structure.

In contrast with the kinematics in the primary direction, large differences in the Z-axis head acceleration of the HNM and ATD were observed, with the HNM exhibiting higher values. This was caused by the higher axial compliance of the HNM neck, compared to the rubber and metal components in the ATD neck. However, this difference did not contribute to large differences in assessment criteria (HIC, BRIC, HIP) because the peak magnitude of the Z acceleration was less than half that of the X acceleration in all HNM impacts. The differences in axial neck compression (Figure 5.4) should be considered in future studies with impacts directed along the neck. In this study, the neck angle was 15 degrees from horizontal, so the majority of the head acceleration was not transmitted axially along the neck. In future studies, especially reconstructions with a striking and struck human surrogate, it will be important to consider the difference in compressive stiffness of the neck between the ATD and HNMs.

The HNM behaved most similarly to the ATD head and neck in the lateral and rear orientation, while it behaved less similarly in the frontal impact. The lateral and rear orientations had impact vectors normal to

the struck surface (helmet or head), resulting in minimal sliding during the initial impact in both the ATD and HNM simulation, and subsequently, similar helmet motion. In contrast, the frontal impact exhibited more sliding at the contact surface, in part due to the forward-angled neck and corresponding highly non-normal impact vector. In the bare head impact, the differences in head shape and neck compliance between the ATD and HNM influenced how the impactor first stuck, then slid over the head. In the helmeted frontal impact, the impactor slid over the front edge of the helmet differently in the HNM simulation, compared to the ATD simulation, because the helmet sat slightly differently on the ATD and HNM due to head shape. Post et al. [20] also noted that small changes in helmet geometry at the contact surface had a large influence on helmet motion, and this could be related to the impactor interaction with the helmet. In general, the frontal orientation experienced lower head accelerations. This was thought to be caused by the frontal impact vector acting further from the head COG compared to the lateral and rear impact vectors, which were very close to the head COG.

The lower accelerations experienced in the frontal impacts of the ATD and HNM, compared to the lateral and rear orientations, could potentially be explained by the deformation of the impactor foam. Only the bottom edge of the impactor was compressed in the frontal bare head impact, and less localized foam deformation was observed in the frontal helmeted impact, but still not as much as in the rear and lateral impacts where the foam was uniformly compressed at the time of peak acceleration. This offset foam deformation resulted in a more compliant impacting surface that allowed more displacement, which spread the impact out over a longer period of time. This explanation was supported by the wider, flatter peak in the contact force that was observed in both the bare-head and helmeted frontal impact compared to the lateral and rear impact (Figure 5.3 and Appendix C, Figure C1) and the increased time that the impactor was in contact with the head in the frontal impacts. The difference in impactor foam deformation in the bare-head case compared to the helmeted case could explain the lower effectiveness of the helmet in reducing head response metrics in this orientation. Dawson et al. [148] observed something similar, in a bare-head linear impactor test. Using a smaller impactor resulted in less than half the peak head acceleration of a larger impactor, and the smaller impactor deformed more [148]. The frontal impact was also further from the head COG than the lateral and rear impact; impacts closer to the COG have been shown to result in higher linear acceleration of the Hybrid III ATD head and neck impacts [20,21,79].

5.3.2. The Effect of Muscle Activation on Head Kinematics

The activation of the neck muscles had a very small effect on the kinematics of the head. Although the total active component of the muscle force at the time of impact was approximately 1.1 kN, this force did not result in a large change in the overall head kinematics. Considering the helmeted simulations, the reaction

moment at the T1 was only 11% – 16% higher for the HNM with balanced activation compared to the HNM with no activation, despite the large difference in muscle force. Once the contact force from the impactor had dropped later in the impact, the neck musculature then had a larger effect on the resulting kinematics, starting at 20 - 30 ms, which was after most of the peak response metrics had developed.


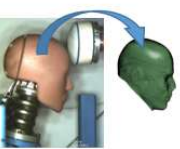


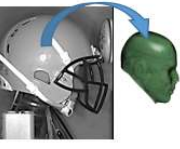
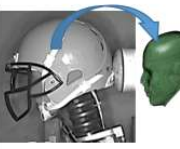
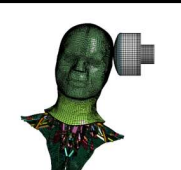
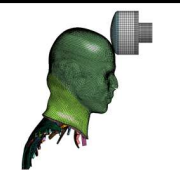
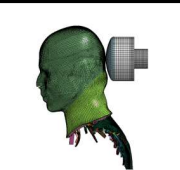
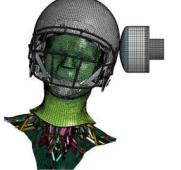
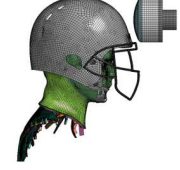
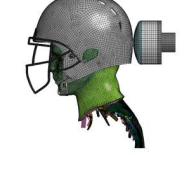
In both the bare head and helmeted cases, the CORA ratings were generally higher for the HNM with balanced activation, compared to the HNM with no activation, suggesting that the ATD was more similar to a human fully braced for impact, attributed to the stiffened neck of the HNM when the muscles are activated. The kinetics and kinematics most affected by active musculature were those measured at T1, which was furthest from the impact site, while those closest to the impact site were affected the least. Active musculature had the largest effect on the motion and moment at the T1 (differences of 4 to 6% in the CORA rating), while it had a lesser effect on the primary direction head kinematics (differences ranging from 1 to 4%), and an even smaller effect on the impactor kinematics (0 to 1% difference), on average. The small effect of balanced muscle activation on angular velocity in the current study contrasted somewhat with some of the findings of Jin et al. [25]. The Jin et al. study [25] found that adding muscle activation prior to impact resulted in a 20% reduction on the angular velocity of the head when comparing a HNM with no muscle activation and an HNM with early muscle activation. In the current study, in the helmeted lateral impact at 9.3 m/s, only a 2% decrease was observed in the angular velocity when comparing the HNM with balanced activation to the HNM with no activation. The linear kinematics of this impact were comparable to the impacts by Jin et al. [25] at 9.5 m/s when comparing translational acceleration in the y direction, with a similar peak timing (within 1 ms), value (approximately 1100 m/s²), and subsequent fall to zero (at 20 ms). A possible explanation for the difference in angular velocity reduction between the studies is that the Jin et al. [25] study used the same muscle Activation Level (AL) for the flexor and extensor muscles, which provides much more extensor force than the 0.15:1 ratio used in the current study. If unconstrained, the GHBM head would be moving backwards with a significant angular velocity if the flexor and extensor muscles were activated with the same AL curve. The results of the Jin et al. [25] study could be attributed to the head moving into a different position with the early activation scheme that was used.

Eckner et al. [115], in which volunteers were tested at non-injurious levels, found a 15% change in head angular velocity due to anticipatory muscle activation, which was a larger effect compared to the current study. The magnitude of the angular velocity in the current study was much higher (8 to 20x) than in the Eckner et al. study, indicating that the applied loading in the current study was much larger, and thus muscle activation had a smaller effect as the muscles could only exert a certain amount of force. Accordingly, in the current study, muscle activation had a larger influence on BrIC at 5.5 m/s, and would likely have a larger effect if a lower impact velocity was used. However, impact speeds of 5.5 m/s and lower do not

typically cause concussions [13,76]. Interestingly, balanced muscle activation slightly increased the peak angular velocity in the frontal and rear orientation in the current study, while peak angular velocity was decreased slightly in the lateral orientation, indicating the need to consider multiple loading directions in future assessment and optimization studies.

6. Study 2: Simulated and Experimental Boundary Conditions for a Human Head Model Comparing Brain Response in Football Helmet Impacts

The purpose of this chapter is to assess two boundary conditions for a head model: (1) the simulated impact of a helmeted HNM (“simulated HBM impact”), and (2) an isolated head model driven by experimental kinematics from an ATD impact (“prescribed kinematics”) (Figure 6.1). The model results were assessed using two brain deformation metrics: Maximum Principal Strain (MPS) of the brain and Cumulative Strain Damage Measure (CSDM) with a threshold of 0.15, which were assessed first for the whole brain, and additionally in the corpus callosum, thalamus and midbrain regions. The results derived from the ATD experimental kinematics and HNM impact simulations were compared quantitatively, in terms of time history, peak values, and peak timing of the two strain metrics. Three impact speeds (5.5 m/s, 7.4 m/s, 9.3 m/s) were investigated, in the lateral, frontal and rear impact orientations (Figure 6.1). Muscle activation was investigated in the HNM using the same muscle activation schemes as outlined in the previous chapter (“balanced activation” and “no activation”). Helmeted impacts are presented in this chapter, and the results from the bare-head impacts can be found in Appendices C, D and E.

		Lateral	Frontal	Rear	
Prescribed Kinematics	Bare Head				5.5 m/s
	Helmeted				5.5 m/s 7.4 m/s 9.3 m/s
HNM with No Muscle Activation	Bare Head				5.5 m/s 7.4 m/s 9.3 m/s
	Helmeted				5.5 m/s 7.4 m/s 9.3 m/s

HNM with Balanced Muscle Activation	Bare Head				5.5 m/s 7.4 m/s 9.3 m/s
	Helmeted				5.5 m/s 7.4 m/s 9.3 m/s

Figure 6.1 Simulation matrix, Study 2

6.1. General Description of Brain Response

6.1.1. Frontal Impact

Generally, the deformation of the brain in all frontal impacts followed a similar pattern, with the outer brain tissues rotating relative to the tissues in the middle of the brain in the sagittal plane, which induced shear in the tissue. Initially, the skull began to rotate backwards in the sagittal plane, and the outside of the cerebrum grey matter started to rotate first. The rotation of the stiffer, inner white matter of the cerebrum lagged behind the grey matter of the brain, inducing shear in the softer grey matter and the connected white matter. Regions of highest strain in the full brain occurred at the top-center of each hemisphere of the cerebrum, and also in the center of the cranial fissure, in both hemispheres. The elements in these regions first sheared in one direction, corresponding with the first peak of MPS, then sheared in the opposite direction which corresponded with the second peak of MPS (Figure 6.2).

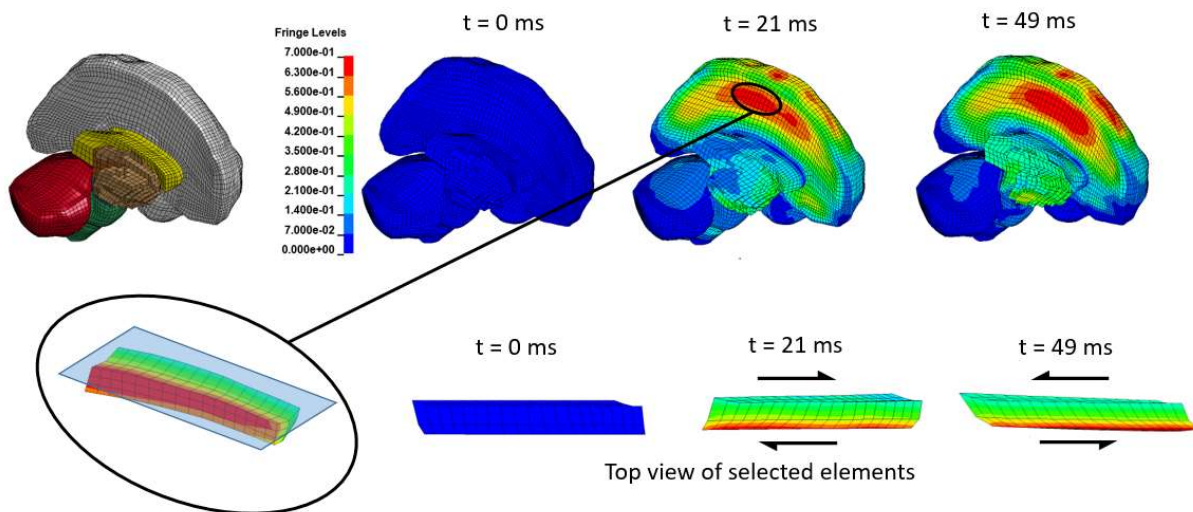


Figure 6.2 Progression of maximum principal strain in a frontal helmeted impact of the HNM (no activation) at 9.3 m/s. The visible shearing of the cerebrum grey and white matter elements in the center of the cranial fissure is highlighted.

There was also notable downward movement of the center of the thalamus and midbrain, relative to the outer cerebrum and the bottom of the brainstem, which induced some shear in the thalamus and midbrain. The outer regions of the basal ganglia moved backwards relative to the cerebrum grey matter, and the center of the corpus callosum twisted forwards in the sagittal plane relative to the outer cerebrum (Figure 6.3).

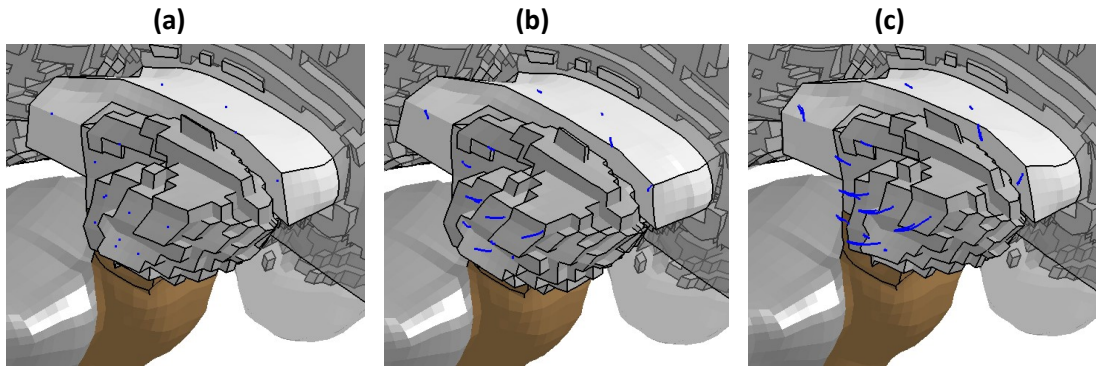


Figure 6.3 Nodal traces showing the movement of the middle of the brain in a frontal impact, relative to the cerebrum grey matter

6.1.2. Lateral Impact

In the lateral impacts, the inner white matter lagged behind the outer grey matter, inducing shear deformation that was highest at boundaries between brain structures. Initially, motion was transmitted from the skull to the outer tissues of the brain. The coronal rotation of the tissue at the center of the brain (corpus callosum and thalamus) visibly lagged the outer structures of the brain. These regions translated relative to the skull, inducing tension in one hemisphere of the cerebrum and compression in the other. Small brain tissue deformations occurred in the transverse plane of the head, and the inner tissues also lagged behind the transverse rotation of the outer brain tissues and the skull.

The locations of high strain were markedly different in the lateral impact than the frontal impact (Figure 6.4). The strain concentrated in the body of the corpus callosum in the lateral impact, and at the outer boundary between the grey matter and the white matter at the most lateral aspect of both cerebral hemispheres. In the lateral impact, the corpus callosum, thalamus, and midbrain rotated predominantly in the coronal plane while in the frontal and rear impact, these brain regions rotated in the sagittal plane. The space between the hemispheres of the brain was visibly curved in the coronal plane view of the brain in the

lateral impact and the corpus callosum was visibly sheared compared to the frontal impact (Figure 6.4). The direction of this curvature reversed later in time, corresponding with the second peak of MPS (Figure 6.6).

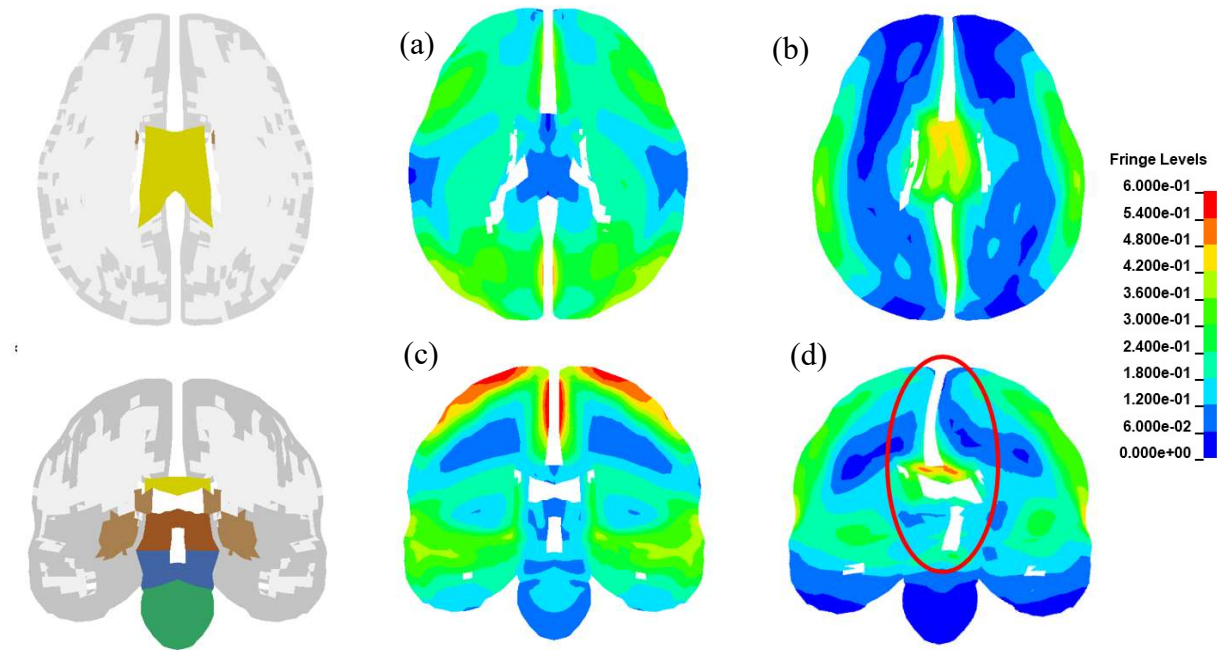


Figure 6.4 Maximum Principal Strain of the brain, at the time of peak deformation in a simulated 9.3 m/s impact of the HNM with No Activation. (a) Frontal orientation, transverse plane, (b) lateral orientation, transverse plane, (c) frontal orientation, coronal plane, (d) lateral orientation, coronal plane.

6.1.3. Rear Impact

The rear impacts created a nearly identical pattern of brain deformation to the frontal impact, with peak strains occurring in the same locations in all rear and frontal simulations; in the mid cerebrum at the uppermost surface of each hemisphere of the cerebrum, and also in the center of the cranial fissure in each hemisphere (Figure 6.5). Intuitively, the shear deformation of in the cranial fissure initially occurred in the opposite direction as that in the frontal impact, then reversed later in time, corresponding with the second peak strain peak (Figure 6.5). The magnitude of strain was considerably lower in all rear impacts of the HNM, compared to the frontal impact.

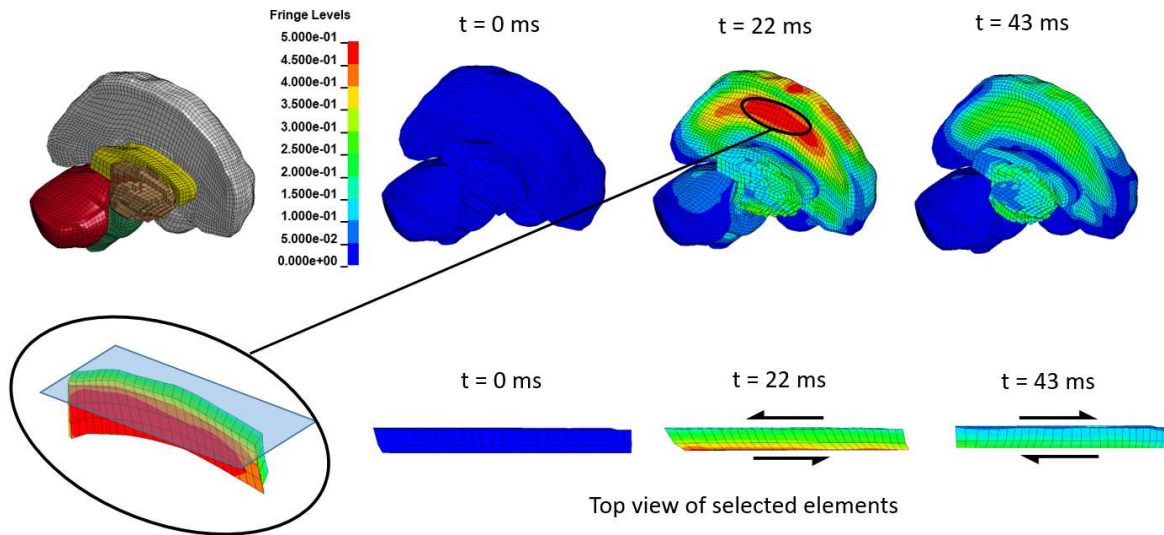


Figure 6.5 Progression of maximum principal strain in a rear helmeted impact of the HNM (no activation) at 9.3 m/s.

6.2. Results - Comparison of Simulated Impact and Prescribed Kinematics

The HNM with no muscle activation was first compared to the head model driven by experimental kinematics (“Prescribed Kinematics” approach).

6.2.1. Whole Brain Maximum Principal Strain

In most of the brain regions, with both the prescribed kinematics approach and the simulated HNM impact, the 95th percentile MPS had two distinct peaks (Figure 6.6), which each corresponded with a maximum shear deformation in two opposite directions. The first peak occurred between 15 and 32 ms, and the second peak occurred between 40 and 60 ms. In the lateral impacts, the time between peaks was typically shorter than in the frontal and rear (sagittal plane) impacts. While the patterns of brain deformation were similar, the simulated HNM impact exhibited predominantly higher values of whole brain MPS (-1% to 43%, average of 23%) than the prescribed kinematics approach (Table 6.1), most notably in the frontal impact, where higher values of angular velocity were observed. No clear trend was observed in whole brain MPS when comparing sagittal plane (frontal and rear) to coronal plane (lateral) impacts. Considering the prescribed kinematics approach in the 9.3 m/s impacts, the first peak for whole brain MPS occurred at a similar time to the HNM in the lateral impact (within 1 ms), 6 ms later in the frontal impact and 6 ms earlier in the rear impact (Table 6.1). In terms of timing, the maximum value of 95th percentile MPS typically occurred before the maximum angular velocity (Table 6.1 and Table 6.3). In most simulations, the first peak of MPS was the highest value of MPS, however in some simulations the second peak was higher (HNM, frontal, 5.5 m/s and Prescribed Kinematics, rear, 9.3 m/s).

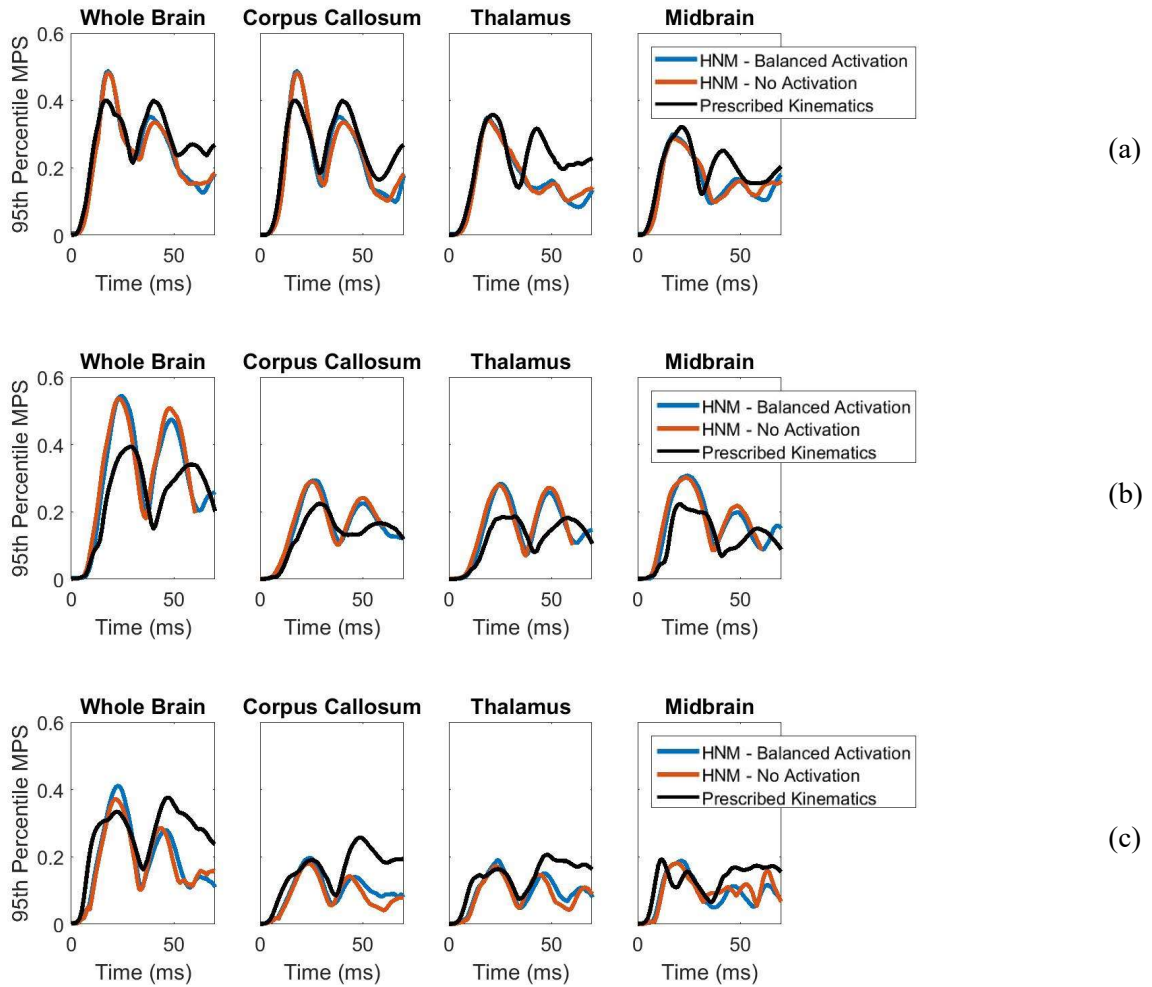


Figure 6.6 9.3 m/s impact, 95th percentile MPS in the (a) lateral orientation, (b) frontal orientation, (c) rear orientation

Orientation	Speed	95th Percentile MPS			95th Percentile MPS – Time of Max. Value		
		HNM - Balanced Activation	HNM - No Activation	Prescribed Kinematics	HNM - Balanced Activation	HNM - No Activation	Prescribed Kinematics
Lateral	5.5 m/s	0.33	0.33	0.28	21	22	18
	9.3 m/s	0.49	0.48	0.40	18	18	17
Frontal	5.5 m/s	0.34	0.32	0.22	54	53	32
	9.3 m/s	0.54	0.54	0.39	24	23	29
Rear	5.5 m/s	0.26	0.25	0.20	22	23	18
	9.3 m/s	0.41	0.37	0.38	23	21	47

Table 6.1 MPS peak values and timing for the whole brain (darker red boxes indicate higher peak values, while darker green values indicate earlier peak values)

6.2.2. Whole Brain Cumulative Strain Damage Measure

CSDM varied more than MPS when considering the prescribed kinematics and simulated impact approaches, with differences ranging from -25% to +187% observed (Table 6.2 and Table 6.3). Interestingly, the maximum value of CSDM for the whole brain always developed after 44 ms in the simulation (Table 6.2), after peak angular velocity occurred (Table 6.3). The increases in whole brain CSDM after 40 ms were generally not large, with only one simulation exhibiting a change higher than 0.1 (rear 9.3 m/s, prescribed kinematics) after this time.

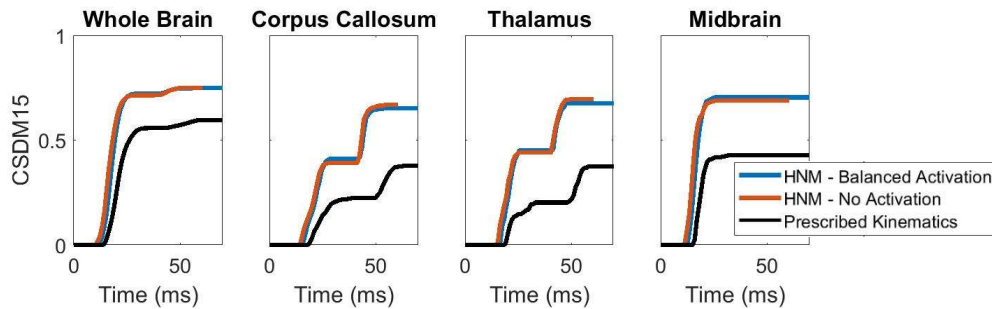


Figure 6.7 9.3 m/s impact, CSDM15 in the frontal orientation

Orientation	Speed	CSDM15			CSDM15 – Time of Max. Value		
		HNM - Balanced Activation	HNM - No Activation	Prescribed Kinematics	HNM - Balanced Activation	HNM - No Activation	Prescribed Kinematics
Lateral	5.5 m/s	0.18	0.17	0.13	55	59	44
	9.3 m/s	0.47	0.46	0.61	48	56	67
Frontal	5.5 m/s	0.48	0.41	0.14	56	55	68
	9.3 m/s	0.75	0.75	0.59	68	52	58
Rear	5.5 m/s	0.23	0.19	0.09	48	44	70
	9.3 m/s	0.58	0.52	0.58	47	45	64

Table 6.2 CSDM15 peak values and timing for the whole brain (darker red boxes indicate higher peak values, while darker green values indicate earlier peak values)

Orientation	Speed	Resultant Angular Velocity			Resultant Angular Velocity - Time of Max. Value		
		HNM - Balanced Activation	HNM - No Activation	Prescribed Kinematics	HNM - Balanced Activation	HNM - No Activation	Prescribed Kinematics
Lateral	5.5 m/s	29.9	32.5	29.7	23	26	25
	9.3 m/s	44.6	46.1	48.8	24	26	21
Frontal	5.5 m/s	34.4	31.3	22.0	30	30	50
	9.3 m/s	54.5	52.6	41.5	27	26	31
Rear	5.5 m/s	25.4	23.3	23.5	25	24	38
	9.3 m/s	40.1	37.9	40.6	23	53	24

Table 6.3 Angular velocity peak values and timing for the whole brain (darker red boxes indicate higher peak values, while darker green values indicate earlier peak values)

6.2.3. Regional Brain Response

In the sagittal plane impacts (frontal and rear), MPS was consistently lower in the corpus callosum, thalamus and midbrain when compared to the lateral impact. In the simulated lateral impacts of the HNM at 9.3 m/s, the peak MPS in the corpus callosum was always equal to the whole brain MPS, while the MPS in the thalamus and midbrain were 71% of the whole brain MPS, and 60% of the whole brain MPS respectively (Figure 6.8). Using the prescribed kinematics approach, the MPS in the corpus callosum was equal to the full brain MPS as well, while the MPS in the thalamus was 89% of the whole brain MPS and the MPS in the midbrain was 80% of the full brain MPS. In contrast, in the frontal and rear impacts, the MPS in the inner brain regions was 51% of the whole brain MPS on average for the simulated HNM impact (ranging from 48 to 56%), and 56% on average for the prescribed kinematics approach (ranging from 47 to 69% of the whole brain MPS). In spite of the higher variability of CSDM, all lateral impacts had consistently higher values of CSDM in the inner regions of the brain than frontal and rear impacts (Appendix D). Notably, CSDM in certain brain regions had larger increases (up to 0.2) than whole brain CSDM after 40 ms; for example in the corpus callosum and thalamus in the Frontal impact at 9.3 m/s (Figure 6.7).

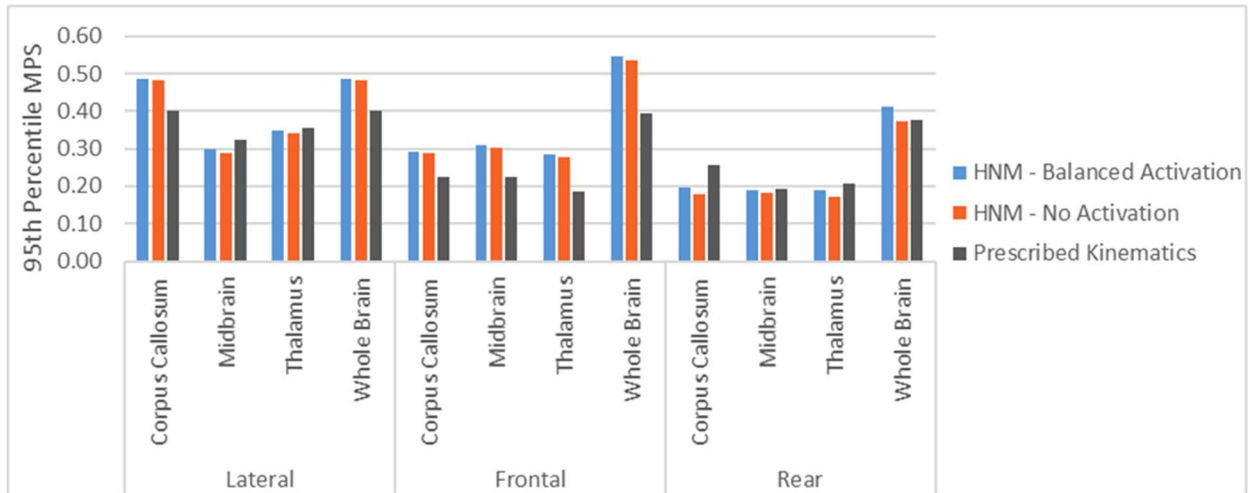


Figure 6.8 9.3 m/s impact, maximum value of 95th percentile MPS in each brain region across impact orientations

6.2.4. Effect of Balanced Muscle Activation

Overall, very small increases in peak whole brain MPS were observed with balanced muscle activation (1 to 10%) compared to the HNM with no activation (Table 6.1). The increase in MPS was smaller in the lateral orientation (1% in both the 5.5 and 9.3 m/s impact). Generally, the first MPS peak occurred at the same time (within 2 ms) in all HNM simulations. CSDM (Table 6.2) exhibited larger increases than MPS, but these were still small (0 to 19%).

6.3. Discussion - Simulated Impact and Prescribed Kinematics Approach

The primary objective of the current study was to compare two methodologies of assessing brain deformation: (1) prescribing kinematics from an ATD experiment to a FE brain model (“Prescribed Kinematics” approach), and (2) simulating the entire impact using a HNM with two muscle activation schemes (“Simulated HNM Impact” approach). Two brain deformation metrics (MPS and CSDM) were investigated for the whole brain, and selected regions of the brain that are associated with concussion.

6.3.1. Comparison of Prescribed Kinematics Approach and Simulated HNM Impacts

The “Prescribed Kinematics” approach generally predicted lower values of whole brain MPS than the “Simulated HNM Impact” approach. The largest differences in whole brain MPS were observed in the frontal impact, where the sagittal angular velocity exhibited larger differences between the two

methodologies. It has been previously shown that in the frontal orientation, the impactor foam can experience complex deformation and sliding [44], which is sensitive to small changes at the contact surface [Bruneau 2019]. Frontal impacts occurring predominantly in the sagittal plane have been shown to result in more widely varying angular kinematic responses than other orientations, with variations up to a factor of 3 in head angular acceleration observed between helmet models [111] in a previous study. Differences in peak timing of MPS between the two methodologies in the current study could be attributed to the helmet fit on the surrogate, with the helmet sitting forward on the HNM head with a slight gap at the front, and a different fit on the ATD head. The fit in the lateral orientation is similar, which could explain the similar peak timing observed in this orientation.

The current study found that the peak value of MPS often, but not always, developed before 40 ms, but the CSDM maximum value always occurred later in time. With both methodologies, the strains in the whole brain exhibited a response with two peaks, with each peak corresponding with shear deformation in opposite directions. Although the first peak was usually the maximum value of MPS, the late peak was sometimes higher than the early peak in the rear and frontal impacts. CSDM always reached maximum values after 40 ms, despite many previous studies considering only a 30 – 40 ms interval after impact [90]. While the increase in CSDM after 40 ms was often very small, CSDM doubled in some brain regions after 40 ms (Figure 6.7). These results reinforce the assertion made by Sanchez et al. [90] that considering brain deformation after 40 ms is important when simulating the brain in using kinematics from impact reconstructions [90]. The shorter interval used in previous studies could partially explain the weaker correlation of CSDM with observed concussions, in addition to the known sensitivity to the chosen threshold. The current study also suggests that CSDM is more sensitive than MPS to small differences in head kinematics, for example in the rear impact at 9.3 m/s, where strain in the corpus callosum and thalamus both varied by 50% while the angular velocity varied by 17%. The high sensitivity to small differences in input kinematics is a potential explanation for the lower correlation of CSDM with concussion than MPS [35,36,40,56].

The relative magnitudes of MPS between the lateral orientation and frontal orientation predicted using the prescribed kinematics approach in the current study fell within the range observed by Elkin et al. [21], using similar experiments and the same brain model. The lateral impact in the current study exhibited 25% higher MPS than in the frontal impact at 5.5 m/s (Elkin et al.[21] observed 29% higher MPS), and less discrepancy (1%) between whole brain MPS in the frontal and lateral impact at 9.3 m/s (Elkin et al. [21] observed 7%). However, differences in the magnitude of whole brain MPS were noted when comparing the frontal and rear orientation; the current study had higher full brain MPS in the frontal impact than the rear impact (13% and 5% higher at 5.5 and 9.3 m/s respectively), while the reverse was true in that study (31% and 7% lower

at 5.5 and 9.3 m/s respectively). The difference in the magnitude of MPS in frontal and rear impacts in the current study could be potentially explained by the differences in the helmets used in the current study and that study. In the Elkin et al. [21] study, it can be seen that the angular velocity in the frontal impact at 9.3 m/s is lower than in the current study at the same impact speed and using the same standard impact configuration. An image in that study shows that the impactor is above the ridge in the top of the facemask, while the impactor in the current study slides over the helmet, which in turn allows the head to gain a higher angular velocity. This is supported by the angular velocity in that study, which exhibited a peak at 20 ms and another peak at 40 ms, compared to the single peak at 30 ms in the current study. The differences in angular velocity highlight an important discrepancy between helmets; while the Xenith helmet in the current study allowed the head to rotate in the standard frontal impact, the Riddell helmet in did not allow the head to rotate considerably. Small geometric discrepancies can lead to the impactor exhibiting different “catching” or sliding behavior over the brim of the helmet, which has been noted previously [20]. While rotation of the head tends to lead to concussion, compression and shearing of the neck could result in neck injury. It is an interesting consequence of the experimental design that the helmet performance metrics (BrIC) are improved when the brim of the helmet gets jammed under the head of the impactor.

The patterns of strain observed in all impacts are in good agreement with the centripetal theory of concussion, as strains in the brain arise from rotational motion of the tissue, and tend to concentrate at sites of structural inhomogeneity. It has been theorized [7,52] that impingement of the falx causes brain deformation to concentrate in the corpus callosum in coronal impacts. This appeared to be the case in the lateral impacts in the current study, where strain was at a maximum in the body of the corpus callosum at the location of contact with the edges of the falx. This was an example of a site of structural homogeneity incurring higher strain than other regions, as suggested by the centripetal theory of concussion [12]. It is theorized that the impingement of the falx enhances the deformation that is partially caused by the inner brain tissue structures lagging the motion of the outer tissues.

6.3.2. Regional Brain Response

While the relative magnitude of whole brain MPS was higher using the simulated HNM impact compared to the prescribed kinematics approach, both methodologies predicted considerably higher strains in the sensitive inner brain regions in the lateral orientation, compared to the frontal and rear impact orientations where the strain was highest elsewhere in the brain. The inner regions of the brain, including the corpus callosum [34,35,39,40,55–57], the thalamus [37,39] and the midbrain [35,37,71] have been more commonly correlated with observed concussions than other brain regions. Furthermore, proposed strain thresholds for concussion in the corpus callosum and thalamus in the literature are 30 – 100% less than that

in the cerebrum [35,40,56,62]. Interestingly, in every lateral impact in the current study, the corpus callosum was the brain region with the highest 95th percentile MPS. In contrast, in all the frontal and rear impacts the strain in the thalamus, corpus callosum and midbrain ranged from 47 – 70% of the whole brain MPS. The strains in the thalamus were consistently higher in the lateral impacts than in frontal and rear impacts using both approaches. The finding that lateral impacts consistently resulted in higher strains in regions linked with concussion supports the consistent observations in the literature that coronal rotations are more likely to cause TBI than sagittal plane impacts [7,11,36,39]. Additionally, the increased strains observed in the inner brain regions could be a key contributor to the disproportionate amount of concussions (over 50%) in the 2015-2016 NFL season that resulted from lateral impacts, compared to other impact orientations [149].

6.3.3. The Influence of Balanced Muscle Activation

The influence of active musculature on MPS on all regions of the brain was smaller than the difference between the two methodologies (less than 10%). In previous work by the authors, it was found that active musculature had a similarly small effect on angular velocity in the linear impactor test, with slight decreases in angular velocity in lateral impacts and slight increases in angular velocity in rear impacts [Bruneau, 2019]. This finding echoes the results of Rousseau et al. [88], who found that doubling the neck stiffness of an ATD in this test setup did not have a significant influence on the resulting strains in the brain. The previous chapter suggests that the reaction moment at the base of the neck is far too small to provide significant resistance to the moment created by the impactor, which consistently exceeded the reaction moment by a factor of 20.

7. Study 3: The Influence of the Whole Body Mass and Inertia on Head Response in Football Helmet Impacts

Continuing from the investigations of head and brain motion with a Head and Neck Model (HNM) in the previous two chapters, the effect of the whole body mass and inertia were investigated by comparing the head and neck response of the HNM to that of an unconstrained FBM (Figure 7.1). The head kinematics and impactor force were compared, and the motions of the cervical vertebrae were investigated. Brain deformation predictions (MPS, CSDM15) from the HNM and the FBM were also compared, which require longer durations to develop than peak accelerations [150]. Although the body below the neck has been shown to contribute little to head kinematics prior to 20 ms [91,151], the remainder of the body may play a role in the development of brain deformation and other longer-term metrics [26].

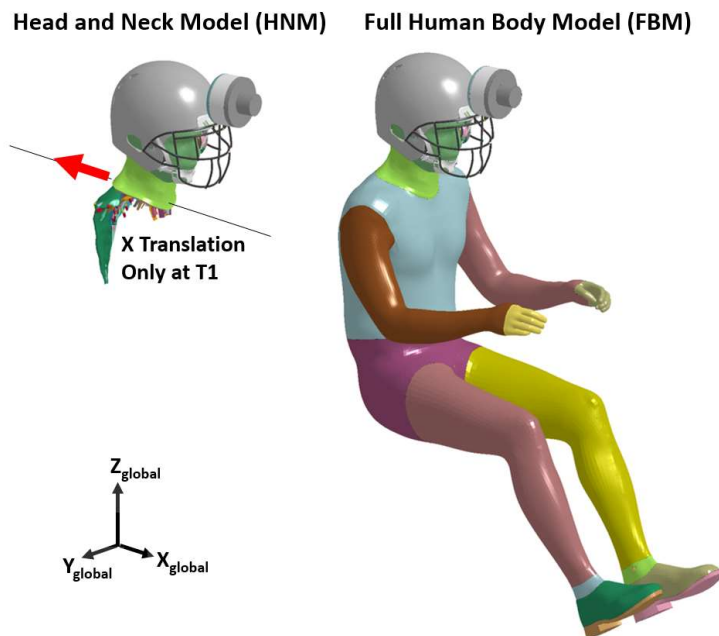


Figure 7.1 Head and Neck Model (HNM), compared to the Full human Body Model (FBM), shown in the frontal configuration

In this study, the same lateral, frontal and rear orientations used in Study 1 and 2 were considered. Only helmeted impacts were considered, and speeds of 5.5 m/s and 9.3 ms/ were examined. The effect of active musculature was also examined in the FBM, to investigate whether the constraint at the T1 in the HNM limited the effect of muscle activation. The test matrix is shown in Figure 7.2.


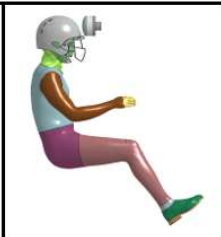
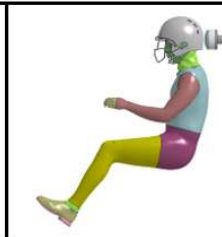


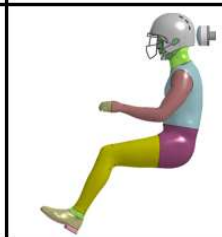
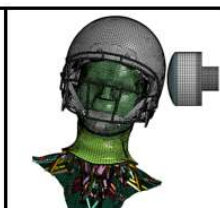
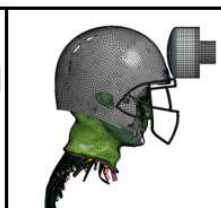
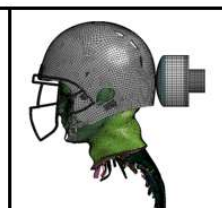

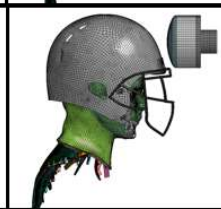
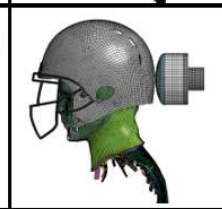
		Lateral	Frontal	Rear	
FBM – Balanced Activation	Helmeted				5.5 m/s 9.3 m/s
FBM – No Activation	Helmeted				5.5 m/s 9.3 m/s
HNM - Balanced Activation	Helmeted				5.5 m/s 9.3 m/s
HNM - No Activation	Helmeted				5.5 m/s 9.3 m/s

Figure 7.2 Simulation Matrix, Full Body Model Compared to Head and Neck Model

7.1. Qualitative Description of Impact Response

The head motion of both the HNM and the FBM in a frontal impact at 5.5 m/s was similar overall (Figure 7.3). There was little visible motion of the head in both the FBM and the HNM at 10 ms, and the impactor deformation was similar. At 30 ms, the head had started to rotate backwards, and small differences in the head and neck position were visible. Differences became more evident at 60 ms, as the neck of the FBM was visibly less compressed and extended compared to the neck of the constrained model.

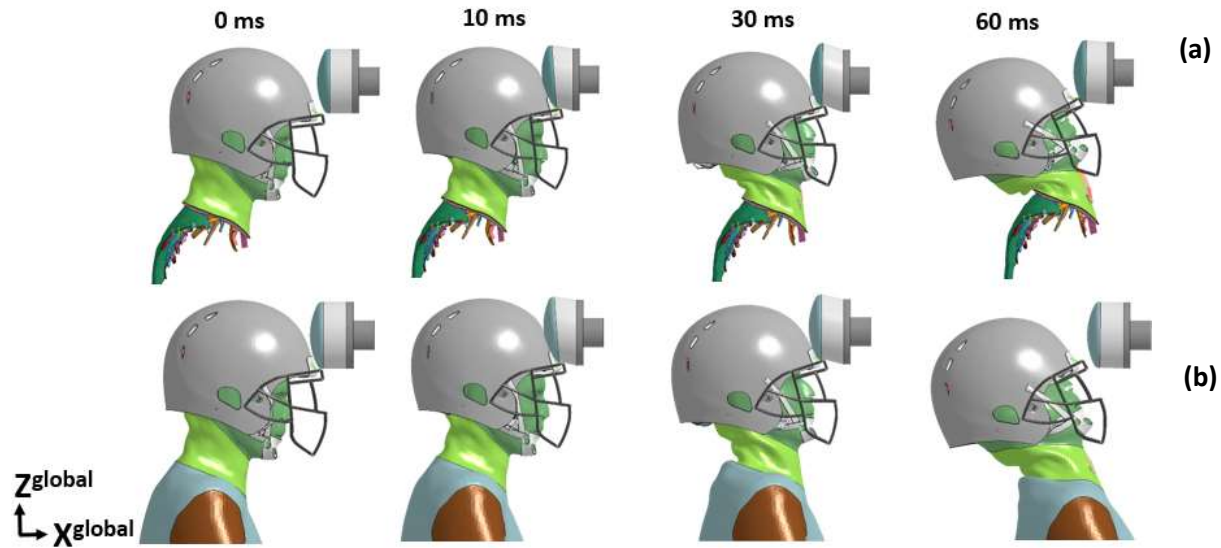
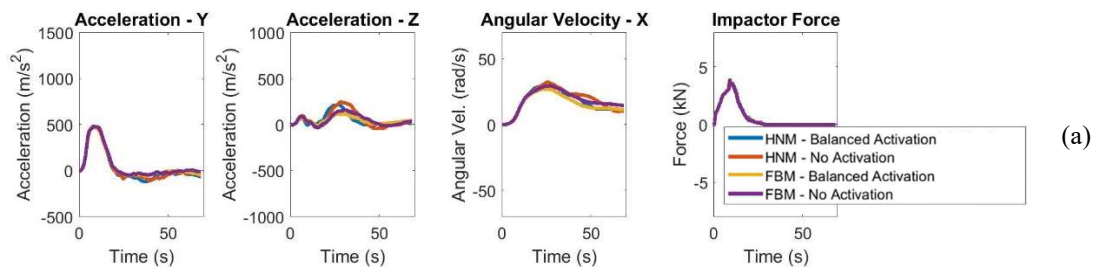


Figure 7.3 Motion of the 5.5 m/s frontal impact (no muscle activation), showing (a) the HNM and (b) the FBM

7.2. Head Kinematics Comparison

Comparing the HNM to the FBM, the early head kinematics (up to 15 – 20 ms) were nearly identical (Figure 7.4). The impactor force trace remained nearly identical for the entire time history, and the X acceleration remained similar until 30 – 40 ms. Considering the acceleration traces in all orientations, the Z acceleration diverged more than the X acceleration. In the HNM, the second peak of Z acceleration was considerably higher (1.6 times higher in the lateral orientation, 2.0 times higher for frontal, and 1.6 times for rear, considering the 9.3 m/s impacts). Z acceleration in the constrained and unconstrained models diverged earlier (between 15 and 20 ms) than X acceleration. Interestingly, angular velocity diverged earlier for the rear orientation (at approximately 20 ms) compared to the frontal and lateral orientations, where divergence occurred at approximately 40 ms.



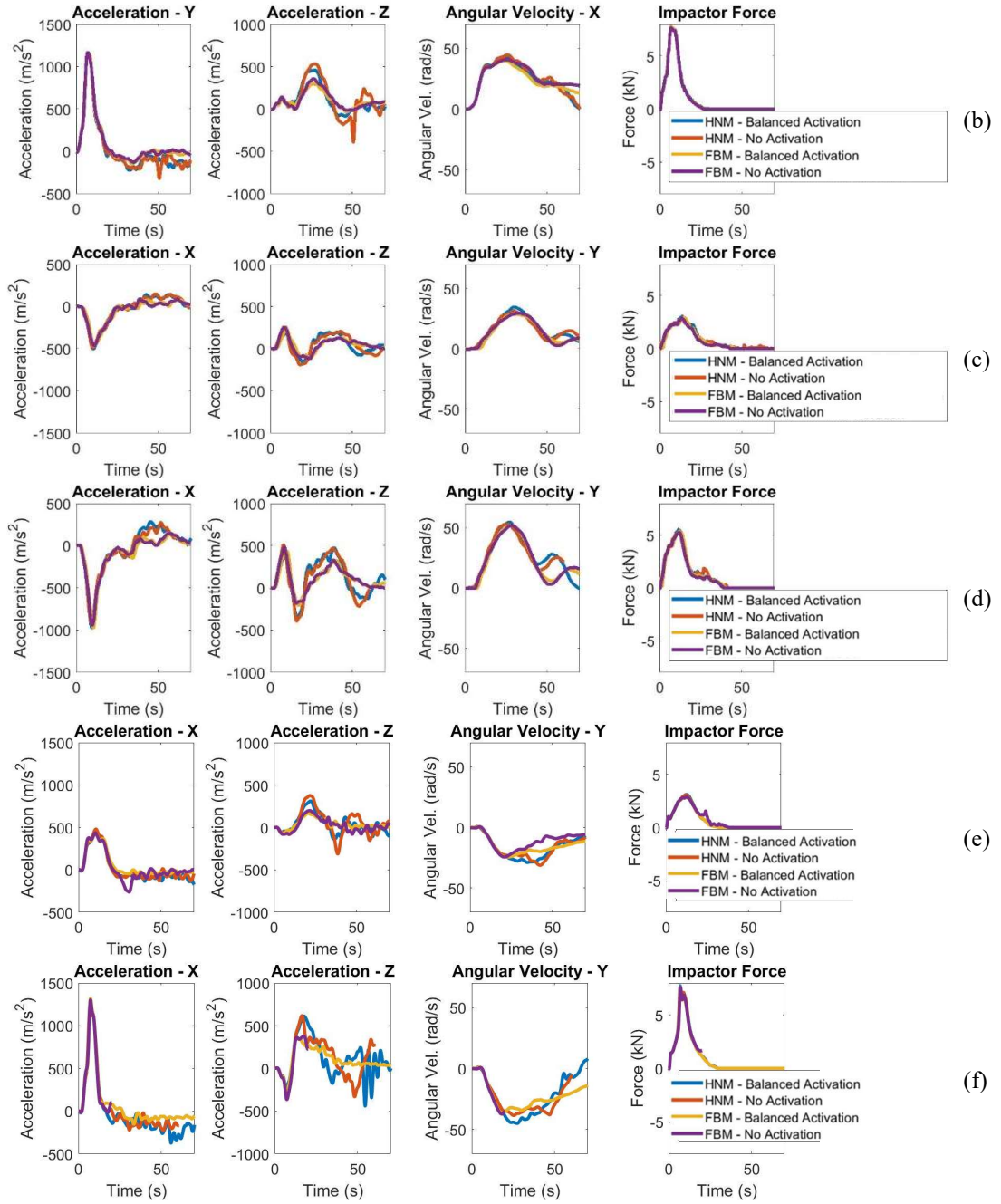


Figure 7.4 Head kinematics and impactor Force (a) lateral 5.5 m/s, (b) lateral 9.3 m/s, (c) frontal 5.5 m/s, (d) frontal 9.3 m/s, (e) rear 5.5 m/s, (f) rear 9.3 m/s

7.3. Spine Kinematics Comparison

7.3.1. T1 Motion

Unlike the kinematics of the head, the motion of the T1 vertebra differed considerably for the FBM, compared to the HNM, where the T1 was constrained so that no rotation could occur and translation could only occur in the global X direction. In the exemplar cases (Figure 7.5), which include 5.5 m/s impacts in the lateral, frontal and rear orientation, there was more displacement in the global X direction in the FBM impacts; 1.5x higher displacement at 70 ms in the lateral and frontal impact were observed, and 1.15x higher displacement in the rear orientation. As expected, there was motion in the global Z direction in all FBM impacts, while there was no Z motion in the head and neck impacts due to the constraint. The Z motion was typically smaller than the motion in the X direction but started earlier in the impact in the lateral and frontal impact, with the Z displacement exceeding 1 mm at 13.4 ms in the frontal impact, and 13.0 ms in the lateral impact. The X displacement exceeded 1 mm at 17.5 ms and 20.2 ms in the lateral and frontal FBM impacts, respectively. It can be seen in all exemplar cases (Figure 7.5) that rotation at the T1 started to occur between 14 and 16 ms after impact, and reached a value between 0.275 and 0.425 radians depending on the orientation. Perhaps most interesting finding was that the initiation of motion at the T1 coincided with the Z acceleration traces of the head starting to diverge, comparing the HNM and FBM (Figure 7.4).

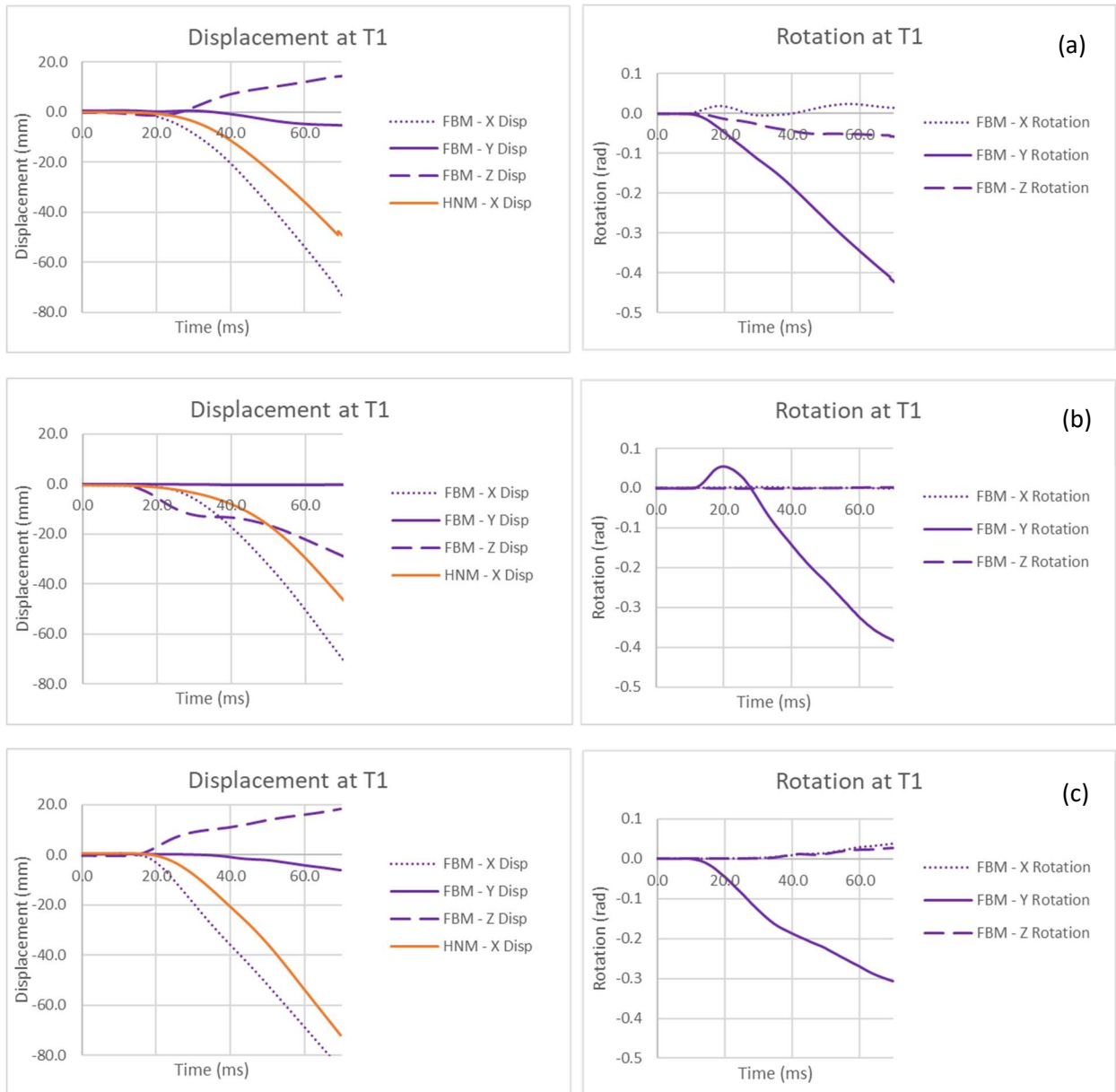


Figure 7.5 T1 displacement and rotation for the FBM and HNM in the global coordinate system, at 5.5 m/s with no muscle activation in the (a) lateral, (b) frontal, and (c) rear orientation. Note that the HNM can only translate in the global X direction.

7.3.2. Full Cervical Spine Motion

Differences in neck deformation were visible when the motion of the cervical spine in the FBM and the HNM were compared (Figure 7.6). The differences between the motion of the FBM and HNM were visible after 20 ms, and became more pronounced later in the simulation, with more flexion occurring in the HNM.

Motion of the neck in the FBM followed a trajectory at approximately 50° downwards, while motion of the HNM was horizontal (in the only direction which was not constrained).

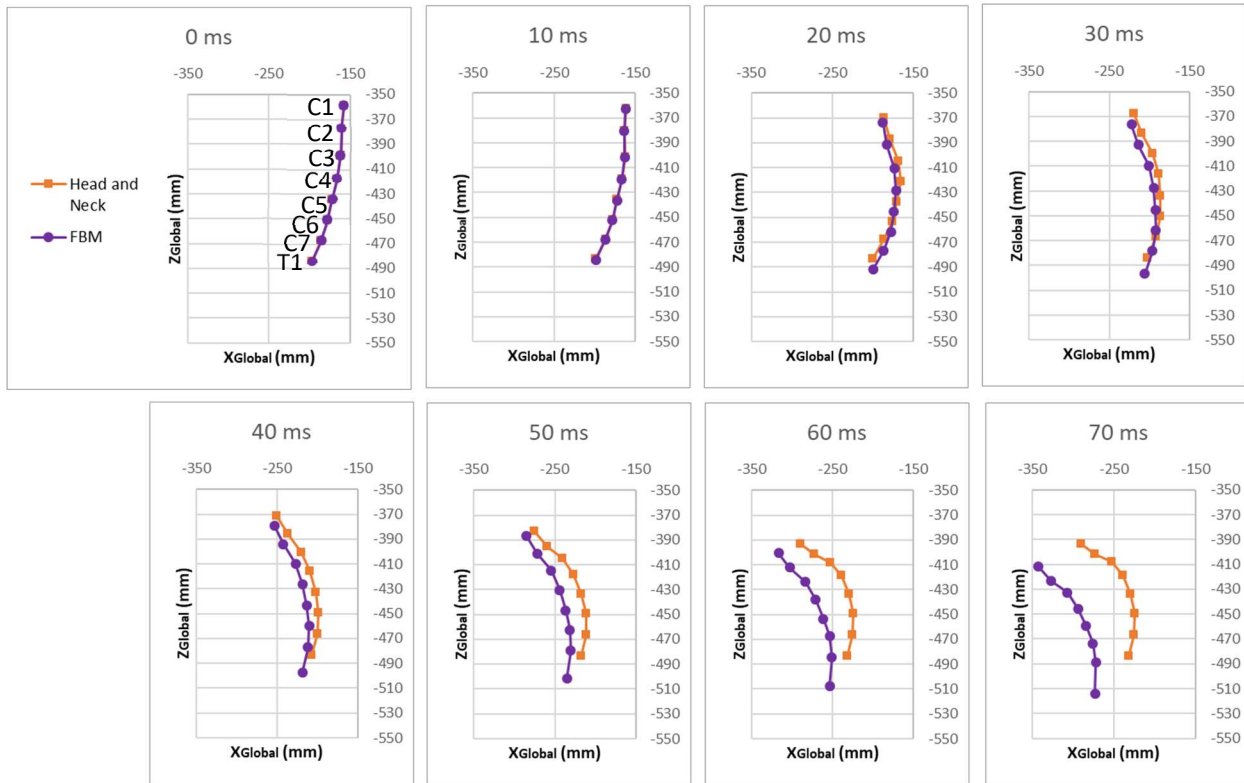


Figure 7.6 Motion of the cervical spine in a 5.5 m/s frontal impact (no muscle activation), comparing the HNM and the FBM

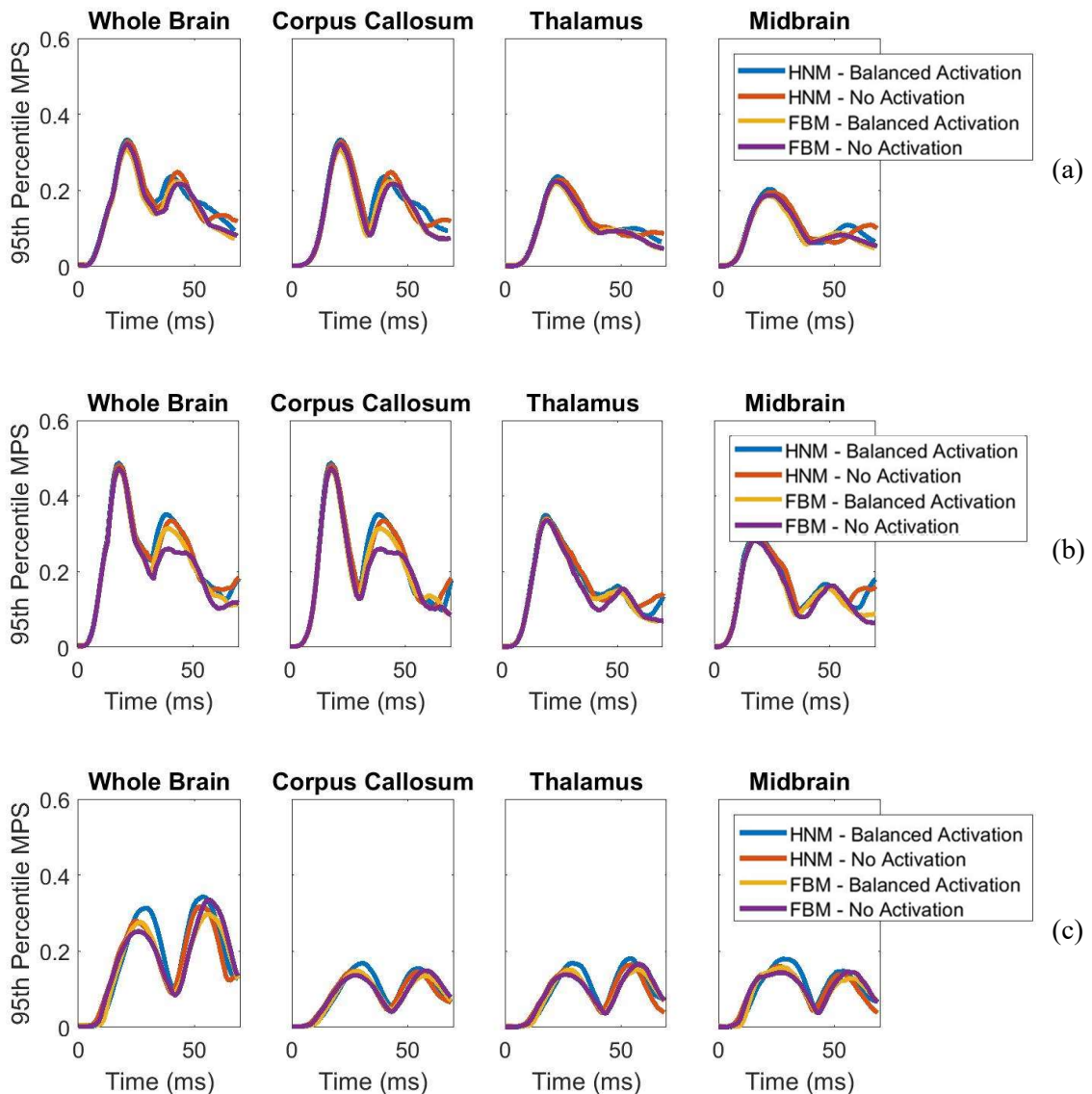
7.4. Brain Deformation Comparison

7.4.1. Maximum Principal Strain

Considering both the FBM and the HNM with no muscle activation, the MPS exhibited a bimodal response in all impact orientations, in most brain regions (Figure 7.7). Overall, both the FBM and the HNM predicted very similar peak MPS at the first peak. At the second peak, there was more variation between the full body model, and after the two peaks, especially after 50 ms, the responses of the full body and the HNM diverged considerably. Interestingly, the response of the FBM and HNM diverged more, and earlier, in the 9.3 m/s impact, in all orientations. Whether the second peak was higher or lower for the constrained and unconstrained models depended on the impact orientation. In the frontal orientation, the second peak was higher in the FBM compared to the HNM, while the second peak was lower in both the lateral and rear orientations.

Similarly, to the second study, the lateral impact orientation exhibited higher brain deformation in the corpus callosum, thalamus and midbrain compared to the frontal and rear (sagittal plane) impacts. Notably, the frontal impact of the FBM exhibited a higher value of whole brain MPS than in the HNM, by 15%.

The effect of muscle activation was similarly small in both the FBM and the HNM, across all impact orientations and brain regions. There was a slight reduction of the first peak of MPS in the lateral orientation with the FBM, while there was a slight increase in the first peak of MPS in the frontal orientation. The reverse was true for the second peak.



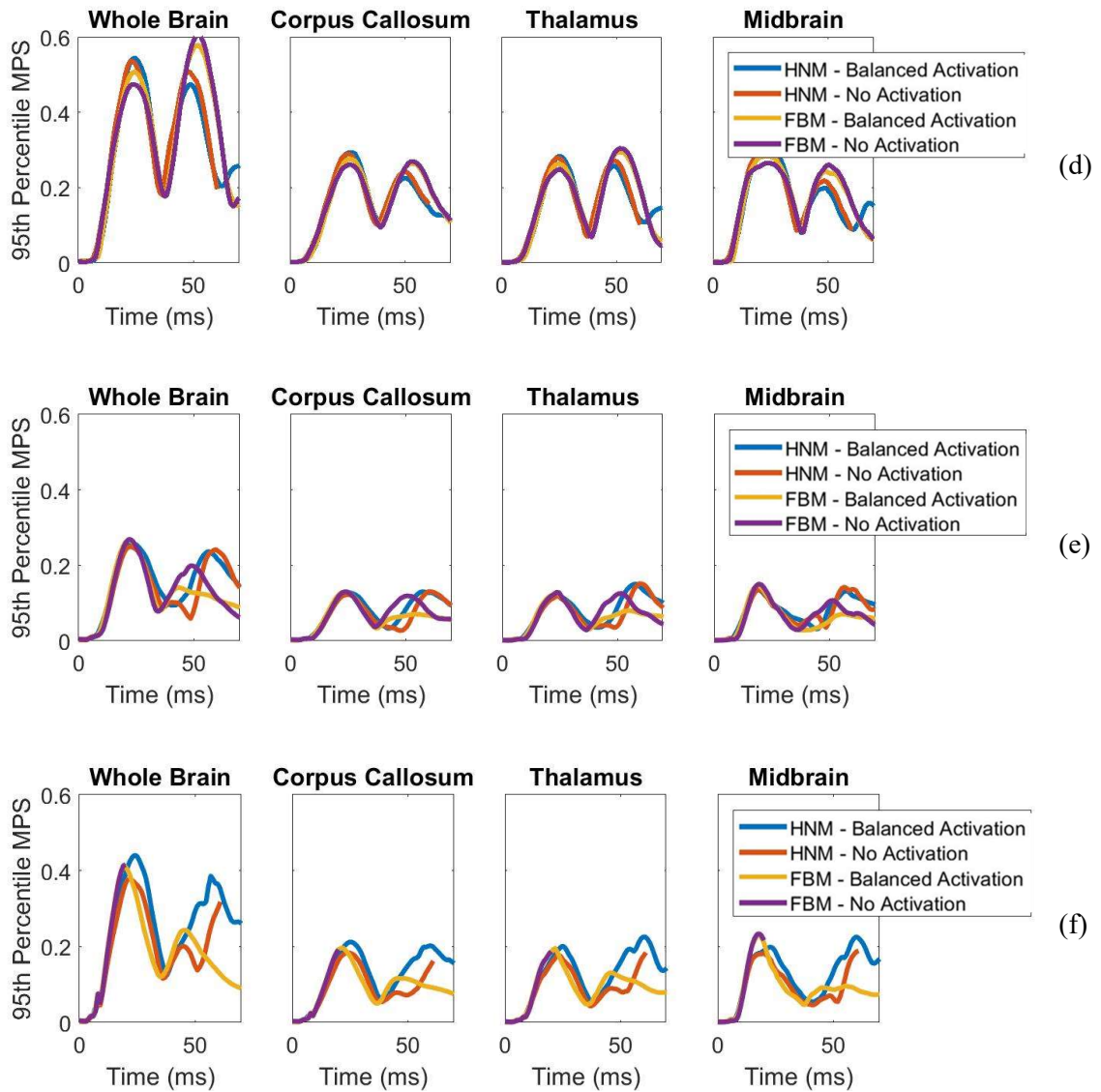
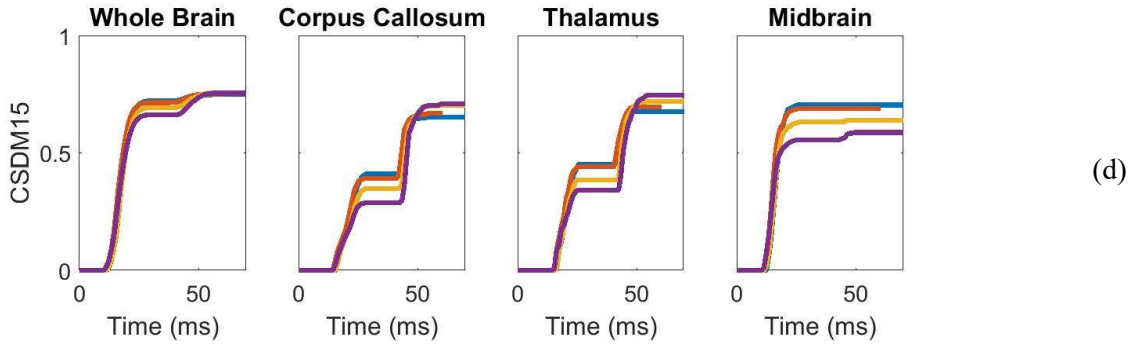
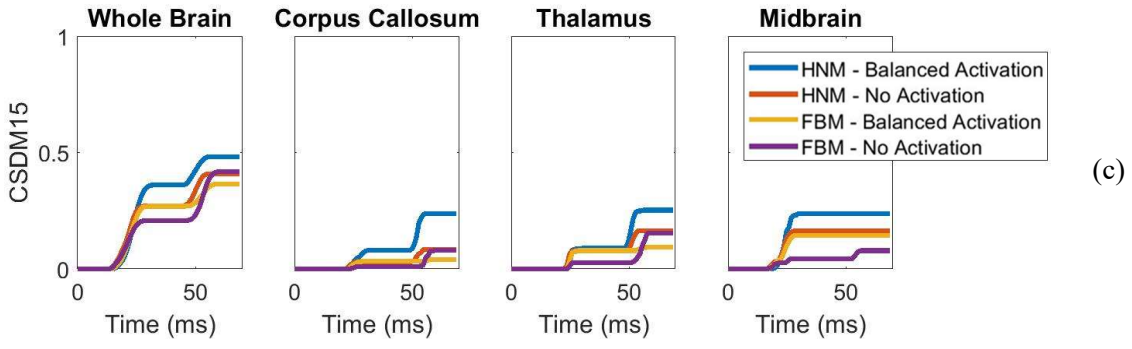
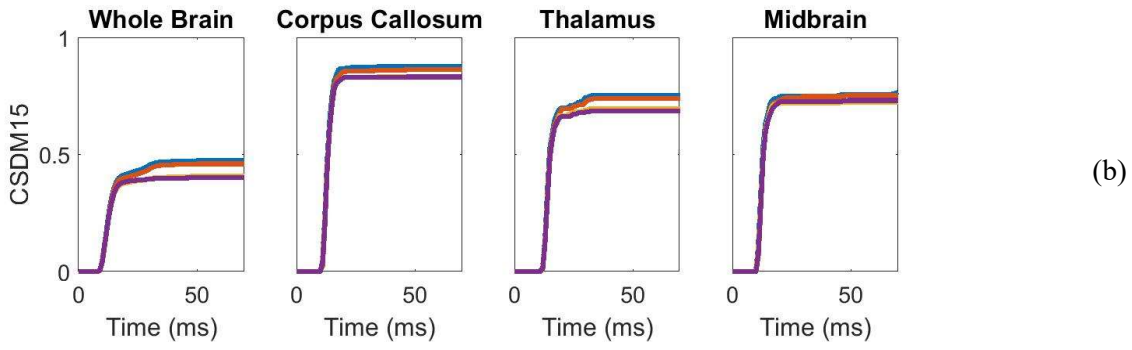
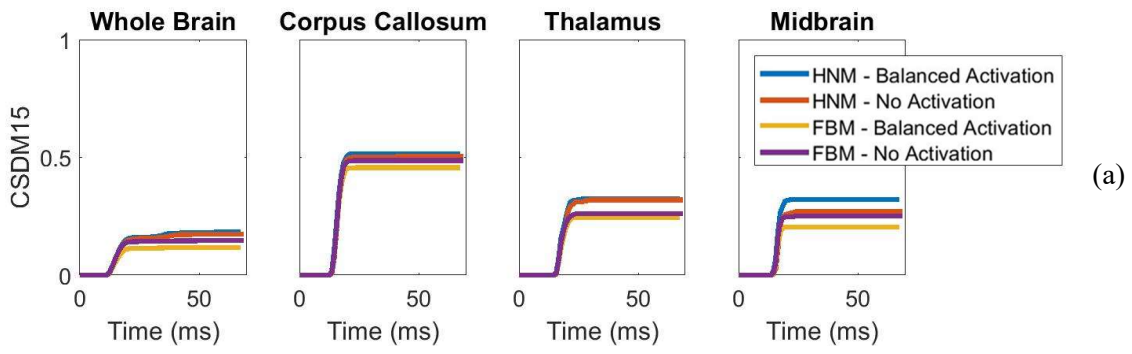


Figure 7.7 95th Percentile Maximum Principal Strain (MPS) in helmeted impacts (a) Lateral 5.5 m/s, (b) Lateral 9.3 m/s, (c) Frontal 5.5 m/s, (d) Frontal 9.3 m/s, (e) Rear 5.5 m/s, (f) Rear 9.3 m/s

7.4.2. Cumulative Strain Damage Measure

Similar to Study 2 (Chapter 6), CSDM exhibited a stepped response, and exhibited more variation than MPS, comparing the FBM and the HNM. Like MPS, in the lateral impacts there were consistently higher values of CSDM in the inner regions of the brain than frontal and rear impacts (Figure 7.8), in both the FBM and the HNM. In some cases, (lateral 9.3 m/s for example) the responses for the FBM and HNM were similar, while in others (frontal 5.5 m/s, rear 9.3 m/s) CSDM response varied between the models.



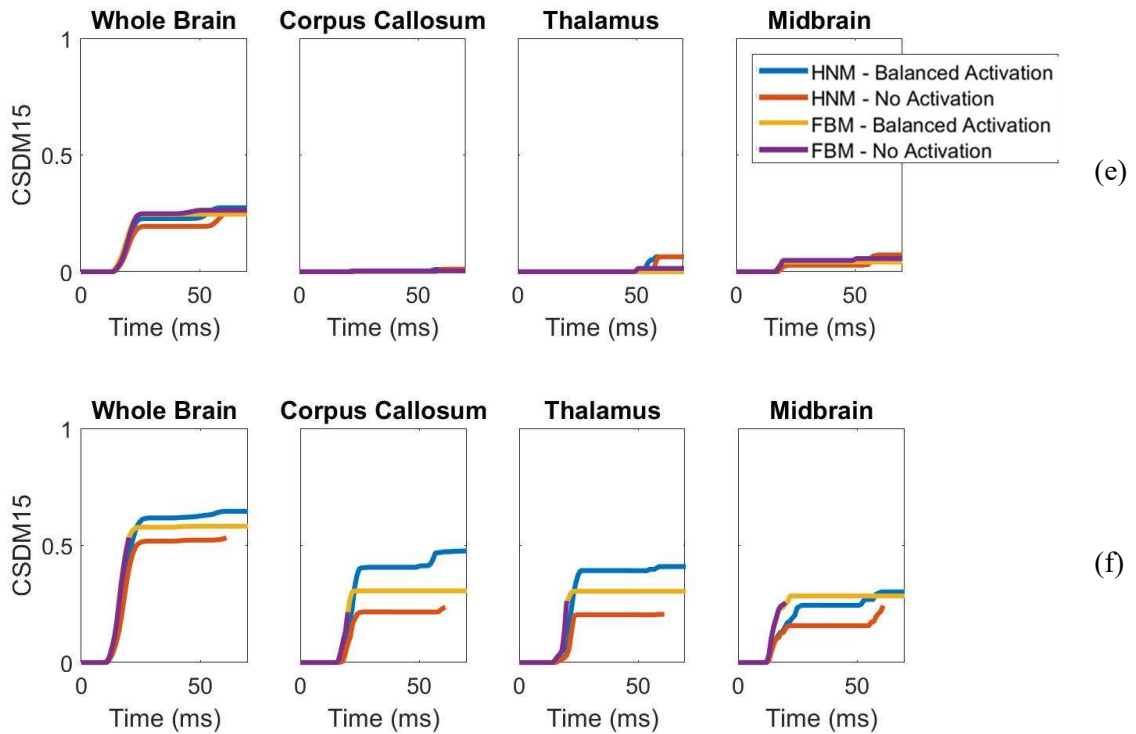


Figure 7.8 Cumulative Strain Damage Measure (CSDM) with a cutoff threshold of 0.15 (CSDM15) in helmeted impacts (a) Lateral 5.5 m/s, (b) Lateral 9.3 m/s, (c) Frontal 5.5 m/s, (d) Frontal 9.3 m/s, (e) Rear 5.5 m/s, (f) Rear 9.3 m/s

7.5. Discussion – The Role of the Whole Body

The purpose of this study was to investigate the influence of whole body mass and inertia on head and neck response, when subjected to a linear ram impact. It is clear from the results presented in this section that the HNM closely replicated the early head kinematics of an FBM in this same test configuration, but not the neck kinematics. In general, head motions and brain deformations that occurred early in the impact (earlier than 15 ms) were nearly unchanged due to the boundary condition at the T1, while head motions later in time were affected more by the boundary condition. In the case of head kinematics, the peak values were unchanged, while the brain deformation metrics were influenced more, often after the peak values occurred.

The similarity of the brain deformation and kinematics early in time was comparable to the result of Study 1 (Chapter 5), where the linear acceleration and angular velocity in the primary impact direction were very similar considering ATD and HNM impacts, despite the differences in the neck. In the Chapter 5 study, the moment at the T1 was different in the HNM and ATD, but was found to be far less than the moment created by the impactor. It was proposed that the differing neck stiffness did not influence the head kinematics because the impactor could not be resisted by the much smaller moment at the base of the neck. It was

thought that for this reason that the FBM and HNM had similar kinematics early in time, because the base of the neck had little effect on primary plane motion until after the impactor force subsides (20 - 25 ms after the onset of impact). By that time, the majority of the angular velocity peaks had occurred and the first peak of brain deformation was occurring. It is worth noting that while MPS response of the HNM and the FBM diverge considerably after 50 ms, especially in the lateral orientation, after the peak MPS had occurred.

In a previous study, Darling et al. [26] simulated helmeted crown and frontal impacts using a simplified helmet model, using the same unconstrained GHBMC FBM as the current study. The impactor was rigid and travelled at 3 m/s. The progression of MPS in the 5.5 m/s frontal impact in the current study and the 3 m/s frontal impact in the Darling et al. study was comparable. The peak MPS in every brain region in the current study occurred between 24 and 25 ms after impact, while in the Darling study it occurred between 19 and 21 ms, depending on the brain region. The magnitude of brain strain was approximately 50% lower in the Darling study compared to the current study. The differences can be explained by the impactor speed, mass, stiffness and impact direction, as well as the differences in the helmet implementation. The Darling study used a lower mass impactor (5 kg vs 15.4 kg), which was rigid. This would result in a shorter duration and higher magnitude pulse delivered to the head, which could result in similar linear acceleration, but lower head angular velocity, which is thought to govern brain deformation [7,10,71]. The compliant, but more massive and faster impactor used in the current study is designed to mimic the mass, speed and stiffness of an incoming player [13]. Comparing a rigid and deformable impactor travelling at a similar speed, the deformable impactor would result in a later strain peak in the brain, because the impactor deformation would delay the peak, similarly to how the helmet delayed the acceleration and angular velocity peaks in the Chapter 5 study. In addition to this, the shape of the incoming impactor was different, as well as the impact angle, which would further influence the distribution of MPS in different brain regions.

In the current study it was found that Z acceleration of the FBM and the HNM diverged earlier than other kinematic parameters. In the FBM, the T1 translation in the Z direction initiated earlier than the X direction, and coincided with the divergence of Z acceleration in the constrained and constrained models. The earlier differences in z motion can be explained by the relative stiffness of the neck in the z direction (axial compression) allowing the impact to transmit to the T1 more quickly, compared to the X and Y direction (bending). This has been shown in the Darling [141] study, where impacts to the crown of the helmeted GHBMC model caused movement (>0.25 mm) of the T1 vertebra 6.8 ms after impact.

In the current study, the FBM was in the default seated position. Although this seated posture did not represent the typical posture of a struck football player, it was clear that the lower body did not influence the early head and brain response as the motion of the body below the torso was minimal prior to 70 ms. However, varying the relative head-neck position and implementing other protective equipment, such as

neck collars and shoulder pads could influence the trajectory of the head early in time, and thus affect the peak head and brain response [108].

Effect of Active Musculature

It was hypothesized that active musculature could have a larger effect on the head response of an unconstrained surrogate, compared to a HNM, however the results of the current study do not support this hypothesis for the timeframe considered. With the muscle activation scheme used in the current study, muscle activation generally had little influence on brain deformation predictions with the FBM, especially early in time.

Overall, the results of the current study support the use of a HNM to predict MPS of the brain up to 50 ms. The head kinematics are near identical for the first 15 ms, then remain in reasonably good agreement for the first 50 ms. The results of the current study suggest that the linear impactor should not be used to evaluate neck injury, as neck kinematics were considerably different when comparing an unconstrained FBM and constrained HNM.

8. Summary, Conclusions and Recommendations

8.1. Summary and Conclusions

This thesis consists of three studies which were completed to better understand the biofidelity of the standardized linear impactor test for testing football helmets and the effect of boundary conditions on head response. Advanced HBM were used for comparison with the Hybrid III Anthropometric Device (ATD), to provide additional anatomical detail compared to the ATD. The three studies were:

1. A comparison of head kinematics of the ATD and HNM, investigating the effect of active musculature.
2. An evaluation of brain deformation comparing a prescribed kinematics approach using head kinematics from an ATD experiment, and a fully simulated impact approach using the helmeted HNM.
3. Comparing an unconstrained FBM to an HNM using the linear impactor test, to investigate the effect of the whole body mass and inertia.

8.1.1. Comparison of Head Kinematics of the ATD and HNM

In the first study, the ATD head and neck provided a similar estimate of head kinematics in a linear impactor test when compared to a more detailed HNM, in a bare-head and helmeted impact. The prediction of head response metrics was also similar for both the ATD and HNM. In both the HNM and the ATD, the helmet reduced two kinematic response predictors by 38 – 50 % over the range of speeds and orientations, when compared to a bare-head impact with the same compliant impactor.

The HNM was found to have similar linear head acceleration to the ATD simulation in the primary impact direction, with the acceleration-time history receiving an overall average CORrelation and Analysis (CORA) rating of 0.89, indicating good overall correlation. Primary direction angular velocity of the head was also similar, with an average CORA rating of 0.87 considering all orientations.

Across all helmeted and bare-head impacts, the z acceleration of the head was considerably lower in the ATD compared to the HNM, with an overall average CORA rating of 0.44 comparing the HNM simulations to the ATD simulation. In addition, the axial stretching and compression of the ATD neck was close to 5x less than that of the HNM. Though the overall magnitude of the z acceleration was less than the X acceleration in the first study, the results imply that using an ATD to represent an impact with a large z

component could result in a less biofidelic kinematic response, as was done in some of the NFL reconstructions [152].

The contribution of muscle activation to head kinematics was found to be relatively small with a balanced muscle activation scheme. This was because the peak accelerations developed early in time, when the impactor force greatly exceeded the resisting moment from the neck, and the kinematics of the head were dominated by the mass and local stiffness properties of the head, impactor and where applicable, the helmet.

When assessing head response based on peak acceleration, it was found that the bending stiffness of the neck did not play a strong role, within the range that was examined with the ATD and the HNM in the first study.

8.1.2. Prescribed Kinematics vs. Simulated HNM Impact

The second study suggested that the chosen surrogate (HBM or Experimental ATD) has an effect on the magnitudes of the Maximum Principal Strain (MPS) in the brain, but the regional distribution of strains remains similar for a given impact orientation. Cumulative Strain Damage Measure (CSDM) was affected more by the chosen surrogate, because the metric is sensitive to small changes in kinematics.

It was found that the whole brain MPS was less sensitive to impact orientation than the MPS within inner brain regions that have been linked to concussion. When optimizing helmet designs, it may be important to consider the deformation in each brain region, and to attempt to reduce the deformation in more vulnerable brain structures as a priority.

This study offers a possible explanation for the orientation specific prevalence of concussion. MPS measured for the whole brain did not vary with impact orientation as much which regions exhibited the highest MPS. The strains in the inner regions of the brain, especially the corpus callosum, were consistently higher in the lateral impact than in the rear and frontal impacts which occur in the sagittal plane.

For the experimental test setup in the second study, active musculature had little influence on the MPS, and the observed effects with muscle activation consisted of increases in brain deformation in rear impacts and decreases in brain deformation in lateral impacts.

8.1.3. The Role of the Whole Body Mass and Inertia

When comparing an unconstrained FBM to the constrained HNM, it was found that the early head kinematics were similar, especially early in time, while the neck kinematics were considerably different, especially at the T1 vertebra.

The MPS followed the same bimodal pattern in the unconstrained full body and the constrained head and neck. The strain response was similar early in time, then diverged slightly later in time, especially after the two peaks had occurred. The predictions for the first peak of MPS were similar to the constrained HNM, while the second peak diverged slightly.

The spine motion for the constrained HNM and unconstrained FBM were similar for the first 20 ms, then continued to diverge considerably until the end of the impact. The constrained HNM spine was considerably more curved than the FBM, suggesting a higher level of compression. The T1 motion was considerably different, with much more motion present in the unconstrained FBM.

These three studies serve to highlight the benefits and limitations of the most commonly used boundary condition for testing of football helmets, using the best available models. The integrated HBM and helmet models developed in this thesis provide a testbed for investigating the effect of helmet modifications on brain deformation in the future.

8.2. Limitations

The implementation of active musculature was a limitation of the HBM used in this thesis. The Hill-type muscle implementation used in the HBM only changed the axial stiffness of the muscle, not the transverse stiffness. Prescribing the same level of muscle activation to all flexor muscles, and another constant value to all extensor muscles, was a simplification. More electromyography data on football-specific muscle activation, and more detailed implementation in the FE model including transverse stiffness would add realism to future studies. A new muscle implementation with decreased compressive stiffness and a three-dimensional implementation of muscle activation could influence the motion of the head and subsequent brain deformation. Notwithstanding, it was clear that the contribution of active musculature was small in the linear impactor test, as the total muscle force prior to impact in the current study was within 10% of the muscle force measured during maximum voluntary contraction in a previous study [144].

The construction of the linear impactor created a challenging boundary condition in the frontal impact orientation, where there was considerable sliding, shearing and sometimes detachment of the impactor end cap and foam. The physical impactor comprised of three components attached together with Velcro. In the lateral and rear impacts, this resulted in relatively little shearing of the foam and a predominantly compressive load to the impactor. In the frontal impact, the impactor experienced tension and compression, which resulted in the Velcro disconnecting and in some cases the impactor foam separated completely from the impactor later in the impact (always >25ms after impact), which was not modelled in the simulation. The Velcro was modelled using a tied contact in the simulations, which may have induced some tensile

force in the impactor. Even so, the average CORA rating of 0.87 for the bare-head experiment and simulation of the ATD linear impactor test indicated that the response of the head was in good agreement with the experiment [44].

A limited number of impact orientations were tested in the current work. More impact orientations could be considered in future studies, to better understand the effects examined. For example, introducing more axial rotation of the head could highlight additional differences between the ATD and HBM. In addition, a 50th percentile male may not be representative of a typical football player, which are typically larger than average males. It is likely that different impact kinematics would be observed in a larger human surrogate. Finally, the brain model was also a limitation of this thesis. The brain model was developed from cadaveric material and brain displacement data [32], which is known to behave differently than in vivo tissue. It would be beneficial to use multiple brain models to see if the trends in brain deformation are similar to those of the GHBMC model.

8.3. Recommendations

The three studies in this thesis have indicated that linear impactor testing of both the ATD and HNM provide similar estimates of head kinematics and brain deformation, and that the boundary condition has a small influence on the head motion. This indicates that both surrogates are suitable for evaluating improvements to football helmets.

The most obvious area for future work is optimizing the performance of the football helmet model using the HNM with no activation. The existing Xenith X2e helmet model could be modified, in particular to examine the effect of stiffening or softening different components, or redesigning the shock absorption components to add progressive stiffness. The effect of strap tightness and helmet fit could also be investigated with the existing helmet model.

The successful use of HBMs in investigating helmeted impacts could be used to investigate other protective equipment, such as shoulder pads or neck collars, which have been shown to influence head response using ATDs [108]. In the 2015-2016 National Football League (NFL) season, the three most common sources of concussive impact were the ground (19%), and the helmet (36%) and shoulder (17%) of the striking player [149]. No standard test has assessed helmet-to-shoulder impacts, and the limited existing research on helmet-to-shoulder impacts has focused on ice hockey [153,154]. HBMs could be used to investigate helmet-to-shoulder impacts and make improvements to football shoulder pads to reduce the risk of concussion in the struck player.

Another potentially interesting study would be to replace the linear impactor with an incoming HBM, to represent both the striking and struck players with HBM. Using two unconstrained HBM, more biofidelic

head motion may be achieved in the struck player. By simulating the standard NFL impact orientations, one could compare the struck HBM head kinematics to those achieved in the linear impactor test. If there are significant differences, one could then optimize the mass and stiffness of both the impactor and Hybrid III ATD in the linear impactor test, to match the HBM head kinematics as closely as possible.

9. References

- [1] Montenegro, P. H., Alosco, M. L., Martin, B. M., Daneshvar, D. H., Mez, J., Chaisson, C. E., Nowinski, C. J., Au, R., McKee, A. C., Cantu, R. C., McClean, M. D., Stern, R. A., and Tripodis, Y., 2017, “Cumulative Head Impact Exposure Predicts Later-Life Depression, Apathy, Executive Dysfunction, and Cognitive Impairment in Former High School and College Football Players,” *J. Neurotrauma*, **34**(2), pp. 328–340.
- [2] Mez, J., Daneshvar, D. H., Kiernan, P. T., Abdolmohammadi, B., Alvarez, V. E., Huber, B. R., Alosco, M. L., Solomon, T. M., Nowinski, C. J., McHale, L., Cormier, K. A., Kubilus, C. A., Martin, B. M., Murphy, L., Baugh, C. M., Montenegro, P. H., Chaisson, C. E., Tripodis, Y., Kowall, N. W., Weuve, J., McClean, M. D., Cantu, R. C., Goldstein, L. E., Katz, D. I., Stern, R. A., Stein, T. D., and McKee, A. C., 2017, “Clinicopathological Evaluation of Chronic Traumatic Encephalopathy in Players of American Football,” *JAMA - J. Am. Med. Assoc.*, **318**(4), pp. 360–370.
- [3] IQVIA, 2019, “Incidence of Concussion - 2012 - 2017” [Online]. Available: <https://www.playsmartplaysafe.com/newsroom/reports/2017-injury-data/>. [Accessed: 19-Jan-2019].
- [4] Casson, I. R., Viano, D. C., Powell, J. W., and Pellman, E. J., 2010, “Twelve Years of National Football League Concussion Data,” *Sports Health*, **2**(6), pp. 471–483.
- [5] Daneshvar, D. H., Nowinski, C. J., Cantu, R. C., and McKee, A., 2011, “The Epidemiology of Sport-Related Concussion,” *Clin. Sports Med.*, **30**(1), pp. 1–17.
- [6] Hoshizaki, T. B., Brien, S. E., Bailes, J. E., Maroon, J. C., Kaye, A. H., and Cantu, R. C., 2004, “The Science and Design of Head Protection in Sport,” *Neurosurgery*, **55**(4), pp. 956–967.
- [7] Meaney, D. F., and Smith, D. H., 2012, “Biomechanics of Concussion,” *Clin. Sport. Med.*, **30**(1), pp. 14–27.
- [8] Hernandez, F., Shull, P. B., and Camarillo, D. B., 2015, “Evaluation of a Laboratory Model of Human Head Impact Biomechanics,” *J. Biomech.*, **48**(12), pp. 3469–3477.
- [9] Gabler, L. F., Crandall, J. R., and Panzer, M. B., 2018, “Development of a Metric for Predicting Brain Strain Responses Using Head Kinematics,” *Ann. Biomed. Eng.*, **46**(7), pp. 972–985.
- [10] Kleiven, S., 2013, “Why Most Traumatic Brain Injuries Are Not Caused by Linear Acceleration but Skull Fractures Are,” *J. Athl. Train.*, **1**(November), pp. 1–5.
- [11] Gennarelli, T. A., Thibault, L. E., Adams, J. H., Graham, D. I., Thompson, C. J., and Marcincin, R.

- P., 1982, "Diffuse Axonal Injury and Traumatic Coma in the Primate," *Ann. Neurol.*, **12**(6), pp. 564–574.
- [12] OMMAYA, A. K., and GENNARELLI, T. A., 1974, "Cerebral Concussion and Traumatic Unconsciousness," *Brain*, **97**(1), pp. 633–654.
- [13] Viano, D. C., Withnall, C., and Halstead, D., 2012, "Impact Performance of Modern Football Helmets," *Ann. Biomed. Eng.*, **40**(1), pp. 160–174.
- [14] BIOCORE, 2017, "BIOCORE Drop Tower Testing for Numerical Crowdsourcing," pp. 1–10 [Online]. Available: <http://biocorellc.com/resources/>. [Accessed: 20-Apr-2019].
- [15] Bland, M., 2017, "Specification of Experimental Methods: Pendulum Impactor Tests to an Unhelmeted and Helmeted Hybrid III Headform," pp. 1–6.
- [16] NOCSAE, 2017, "Standard Performance Specification for Newly Manufactured Football Helmets," pp. 2–6 [Online]. Available: <https://nocsae.org/standard/standard-performance-specification-for-newly-manufactured-football-helmets-3/>.
- [17] Funk, J. R., Crandall, J., Wonnacott, M., and Withnall, C., 2017, "Linear Impactor Helmet Test Protocol," *Biomech. Consult. Res. LC* [Online]. Available: <http://biocorellc.com/resources/>. [Accessed: 20-Apr-2019].
- [18] Pellman, E. J., Viano, D. C., Withnall, C., Shewchenko, N., Bir, C. A., and Halstead, P. D., 2006, "Concussion in Professional Football: Helmet Testing to Assess Impact Performance - Part 11," *Neurosurgery*, **58**(1), pp. 78–95.
- [19] Gwin, J. T., Chu, J. J., Diamond, S. G., Halstead, P. D., Crisco, J. J., and Greenwald, R. M., 2010, "An Investigation of the NOCSAE Linear Impactor Test Method Based on In Vivo Measures of Head Impact Acceleration in American Football," *J. Biomech. Eng.*, **132**(1), p. 011006.
- [20] Post, A., Oeur, A., Hoshizaki, B., and Gilchrist, M. D., 2013, "An Examination of American Football Helmets Using Brain Deformation Metrics Associated with Concussion," *Mater. Des.*, **45**(March), pp. 653–662.
- [21] Elkin, B. S., Gabler, L. F., Panzer, M. B., and Siegmund, G. P., 2019, "Brain Tissue Strains Vary with Head Impact Location: A Possible Explanation for Increased Concussion Risk in Struck versus Striking Football Players," *Clin. Biomech.*, **64**(April), pp. 49–57.
- [22] Post, A., Oeur, A., Walsh, E., Hoshizaki, B., and Gilchrist, M. D., 2014, "A Centric/Non-Centric Impact Protocol and Finite Element Model Methodology for the Evaluation of American Football

- Helmets to Evaluate Risk of Concussion,” *Comput. Methods Biomech. Biomed. Engin.*, **17**(16), pp. 1785–1800.
- [23] Kallieris, D., Rizzetti, A., and Mattern, R., 1995, “The Biofidelity of Hybrid III Dummies,” *International Research Council on Biomechanics of Injury*, IRCOBI, pp. 135–154.
- [24] Karton, C. M., Hoshizaki, T. B., and Gilchrist, M. D., 2014, “The Influence of Impactor Mass on the Dynamic Response of the Hybrid III Headform and Brain Tissue Deformation,” *Mech. Concussion Sport.*, **40**(STP1552), pp. 23–40.
- [25] Jin, X., Feng, Z., Mika, V. H., Li, H., Viano, D., and Yang, K. H., 2017, “The Role of Neck Muscle Activities on the Risk of Mild Traumatic Brain Injury in American Football,” *J. Biomech. Eng.*, **139**(October 2017).
- [26] Darling, T., Muthuswamy, J., and Rajan, S. D., 2016, “Finite Element Modeling of Human Brain Response to Football Helmet Impacts,” *Comput. Methods Biomech. Biomed. Engin.*, **19**(13), pp. 1432–1442.
- [27] Yang, K. H., Barker, J., Cronin, D. S., Gierczycka, D., Hu, J., Iwamoto, M., Jin, X., Kalra, A., Mao, H., Presley, B. R., Shen, D., Singh, D., and Zhu, F., 2018, *Basic Finite Element Method as Applied to Injury Biomechanics*, Academic Press - Elsevier.
- [28] Panzer, M. B., Fice, J. B., and Cronin, D. S., 2011, “Cervical Spine Response in Frontal Crash,” *Med. Eng. Phys.*, **33**(9), pp. 1147–1159.
- [29] Fice, J. B., Cronin, D. S., and Panzer, M. B., 2011, “Cervical Spine Model to Predict Capsular Ligament Response in Rear Impact,” *Ann. Biomed. Eng.*, **39**(8), pp. 2152–2162.
- [30] Dibb, A. T., Cox, C. A., Nightingale, R. W., Luck, J. F., Cutcliffe, C., Myers, B. S., Arbogast, K. B., Seacrist, T., and Bass, R., 2013, “Importance of Muscle Activations for Biofidelic Pediatric Neck Response in Importance of Muscle Activations for Biofidelic Pediatric Neck Response in Computational Models,” *Traffic Inj. Prev.*, (November).
- [31] Giudice, J. S., Zeng, W., Wu, T., Alshareef, A., Shedd, D. F., and Panzer, M. B., 2018, “An Analytical Review of the Numerical Methods Used for Finite Element Modeling of Traumatic Brain Injury,” *Ann. Biomed. Eng.*, pp. 1–18.
- [32] Mao, H., Zhang, L., Jiang, B., Genthikatti, V. V., Jin, X., Zhu, F., Makwana, R., Gill, A., Jandir, G., Singh, A., and Yang, K. H., 2013, “Development of a Finite Element Human Head Model Partially Validated With Thirty Five Experimental Cases,” *J. Biomech. Eng.*, **135**(11), p. 111002.

- [33] Takhounts, E. G., Eppinger, R. H., Campbell, J. Q., Tannous, R. E., Power, E. D., and Shook, L. S., 2003, "On the Development of the SIMon Finite Element Head Model," *Stapp Car Crash J.*, **47**(October), pp. 107–33.
- [34] Zhao, W., Cai, Y., Li, Z., and Ji, S., 2017, "Injury Prediction and Vulnerability Assessment Using Strain and Susceptibility Measures of the Deep White Matter," *Biomech. Model. Mechanobiol.*, **16**(5), pp. 1709–1727.
- [35] Giordano, C., and Kleiven, S., 2014, "Evaluation of Axonal Strain as a Predictor for Mild Traumatic Brain Injuries Using Finite Element Modeling," *Stapp Car Crash J.*, **58**(14), pp. 29–61.
- [36] Hernandez, F., Wu, L. C., Yip, M. C., Laksari, K., Hoffman, A. R., Lopez, J. R., Grant, G. A., Kleiven, S., and Camarillo, D. B., 2015, "Six Degree-of-Freedom Measurements of Human Mild Traumatic Brain Injury," *Ann. Biomed. Eng.*, **43**(8), pp. 1918–1934.
- [37] Zhang, L., Yang, K. H., and King, A. I., 2004, "A Proposed Injury Threshold for Mild Traumatic Brain Injury," *J. Biomech. Eng.*, **126**(2), p. 226.
- [38] Marjoux, D., Baumgartner, D., Deck, C., and Willinger, R., 2008, "Head Injury Prediction Capability of the HIC, HIP, SIMon and ULP Criteria," *Accid. Anal. Prev.*, **40**(3), pp. 1135–1148.
- [39] Patton, D., McIntosh, A., and Kleiven, S., 2013, "The Biomechanical Determinants of Concussion: Finite Element Simulations To," *J. Appl. Biomech.*, pp. 721–730.
- [40] Kleiven, S., 2007, "Predictors for Traumatic Brain Injuries Evaluated through Accident Reconstructions," *Stapp Car Crash J.*, **51**(October), pp. 81–114.
- [41] Eckersley, C. P., Nightingale, R. W., Luck, J. F., and Bass, C. R., 2020, "The Role of Cervical Muscles in Mitigating Concussion," *J. Sci. Med. Sport*, (2019), pp. 5–9.
- [42] (GHBMCM), G. H. B. M. C., 2019, "Resources" [Online]. Available: <https://www.elemance.com/resources/>.
- [43] Cronin, D., Barker, J., Gierczycka, D., Bruneau, D., Bustamante, M., and Corrales, M., 2018, "User Manual - Finite Element Model of 2016 Xenith X2E (Safety Equipment Institute Model X2E) Version 1.0 for LS-DYNA" [Online]. Available: <http://biocorellc.com/resources/>.
- [44] Giudice, J. S., Park, G., Kong, K., Bailey, A., Kent, R., and Panzer, M. B., 2018, "Development of Open-Source Dummy and Impactor Models for the Assessment of American Football Helmet Finite Element Models," *Ann. Biomed. Eng.*, (434), pp. 1–27.
- [45] Bruneau, D., Cronin, D., Giudice, J. S., Panzer, M. B., and Kent, R., 2018, "Comparison of the

- Hybrid III Head and Neck to a Detailed Head and Neck Finite Element Model with Active Musculature, in a Football Impact Scenario,” *IRCOBI Conference*, IRCOBI, Athens, Greece, pp. 322–323.
- [46] Bustamante, M., Bruneau, D., Barker, J., Gierczycka, D., Corrales, M., and Cronin, D., 2019, “Component-Level Finite Element Model and Validation for a Modern American Football Helmet,” *J. Dyn. Behav. Mater.*
- [47] Barker, J., Corrales, M., Gierczycka, D., Bruneau, D., Bustamante, M. C., and Cronin, D., 2018, “Contribution of Energy-absorbing Structures to Head Kinematics in Football Helmet Impacts,” *IRCOBI Conference*, IRCOBI, Athens, Greece, pp. 315–316.
- [48] Yoganandan, N., Pintar, F. A., Zhang, J., and Baisden, J. L., 2009, “Physical Properties of the Human Head: Mass, Center of Gravity and Moment of Inertia,” *J. Biomech.*, **42**(9), pp. 1177–1192.
- [49] “Anatomical Terminology,” Natl. Cancer Inst. - Training Modul. [Online]. Available: <https://training.seer.cancer.gov/anatomy/body/terminology.html>. [Accessed: 30-Oct-2018].
- [50] Standring, S., Borley, N., Collins, P., Crossman, A., Gatzoulis, M., Healy, J., Johnson, D., Mahadevan, V., Newell, R., and Wigley, C., eds., 2008, *Gray’s Anatomy: The Anatomical Basis of Clinical Practice*, Churchill Livingstone Elsevier.
- [51] Sinclair, A. J., 2012, “Cerebrospinal Fluid and Lumbar Puncture : A Practical Review,” *Neurology*, **259**, pp. 1530–1545.
- [52] Ho, J., Zhou, Z., Li, X., and Kleiven, S., 2017, “The Peculiar Properties of the Falx and Tentorium in Brain Injury Biomechanics,” *J. Biomech.*, **60**, pp. 243–247.
- [53] Mysid, and Team, S. D., “Meninges of the Central Nervous Parts” [Online]. Available: <https://commons.wikimedia.org/wiki/File:Meninges-en.svg>. [Accessed: 30-Oct-2018].
- [54] Budday, S., Sommer, G., Birkl, C., Langkammer, C., Haybaeck, J., Kohnert, J., Bauer, M., Paulsen, F., Steinmann, P., Kuhl, E., and Holzapfel, G. A., 2017, “Mechanical Characterization of Human Brain Tissue,” *Acta Biomater.*, **48**, pp. 319–340.
- [55] Post, A., Blaine Hoshizaki, T., Gilchrist, M. D., and Cusimano, M. D., 2017, “Peak Linear and Rotational Acceleration Magnitude and Duration Effects on Maximum Principal Strain in the Corpus Callosum for Sport Impacts,” *J. Biomech.*, **61**, pp. 183–192.
- [56] Patton, D., McIntosh, A., and Kleiven, S., 2015, “The Biomechanical Determinants of Concussion: Finite Element Simulations to Investigate Tissue-Level Predictors of Injury During Sporting

- Impacts to the Unprotected Head,” *J. Appl. Biomech.*, pp. 721–730.
- [57] McAllister, T. W., Ford, J. C., Ji, S., Beckwith, J. G., Flashman, L. A., Paulsen, K., and Greenwald, R. M., 2012, “Maximum Principal Strain and Strain Rate Associated with Concussion Diagnosis Correlates with Changes in Corpus Callosum White Matter Indices,” *Ann. Biomed. Eng.*, **40**(1), pp. 127–140.
- [58] Hernandez, F., Giordano, C., Goubran, M., Parivash, S., Grant, G., and Zeineh, M., 2019, “Lateral Impacts Correlate with Falx Cerebri Displacement and Corpus Callosum Trauma in Sports - Related Concussions,” *Biomech. Model. Mechanobiol.*, (0123456789).
- [59] Jones, E. G., 1985, *The Thalamus*, Springer Science+Business Media LLC, Irvine, California, USA.
- [60] Fice, J. B., 2010, “Numerical Modeling of Whiplash Injury,” University of Waterloo.
- [61] Salo, P. K., Kautiainen, H., and Há, A. H., 2006, “Isometric Strength of the Cervical Flexor , Extensor , and Rotator Muscles in 220 Healthy Females Aged 20 to 59 Years,” *J. Orthop. Sport. Phys. Ther.*, **36**(7), pp. 495–502.
- [62] Beckwith, J. G., Zhao, W., Ji, S., Ajamil, A. G., Bolander, R. P., Chu, J. J., McAllister, T. W., Crisco, J. J., Duma, S. M., Rowson, S., Broglio, S. P., Guskiewicz, K. M., Mihalik, J. P., Anderson, S., Schnebel, B., Gunnar Broolinson, P., Collins, M. W., and Greenwald, R. M., 2018, “Estimated Brain Tissue Response Following Impacts Associated With and Without Diagnosed Concussion,” *Ann. Biomed. Eng.*, **46**(6), pp. 819–830.
- [63] Morris, S.-A., Jones, W. H., Proctor, M. R., and Day, A. L., 2014, “Emergent Treatment of Athletes With Brain Injury,” *Neurosurgery*, **75**(4), pp. S96–S105.
- [64] Omalu, B. I., DeKosky, S. T., Hamilton, R. L., Minster, R. L., Kamboh, M. I., Shakir, A. M., and Wecht, C. H., 2006, “Chronic Traumatic Encephalopathy in a National Football League Player: Part II,” *Neurosurgery*, **59**(5), pp. 1086–1092.
- [65] Mckee, A. C., Cantu, R. C., Nowinski, C. J., Hedley-whyte, E. T., Gavett, B. E., Budson, A. E., Santini, V. E., Lee, H., Kubilus, C. A., and Stern, R. A., 2009, “Chronic Traumatic Encephalopathy in Athletes : Progressive Tauopathy After Repetitive Head Injury,” **68**(7), pp. 709–735.
- [66] Johnson, K. L., Chowdhury, S., Lawrimore, W. B., Mao, Y., Mehmani, A., Prabhu, R., Rush, G. A., and Horstemeyer, M. F., 2016, “Constrained Topological Optimization of a Football Helmet Facemask Based on Brain Response,” *Mater. Des.*, **111**, pp. 108–118.
- [67] Gennarelli, T. A., 2015, “The Centripetal Theory of Concussion (CTC) Revisited after 40 Years and

- a Proposed New Symptomcentric Concept of the Concussions,” *IRCOBI Conference 2015*, pp. 1131–1138.
- [68] Khong, E., Odenwald, N., Hashim, E., and Cusimano, M. D., 2016, “Diffusion Tensor Imaging Findings in Post-Concussion Syndrome Patients after Mild Traumatic Brain Injury: A Systematic Review,” *Front. Neurol.*, **7**(SEP), pp. 1–8.
- [69] Stone, J. R., Okonkwo, D. O., Dialo, A. O., Rubin, D. G., Mutlu, L. K., Povlishock, J. T., and Helm, G. A., 2004, “Impaired Axonal Transport and Altered Axolemmal Permeability Occur in Distinct Populations of Damaged Axons Following Traumatic Brain Injury,” *Exp. Neurol.*, **190**(1), pp. 59–69.
- [70] Viano, D. C., Casson, I. R., Pellman, E. J., Zhang, L., King, A. I., and Yang, K. H., 2005, “Concussion in Professional Football: Brain Responses by Finite Element Analysis: Part 9,” *Neurosurgery*, **57**(5), pp. 891–915.
- [71] King, A. I., Yang, K. H., Zhang, L., Hardy, W., and Viano, D. C., 2003, “Is Head Injury Caused by Linear or Angular Acceleration?,” *IRCOBI Conference*, IRCOBI, Lisbon, Portugal, pp. 1–12.
- [72] Thomas A. Gennarelli, Lawrence E. Thibault, G. Tomei, R. Wisner, D. G. and J. A., 1897, “Directional Dependence of Axonal Brain Injury Due to Centroidal and Non-Centroidal Acceleration,” *SAE Transactions 96*, pp. 1355–359.
- [73] Lessley, D. J., Kent, R. W., Funk, J. R., Sherwood, C. P., Cormier, J. M., Crandall, J. R., Arbogast, K. B., and Myers, B. S., 2018, “Video Analysis of Reported Concussion Events in the National Football League During the 2015-2016 and 2016-2017 Seasons,” *Am. J. Sports Med.*, **46**(14), pp. 3502–3510.
- [74] Pellman, E. J., Viano, D. C., Tucker, A. M., Casson, I. R., Valadka, A. B., Maroon, J. C., Bailes, J. E., Kelly, D. F., and Levy, M. L., 2003, “Concussion in Professional Football: Location and Direction of Helmet Impacts - Part 2,” *Neurosurgery*, **53**(6), pp. 1328–1341.
- [75] Broglio, S. P., Sosnoff, J. J., Shin, S., He, X., Alcaraz, C., and Zimmerman, J., 2009, “Head Impacts During High School Football: A Biomechanical Assessment,” **44**(4), pp. 342–349.
- [76] Pellman, E. J., Viano, D. C., Tucker, A. M., Casson, I. R., Waeckerle, J. F., Maroon, J. C., Lovell, M. R., Collins, M. W., Kelly, D. F., Valadka, A. B., Cantu, R. C., Bailes, J. E., and Levy, M. L., 2003, “Concussion in Professional Football: Reconstruction of Game Impacts and Injuries,” *Neurosurgery*, **53**(4), pp. 799–814.
- [77] NOCSAE, 2015, *Standard Pneumatic Ram Test Method and Equipment Used in Evaluating the*

Performance Characteristics of Protective Headgear and Face Guards.

- [78] Spittle, E., Shipley, B. W., and Kaleps, I., 1992, *Hybrid II and Hybrid III Dummy Neck Properties for Computer Modeling*, Dayton, OH.
- [79] Bartsch, A., Benzel, E., Miele, V., Morr, D., and Prakash, V., 2012, “Hybrid III Anthropomorphic Test Device (ATD) Response to Head Impacts and Potential Implications for Athletic Headgear Testing,” *Accid. Anal. Prev.*, **48**, pp. 285–291.
- [80] Giudice, J. S., Park, G., Kong, K., Bailey, A., Kent, R., and Panzer, M. B., 2019, “Development of Open-Source Dummy and Impactor Models for the Assessment of American Football Helmet Finite Element Models,” *Ann. Biomed. Eng.*, **47**(2), pp. 464–474.
- [81] Kaleps, I., White, R. P., Beecher, R. M., Whitestone, J., and Obergefell, L. A., 1988, *Measurement of Hybrid III Dummy Properties and Analytical Simulation Data Base Development*, Ohio, USA.
- [82] Funk, J., Cormier, J., Bain, C., Guzman, H., and Bonugli, E., 2009, “Validation and Application of a Methodology to Calculate Head Accelerations and Neck Loading in Soccer Ball Impacts,” *SAE Int.*, pp. 2009-01–0251.
- [83] Cheng, Y., Kheng Leow, W., and Chye Lim, T., 2012, “Automatic Identification of Frankfurt Plane and Mid-Sagittal Plane of Skull,” *Proc. IEEE Work. Appl. Comput. Vis.*, pp. 233–238.
- [84] Butz, R. C., Knowles, B. M., Newman, J. A., and Dennison, C. R., 2015, “Effects of External Helmet Accessories on Biomechanical Measures of Head Injury Risk: An ATD Study Using the HYBRIDIII Headform,” *J. Biomech.*, **48**(14), pp. 3816–3824.
- [85] BIOCORE, 2019, “Resources” [Online]. Available: <http://biocorellc.com/resources/>.
- [86] Yoganandan, N., Sances, A., and Pintar, F. A., 1989, “Biomechanical Evaluation of the Axial Compressive Responses of the Human Cadaveric And,” **111**(August 1989).
- [87] Giordano, C., Cloots, R. J. H., van Dommelen, J. A. W., and Kleiven, S., 2014, “The Influence of Anisotropy on Brain Injury Prediction,” *J. Biomech.*, **47**(5), pp. 1052–1059.
- [88] Rousseau, P., Hoshizaki, T. B., and Gilchrist, M. D., 2010, “Estimating the Influence of Neckform Compliance on Brain Tissue Strain during a Helmeted Impact,” *Stapp Car Crash J.*, **11**(54), pp. 37–48.
- [89] Rousseau, P., and Hoshizaki, T. B., 2009, “The Influence of Deflection and Neck Compliance on the Impact Dynamics of a Hybrid III Headform,” *Proc. Inst. Mech. Eng. Part P J. Sport. Eng. Technol.*, **223**(3), pp. 89–97.

- [90] Sanchez, E. J., Gabler, L. F., Good, A. B., Funk, J. R., Crandall, J. R., and Panzer, M. B., 2019, “A Reanalysis of Football Impact Reconstructions for Head Kinematics and Finite Element Modeling,” *Clin. Biomech.*, **64**(April), pp. 82–89.
- [91] Newman, J. A., Beusenbergh, M. C., Shewchenko, N., Withnall, C. A., and Fournier, E., 2005, “Verification of Biomechanical Methods Employed in a Comprehensive Study of Mild Traumatic Brain Injury and the Effectiveness of American Football Helmets,” **38**, pp. 1469–1481.
- [92] Withnall, C., Shewchenko, N., Gittens, R., and Dvorak, J., 2005, “Biomechanical Investigation of Head Impacts in Football,” *Br. J. Sports Med.*, **39**(SUPPL. 1), pp. 49–58.
- [93] Takhounts, E. G., Craig, M. J., Moorhouse, K., McFadden, J., and Hasija, V., 2013, “Development of Brain Injury Criteria (BrIC),” *Stapp Car Crash J.*, **57**(November), p. 243.
- [94] Hutchinson, J., Kaiser, M. J., and Lankarani, H. M., 1998, “The Head Injury Criterion (HIC) Functional,” *Appl. Math. Comput.*, **96**(1), pp. 1–16.
- [95] Gabler, L. F., Crandall, J. R., and Panzer, M. B., 2016, “Assessment of Kinematic Brain Injury Metrics for Predicting Strain Responses in Diverse Automotive Impact Conditions,” *Ann. Biomed. Eng.*, **44**(12), pp. 3705–3718.
- [96] Morrison, B., Elkin, B. S., Dollé, J.-P., and Yarmush, M. L., 2011, “In Vitro Models of Traumatic Brain Injury,” *Annu. Rev. Biomed. Eng.*, **13**(1), pp. 91–126.
- [97] Simms, C., and Wood, D., 2009, *Pedestrian and Cyclist Impact: A Biomechanical Perspective*, Springer, Dordrecht Heidelberg London New York.
- [98] Hardy, W. N., Mason, M. J., Foster, C. D., Shah, C. S., Kopacz, J. M., Yang, H., King, A. I., Bishop, J., and Bey, M., 2008, “A Study of the Response of the Human Cadaver Head to Impact,” *Stapp Car Crash J.*, **51**, pp. 17–80.
- [99] Miller, L. E., Urban, J. E., and Stitzel, J. D., 2017, “Validation Performance Comparison for Finite Element Models of the Human Brain,” *Comput. Methods Biomech. Biomed. Engin.*, **20**(12), pp. 1273–1288.
- [100] Takhounts, E., Danelson, K., Stitzel, J., Rowson, S., and Duma, S., 2008, “Investigation of Traumatic Brain Injuries Using the next Generation of Simulated Injury Monitor (SIMon) Finite Element Head Model Simulated Injury Monitor (SIMon) Finite Element Head Model,” *Stapp Car Crash J.*, **52**(January), pp. 1–31.
- [101] Kimpara, H., Nakahira, Y., Iwamoto, M., and Miki, K., 2006, “Investigation of Anteroposterior

- Head-Neck Responses during Severe Frontal Im ...,” *Stapp Car Crash J.*, **50**(November), pp. 509–544.
- [102] Horgan, T. J., and Gilchrist, M. D., 2003, “The Creation of Three-Dimensional Finite Element Models for Simulating Head Impact Biomechanics,” *Int. J. Crashworthiness*, **8**(4), pp. 353–366.
- [103] Ji, S., Zhao, W., Ford, J. C., Beckwith, J. G., Bolander, R. P., Greenwald, R. M., Flashman, L. A., Paulsen, K. D., and McAllister, T. W., 2015, “Group-Wise Evaluation and Comparison of White Matter Fiber Strain and Maximum Principal Strain in Sports-Related Concussion,” *J. Neurotrauma*, **32**(7), pp. 441–454.
- [104] Chatelin, S., Constantinesco, A., and Willinger, R., 2010, “Fifty Years of Brain Tissue Mechanical Testing: From in Vitro to in Vivo Investigations,” *Biorheology*, **47**(5–6), pp. 255–276.
- [105] Ji, S., Ghadyani, H., Bolander, R. P., Beckwith, J. G., Ford, J. C., McAllister, T. W., Flashman, L. A., Paulsen, K. D., Ernstrom, K., Jain, S., Raman, R., Zhang, L., and Greenwald, R. M., 2014, “Parametric Comparisons of Intracranial Mechanical Responses from Three Validated Finite Element Models of the Human Head,” *Ann. Biomed. Eng.*, **42**(1), pp. 11–24.
- [106] Mao, H., Gao, H., Cao, L., Genthikatti, V. V., and King, H., 2013, “Development of High-Quality Hexahedral Human Brain Meshes Using Feature-Based Multi-Block Approach,” *Comput. Methods Biomech. Biomed. Engin.*, **5842**.
- [107] Zhao, W., and Ji, S., 2019, “Mesh Convergence Behavior and the Effect of Element Integration of a Human Head Injury Model,” **47**(2), pp. 475–486.
- [108] Rowson, S., 2008, “Impact Biomechanics of the Head and Neck in Football.Pdf,” Virginia Polytechnic Institute and State University, Virginia, USA.
- [109] NHTSA, 2019, “New CSDM Calculation for New SIMon Model” [Online]. Available: <https://www.nhtsa.gov/DOCUMENT/SIMON-MODELZIP> . [Accessed: 20-Apr-2019].
- [110] Zhang, L., Yang, K. H., and King, A. I., 2001, “Comparison of Brain Responses Between Frontal and Lateral Impacts by Finite Element Modeling,” *J. Neurotrauma*, **18**(1), pp. 21–30.
- [111] Post, A., Kendall, M., Cournoyer, J., Karton, C., Oeur, R. A., Dawson, L., Hoshizaki, T. B., Post, A., Kendall, M., Cournoyer, J., Karton, C., and Oeur, R. A., 2018, “Brain Tissue Analysis of Impacts to American Football Helmets,” *Comput. Methods Biomech. Biomed. Engin.*, **5842**, pp. 1–14.
- [112] GlobalHumanBodyModelsConsortium, 2015, “Global Human Body Models Consortium, LLC User Manual: M50 Occupant Version 4.4 for LS-DYNA.”

- [113] Brolin, K., Halldin, P., and Leijonhufvud, I., 2005, “The Effect of Muscle Activation on Neck Response,” *Traffic Inj. Prev.*, **6**(1), pp. 67–76.
- [114] Östh, J., Mendoza-Vazquez, M., Sato, F., Svensson, M. Y., Linder, A., and Brolin, K., 2017, “A Female Head–Neck Model for Rear Impact Simulations,” *J. Biomech.*, **51**, pp. 49–56.
- [115] Eckner, J. T., Oh, Y. K., Joshi, M. S., Richardson, J. K., and Ashton-Miller, J. A., 2014, “Effect of Neck Muscle Strength and Anticipatory Cervical Muscle Activation on the Kinematic Response of the Head to Impulsive Loads,” *Am. J. Sports Med.*, **42**(3), pp. 566–576.
- [116] Schmidt, J. D., Guskiewicz, K. M., Blackburn, J. T., Mihalik, J. P., Siegmund, G. P., and Marshall, S. W., 2014, “The Influence of Cervical Muscle Characteristics on Head Impact Biomechanics in Football,” *Am. J. Sports Med.*, **42**(9), pp. 2056–2066.
- [117] Mihalik, J. P., Cat, C., Guskiewicz, K. M., Marshall, S. W., Greenwald, R. M., Blackburn, J. T., and Cantu, R. C., 2011, “Does Cervical Muscle Strength in Youth Ice Hockey Players Affect Head Impact Biomechanics ?,” **21**(5), pp. 416–421.
- [118] Morimoto, K., Sakamoto, M., Fukuhara, T., and Kato, K., 2013, “Electromyographic Study of Neck Muscle Activity According to Head Position in Rugby Tackles,” *J. Phys. Ther. Sci.*, **25**(5), pp. 563–566.
- [119] Herbert, R., 1988, “The Passive Mechanical Properties of Muscle and Their Adaptations to Altered Patterns of Use,” *Aust. J. Physiother.*, **34**(3), pp. 141–149.
- [120] Alvarez, V. S., Halldin, P., and Kleiven, S., 2014, “Influence of Neck Muscle Tonus and Posture on Brain Tissue Strain during Pedestrian Impacts,” 11th. World Congr. Comput. Mech. (WCCM XI), 5th. Eur. Conf. Comput. Mech. (ECCM V), **58**(April 2016), pp. 2006–2007.
- [121] Panzer, M. B., 2006, “Numerical Modelling of the Human Cervical Spine in Frontal Impact,” University of Waterloo.
- [122] Osth, J., Eliasson, E., Happee, R., and Brolin, K., 2014, “A Method to Model Anticipatory Postural Control in Driver Braking Events,” *Gait Posture*, **40**, pp. 664–669.
- [123] Ewing, C. L., and Thomas, D. J., 1972, *Human Head and Neck Response To Impact Acceleriation*, Springfield, VA.
- [124] Thunnissen JGM, Wismans J, Ewing CL, T. D., 1995, “Human Volunteer Head-Neck Response in Frontal Flexion: A New Analysis,” *SAE Trans.*, **104**(SECTION 6: JOURNAL OF PASSENGER CARS, Part 2), pp. 3065–3086.

- [125] Deng, B., 1999, “Kinematics of Human Cadaver Cervical Spine During Low Speed Rear-End Impacts,” Wayne State University, Michigan, USA.
- [126] Barker, J. B., Cronin, D. S., and Nightingale, R. W., 2017, “Lower Cervical Spine Motion Segment Computational Model Validation: Kinematic and Kinetic Response for Quasi-Static and Dynamic Loading,” *J. Biomech. Eng.*, **139**(6), p. 061009.
- [127] Mattucci, S. F. E., Moulton, J. A., Chandrashekar, N., and Cronin, D. S., 2012, “Strain Rate Dependent Properties of Younger Human Cervical Spine Ligaments,” *J. Mech. Behav. Biomed. Mater.*, **10**, pp. 216–226.
- [128] Barker, J. B., and Cronin, D. S., 2014, “High Rotation Rate Behavior of Cervical Spine Segments in Flexion and Extension,” **136**(December 2014), pp. 1–10.
- [129] Lasswell, T. L., Cronin, D. S., Medley, J. B., and Rasoulinejad, P., 2017, “Incorporating Ligament Laxity in a Finite Element Model for the Upper Cervical Spine,” *Spine J.*, **17**(11), pp. 1755–1764.
- [130] Cronin, D. S., 2010, *Global Human Body Models Consortium, LLC, Project Report - Neck Model (Sept. 1, 2010 - Nov. 30, 2010)*.
- [131] Hallquist, J., 2006, *LS-DYNA Theory Manual*, Livermore Software Technology Corporation, Livermore, California.
- [132] White, N. A., Danelson, K. A., Scott Gayzik, F., and Stitzel, J. D., 2014, “Head and Neck Response of a Finite Element Anthropomorphic Test Device and Human Body Model During a Simulated Rotary-Wing Aircraft Impact,” *J. Biomech. Eng.*, **136**(11), p. 111001.
- [133] Thunert, C., 2012, “CORAS Release 3.6 User’s Manual,” Partnersh. Dummy Technol. Biomech. [Online]. Available: <http://www.pdb-org.com/en/information/18-cora-download.html>.
- [134] Vavalle, N. A., Jelen, B. C., Moreno, D. P., Stitzel, J. D., and Gayzik, F. S., 2013, “An Evaluation of Objective Rating Methods for Full-Body Finite Element Model Comparison to PMHS Tests,” *Traffic Inj. Prev.*, **14**(SUPPL1), pp. S87–S94.
- [135] Poulard, D., Kent, R. W., Kindig, M., Li, Z., and Subit, D., 2015, “Thoracic Response Targets for a Computational Model: A Hierarchical Approach to Assess the Bio Fidelity of a 50th-Percentile Occupant Male Finite Element Model,” *J. Mech. Behav. Biomed. Mater.*, **45**, pp. 45–64.
- [136] Zhang, L., Ramesh, D., Yang, K. H., and King, A. I., 2003, “EFFECTIVENESS OF THE FOOTBALL HELMET ASSESSED BY FINITE ELEMENT MODELING AND IMPACT TESTING,” *IRCOBI Conference*, pp. 27–38.

- [137] Johnston, J. M., Ning, H., Kim, J. E., Kim, Y. H., Soni, B., Reynolds, R., Cooper, L., Andrews, J. B., and Vaidya, U., 2015, "Simulation, Fabrication and Impact Testing of a Novel Football Helmet Padding System That Decreases Rotational Acceleration," *Sport. Eng.*, **18**(1), pp. 11–20.
- [138] Craig, M. J., 2007, "Biomechanics of Jaw Loading in Football Helmet Impacts," Wayne State University, Detroit, Michigan, USA.
- [139] Rush, G. A., 2016, "Design of an American Football Helmet Liner for Concussion Mitigation," Mississippi State University, Mississippi, USA.
- [140] Xenith LLC, 2019, "X2E Varsity," Xenith, LLC [Online]. Available: <https://www.xenith.com/products/x2e-plus-varsity-helmet>. [Accessed: 14-May-2019].
- [141] Darling, T., 2014, "Finite Element Modeling of Human Brain Response to Football Helmet Impacts," ARIZONA STATE UNIVERSITY, Arizona, USA.
- [142] Luo, Y., and Liang, Z., 2013, "Sport Helmet Design and Virtual Impact Test by Image-Based Finite Element Modeling," *Conf. Proc. ... Annu. Int. Conf. IEEE Eng. Med. Biol. Soc. IEEE Eng. Med. Biol. Soc. Annu. Conf.*, **2013**, pp. 7237–7240.
- [143] Newell, R. S., Blouin, J., Street, J., Cripton, P. A., and Siegmund, G. P., 2018, "The Neutral Posture of the Cervical Spine Is Not Unique in Human Subjects," *J. Biomech.*, **80**, pp. 53–62.
- [144] Cheng, C., Chien, A., Hsu, W., and Chen, C. P., 2016, "Investigation of the Differential Contributions of Superficial and Deep Muscles on Cervical Spinal Loads with Changing Head Postures," *PLoS One*, pp. 1–12.
- [145] Bandak, F. A., Zhang, A. X., Tannous, R. E., Dimasi, F., Masiello, P., and Eppinger, R., "SIMon: A SIMULATED INJURY MONITOR; APPLICATION TO HEAD INJURY ASSESSMENT," pp. 1–7.
- [146] Giudice, J. S., Kong, K., Caudillo, A., Mukherjee, S., and Panzer, M. B., 2018, "User Manual - Finite Element Models of Helmet Assessment Tools" [Online]. Available: <http://biocorellc.com/resources/>.
- [147] Cronin, D. S., 2013, *Project Quarterly Report, July 22, 2013, Neck Model*.
- [148] Dawson, L. E., Oeur, R. A., and Hoshizaki, T. B., 2014, "The Influence of Striker Cap Size on the Dynamic Response of a Hybrid III Headform," *The Mechanism of Concussion in Sports*, ATSM International, pp. 13–22.
- [149] Crandall, J., 2017, "New Video Review Data to Help Improve Designs for Protective Equipment"

- [Online]. Available: <https://www.playsmartplaysafe.com/focus-on-safety/advanced-technology/new-video-review-data-help-improve-designs-protective-equipment/>.
- [150] Maas, A. I. R., Menon, D. K., Adelson, P. D., Andelic, N., Bell, M. J., Belli, A., Bragge, P., Brazinova, A., Büki, A., Chesnut, R. M., Citerio, G., Coburn, M., Cooper, D. J., Crowder, A. T., Czeiter, E., Czosnyka, M., Diaz-Arrastia, R., Dreier, J. P., Duhaime, A. C., Ercole, A., van Essen, T. A., Feigin, V. L., Gao, G., Giacino, J., Gonzalez-Lara, L. E., Gruen, R. L., Gupta, D., Hartings, J. A., Hill, S., Jiang, J. yao, Ketharanathan, N., Kompanje, E. J. O., Lanyon, L., Laureys, S., Lecky, F., Levin, H., Lingsma, H. F., Maegele, M., Majdan, M., Manley, G., Marsteller, J., Mascia, L., McFadyen, C., Mondello, S., Newcombe, V., Palotie, A., Parizel, P. M., Peul, W., Piercy, J., Polinder, S., Puybasset, L., Rasmussen, T. E., Rossaint, R., Smielewski, P., Söderberg, J., Stanworth, S. J., Stein, M. B., von Steinbüchel, N., Stewart, W., Steyerberg, E. W., Stocchetti, N., Synnot, A., Te Ao, B., Tenovuo, O., Theadom, A., Tibboel, D., Videtta, W., Wang, K. K. W., Williams, W. H., Wilson, L., and Yaffe, K., 2017, “Traumatic Brain Injury: Integrated Approaches to Improve Prevention, Clinical Care, and Research,” *Lancet Neurol.*, **16**(12), pp. 987–1048.
- [151] Newman, J., Beusenbergh, M., Fournier, E., Shewchenko, N., King, A., Yang, K., Zhang, L., Mcelhaney, J., Carolina, N., Thibault, L., and McGinnis, G., 1999, “A New Biomechanical Assessment of Mild Traumatic Brain Injury: Part 1 - Methodology,” *IRCOBI Conference*, IRCOBI, Sitges (Spain), pp. 17–36.
- [152] Viano, D. C., Casson, I. R., and Pellman, E. J., 2007, “Concussion in Professional Football: Biomechanics of the Struck Player - Part 14,” *Neurosurgery*, **61**(2), pp. 313–327.
- [153] Virani, S., Russell, C. N., Bruschetta, M. L., Hua, K. N., Potvin, B. M., Cox, D. N., and Robinovitch, S. N., 2017, “The Effect of Shoulder Pad Design on Head Impact Severity during Checking,” *Med. Sci. Sports Exerc.*, **49**(3), pp. 573–580.
- [154] Rousseau, P., 2014, “Analysis of Concussion Metrics of Real-World Concussive and Non-Injurious Elbow and Shoulder to Head Collisions in Ice Hockey,” University of Ottawa, Ontario, Canada.

Appendix A: Verification of HNM Response

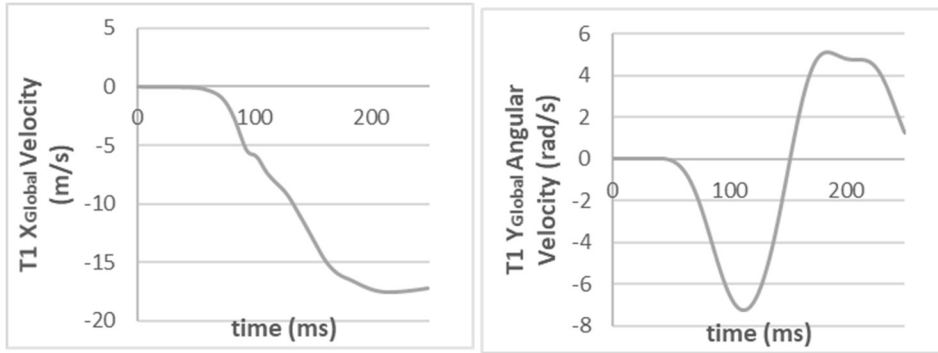


Figure A1 T1 inputs from 15g frontal case

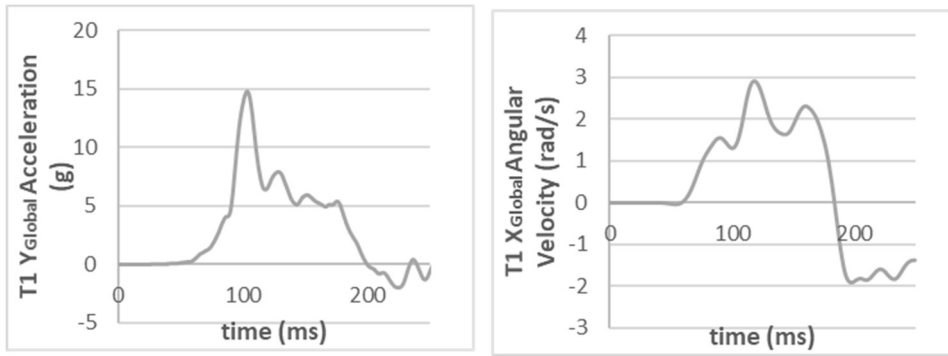


Figure A2 T1 inputs from 7g lateral case

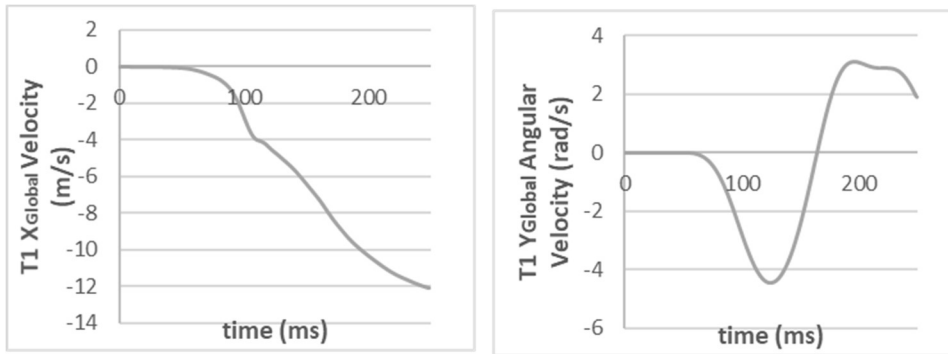


Figure A3 T1 inputs from 8g frontal case

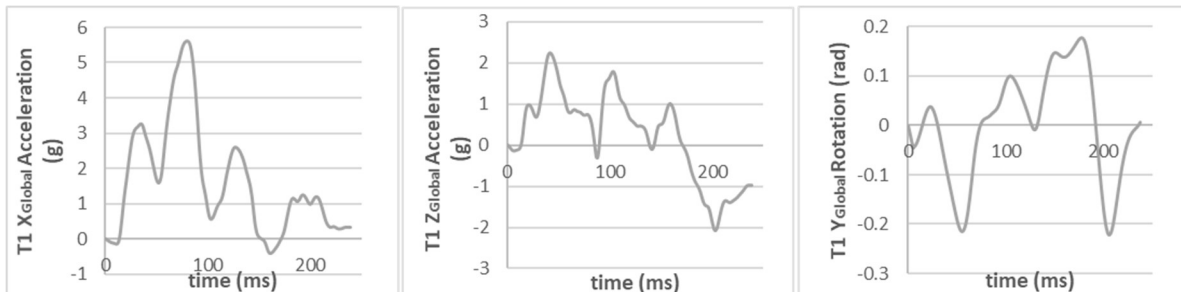


Figure A4 7g rear T1 inputs

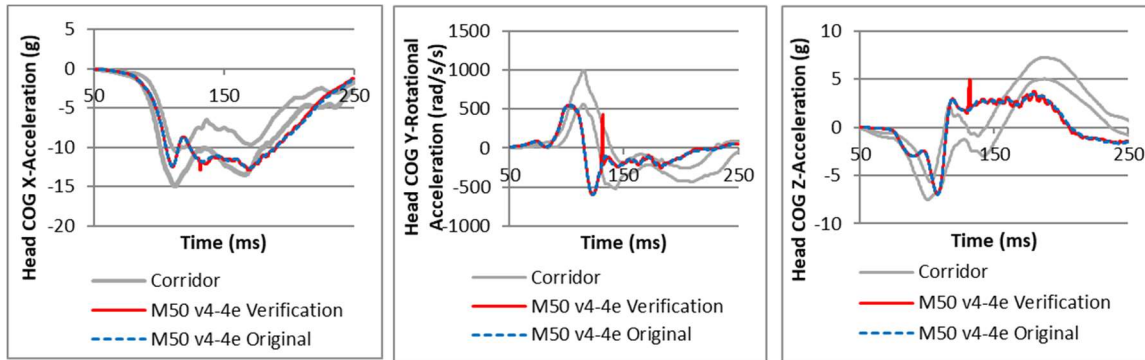


Figure A5 8g Frontal Model and Experimental Response

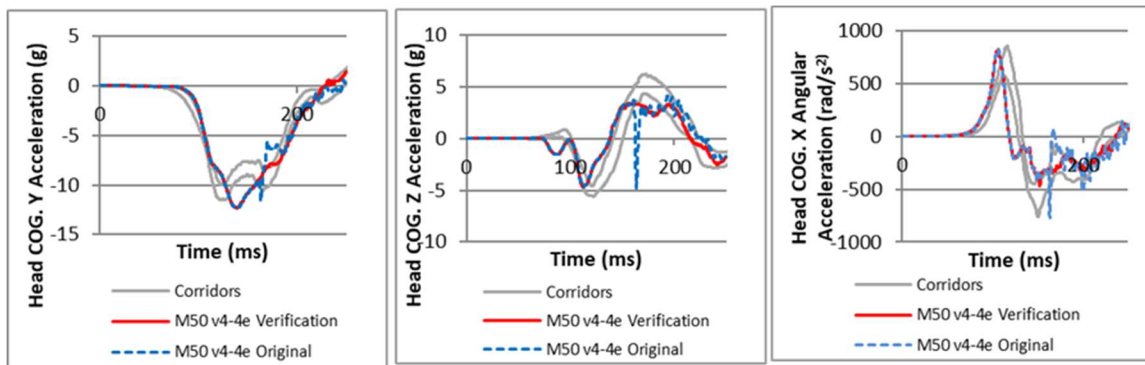


Figure A6 15g Frontal Model and Experimental Response

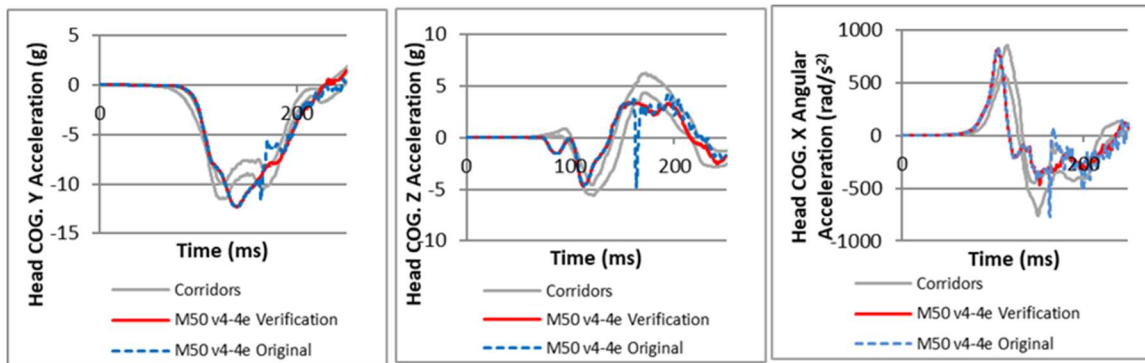


Figure A7 7g Lateral Model and Experimental Response

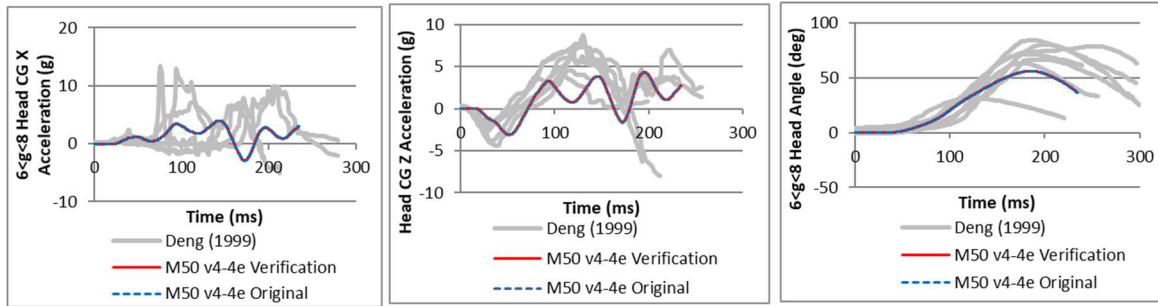


Figure A8 7g Rear Model and Experimental Response

Appendix B: Progression of Bare Head Impact

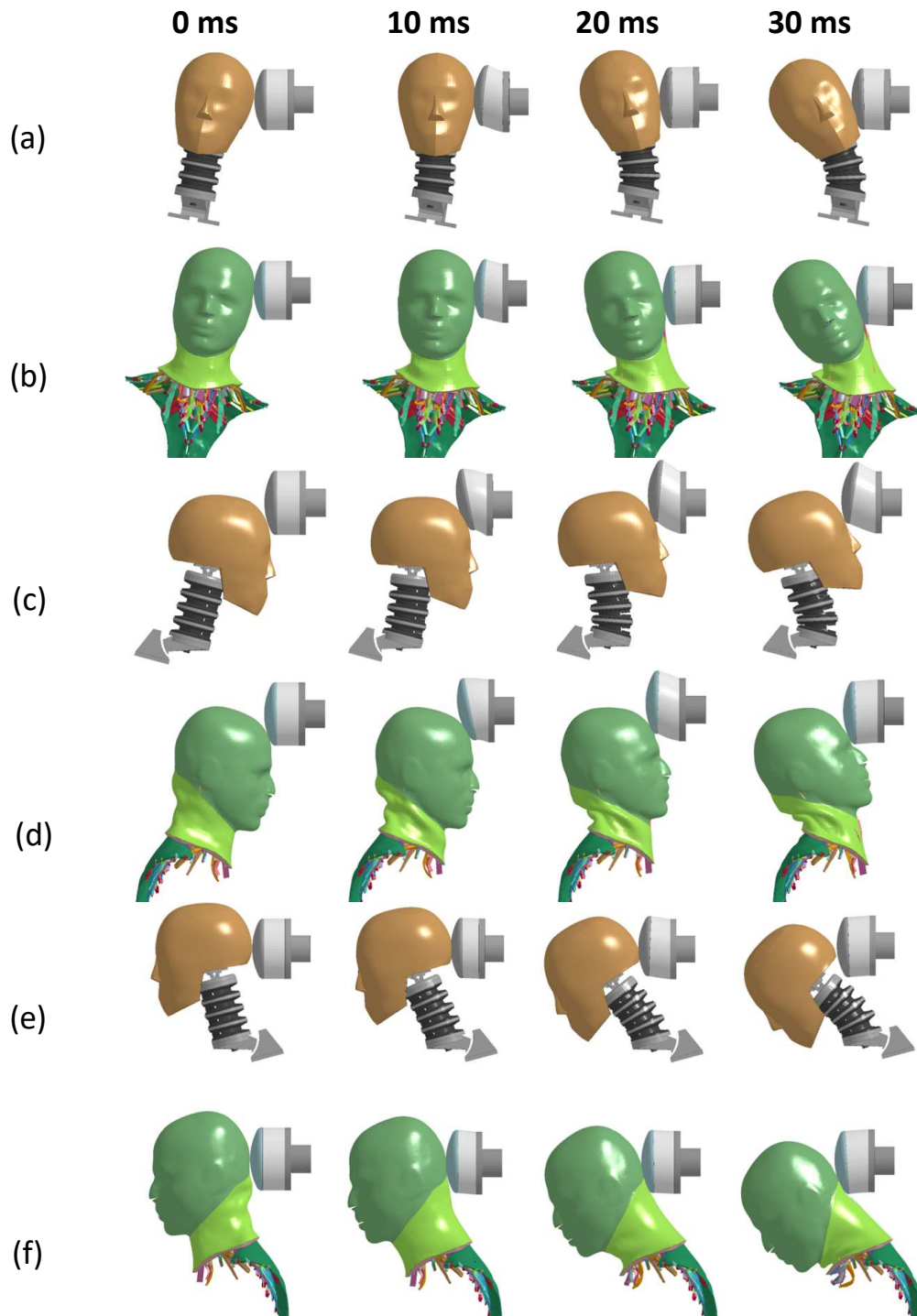


Figure B1 Progression of Bare Head Impacts: (a) ATD Simulation, Lateral 5.5 m/s, (b) HNM w. No Activation, Lateral 5.5 m/s, (c) ATD Simulation, Frontal 5.5 m/s, (d) HNM w. No Activation, Frontal 5.5 m/s, (e) ATD Simulation, Rear 5.5 m/s, (f) HNM w. No Activation, Rear 5.5 m/s

Appendix C: Head Kinematics and Other Metrics in All Impacts

Head Kinematics and Kinetics for All Cases

	5.5 m/s
	7.4 m/s
	9.3 m/s
<i>C, Bare-Head Impact</i>	
	5.5 m/s
	7.4 m/s

	9.3 m/s
<i>F, Bare-Head Impact</i>	
	5.5 m/s
	7.4 m/s
	9.3 m/s
<i>R, Bare-Head Impact</i>	
	5.5 m/s

	<p>7.4 m/s</p>
	<p>9.3 m/s</p>
<p><i>C, Helmeted Impact</i></p>	

	<p>5.5 m/s</p>
	<p>7.4 m/s</p>
	<p>9.3 m/s</p>
<p><i>F, Helmeted Impact</i></p>	

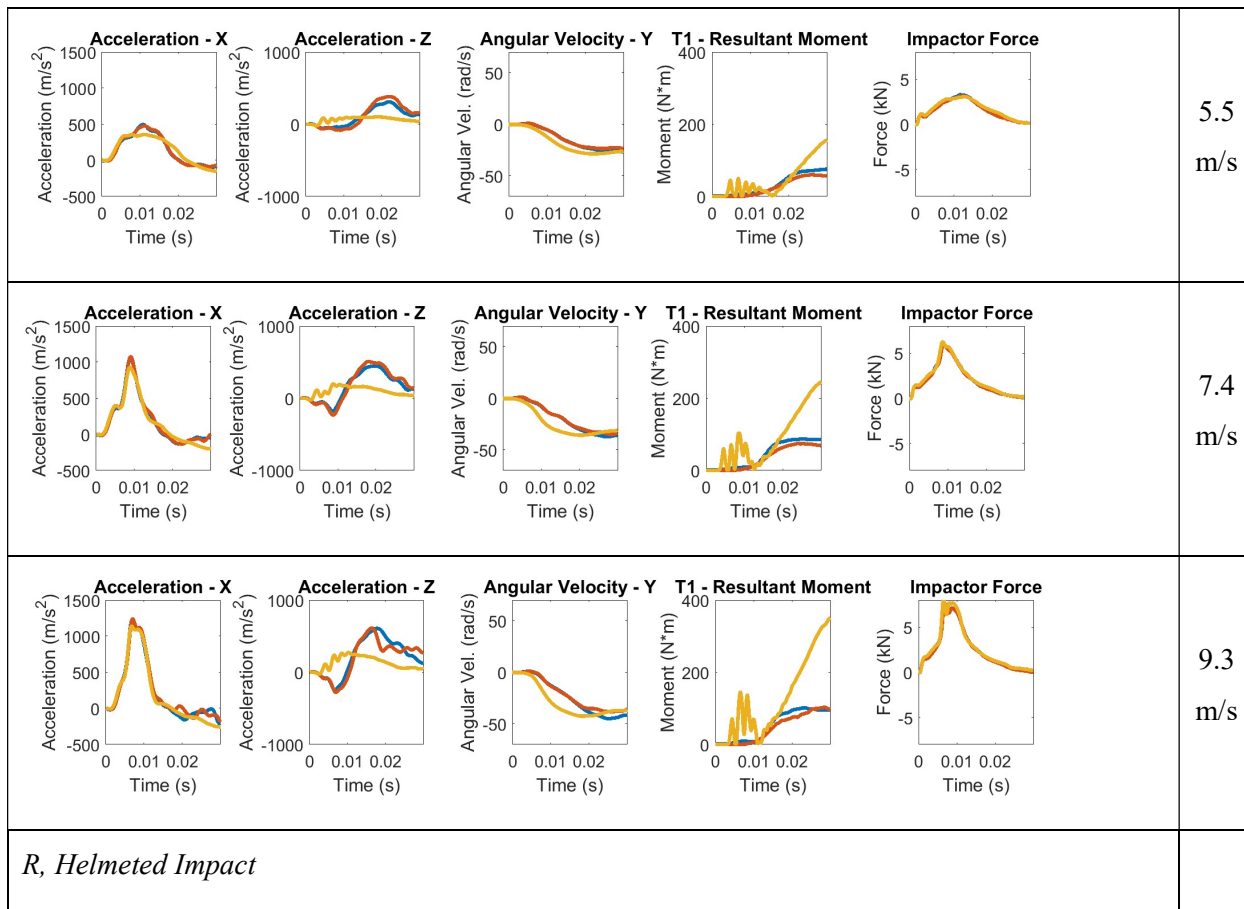
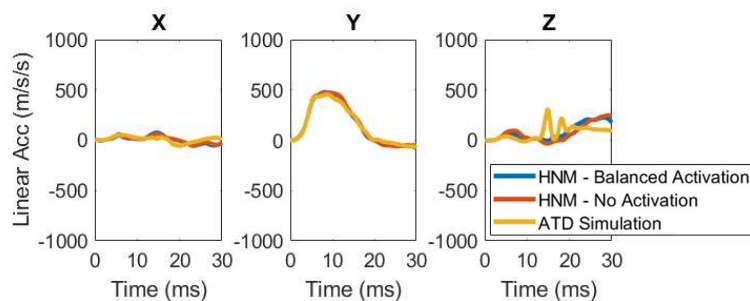


Figure C1 Kinematics and kinetics in all impacts

Out of Plane Kinematics

Kinematics in the primary plane of motion (global Y-Z for lateral orientation, global X-Z for frontal and rear) were examined in Chapter 5. The orientations used were chosen to minimize out-of-plane motion, to exercise the neck primarily in bending and axial compression. The 6 DOF kinematics are shown for the helmeted cases at 5.5 m/s, showing close to zero out-of-plane motion in the rear and frontal impacts, and small out of plane motions in the lateral impact (Figure C2, Figure C3).



(a)

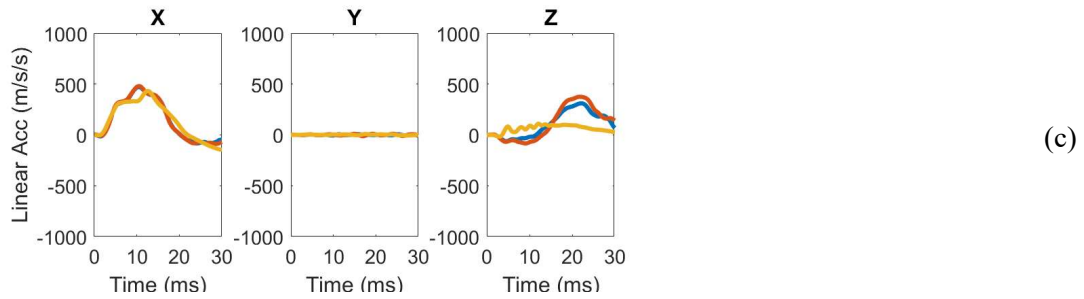
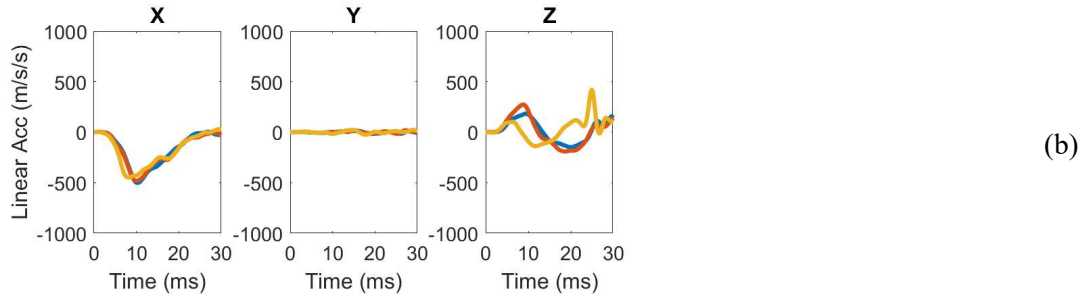


Figure C2 Helmeted Impact, 3DOF Linear Acceleration, 5.5 m/s, (a) Lateral, (b) Frontal, (c) Rear

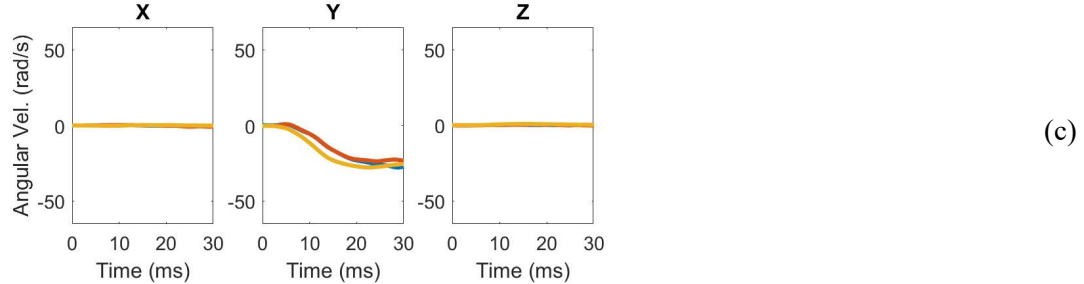
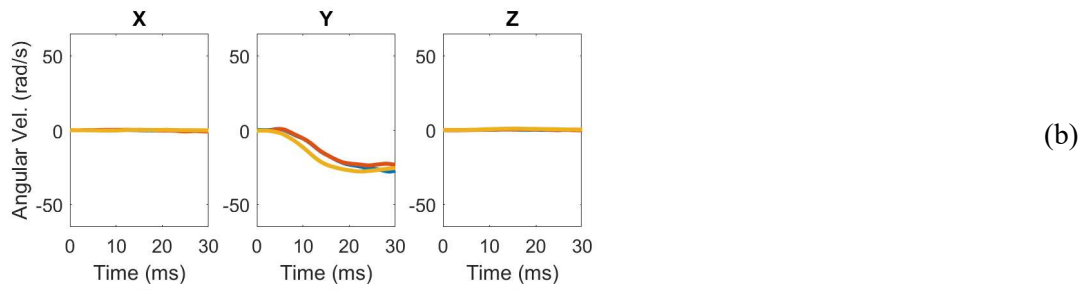
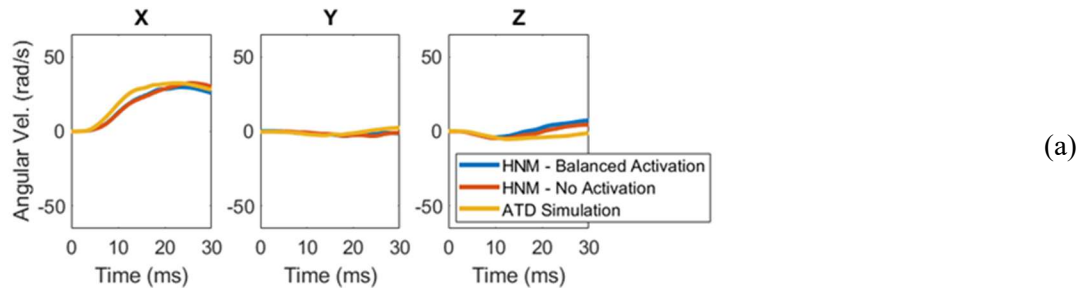
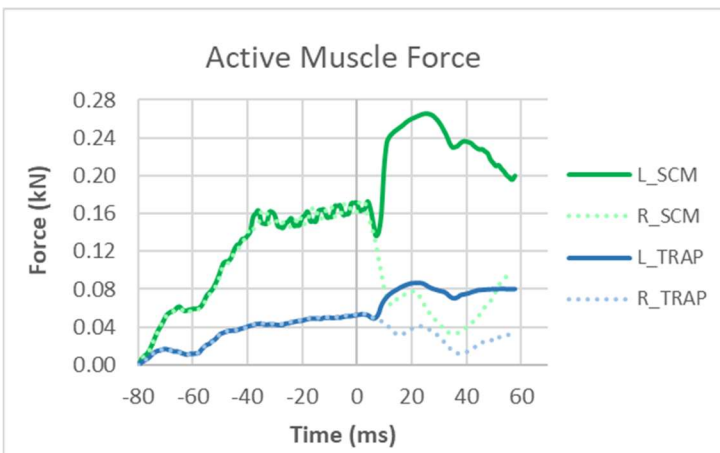


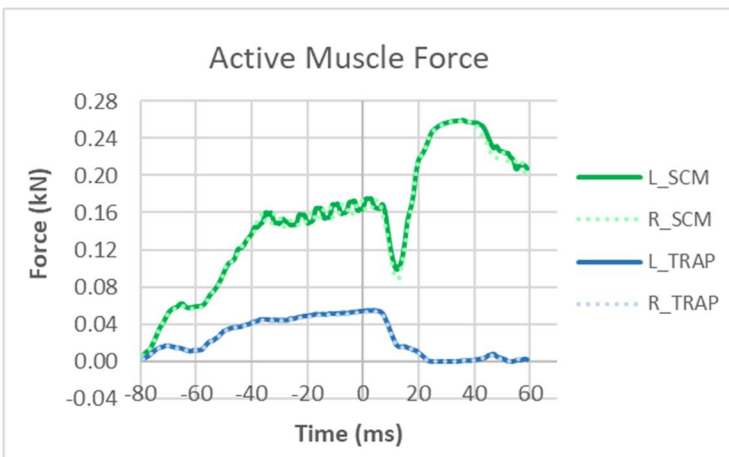
Figure C3 **Helmeted Impact, 3DOF Angular Velocity, 5.5 m/s, (a) Lateral, (b) Frontal, (c) Rear**

Muscle Force-Time Profiles

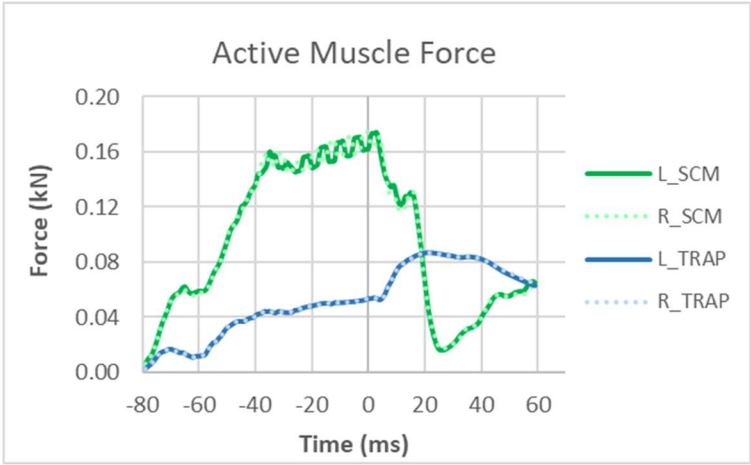
The level of active muscle force (the total force in the 1D Hill elements) is shown in the left and right sternocleidomastoid (L_SCM and R_SCM) and trapezius (L_TRAP and R_TRAP), at a cross-section 10 mm below the hyoid bone. In frontal and rear impacts (sagittal plane impacts) the left and right side had a nearly identical progression of muscle force (Figure C4b and Figure C4c), while in the lateral impact, the left and right side differed (Figure C4a). The muscle force decreased when a muscle went into compression, and increased when the muscle went into tension, in agreement with the behavior in the load curves in the Hill model. Increases in muscle force of up to 65% were observed when the Sternocleidomastoid went into tension in the frontal impact, while force decreased nearly to zero after the rear impact.



(a)



(b)



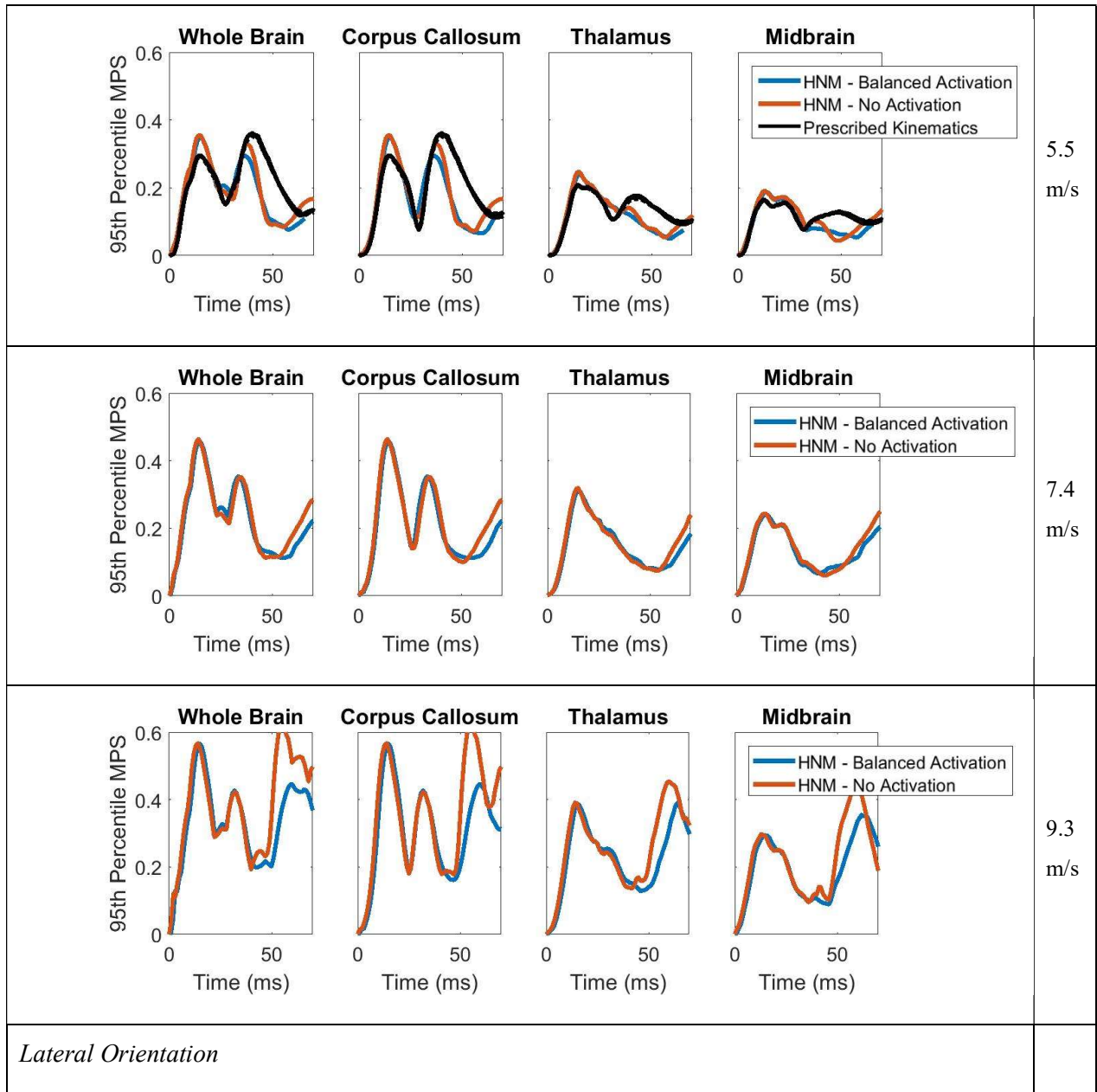
(c)

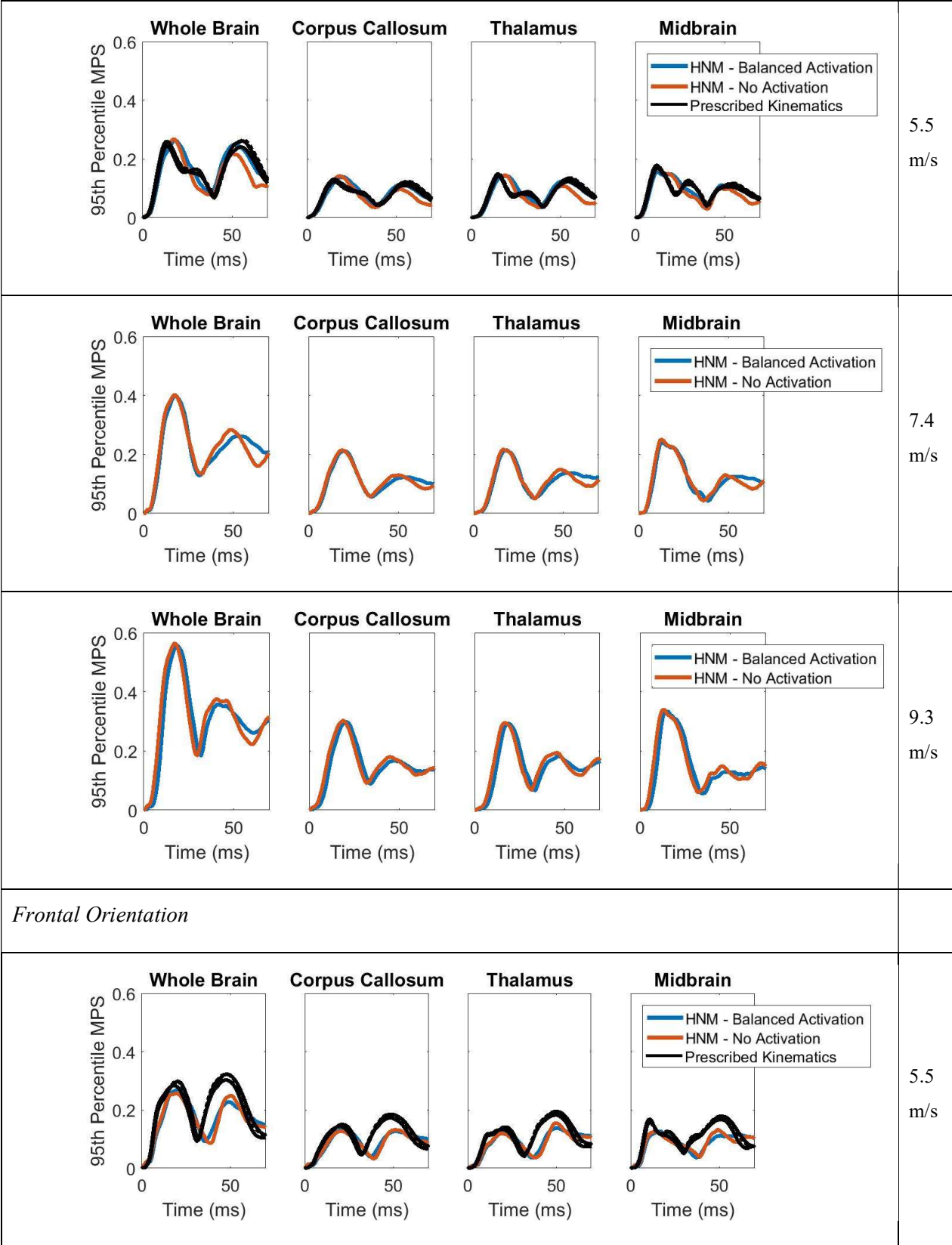
Figure C4 Helmeted impact at 5.5 m/s, active component of muscle force, (a) Lateral, (b) Frontal, (c) Rear

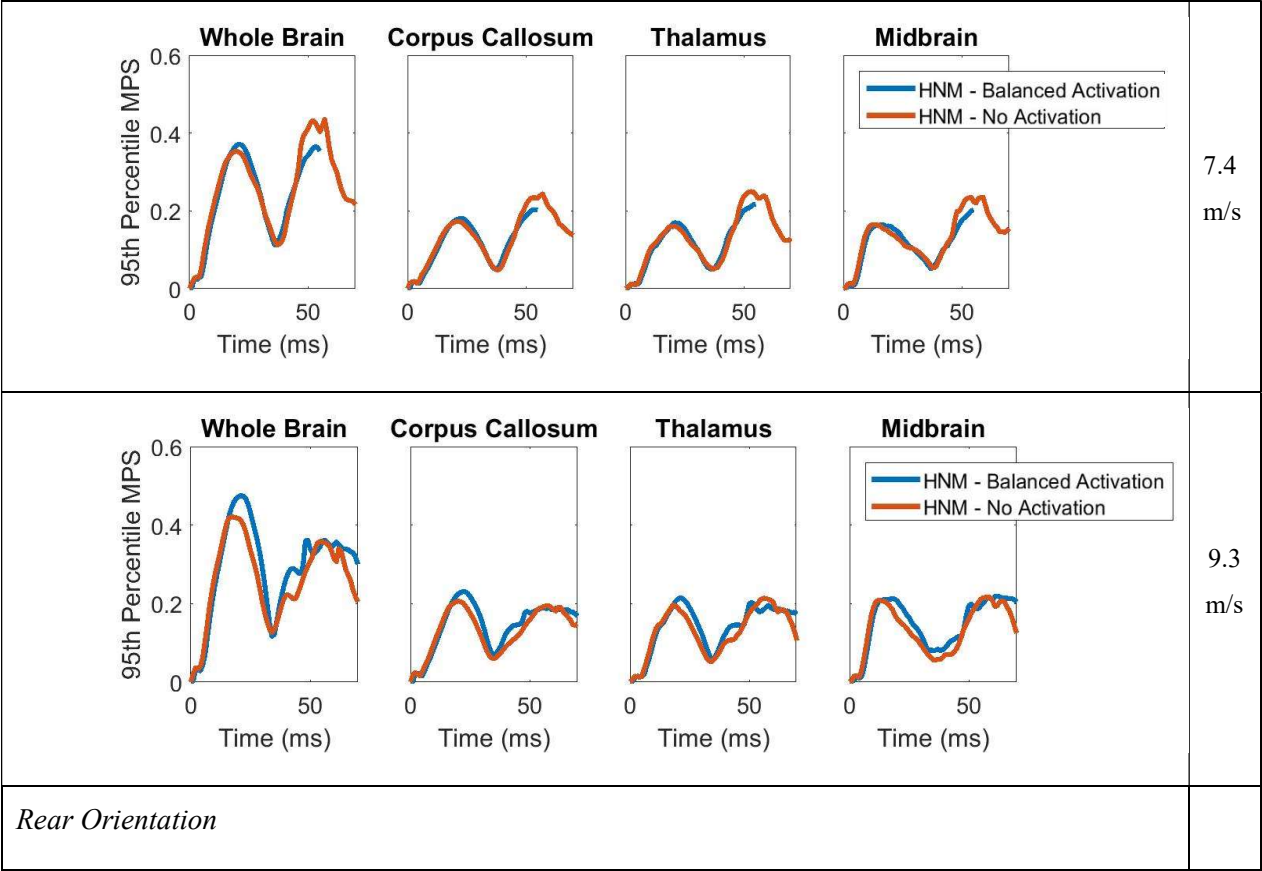
Appendix D: Brain Deformation of Simulated HNM Impacts and Prescribed Kinematics approach

Maximum Principal Strain (95th Percentile)

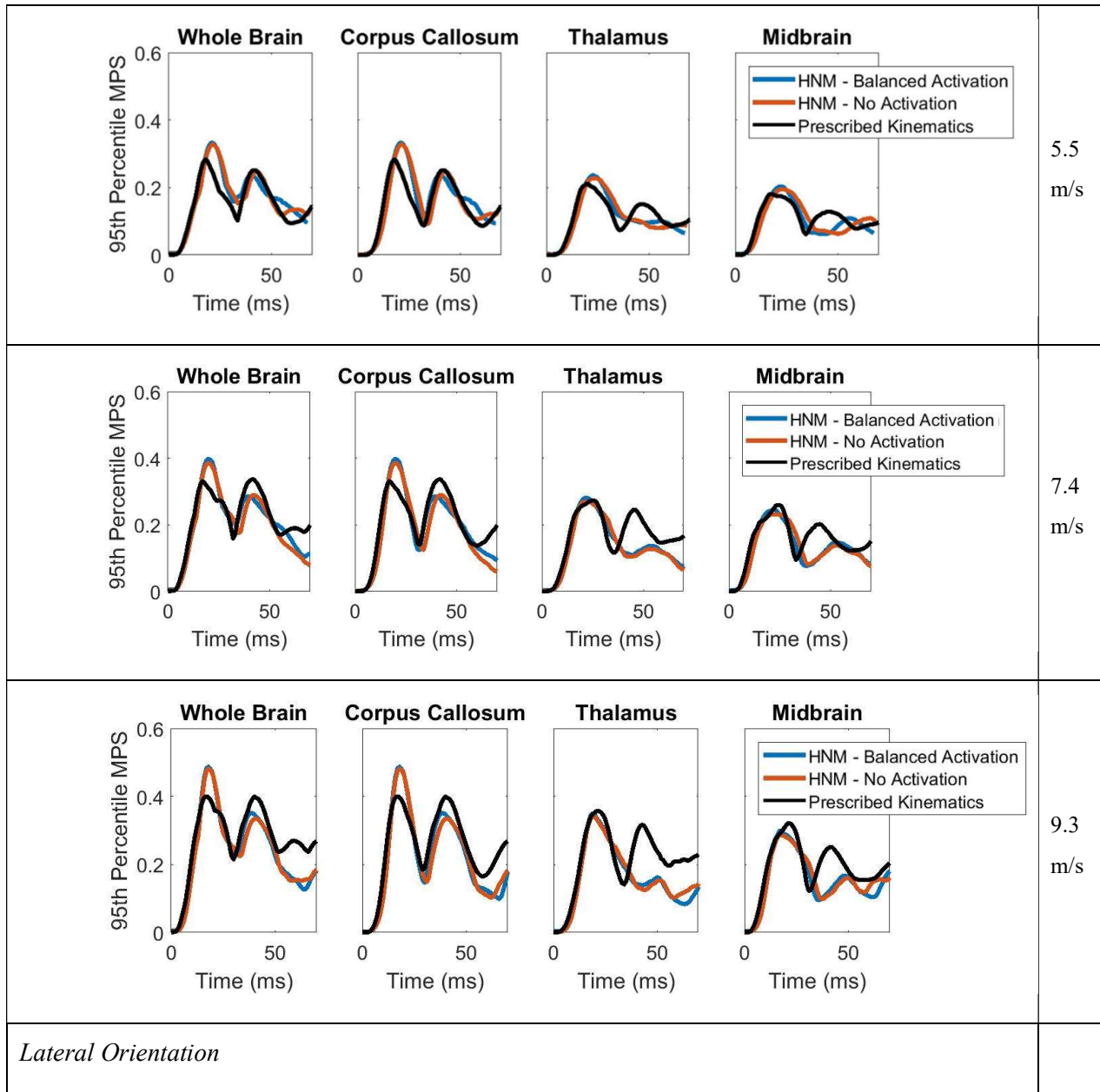
Bare-Head Impact

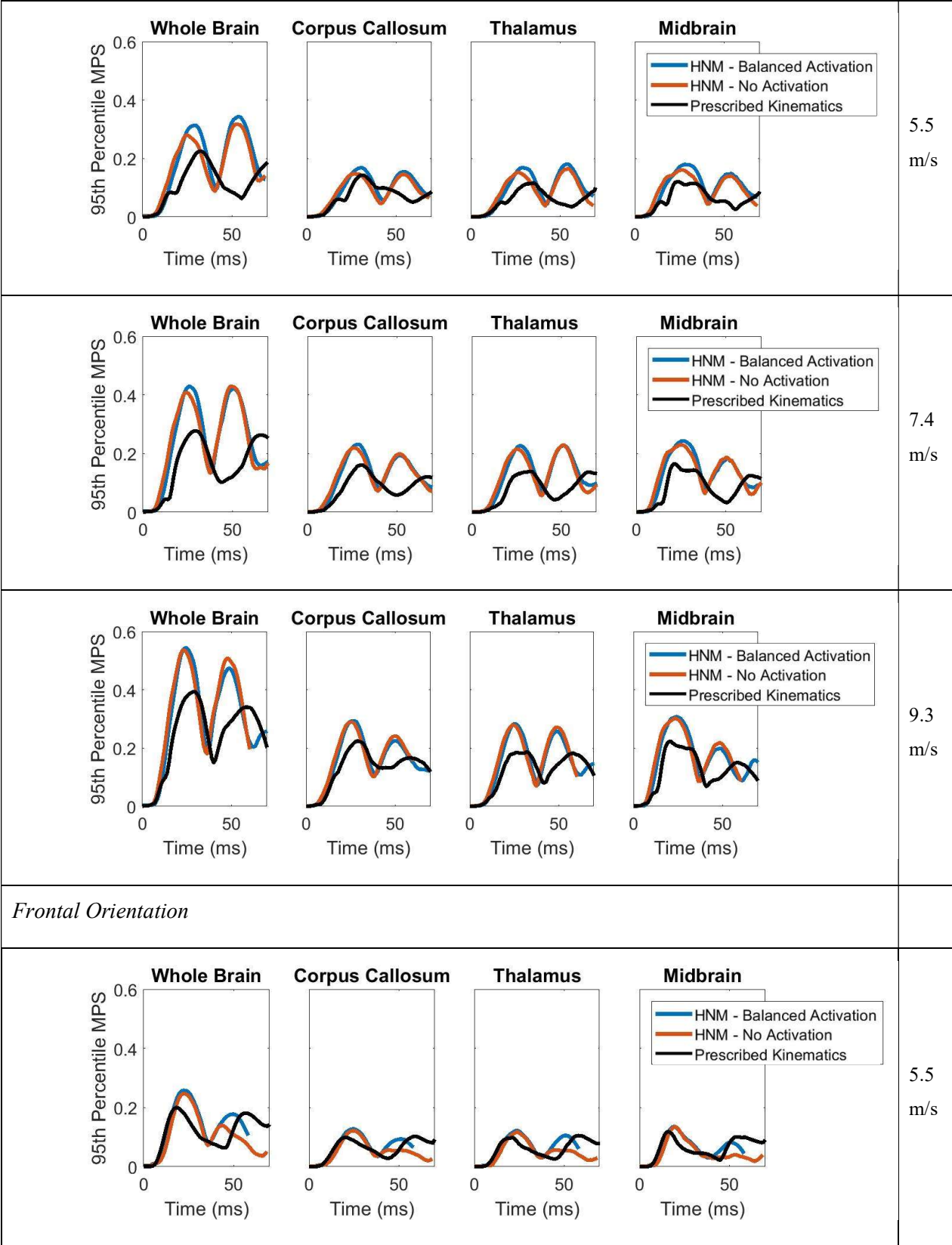


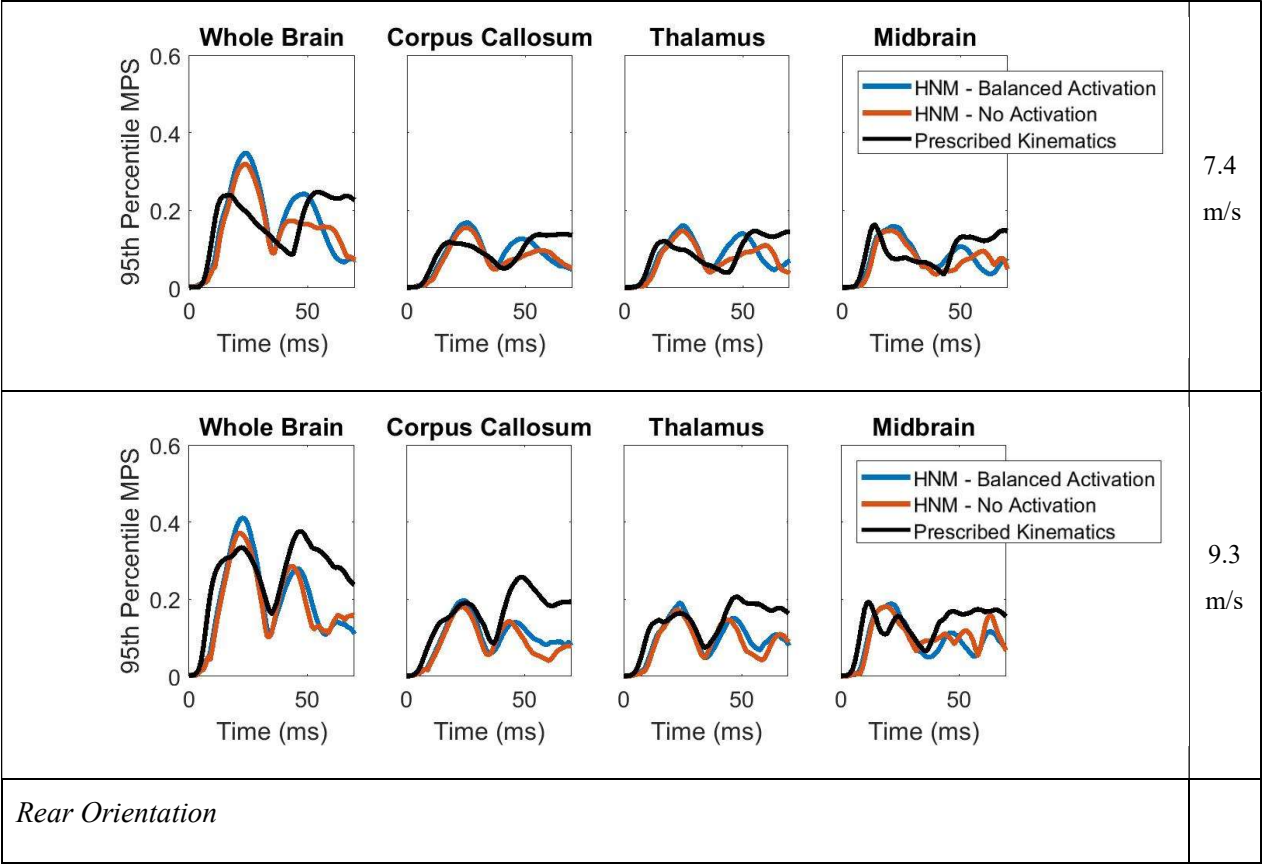




Helmeted Impact

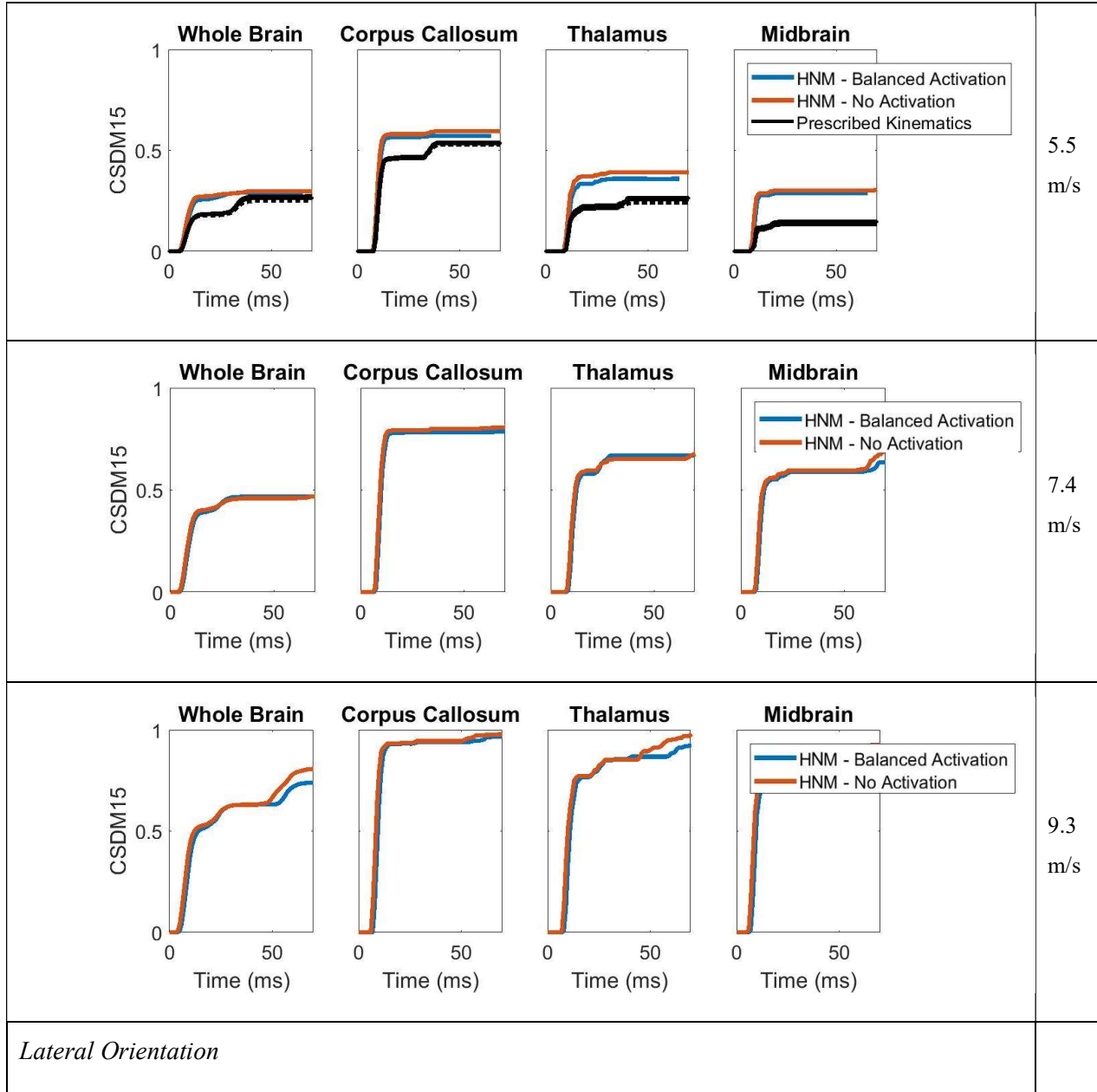


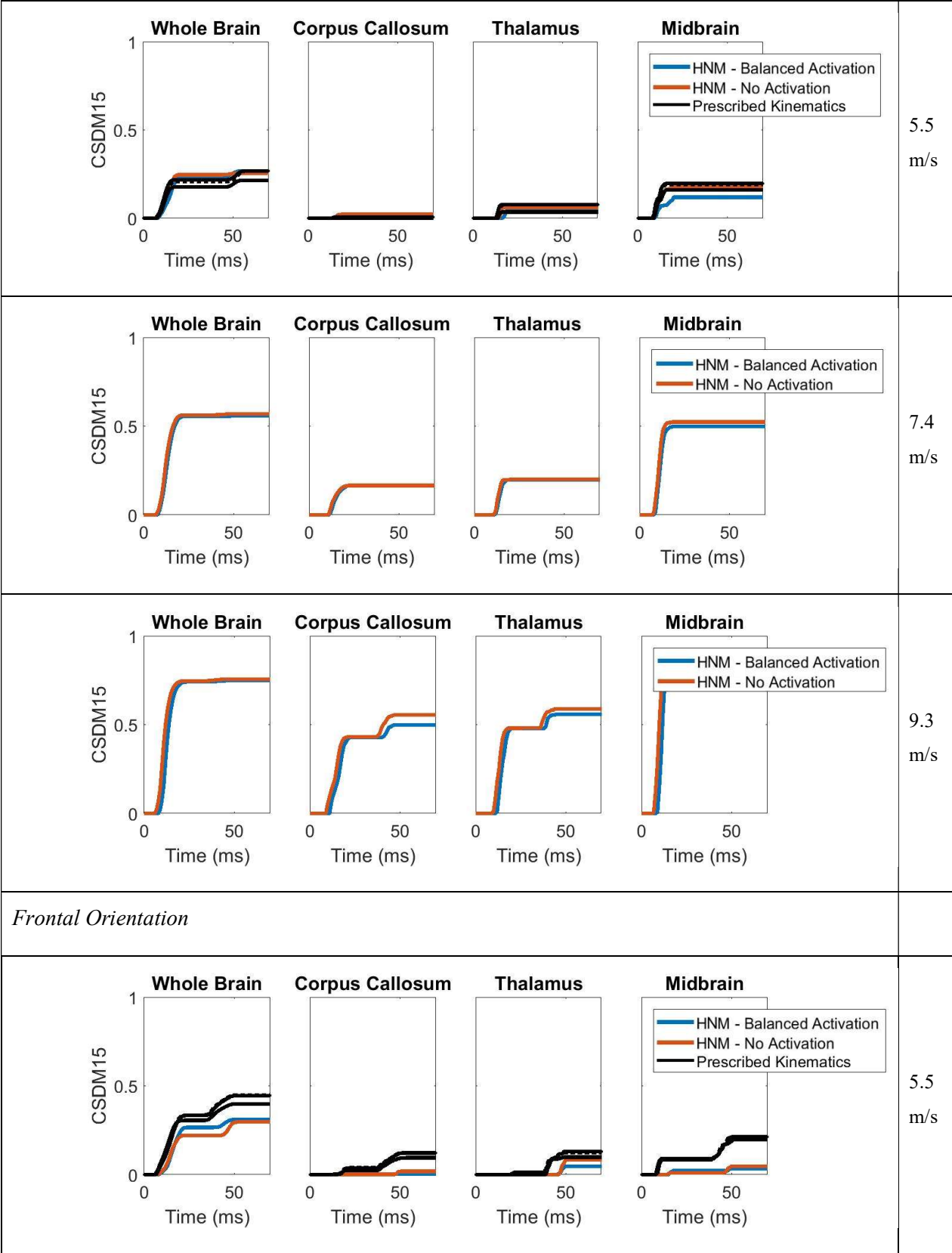


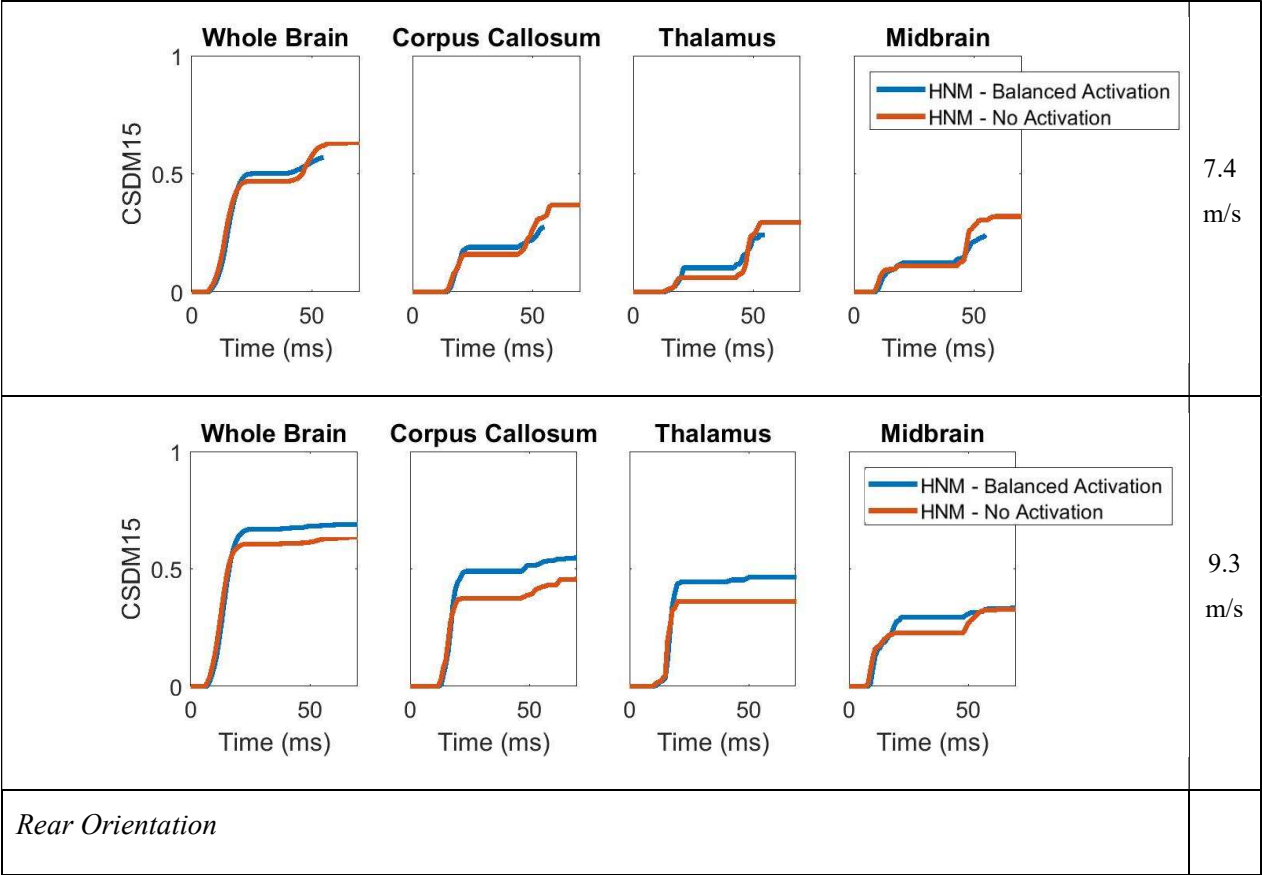


Cumulative Strain Damage Measure (CSDM15) in all impacts

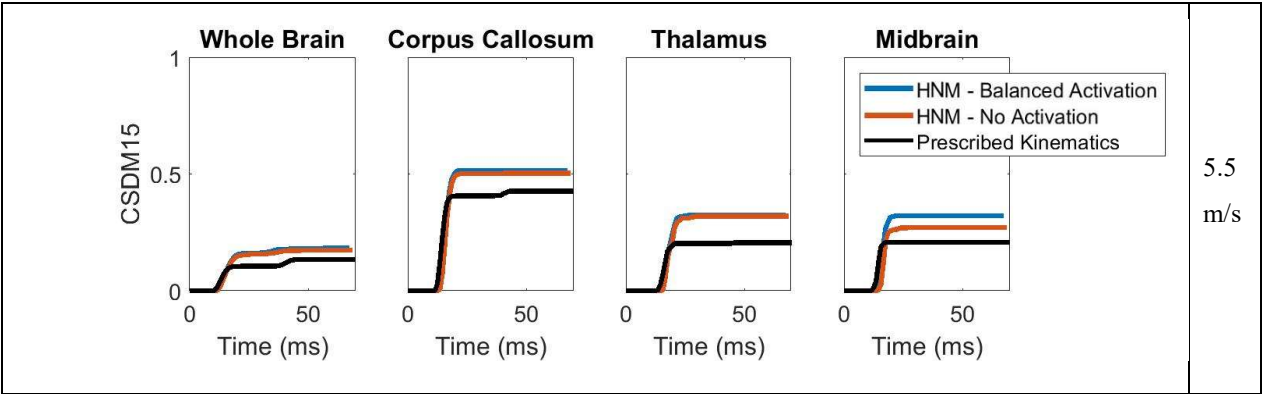
Bare-Head Impact

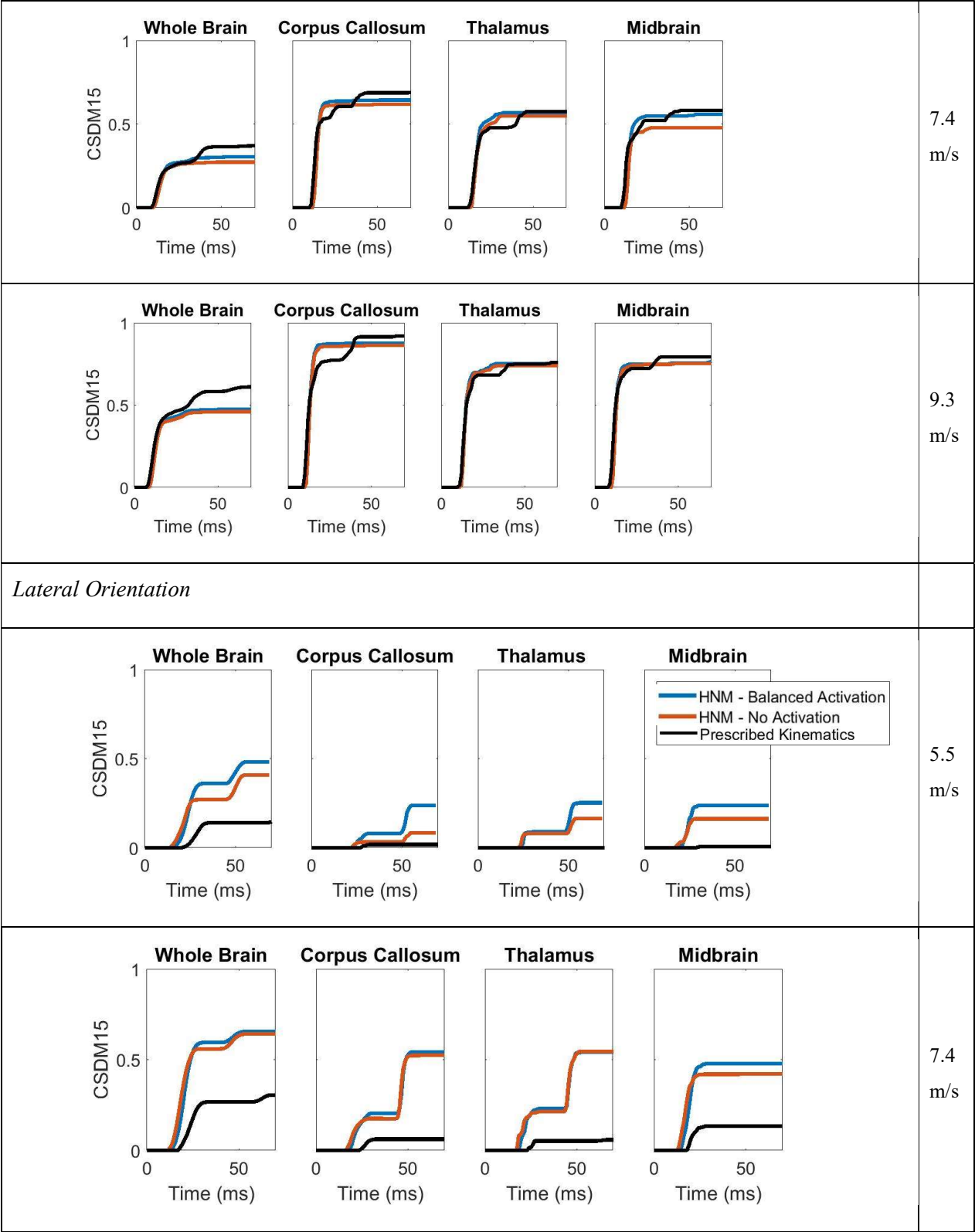


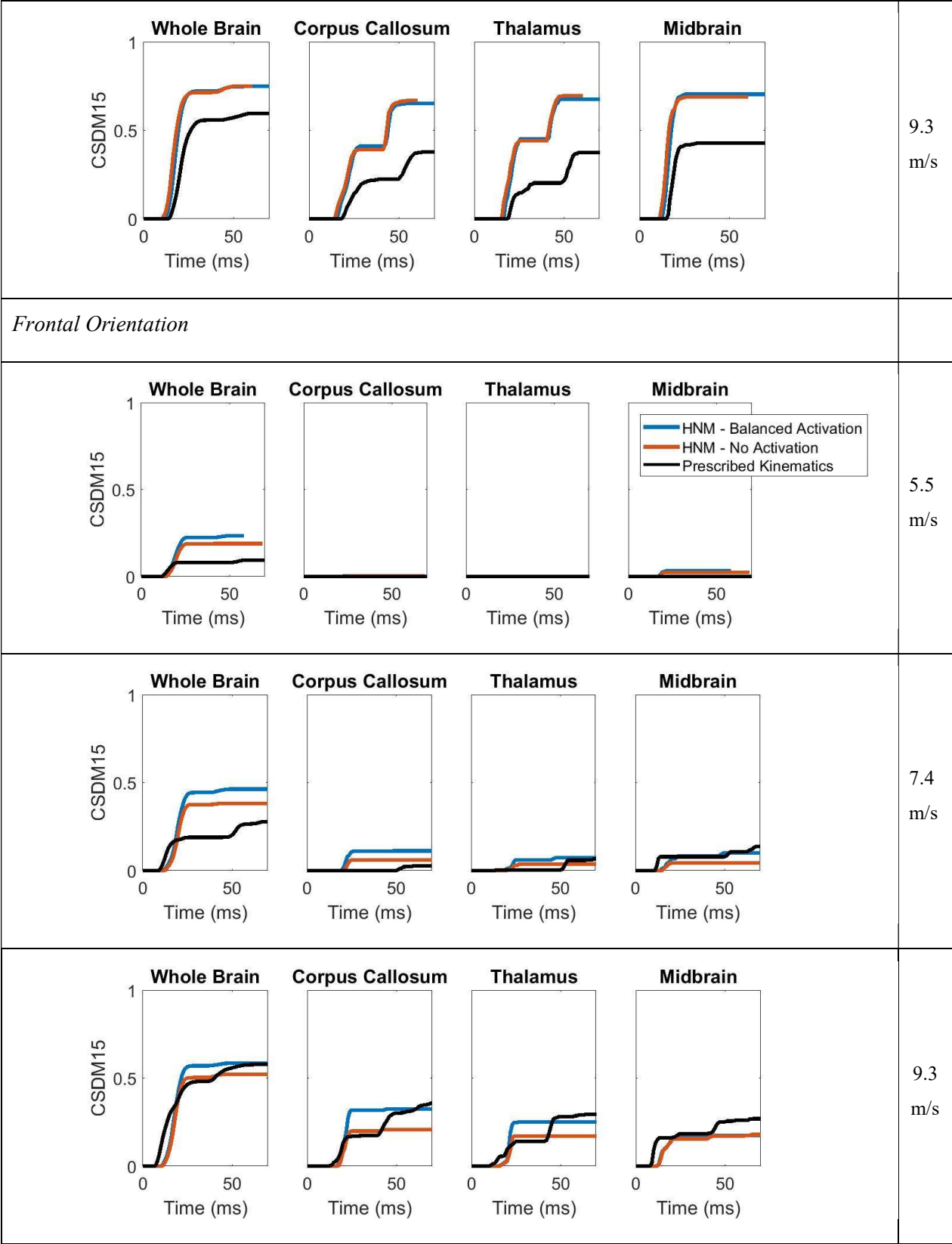




Helmeted Impact

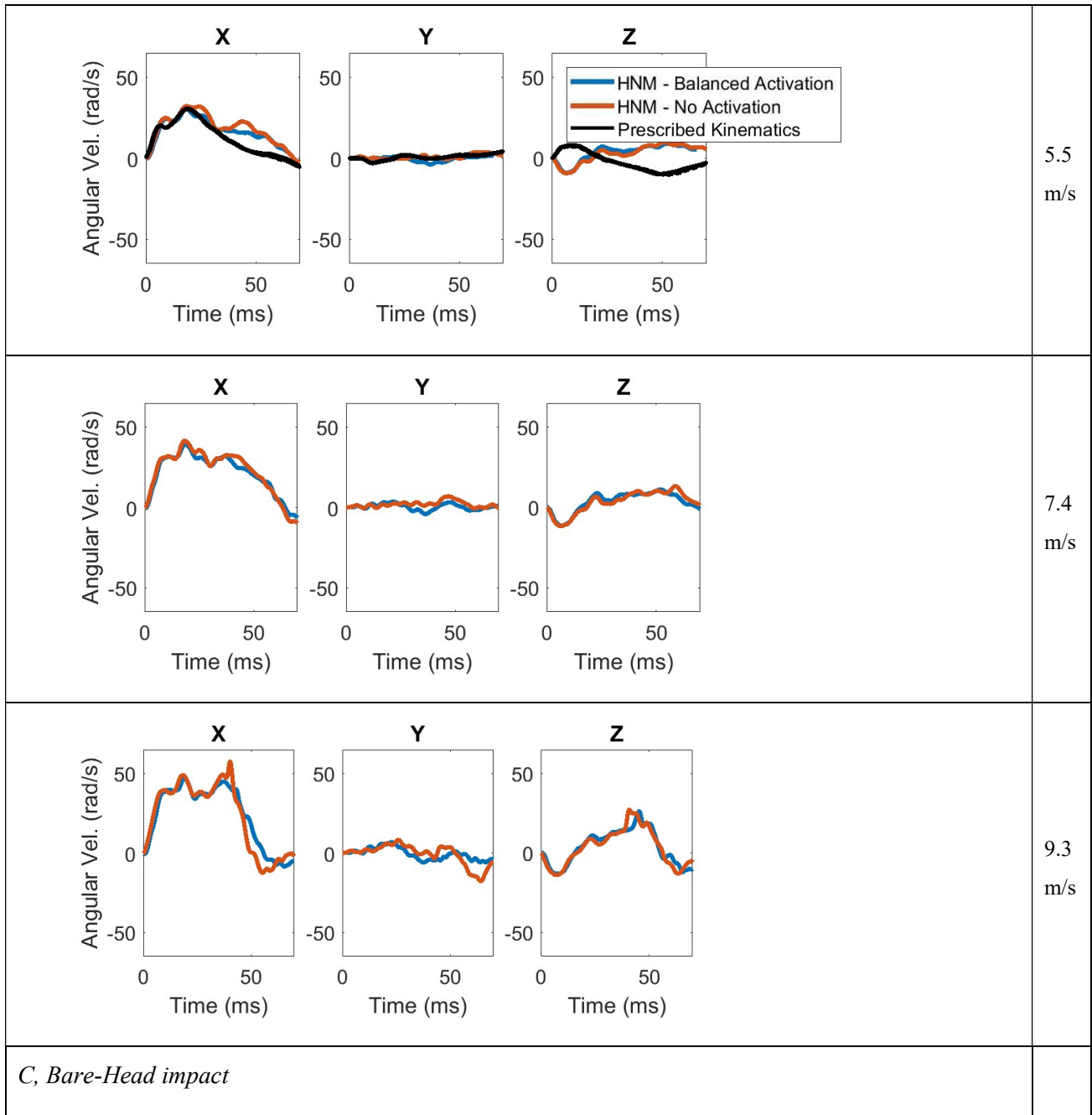


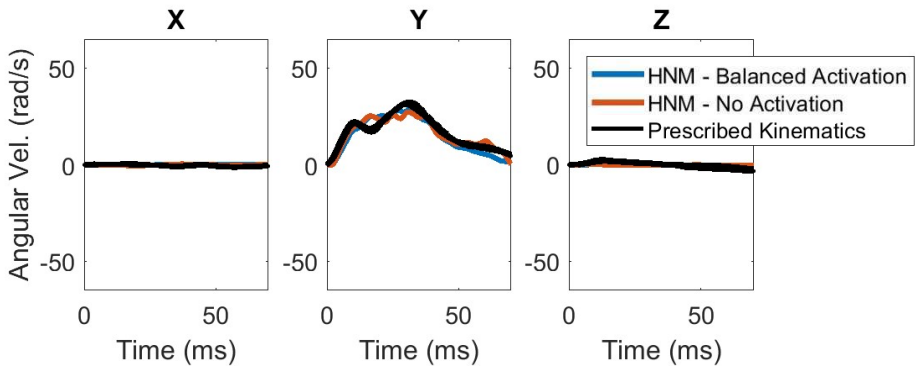
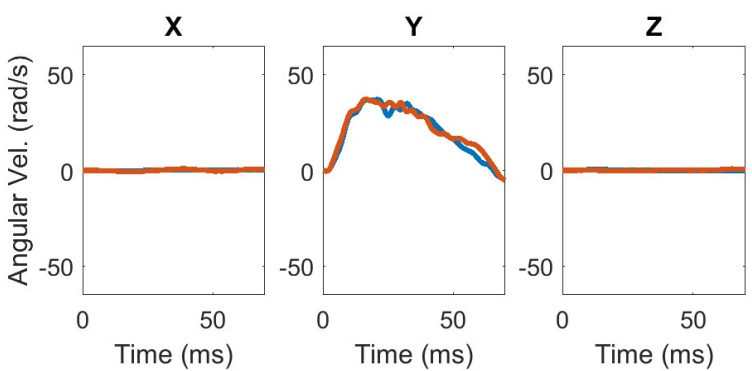
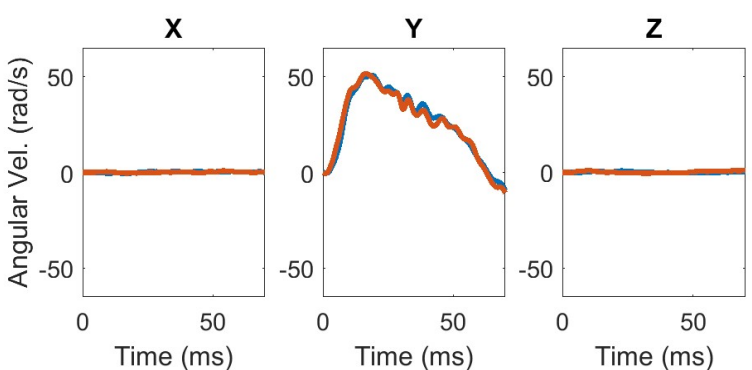


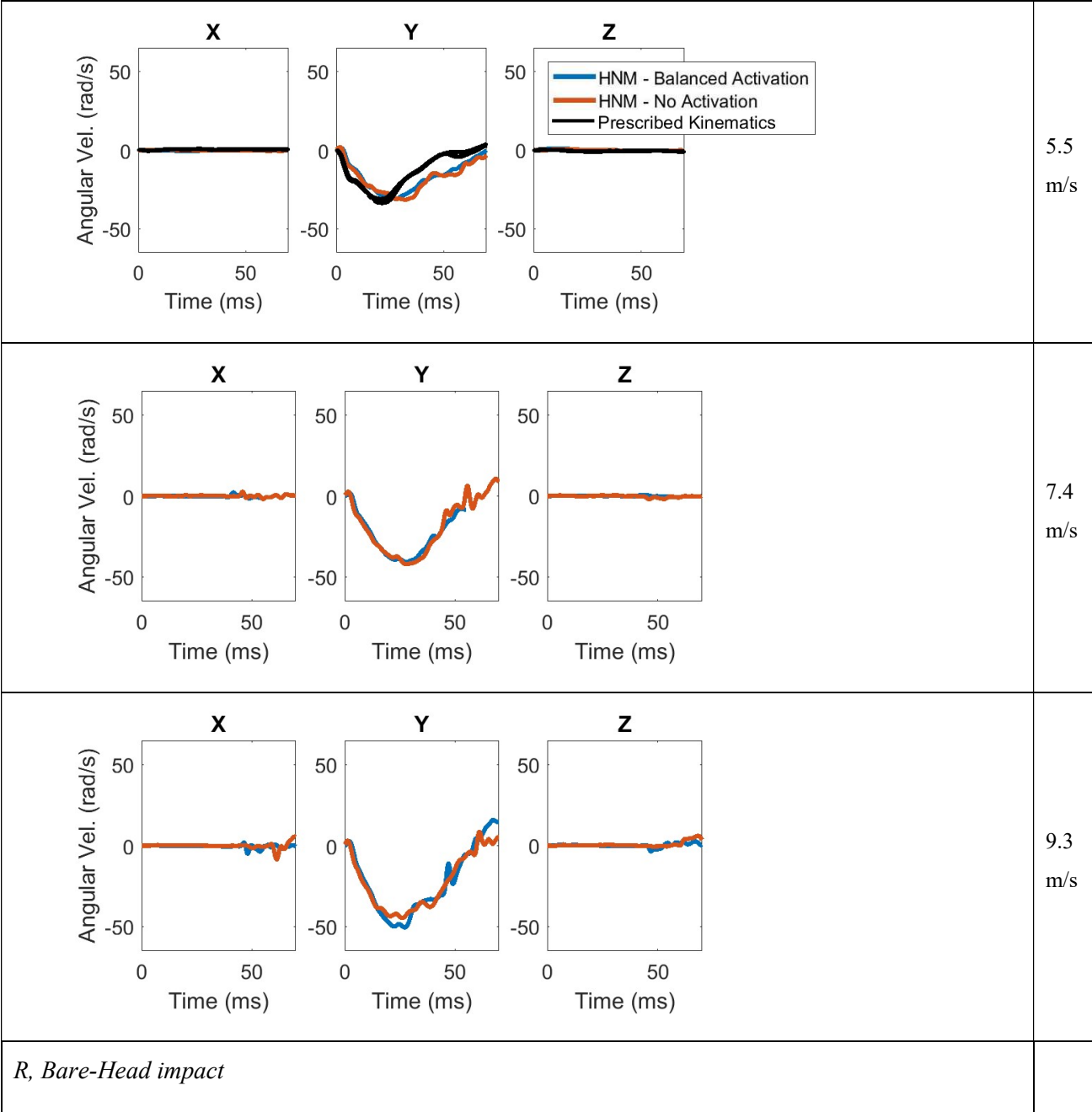


Rear Orientation

Appendix E – 3 DOF Angular Head Kinematics of HNM and ATD – experiment

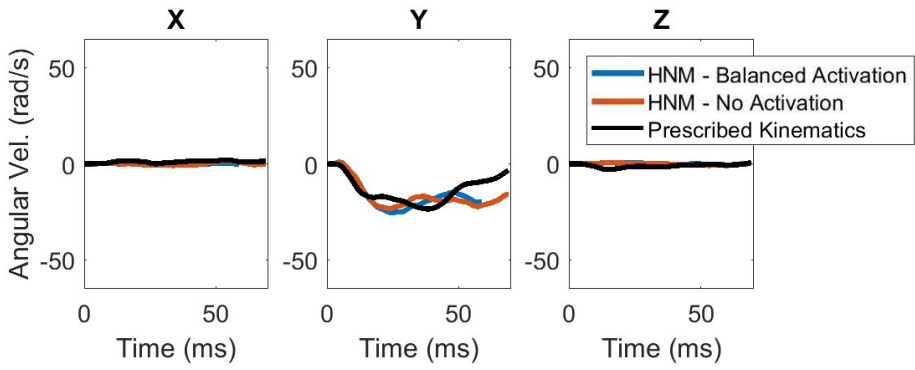
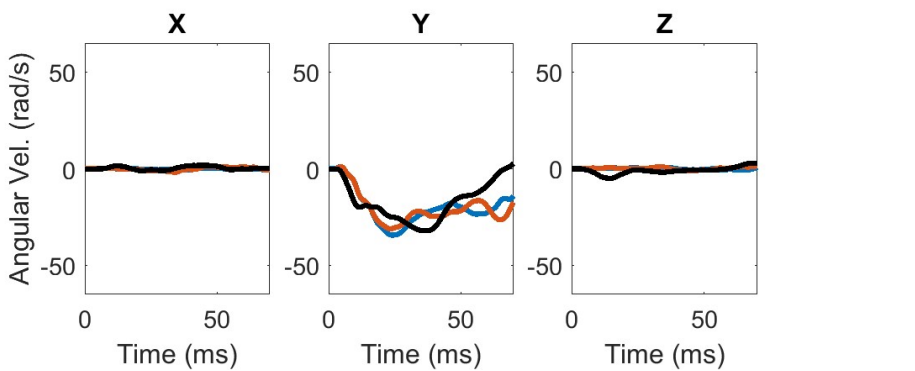
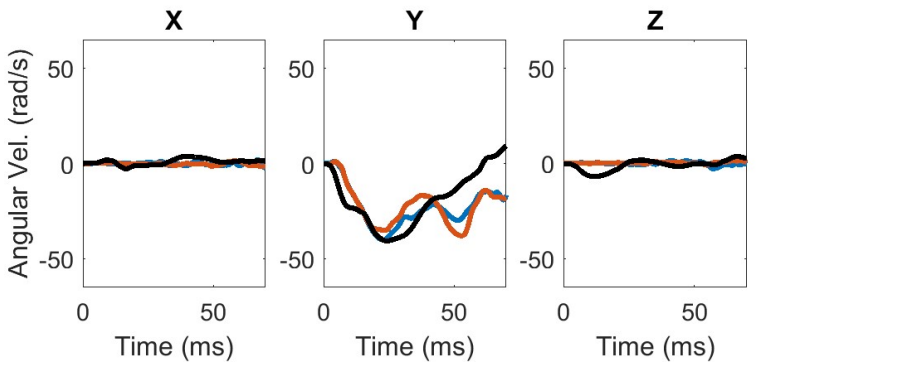


	<p>5.5 m/s</p>
	<p>7.4 m/s</p>
	<p>9.3 m/s</p>
<p><i>F, Bare-Head impact</i></p>	



	5.5 m/s
	7.4 m/s
	9.3 m/s
<i>C, Helmeted Impact</i>	

	5.5 m/s
	7.4 m/s
	9.3 m/s
<i>F, Helmeted Impact</i>	

	5.5 m/s
	7.4 m/s
	9.3 m/s
<i>R, Helmeted Impact</i>	